NOTE TO USERS

This reproduction is the best copy available.

SENSITIVITY ANALYSIS OF A BEAMFORMING TECHNIQUE FOR ACOUSTIC MEASUREMENTS

by

Pushpinder Singh Bhullar
B.E. (Mechanical Engineering),
Punjab Technical University, India, 1998

A Thesis
Presented to Ryerson University
In partial fulfillment of the
Requirements for the degree of

Masters of Applied Science

In the Department of
Mechanical and Industrial Engineering

Toronto, Ontario, Canada, 2004

Borrower's Page

Ryerson University requires the signatures of all persons using or photocopying this thesis. Please sign below, and give address and date.

Name	Address	Date

Acknowledgements

I would like to express my thanks and gratitude to my supervisors, Dr. Ramani Ramakrishnan and Dr. Greg Kawall, without whose help completion of this thesis would not have been possible.

I would like to thank Dr. Norman Ball and his colleagues at the National Research Council (NRC) of Canada, Ottawa, for supporting this project and for providing the opportunity to conduct experiments at the NRC acoustic laboratory. I am grateful to Subajini Kandasamy for her invaluable help.

Finally, my gratitude goes to my wife, Manmeet Bhullar, for her patience, encouragement and help.

Abstract

Sensitivity Analysis of a Beamforming Technique for Acoustic Measurements

Master of Applied Science
in the program of
Mechanical Engineering
Ryerson University

Beamforming is a technique that is used to determine the location of an acoustic source and the sound level spectrum of the signal produced by the source. This technique involves an array of microphones which record acoustic signals at multiple locations. A detailed analysis of the beamforming technique was carried out for three different array geometries: a uniform linear array, a uniform planar array, and a random array. The effect of various parameters, such as the number of microphones in an array, on the applicability of the technique was examined using both simulations and experiments. The simulation results established that the source localization capability of a uniform linear array is limited to an acoustic source lying in the plane of the array. In contrast, a planar array (either uniform or random) does not suffer the above limitation. These results also showed that a random array (e.g., a spiral array) is the best of all the array geometries. The experimental results demonstrated the robustness of the beamforming technique in localizing an acoustic source and also confirmed the superiority of a uniform planar array over a uniform linear array.

Table of Contents

List of Figures

Uniform Linear Array-near field beamforming

Uniform Planar Array-near field beamforming

Comparison between a ULA and a UPA with a near field source

Random Array – near field beamforming

Horizontal Uniform Linear Array

Comparison between a Vertical Uniform Linear Array (VULA) and an HULA

Cross Array

Comparison between an HULA, a VULA, and a Cross array

Appendix B

List of Tables

Nomenclature

a	Diameter of circular array, m
A	Amplitude of source signal, Pa
b	Index, 1, 2, 3,...
c	Speed of sound in air, 344 m/s
CSM	Cross spectral matrix
d	Inter-microphone distance for ULA, m
d^*	Inter-microphone distance to satisfy Shannon's criterion (=$\lambda/2$)
d_1, d_2	Inter-microphone distance along the x & y axes for UPA, m
D	Array aperture, m
e	Steering vector
e'	Hermitian transpose of steering vector
f	Frequency, Hz
f_s	Sampling frequency, Hz
f_{max}	Maximum frequency present in signal, Hz
f_k	Frequency for kth frequency bin, Hz
FFT	Fast Fourier Transform
$G_n(f)$	Auto spectrum of noise signal
$G_s(\omega)$	Auto spectrum of source signal
$\tilde{G}_s(\omega;T)$	"Raw" auto spectrum of the source signal
$G(\omega)$	Cross spectral matrix of the source signal
$G_{ii}(\omega)$	Auto spectrum of the ith microphone i.e., diagonal elements of the CSM
$G_{ij}(\omega)$	Cross spectra of the ith and jth microphones i.e., off-diagonal elements of the CSM
$\tilde{G}_{ij}(\omega;T)$	"Raw" cross spectra of the ith and jth microphones
$\hat{G}_{ij}(\omega)$	Averaged cross spectra of the ith and jth microphones
G_{ij_k}	CSM element for ith and jth microphones at frequency f_k

$\hat{G}_{ij_k}$	Averaged CSM element for ith and jth microphones at frequency f_k
$[G]_k$	CSM at frequency f_k
$\lvert\hat{G}\rvert_k$	Averaged CSM at frequency f_k
$H(\omega)$	Array pattern for far field beamforming for ULA
$H(\theta,\varphi)$	Array pattern for far field beamforming for UPA
i	Index, 1, 2, 3...
i	Imaginary unit, $\sqrt{-1}$
I	Integer number, 1, 2, 3...
j	Index, 1,2 3, ...
k	Index, 1,2,3,...
$\vec{k}$, k	Wave number vector, wave number
l	Index, 1,2 ,3...
L	Total number of blocks per microphone
m	Index, 1, 2, 3 ...
M_T	Total number of data points per microphone = $\frac{T}{\Delta t} = ML$
M	Number of data points per block
n	Microphone index for ULA, 1,2,3...
$n_1 n_2$	Microphone index for UPA, 11, 12, 13 ..., 21, 22, 23...
N	Number of microphones for ULA
N_1, N_2	Number of microphones along x and y axes for UPA
p	Acoustic pressure, p(x, y, z, t)
$P(\omega)$	Array power response
$\hat{P}_k$	Array power for kth frequency bin
$\bar{r}$	Distance between the acoustic source and the given microphone, m
r	Actual distance between array centre and acoustic source, m
r_n	Actual distance between acoustic source and nth microphone, m
r'	Assumed distance between array centre and acoustic source, m

r'_n	Assumed distance between acoustic source and nth microphone, m
$R(\tau)$	Cross correlation matrix (CCM)
$R_{ii}(\tau)$	Auto correlation function of the *i*th microphone i.e., diagonal elements of the CCM
$R_{ij}(\tau)$	Cross correlation function of the *i*th and *j*th microphone i.e., diagonal elements of the CCM
$R_s(\tau)$	Auto correlation of source signal, *s(t)*
$R_{sn_n}(\tau)$	Cross-correlation function of source signal and the noise signal of *n*th microphone
$R_{n_i n_j}(\tau)$	Cross-correlation between noise signals at *i*th and *j*th microphones
$R_n(\tau)$	Autocorrelation function of noise signal
$s(t)$	Source signal
$\overline{s^2}$	Mean square value of the source signal
$s[m]$	Digitized form of the source signal
S	Noise scaling factor
$S(\omega;T)$	Finite Fourier Transform (FT) of the signal *s(t)*
SR	Sampling rate, Hz
SNR	Signal-to-noise ratio of an array
SNR_o	Signal-to-noise ratio of a single microphone
SPL	Sound pressure level, dB
t	Time, s
T	Total duration of signal per microphone, s
T_l	Duration of signal for one block, s ($=M\Delta t$)
T_p	Period of one sine wave cycle, s
W_n	Weight applied to nth microphone
$W(k,x',x)$	Array pattern for near field beamforming: ULA and UPA
$y_n(t)$	Signal at nth microphone
$y_n[m]$	Digitized signal at *nth* microphone

$Y_n(\omega)$	Fourier Transform (FT) of signal $y_n(t)$
$Y_n(\omega;T)$	Finite Fourier Transform (FT) of signal $y_n(t)$
$Y_n[k]$	Discrete Fourier Transform of $y_n[m]$
$Y_i[k]$	Discrete Fourier Transform for the *ith* microphone for *k*th frequency bin
$Y_j[k]$	Discrete Fourier Transform for the *jth* microphone for *k*th frequency bin
$[Y]_k$	FFT coefficients column matrix for kth frequency bin (all microphones)
$z(t)$	Microphone array output in time domain
$z[m]$	Discrete version of $z(t)$
$Z(\omega)$	Microphone array output in frequency domain: FT of signal $z(t)$
$Z[k]$	Discrete version of $Z(\omega)$
x, y, z	Cartesian coordinates, m
X, Y, Z	Position of a source along x, y, and z-axis, m
φ	Elevation angle, radians
θ	Azimuth angle, radians
σ_{ym}^2	Mean square value of *mth* microphone signal
σ_s^2	Mean square value of source signal
σ_{nm}^2	Mean square value of noise signal at *mth* microphone
Δ_n	Time delay for *nth* microphone (with respect to reference microphone or position): ULA
Δ_{n1n2}	Time delay for $n_1 n_2$ microphone in far field: UPA
ω	Radian frequency, Hz
λ	Wave-length = *c/f*, m
$\lambda_{\min}$	Minimum wave-length = c / $f_{\max}$, m
Δt	Time spacing between sampled points =1/*SR*, s
Δf	Frequency resolution $= \frac{SR}{M} = \frac{1}{T_l}$, Hz

Chapter 1

Introduction

1.0 Background

The identification of an acoustic source, its location in space, and its acoustic output, is a challenging and important research area in the field of aeroacoustics. This field concerns the study of fluid-mechanically generated sound, and acoustic source identification has become an important research area due to the growing need to control aircraft and automobile noise. This area has expanded with the development of special wind tunnels designed for model studies that involve the simulation of noise generating vehicles. An essential aspect of these studies is the use of microphones to measure acoustic signals generated by a model.

A single microphone provides the sound pressure spectrum of the acoustic signal from a given source, recorded at the location of the microphone. In general, the spectrum is contaminated by noise when measurements are conducted in hard-wall wind tunnels (which reflect sound) and the resulting measurements are hampered by poor signal-to-noise ratio. Therefore, the use of a single microphone would not provide the required information concerning source location and the correct sound pressure spectrum, and the development of source localization techniques to provide the correct location of an acoustic source and the correct associated sound level spectrum is required. There are various source identification techniques used in acoustics. One of the most effective of these is the beamforming technique.

This chapter briefly outlines the basic aspects of source identification, various source identification techniques used in acoustics, including the beamforming technique, a brief history of beamforming, and the objective of the thesis.

1.1 Basic aspects of source identification

In aeroacoustic testing, a model is placed in a wind tunnel and exposed to an air flow. The model responds by producing a complex array of sounds. The two primary objectives of acoustic measurements are to localize the sound producing regions (i.e., acoustic sources) and to quantify their acoustic strength [1]. These sound producing regions can be in the near field or in the far field depending upon the distance of a given source from a microphone. When the

wavefront of a propagating acoustic signal is *spherical* at the location of the microphone, the source is said to be in the near field; and when the wavefront can be considered *plane*, the source is said to be in the far field, as depicted in Figures 1.1(a) and 1.1(b), where θ defines the direction of arrival (DOA).These figures pertain to situations in which the source and microphone lie in the same plane (viz., the x-y plane). In general, this is not the case.

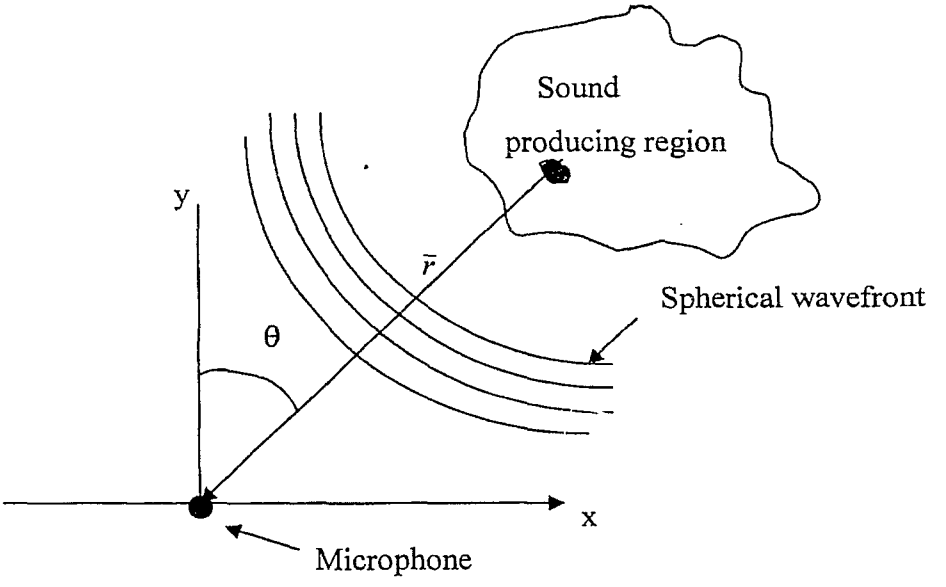

Figure 1.1 (a): Depiction of near field source location.

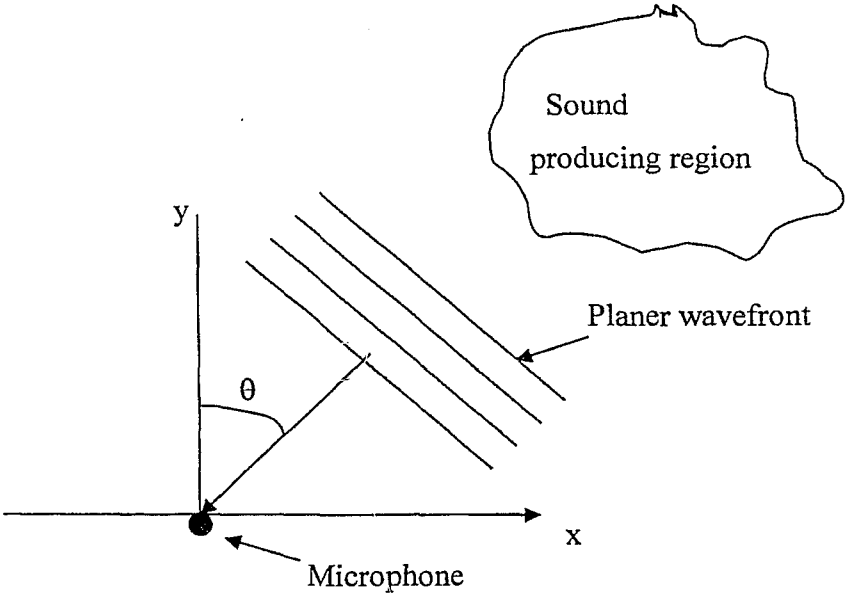

Figure1.1 (b): Depiction of far field source location.

1.1.1 Far field source location

The general wave equation in terms of the acoustic pressure is given by [2]:

$$\frac{\partial^2 p}{\partial x^2}+\frac{\partial^2 p}{\partial y^2}+\frac{\partial^2 p}{\partial z^2}=\frac{1}{c^2}\frac{\partial^2 p}{\partial t^2} \tag{1.1}$$

where, c is the speed of sound in air, $p = p(x, y, z, t)$ represents the acoustic pressure, and x, y, z are Cartesian coordinates.

In practice, the most important type of solution of the wave equation is the harmonic solution. This solution pertains to situations for which p has harmonic spatial and temporal variations, i.e., p is a periodic function of x, y, z, and t. For convenience, the solution of equation (1.1) is expressed in complex form, with the understanding that the actual solution is the real part of the complex solution.

When a source is far from a microphone, *a plane* wave will be received by the microphone, and the solution of the wave equation is given by [2]:

$$p(x,y,z,t) = A\exp\{i(\omega t+\phi-k_x x-k_y y-k_z z)\}$$

$$= A\exp\{i(\omega t+\phi-\vec{k}\bullet\vec{x})\}, \tag{1.2}$$

where A is the amplitude of the pressure wave, ϕ is an arbitrary phase angle, and $\vec{k}$ is the wave number vector with Cartesian components, k_x, k_y, and k_z. The magnitude of $\vec{k}$ is related to the speed of sound (c) and the angular frequency of source (ω) as follows:

$$k=\frac{\omega}{c}. \tag{1.3}$$

For a microphone located at x^*, y^*, z^*, equation (1.2) yields:

$$p(x^*,y^*,z^*,t) = A\exp\{i(\omega t+\phi-\phi^*)\}$$

$$= A\cos(\omega t+\phi-\phi^*)+iA\sin(\omega t+\phi-\phi^*) \tag{1.4}$$

where $\phi^* = \vec{k}\bullet\vec{x}$ is fixed, so that the actual plane pressure wave, i.e., the signal pertaining to the microphone, is given by:

$$p(x^*,y^*,z^*,t) = A\cos(\omega t+\phi-\phi^*). \tag{1.5}$$

Without loss of generality, ϕ can be taken as $\phi^*+\pi/2$. Hence, equation (1.5) becomes:

$$p(x^*,y^*,z^*,t) = A\sin\omega t \tag{1.6}$$

Therefore, for a far-field source location, the amplitude (A), and frequency (ω), or, more generally, the spectrum of the signal, and the direction of arrival (DOA) of the acoustic signal need to be determined.

1.1.2 Near field source location

When the source is near to the microphone, a spherical wave will be received by the microphone, and the general wave equation, for spherically symmetric problems, becomes in spherical coordinates [2]

$$\frac{1}{\bar{r}^2}\frac{\partial}{\partial \bar{r}}\left(\bar{r}^2\frac{\partial p}{\partial \bar{r}}\right)=\frac{1}{c^2}\frac{\partial^2 p}{\partial t^2} \tag{1.7}$$

where $\bar{r}$ is the distance between the source and a given microphone.

The solution to equation (1.7) is given by [2]:

$$p(\bar{r},t)=\left(\frac{A}{\bar{r}}\right)\exp.\{i(\omega t+\phi-k\bar{r})\} \tag{1.8}$$

Since, from equation (1.3), $k=\omega/c$, equation (1.8) can be expressed as:

$$\begin{aligned} p(\bar{r},t) &= \left(\frac{A}{\bar{r}}\right)\exp.\{i[\omega(t-\frac{\bar{r}}{c})+\phi]\} \\ &= \left(\frac{A}{\bar{r}}\right)\cos[\omega(t-\frac{\bar{r}}{c})+\phi]+i\left(\frac{A}{\bar{r}}\right)\sin[\omega(t-\frac{\bar{r}}{c})+\phi] \end{aligned} \tag{1.9}$$

Hence, the actual pressure wave received by the microphone is given by:

$$p(\bar{r},t)=\left(\frac{A}{\bar{r}}\right)\cos[\omega(t-\frac{\bar{r}}{c})+\phi]. \tag{1.10}$$

Without loss of generality ϕ can be taken as $\pi/2$. Hence equation (1.10) becomes:

$$p(\bar{r},t)=\left(\frac{A}{\bar{r}}\right)\sin[\omega(t-\frac{\bar{r}}{c})] \tag{1.11}$$

Therefore, for a near-field source, the spectrum of the signal, the location of the source $(\bar{r})$, and the direction of arrival (DOA) of the signal must be determined.

1.2 Source identification techniques in acoustics

1.2.1 The sound intensity technique

The sound intensity technique involves the use of a special probe to measure sound intensity. This probe consists of two microphones separated by a spacer; it enables the cross-spectrum of the pressure signals at the two microphones to be calculated. The acoustic intensity provides the magnitude and the direction of the acoustic energy flow, so that the acoustic source can be determined. This technique is time consuming, and very sensitive to measurement errors. Also, the intensity field is not a significant parameter for source identification in highly reverberant environments, such as hard-wall wind tunnels [3].

1.2.2 The time delay estimation (TDE) technique

The time delay estimation (TDE) technique involves the use of two (or more) microphones. It is based on a two-step process. The first step consists of the estimation of the time delay between the various microphones by cross-correlation of the microphone signals. The second-step combines the known geometry of the microphones configuration and the time delay to find the direction of arrival (DOA) of the source signal [4, 5]. This technique is used when reverberation is not severe and is effective only for a single source. Also, the acoustic measurements require low background noise and acoustic reflections for accurate results, and these requirements are difficult in most wind tunnels.

1.2.3 The acoustic mirror technique

Aeroacoustic researchers use the "acoustic mirror" technique to localize acoustic sources in wind tunnels. In this technique, a large concave elliptic mirror and a single microphone are used. The microphone is placed at one focal point of the mirror, and the other focal point is located within the acoustic source region. This technique has many limitations. The size of the mirror must be large for low frequency sources, and the mechanical movement of the mirror around the model is difficult. However, these systems are still used in large test facilities [6, 7].

1.2.4 Acoustic array techniques

To overcome the limitations of the above given techniques (i.e., the sound intensity, TDE, and acoustic mirror techniques), an array of microphones is required. Acoustic array techniques

involve the collection of a large quantity of spatial data from an array of microphones [8], and they can be classified as:

- The near-field acoustical holography (NAH) technique.
- The beamforming technique.

1.2.4.1 The near-field acoustical holography (NAH) technique

As mentioned in section 1.1, when the distance between the source and the microphone is small, the wave front of the acoustic signal is curved and the source is said to be in the near field. The near-field acoustical holography (NAH) technique is the source identification technique generally used for the localization of acoustic sources from near-field pressure and velocity measurements [8]. These measurements describe the acoustic properties of the sources. Applications of this technique include the localization of machinery noise and, in the automotive industry, the determination of acoustic energy distribution in various areas of a car (such as doors, windscreen, roof etc.) [4, 7, 8, and 9]. There are frequency limitations on this technique. Specifically, for a closed volume, the reverberant field will impose a limit on low frequencies [10]. Also, high frequencies are limited by the distance between microphones [10].

1.2.4.2 The beamforming technique

This is a spectral based technique for calculating source characteristics such as the location of an acoustic source, the sound pressure level (SPL) of the source, and the frequency of the source. In beamforming, the array of microphones is steered towards the source algorithmically, i.e., the microphone signals are processed in such a way that the effect is the same as that obtained by physical movement of the microphones. This involves the calculation of the microphone array output power (i.e., mean square pressure values) for different possible locations of the source. The maximum power corresponds to the location of the source [11].

In microphone directional array (beamforming) testing, several spatially separated microphones provide pressure fluctuations at multiple locations and can be used to reduce the effect of extraneous noise and extract the desired source location and sound pressure level information from the middle of noisy, reverberant, non-acoustic wind tunnels [1]. Note that, as mentioned previously, the other source localization techniques, viz., acoustic intensity, TDE, and acoustic mirror techniques, are time consuming, and have poor resolution when strong reverberation (noise) is present. Therefore, the use of a microphone directional array adds a

powerful measurement capability to aeroacoustic research [1]. The advantages of an array of microphones over a single microphone are: improved signal-to-noise ratio and the localization of the acoustic sources. It should be noted that by using a microphone directional array, the capability to conduct *simultaneous* aerodynamic and acoustic testing of a model is possible in a traditionally designed aerodynamic hard-wall wind tunnel [1].

1.3 A brief history of beamforming

Beamforming has been used for many years in RADAR (RAdio Detection And Ranging), SONAR (SOund Navigation And Ranging), communications, imaging, geophysical exploration, and bio-medical research [12]. Large fixed electromagnetic antennas are used for RADAR systems and phase shifts are applied to the received signals to detect the DOA of the signal. Most of the applications of beamforming for RADAR and communications involve narrowband signals. The applications of beamforming to underwater acoustics started with active SONAR where a known narrowband signal is generated, and a corresponding reflected signal (echo) provides information about an underwater object. Passive SONAR was subsequently used to find out the location of a ship or submarine, and, in the 1970's, passive localization efforts focused on determining not only the bearing but also the range [13]. It should be noted that passive SONAR involves broadband frequency signals.

In aeroacoustics, aircraft and automotive manufacturers have always been interested in improving the acoustic measurement capabilities in non-anechoic wind tunnels. Until the 1990's, researchers and engineers used only one microphone or a pair of microphones for *most* of the acoustic measurements because data acquisition systems were relatively expensive. In 1975, Soderman and Noble [14], for the first time, used four and eight- element microphone arrays, in conjunction with time domain beamforming, in the NASA Ames 40- by 80-foot hard-walled wind tunnel. In 1987, Brooks and Marcolini [15] tested an out-of-flow directional microphone array in an anechoic wind tunnel to examine the acoustic sources over a helicopter rotor model. In 1990, Elias [16], did more work with a linear array by using frequency domain beamforming to localize acoustic sources. In 1992, Dine, Gely and Elias [17] evaluated the performance of a linear array in an anechoic open jet wind tunnel. In 1995, Gramann and Mocio [18], used a linear array by incorporating inexpensive microphones, in conjunction with the delay and sum beamforming (DSB) and adaptive beamforming, in a conventional low

speed wind tunnel to measure the source location and sound level of signals from a loudspeaker. Brooks, and Marcolini [19], Underbrink J.R. [20], and Barns, Watts and Mosher [21, 22] expanded the linear array to the planar (two dimensional) array geometry, using frequency domain beamforming. With the expansion of work on microphone arrays, in 1995, NASA and Boeing built data acquisition systems for closed and open wind tunnels, and efforts have been made to improve array design and algorithms for optimization of results [7].

In North America, mainly NASA and Boeing are active in microphone array research and are very focused on reducing the noise (especially airframe noise) of large aircraft, because, with the development of quieter engines, the noise generated by airframes becomes more significant, particularly during the approach of a flight [23]. In Europe, most of the research work on microphone arrays is published by German Dutch Wind Tunnel (DNW) & National Aerospace Laboratory (NLR) [24] and by ACB Engineering, Paris, France [25, 26, 27, and 28]. Over the last few years, with the success of microphone arrays in localizing aeroacoustic sources in hard-wall wind tunnels, research to find more advanced beamforming algorithms has intensified.

1.4 The objective of this thesis

The main objective of this thesis is to carry out a sensitivity analysis of the delay-and-sum beamforming (DSB) technique used as a source identification tool. This objective is split into two parts: 1) a sensitivity analysis of the DSB technique using simulation data; 2) a sensitivity analysis of the DSB technique using experimental data.

The organization of the thesis is as follows. Chapter 2 discusses the theoretical aspects of the delay and sum beamforming technique. This chapter also describes different geometries used in array signal processing, viz., the uniform linear array, the uniform planar array, and the random array. Chapter 3 provides details on the simulation aspect of the work and discusses the results of the sensitivity analysis using simulation data. The effect of various parameters, such as, number of microphones (N), frequency of acoustic source (f), inter-microphone distance (d), source position, on the efficacy of the technique is examined. Also, three different geometries are considered: a uniform linear array with a far field and a near field source, a uniform square array with a near field source, and a spiral array with a near field source. Chapter 4 provides experimental details and describes the results of the sensitivity analysis

using experimental data obtained with three different geometries: a horizontal uniform linear array, a vertical uniform linear array and a cross array. A comparison between a horizontal uniform linear array, a vertical uniform linear array, and a cross array is also discussed in this chapter. Finally, chapter 5 contains a summary of the work and conclusions, and it describes future work.

Chapter 2
Beamforming in acoustics

2.0 Introduction

Beamforming is a measurement technique applied to focus a microphone array in order to find acoustic source characteristics. In beamforming, the data are collected by spatially separated microphones and summed after required weights have been applied to all the microphones. These weights can be determined in different ways, leading to two basic methods, viz., the *conventional (delay and sum) beamforming method* and the *adaptive beamforming method* [2, 27]. It should be noted that the combination of hardware and software that perform beamforming is called a beamformer.

The basic purpose of a beamformer is to enhance signals from a particular direction while rejecting signals from other directions. The beamformer acts as a spatio-temporal filter for incoming signals and produces an acoustic source map over a grid of points in space. The characteristics of a beamforming map, shown in Figure 2.1, are the mainlobe and the sidelobes [1, 2, and 29]. The beamforming map is a plot of the array power (i.e., the mean square value of an acoustic pressure signal) versus the *possible* source locations, and this map is calculated by means of the delay and sum beamforming method.

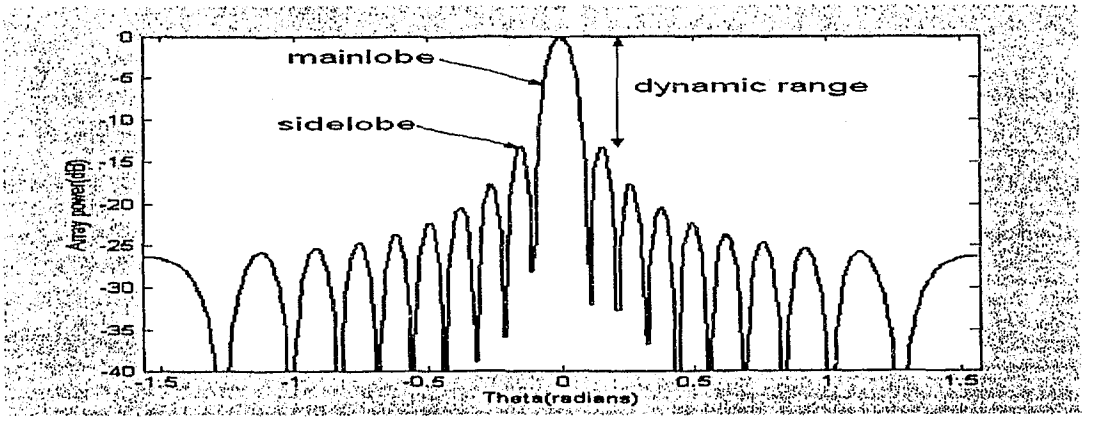

Figure 2.1: A typical beamforming map.

The primary lobe in the beamforming map is called the mainlobe and the secondary lobes are called sidelobes. The mainlobe of a beamformer corresponds to the direction in which a given array is steered and indicates the ability of the array to locate a source. In comparison to

the mainlobe, the sidelobe magnitudes are lower and indicate an array's ability to filter out spurious signals, i.e., undesirable signals propagating from other directions. The dynamic range of an array is the difference (in dB) between the mainlobe and the highest sidelobe [1], so that the smaller the sidelobe magnitude the greater the dynamic range.

The delay and sum beamforming technique is the method applied in this thesis. The basic theory of the method and details of its application are described below.

2.1 Basic theory of Delay and Sum Beamforming (DSB)

The delay and sum beamforming (DSB) or conventional beamforming technique has been used since the second World War [2, 11]. The basic principle behind the technique is that when an acoustic source signal is detected by an array of microphones, the signal arrives at each microphone with a specific time delay that depends upon the relative position of the microphones with respect to the reference microphone. The various time delays in the array are compensated by appropriate times and the outputs of all the microphones are summed so as to yield a single output signal from the array. This process is called delay and sum beamforming [6]. It is also referred to as data independent beamforming because any weights applied to the beamformer do not depend upon the array input data [12].

Consider an array of N microphones $\{n\}$, n=1, 2 ...N and a signal $s(t)$, where t is time, emanating from a source, as shown in Figure 2.2.

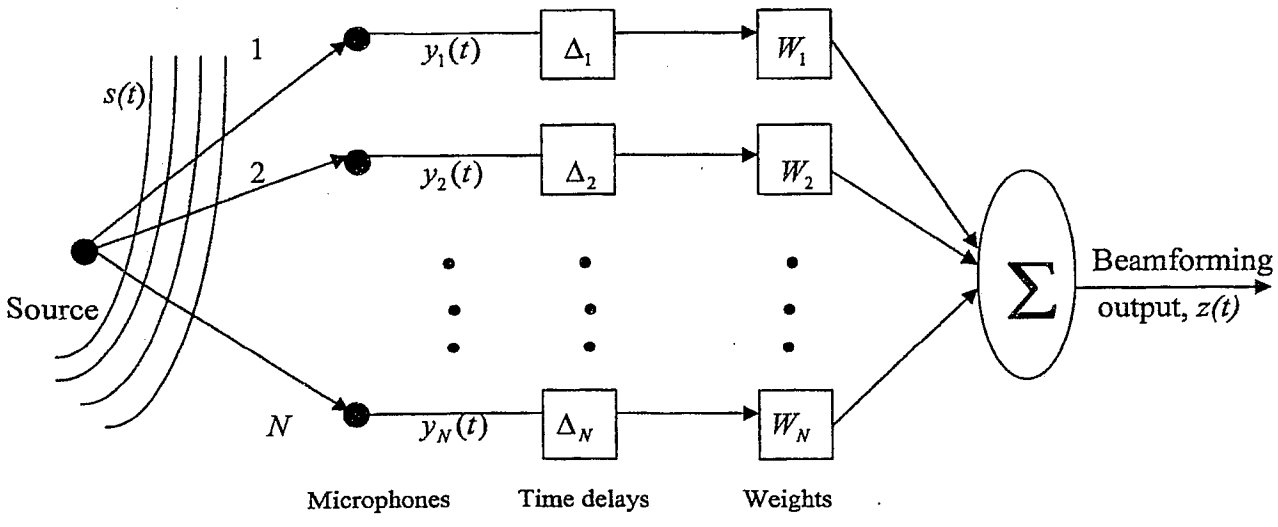

Figure 2.2: Depiction of delay and sum beamforming

The signal measured by the nth microphone is denoted as $y_n(t)$. The signal from the source reaches the microphones at different times because the speed of sound is finite and travels different distances to reach the different microphones. Let $\{\Delta_n\}$, n=1, 2, 3....N, denote the time delays for the various microphones.

In DSB, time delays $\{\Delta_n\}$ and weights $\{W_n\}$ are applied to the microphone signals for a near-field source [18]. The weights serve to compensate for the fact that the wavefront reaching the different microphones is spherical. For a far-field source, only time delays are applied, because the wave front is planar and the weights $\{W_n\}$ are unity. In practice, the time delays and the weights are applied to the incoming signals to steer the array in a direction (with respect to a far field source) or to a location in a grid (with respect to a near field source), and the output of the beamformer, *z(t),* is monitored. This output is:

$$z(t) = \sum_{n=1}^{N} y_n(t - \Delta_n) W_n \tag{2.1}$$

The position of the source corresponds to the steered direction or the location for which the output of the beamformer is maximum [18]. The power associated with the beamformer output signal, *z(t),* can be depicted in a graph (i.e., a beamforming map) showing the mainlobe and sidelobes (see Fig. 2.1). The mainlobe position provides the location of the acoustic source and its height indicates the power of the source. Beamforming can be implemented in the time domain or in the frequency domain. When the time history of an experiment is not of interest, frequency domain beamforming is preferred. It has several benefits over time domain beamforming, viz., reducing sidelobes, narrowing the mainlobe, and reducing statistically independent noise effects [30]. It should be noted that delays in the time domain correspond to phase shifts in the frequency domain; also, in frequency domain beamforming, the Fourier Transform (FT) is applied to, *z(t).* This leads to a complex frequency-domain signal given by:

$$Z(\omega) = FT[z(t)], \tag{2.2}$$

where ω is angular frequency in radians per second.

From equation (2.1), the output of the beamformer in the frequency domain is given by:

$$Z(\omega) = \sum_{n=1}^{N} W_n FT[y_n(t-\Delta_n)]$$

$$= \sum_{n=1}^{N} W_n Y_n(\omega) e(-i\omega\Delta_n) \tag{2.3}$$

where $Y_n(\omega)$ is the Fourier Transform of the input time-domain signal $y_n(t)$, i.e.,

$$Y_n(\omega) = FT[y_n(t)] = \int_{-\infty}^{\infty} y_n(t)\exp(-i\omega t)dt \tag{2.4}$$

It should be noted that if $y_n(t)$ is a *random* (time-domain) signal, and then $Y_n(\omega)$ will also be a *random* (frequency-domain) signal.

Now, the beamformer frequency-domain output signal, $Z(\omega)$, can be expressed in terms of a complex *row* matrix, $[e(\omega)]'$, and a complex *column* matrix, $[Y(\omega)]$, which are given by, respectively:

$$[e(\omega)]' = [W_1\exp(-i\omega\Delta_1), W_2\exp(-i\omega\Delta_2),...,W_N\exp(-i\omega\Delta_N)], \tag{2.5}$$

and

$$[Y(\omega)] = col[Y_1(\omega), Y_2(\omega),...,Y_N(\omega)]. \tag{2.6}$$

From equation (2.5) and (2.6), it follows that:

$$[e(\omega)]'[Y(\omega)] = W_1Y_1(\omega)\exp(-i\omega\Delta_1) + W_2Y_2(\omega)\exp(-i\omega\Delta_2) + ... + W_NY_N(\omega)\exp(-i\omega\Delta_N)$$

$$= \sum_{n=1}^{N} W_nY_n(\omega)\exp(-i\omega\Delta_n),$$

i.e.,

$$Z(\omega) = [e(\omega)]'[Y(\omega)]. \tag{2.7}$$

The Hermitian (complex conjugate) transpose of $[e(\omega)]'$ is a *column* matrix, which is called the *steering vector.*

This is given by:

$$[e(\omega)] = ([e(\omega)]')^* = col[W_1\exp(i\omega\Delta_1), W_2\exp(i\omega\Delta_2),...,W_N\exp(i\omega\Delta_N)], \tag{2.8}$$

where $(.)^*$ denotes the complex conjugate.

For any assumed steering vector, $[e_a(\omega)]$, an apparent array power response, $P_a(\omega)$, can be determined. $P_a(\omega)$ represents the apparent average power associated with the source signal auto spectrum, $G_s(\omega)$, and is given by:

$$P_a(\omega) = [e_a(\omega)]'[G(\omega)][e_a(\omega)]. \tag{2.9}$$

In this expression, $[G(\omega)]$ is an N x N (square) Hermitian matrix called the Cross Spectral Matrix (CSM), which is given by,

$$[G(\omega)] = \begin{bmatrix} G_{11}(\omega)G_{12}(\omega)...G_{1N}(\omega) \\ G_{21}(\omega)G_{22}(\omega)..... \\ . \\ . \\ G_{N1}(\omega).....G_{NN}(\omega) \end{bmatrix}, \omega \geq 0. \tag{2.10}$$

The diagonal elements of the CSM, $\{G_{ii}(\omega)\}; i=1, 2, 3..., N$, are real positive functions of ω and are the auto spectra of the individual microphone signals. The off-diagonal components of the CSM, $\{G_{ij}(\omega)\}, i=1, 2, 3... N, \quad j=1, 2, 3,...., N, i \neq j$, are complex functions of ω and are the cross-spectra of the various pairs of microphone signals; moreover,

$$G_{ji}(\omega) = G_{ij}^*(\omega). \tag{2.11}$$

For stationary random microphone signals, the components of the CSM are defined as [31]:

$$G_{ij}(\omega) = \underset{T\to\infty}{Limit}\left|E\{\tilde{G}_{ij}(\omega;T)\}\right| \tag{2.12}$$

In equation (2.12), T denotes the duration of the signals; $E\{.\}$ denotes the expected value or ensemble average; $\tilde{G}_{ij}(\omega)$ is a "raw" spectrum, which is a random quantity if the microphone signals are random and is given by:

$$\tilde{G}_{ij}(\omega;T) = \frac{2Y_i^*(\omega;T)Y_j(\omega;T)}{T}, \tag{2.13}$$

where $Y_n(\omega;T)$ is the *finite* Fourier Transform of $y_n(t)$, i.e.,

$$Y_n(\omega;T) = \int_0^T y_n(t)\exp(-i\omega t)dt. \tag{2.14}$$

It should be noted that the CSM is twice the Fourier Transform of the cross-correlation matrix (CCM) of the microphone signals [31], i.e.,

$$[G(\omega)] = 2FT[[R(\tau)]]. \tag{2.15}$$

The CCM is given by [31]:

$$[R(\tau)] = \begin{bmatrix} R_{11}(\tau)R_{12}(\tau)...R_{1N_k}(\tau) \\ R_{21}(\tau)R_{22}(\tau)..... \\ . \\ . \\ R_{N1}.....R_{NN}(\tau) \end{bmatrix}, -\infty < \tau < \infty, \tag{2.16}$$

where τ denotes a time lag.

The diagonal elements of the CCM, $\{R_{ii}(\tau)\}$, i=1, 2, 3..., N are real even functions of τ and are the auto correlation functions of the individual microphone signals. The off-diagonal elements of the CCM, $\{R_{ij}(\tau)\}$, i=1, 2, 3..., N, j=1, 2, 3, ..., N. $i \neq j$, are real functions of τ that are neither even nor odd and are the cross-correlation functions of the various pairs of microphone signals; moreover,

$$R_{ji}(\tau) = R_{ij}(-\tau). \tag{2.17}$$

The components of the CCM are given by [31]:

$$R_{ij}(\tau) = \underset{T\to\infty}{Limit} \frac{1}{T} \int_{t_o}^{t_o+T} y_i(t) y_j(t+\tau) dt, \tag{2.18}$$

where t_o is an arbitrary starting time.

The auto spectrum of the source signal, $s(t)$, is defined as [31]:

$$G_s(\omega) = \underset{T\to\infty}{Limit}\ E\{\tilde{G}_s(\omega;T)\} = 2FT[R_s(\tau)], \omega \geq 0. \tag{2.19}$$

In equation (2.19), $\tilde{G}_s(\omega;T)$ is a "raw"autospectrum given by:

$$\tilde{G}_s(\omega;T) = \frac{2S^*(\omega;T)S(\omega;T)}{T}, \tag{2.20}$$

where $S(\omega;T)$ is the *finite* Fourier Transform of the source signal $s(t)$, i.e.,

$$S(\omega;T) = \int_0^T S(t)\exp(-i\omega t)dt; \tag{2.21}$$

and $R_s(\tau)$ is the autocorrelation function of $s(t)$, i.e.,

$$R_s(\tau) = \text{limit}\ \frac{1}{T}\int_{t_o}^{t_o+T} s(t)s(t+\tau)dt. \tag{2.22}$$

In practice, T is finite, $E\{.\}$ is approximated by frequency-domain (block) averaging and the components of the CSM are estimated as follows [31]:

$$G_{ij}(\omega) \cong \hat{G}_{ij}(\omega) = \left(\frac{1}{L}\right)\sum_{l=1}^{L}\{\tilde{G}_{ij}(\omega,T_l)\}_l \tag{2.23}$$

where L denotes a (large) number (>>1) of non-overlapping segments of the various microphone signals. These segments are referred to as blocks, and the duration of each block is given by:

$$T_l = \frac{T}{L}. \tag{2.24}$$

It may be remarked that, in the case of an acoustic source that produces a periodic (harmonic) signal, which is a deterministic (as opposed to a random) quantity,

$$G_{ij}(\omega) \cong \tilde{G}_{ij}(\omega,T), \tag{2.25}$$

where T is the period or an integer multiple of the period of the microphone signals; hence, block averaging is not really required.

Now, for any assumed location of an acoustic source, with the corresponding steering vector determined by means of equation (2.8), the apparent array power response can be determined by equation (2.9). Moreover, if the assumed source location is the *actual* location of the source, then the apparent array power response will be a maximum (for any relevant frequency). Thus, the acoustic source location and, in the absence of extraneous noise, the auto spectrum of the signal generated by the source can be determined by computing $P_a(\omega)$ for a range of assumed source locations and finding the maximum value(s) of $P_a(\omega)$. When the steering vector corresponds to the actual location of the acoustic source, and extraneous noise is absent, the array power response is related to the autospectrum of the source signal as follows:

$$P(\omega) = N^2 G_s(\omega). \tag{2.26}$$

To provide insight into the DSB technique, the above relationship, equation (2.26), is established for a noise-free uniform linear array and a far field acoustic source that lies in the plane of the array and is located at an angle θ with respect to the array, as depicted in Figure 2.3. In this case, with microphone 1 taken as the reference sensor, $\Delta_1 = 0$ and,

$$y_1(t) = s(t), \tag{2.27}$$

where, $s(t)$ is the source signal, which can be either a stationary random signal or a deterministic periodic signal; also, the array weights are all unity.

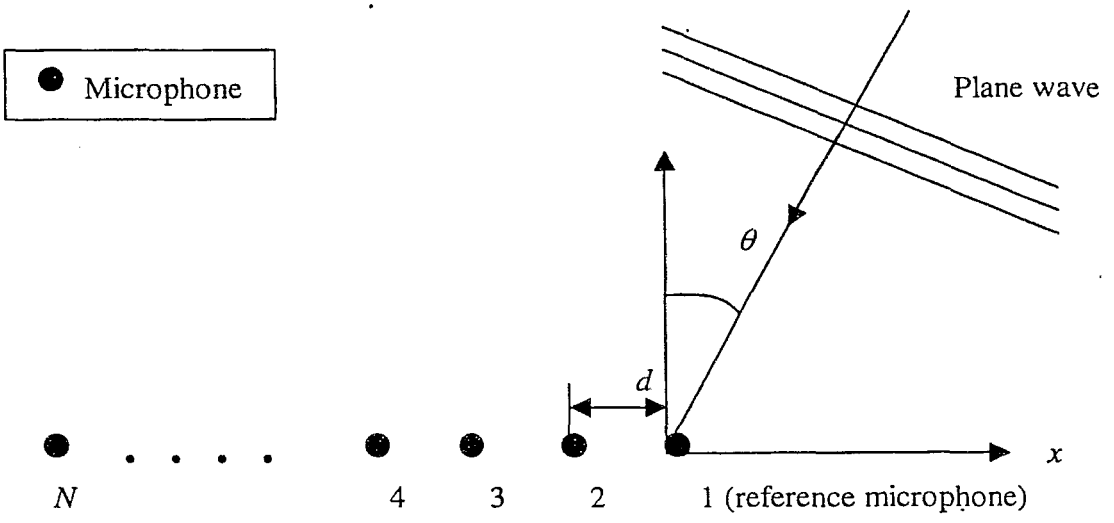

Figure 2.3: Uniform Linear Array (ULA) with a far field source.

Hence, the diagonal elements of the CCM are given by:

$$R_{ii}(\tau) = R_s(\tau), \qquad i=1, 2, 3\ldots N, \tag{2.28}$$

and the off-diagonal elements of the CCM are given by:

$$R_{ii+1}(\tau) = R_s(\tau - \Delta_2), \qquad i=1, 2, 3\ldots N\text{-}1, \tag{2.29}$$

$$R_{ii+2}(\tau) = R_s(\tau - \Delta_3), \qquad i=1, 2, 3\ldots N\text{-}2, \tag{2.30}$$

$$\vdots$$

$$R_{ii+N}(\tau) = R_s(\tau - \Delta_N) \tag{2.31}$$

Moreover, the elements of the CSM are as follows:

$$G_{ii}(\omega) = 2FT[R_{ii}(\tau)]$$
$$= 2\,FT[R_s(\tau)]$$
$$= G_s(\omega), \qquad i=1, 2, 3\ldots N, \tag{2.32}$$

$$G_{ii+1}(\omega) = FT[R_{ii+1}(\tau)]$$
$$= FT[R_s(\tau-\Delta_2)]$$
$$= FT[R_s(\tau)]\exp(-i\omega\Delta_2)$$
$$= G_s(\omega)\exp(-i\omega\Delta_2), \qquad i=1, 2, 3\ldots N\text{-}1, \tag{2.33}$$

Similarly,

$$G_{ii+2}(\omega) = G_s(\omega)\exp(-i\omega\Delta_3), \qquad i=1, 2, 3\ldots N\text{-}2, \tag{2.34}$$

$$\vdots$$

$$G_{1N}(\omega) = G_s(\omega)\exp(-i\omega\Delta_N), \tag{2.35}$$

The corresponding steering vector is given by:

$$[e(\omega)] = col[1, \exp(i\omega\Delta_2), \exp(i\omega\Delta_3), \cdots, \exp(i\omega\Delta_N)]. \tag{2.36}$$

From equations (2.10) and (2.11), with the dependence on ω of the various quantities omitted for convenience, the resulting array power response is:

$$P = [e]'[G][e]$$
$$= [e]'\begin{bmatrix} G_{11}G_{12}\ldots G_{1N} \\ G_{21}G_{22}\ldots\ldots \\ . \\ . \\ G_{N1}\ldots.G_{NN} \end{bmatrix}\begin{bmatrix} 1 \\ \exp(i\omega\Delta_2) \\ . \\ . \\ . \\ \exp(i\omega\Delta_N) \end{bmatrix}$$

$$P = [1, \exp(-i\omega\Delta_2), \cdots, \exp(-i\omega\Delta_N)]\begin{bmatrix} G_{11} + G_{12}\exp(i\omega\Delta_2) + \ldots + G_{1N}\ \exp(i\omega\Delta_N) \\ G_{21} + G_{22}\exp(i\omega\Delta_2) + \ldots + G_{2N}\exp(i\omega\Delta_N) \\ . \\ . \\ G_{N1} + G_{N2}\exp(i\omega\Delta_2) + \ldots + G_{NN}\exp(i\omega\Delta_N) \end{bmatrix}. \tag{2.37}$$

Since the spacing between adjacent microphones is constant, $\Delta_k = (k-1)\Delta_2, k = 1,2,3,\cdots,N-1$.

Hence,

$$P = G_{11} + G_{12}\exp(i\omega\Delta_2) + \cdots + G_{1N}\exp(i\omega\Delta_N)\ \{N\ terms\}$$
$$+ G_{21}\exp(-i\omega\Delta_2) + G_{22} + \cdots + G_{2N}\exp(i\omega\Delta_{N-1})\ \{N\ terms\}$$
$$\vdots$$
$$+ G_{N1}\exp(-i\omega\Delta_N) + G_{N2}\exp(-i\omega\Delta_{N-1}) + \cdots + G_{NN}\ \{N\ terms\} \quad (2.38)$$

Now,

$$G_{11} = G_s \quad (2.39)$$
$$G_{12}\exp(i\omega\Delta_2) = G_s\exp(-i\omega\Delta_2)\exp(i\omega\Delta_2) = G_s \quad (2.40)$$
$$\vdots$$
$$G_{1N}\exp(i\omega\Delta_N) = G_s\exp(-i\omega\Delta_N)\exp(i\omega\Delta_N) = G_s \quad (2.41)$$

$$G_{21}\exp(i\omega\Delta_2) = G_{12}^{*}\exp(-i\omega\Delta_N) = G_s \quad (2.42)$$
$$G_{22} = G_s \quad (2.43)$$
$$\vdots$$
$$G_{2N}\exp(i\omega\Delta_{N-1}) = G_s\exp(-i\omega\Delta_{N-1})\exp(i\omega\Delta_{N-1}) = G_s \quad (2.44)$$
$$G_{N1}\exp(-i\omega\Delta_N) = G_{1N}^{*}\exp(-i\omega\Delta_N) = G_s \quad (2.45)$$
$$G_{N2}\exp(-i\omega\Delta_{N-1}) = G_{2N}^{*}\exp(-i\omega\Delta_{N-1}) = G_s \quad (2.46)$$
$$\vdots$$
$$G_{NN} = G_s. \quad (2.47)$$

Thus, the array power response is given by:

$$P(\omega) = N[G_s(\omega) + G_s(\omega) + \bullet\bullet\bullet + G_s(\omega)]\ \{N\ terms\}$$
$$= N^2 G_s(\omega). \quad (2.48)$$

It should be noted that the CSM captures all relative magnitude and phase relations pertaining to the various pairs of microphones in an array. It therefore contains all of the information required to determine the source location and, in the absence of extraneous noise,

the autospectrum of the source signal [30]. Accordingly, the CSM needs to be computed only *once.*

In practice, the time data collected at each microphone are digitized to form digital time series, and the Fast Fourier Transform (FFT) is applied to the time series.

2.2 Digital data collection and post-processing procedure

Modern beamforming systems exploit the advantage of digital implementation [2]. The pressure signals measured by the microphones in the array are first transformed to analogue voltage signals, $y_n(t)$, (within the microphones). These microphone signals are then digitized with a time spacing of $\Delta t = 1/SR$ between sampled points, where SR is the sampling rate and denotes the number of points per second. Each digitized signal is segmented into L non-overlapping blocks, each of duration T_l, such that

$$T_l = M\Delta t \tag{2.49}$$

where M = number of sampled points per block in time T_l. For application of the FFT, M must be a multiple of 2 (e.g., 512, 1024, etc.).

Two key aspects that must be considered during data collection in order to avoid ambiguous (incorrect) beamforming results are spatial aliasing and temporal aliasing.

2.2.1 Spatial aliasing

Spatial aliasing pertains to the physical deployment of the microphones in an array, i.e., the spacing between microphones. If the spacing is not consistent with the Shannon criterion, grating lobes will appear in the beamforming map and there will be ambiguity in distinguishing between the actual source (represented by the main lobe) and false sources (represented by the grating lobes), as shown in Figure 2.4 (a), for which there is no ambiguity, and 2.4 (b), for which there is ambiguity.

The Shannon criterion is given by:

$$d \leq \frac{\lambda_{\min}}{2}, \tag{2.50}$$

where d is the distance between adjacent microphones and $\lambda_{\min}$ is the minimum wavelength of

the acoustic signal, which is related to the highest frequency present in the signal, f_{max}, as follows:

$$\lambda_{min} = \frac{c}{f_{max}}. \tag{2.51}$$

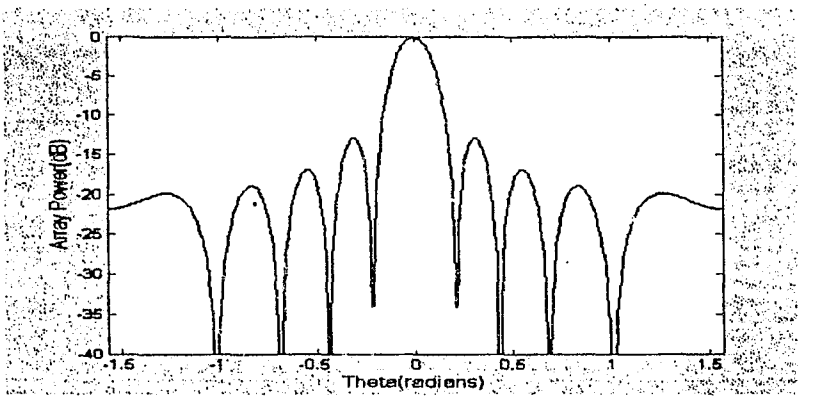

Figure 2.4 (a): Beamforming map for 10 microphones in a linear array with $d = \lambda_{min}/2$

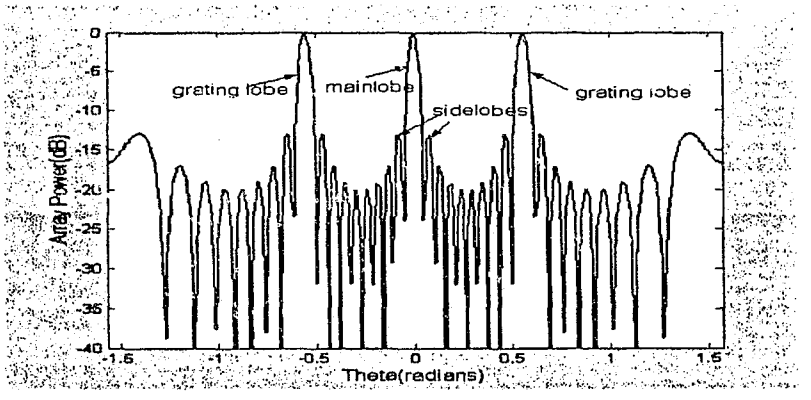

Figure 2.4 (b): Beamforming map for 10 microphones in a linear array with $d = 2\lambda_{min}$

2.2.2 Temporal aliasing

Temporal aliasing pertains to the sampling of a signal, i.e., the conversion of an analogue signal into a time series. If the sampling rate is not consistent with the Nyquist criterion, high frequency components of a signal will impersonate low frequency components and the calculated spectrum of the signal will be erroneous, as depicted in Figure 2.5 (a), for which there is no aliasing, and 2.5 (b), for which there is aliasing, i.e., high frequency information (at 500 Hz) appears at a lower frequency (at 300 Hz).

To avoid temporal aliasing, the sampling rate, SR (or f_s) must satisfy the Nyquist criterion, viz.,

$$SR \geq 2 f_{max}, \tag{2.52}$$

where f_{max} is the highest frequency present in the signal.

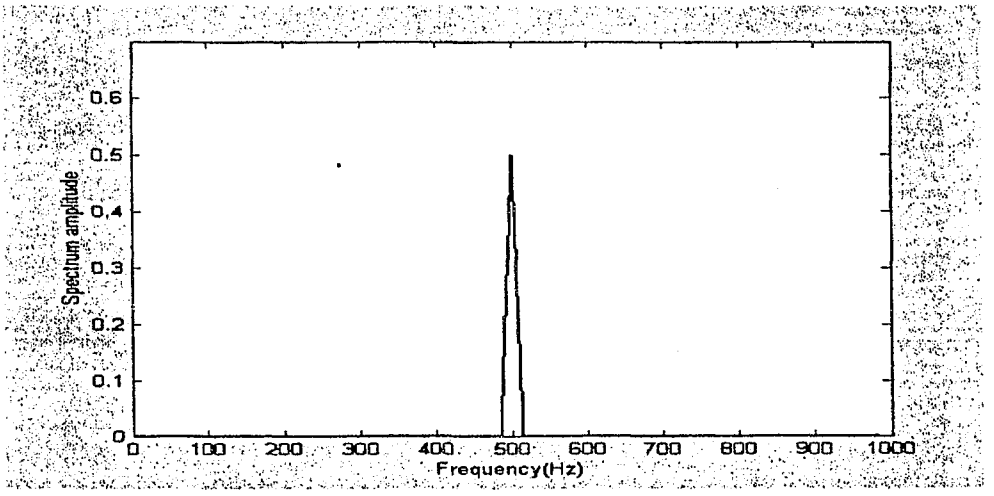

Figure 2.5 (a): Spectrum obtained with $SR > 2f_{max}$.

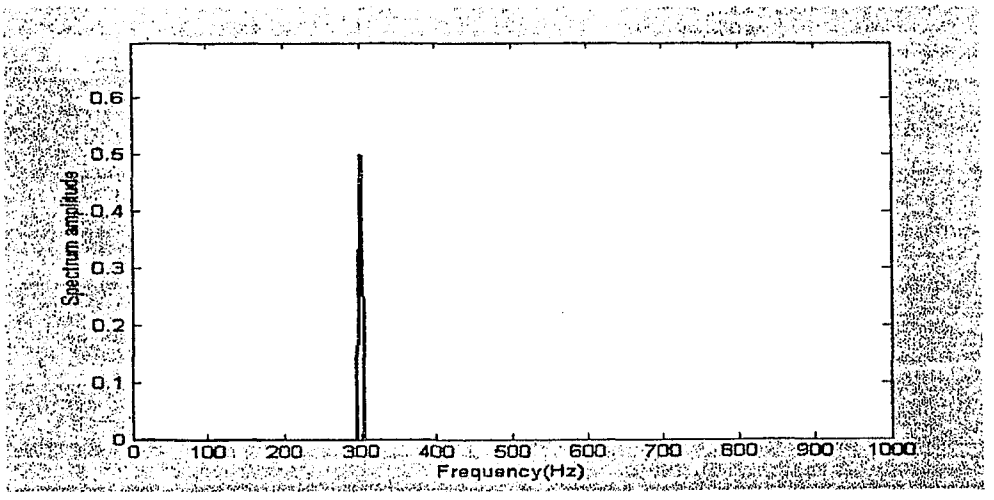

Figure 2.5 (b): Spectrum obtained with $SR < 2f_{max}$.

In practice, an analog to digital (A/D) converter is used to convert the analog signal into digital signals, and the data are stored for post processing.

2.2.3 Data post-processing procedure

The post processing starts with the conversion of the raw voltage data from each microphone (channel) into pressure data via the microphone sensitivity. This is followed by the computation of the cross spectral matrix (CSM) [see section 2.1 for details], which is obtained via the Fast Fourier transform (FFT). Note that the use of an appropriate time window with the FFT can improve the accuracy of the pressure spectrum by reducing temporal leakage [2].

2.2.3.1 Cross spectral matrix (CSM)

Consider an array of N microphones producing analogue signals $y_1(t)$, $y_2(t)$,... $y_N(t)$. The corresponding digital signals are denoted by $y_1[m]$, $y_2[m]$,... $y_N[m]$, where $m = t/\Delta t = 0, 1, 2, \ldots ML$.

With respect to the nth microphone, for each block of data, the frequency-domain data are obtained via the FFT of $Y_n[k]$, which is defined as follows:

$$Y_n[k] = \sum_{m=0}^{M-1} y_n[m] \exp.\{(\frac{-i2\pi km}{M})\} \tag{2.53}$$

where $k = 0, 1, 2 \ldots (M-1)/2$.

These data are assigned to frequency bins given by:

$$f_k = k\Delta f, \tag{2.54}$$

where Δf is the frequency resolution defined as:

$$\Delta f = \frac{1}{T} = \frac{1}{M\Delta t} = \frac{SR}{M} \text{ (Hz)} \tag{2.55}$$

Note that there are $(M/2) + 1$ frequencies bins.

From equation (2.13), each term of the CSM (based on one block of data) for microphones i and j at frequency f_k is calculated as:

$$G_{ij_k} = \Delta f \tilde{G}_{ij_k} = \left(\frac{2}{M^2}\right)\left[Y_i^*[k]Y_j[k]\right] \tag{2.56}$$

where $(\cdot)^*$ denotes the complex conjugate, $i = 1,2,\ldots,N$, $j = 1,2,\ldots,N$, and M is the number of data points per block.

Thus, the N x N CSM at frequency f_k (or at kth frequency bin) is given as:

$$[G]_k = \begin{bmatrix} G_{11_k} G_{12_k} \ldots\ldots\ldots\ldots\ldots\ldots G_{1N_k} \\ G_{21_k} G_{22_k} \ldots\ldots\ldots\ldots\ldots\ldots \\ \\ \ldots\ldots\ldots\ldots\ldots\ldots\ldots\ldots G_{NN_k} \end{bmatrix} \tag{2.57}$$

As mentioned in section 2.1, the diagonal elements of this matrix represent the autospectra of the individual microphone signals. The off-diagonal elements represent the cross-spectra of pairs of microphone signals. Note that the lower triangular elements can be calculated by taking the complex conjugates of the upper triangular elements because the CSM is a Hermitian matrix.

Again as mentioned in section 2.1, the CSM captures all relative magnitude and phase relations between pairs of microphone signals and therefore encapsulates all of the information needed to compute the source location [30]. The procedure for generating the CSM with any array geometry remains the same for both near-field and far-field source locations.

In general, extraneous noise will be present and the source signal may be random in nature. Consequently, frequency domain averaging, i.e., averaging several blocks (L) of frequency-domain data, must be used [30]. In this case, each term of the CSM for microphones i and j at the kth frequency bin is given as [see equation (2.23)]:

$$\hat{G}_{ij_k} = \left(\frac{2}{LM^2} \right) \sum_{l=1}^{L} \left[Y_{il}^{*}[k] Y_{jl}[k] \right] \tag{2.58}$$

The corresponding N x N CSM is given by:

$$[\hat{G}]_k = \begin{bmatrix} \hat{G}_{11_k} \hat{G}_{12_k} \ldots\ldots\ldots\ldots\ldots\ldots \hat{G}_{1N_k} \\ \hat{G}_{21_k} \hat{G}_{22_k} \ldots\ldots\ldots\ldots\ldots\ldots \\ \\ \ldots\ldots\ldots\ldots\ldots\ldots\ldots\ldots \hat{G}_{NN_k} \end{bmatrix} \tag{2.59}$$

It should be noted that if the microphones are affected by stastically independent noise, then such noise can be reduced by frequency-domain averaging, as will be demonstrated by the simulation results in Chapter 3.

2.2.3.2 Steering vector and Array Power

The digital output of the beamformer in the frequency-domain for the *kth* frequency bin [corresponding to equation (2.2)] is given as:

$$Z[k] = \sum_{n=1}^{N} W_n Y_n[k] \exp.(-i\omega\Delta_n) \tag{2.60}$$

From equation (2.8),

$$Z[k] = e'_k [Y]_k \tag{2.61}$$

where (.)' represents the Hermitian transpose and e_k denotes a column "steering vector". This vector contains the weights and the phase shifts applied to the individual microphones to steer the array towards the acoustic source and is given as:

$$e_k = col[W_1 \exp.(-i\omega_k\Delta_1), W_2 \exp.(-i\omega_k\Delta_2), ..., W_N \exp.(-i\omega_k\Delta_N)] \tag{2.62}$$

where $[W_1, W_2, ...W_N]$ represent the weights and $[\Delta_1, \Delta_2, ...\Delta_N]$ represent the time delays for the various microphones.

For a far field beamformer, the weights are '1' for each microphone because the wavefront is planar. But, for a near field beamformer, with the wave front being spherical, a different weight is assigned to each microphone to compensate for the geometric attenuation of radially propagating waves. For the nth microphone, the weight is given as [30]:

$$W_n = \frac{r_n}{r} \tag{2.63}$$

where, r_n is the distance of the nth microphone from the acoustic source, and r is the distance between the array center and the acoustic source.

An additional optional weighting process, called shading or tapering [32], can be applied to reduce the effect of side lobes. (The various types of shading are Triangular, Hanning, Hamming, Dolph-Chebyshev etc.). This process results in a trade-off between the main lobe width and the side lobe level [18, 32].

The array power for the kth frequency bin, which depends on the steering vector, is given by [30]:

$$\hat{P}_k = \frac{e^{'}{}_k [\hat{G}]_k e_k}{N^2} \tag{2.64}$$

Plotting the array power values versus possible source locations yields the beamforming map (as mentioned in section 2.0). The maximum array power value corresponds to the source location. In the absence of noise, this maximum value is the value of the spectrum of the source signal at frequency f_k. Thus, both the location of the source and the power spectrum of the source signal can be estimated by means of the DSB technique.

A MATLAB code, developed at Ryerson University, for implementing the DSB technique using simulation and experimental data is given in Appendix A. Validation of the MATLAB code is discussed in Appendix B.

2.3 Array geometries

Different microphone array geometries are used in beamforming. The most common geometries are as follows:

- Uniform Linear Array (ULA).
- Uniform Planar Array (UPA).
- Random Array.

The different geometries are discussed below.

2.3.1 Uniform Linear Array (ULA)

When the microphones in an array are arranged in a line with a constant distance "*d*" between each other the array is called a uniform linear array (ULA). For a far field source, with an acoustic source lying in the plane of the array, a plane wave reaches the microphones, and the signal generated by the source has a DOA of θ radians, as depicted in Figure 2.3.

2.3.2 Uniform Planar Array (UPA)

When the microphones in an array are arranged within a plane (e.g., the *x*-*y* plane) in a regular pattern, the array is referred to as a uniform planar array (UPA). For a far field source, with the source *not* lying in the plane of the array, a plane wave reaches the microphones, and the DOA of the source signal is defined by two different angles, viz., the angle of elevation, φ,

and the angle of azimuth, θ, as depicted in Figure 2.6. It should be noted that, in this case, the use of a uniform linear array can provide only partial information, viz., θ, whereas the use of a uniform planar array provides both θ and φ [33].

Depending on the specific geometric pattern of the microphones, the UPA is classified as a uniform rectangular, square, cross, or circular array. Two specific type of the UPA are described below.

2.3.2.1 Uniform Rectangular Array (URA)

When the microphones are placed in a rectangular grid in an x-y plane such that the uniform inter-microphone distance along the x-axis is d_1 and along the y-axis is d_2, the array is called a uniform rectangular array. Such an array with a far field source is shown in Figure 2.6. When the microphones are placed at a uniform distance in a square grid in the x-y plane, the array is called a uniform square array and $d_1 = d_2 = d$. It is a special case of the rectangular array.

2.3.2.2 Uniform Circular Array (UCA)

When the microphones are placed on the circumference of a circle with radius "a", as shown in Figure 2.7, the resulting array is called a uniform circular array (UCA) [33].

2.3.3 Random Array

When the microphones are placed in a random fashion to break the regularities of uniform planar arrays, the resulting array is called an irregular or aperiodic or random array [1]. A random array with a far field source is shown in Figure 2.8.

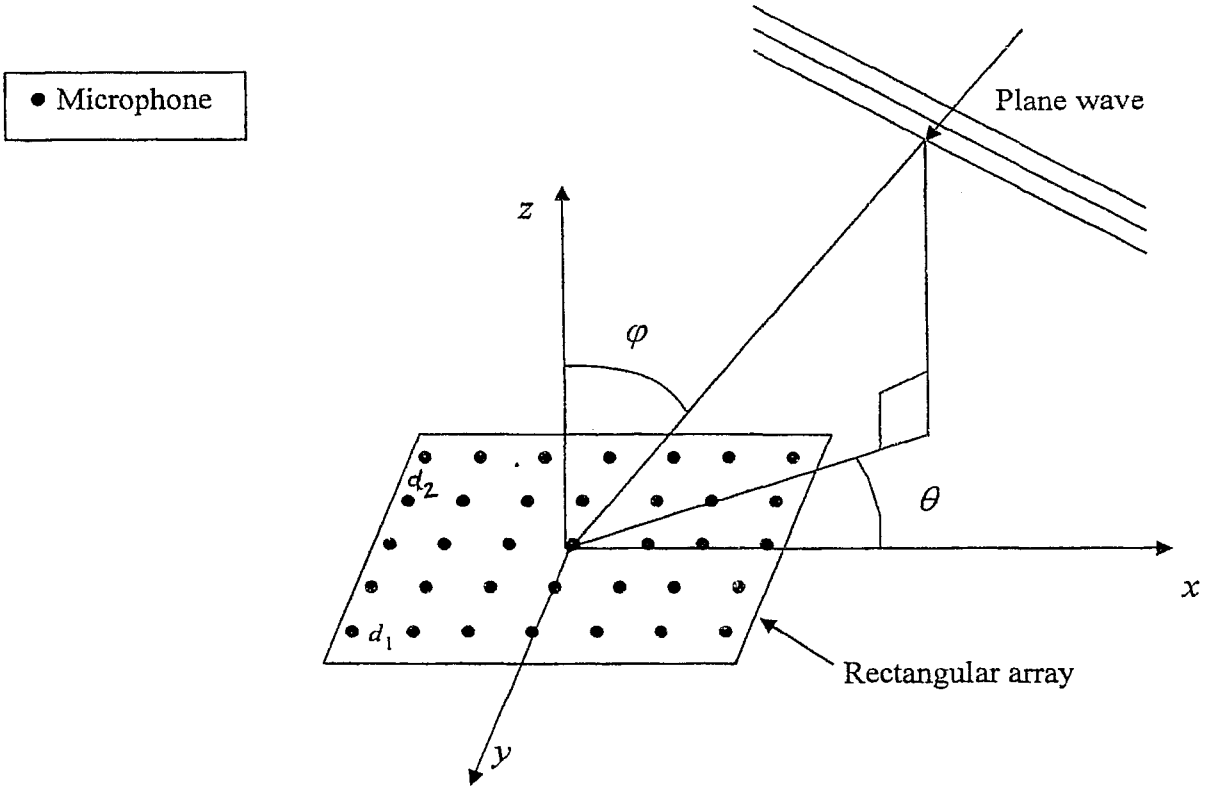

Figure 2.6: Uniform Rectangular Array (URA) with a far field source.

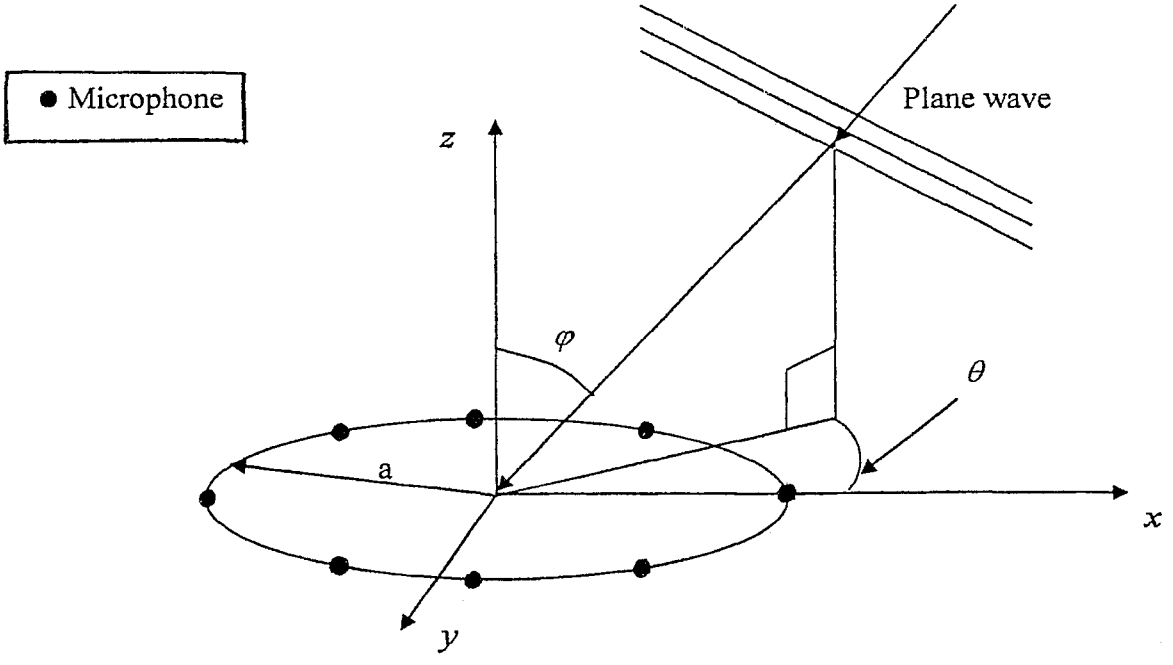

Figure 2.7: Uniform Circular array (UCA) with a far field source.

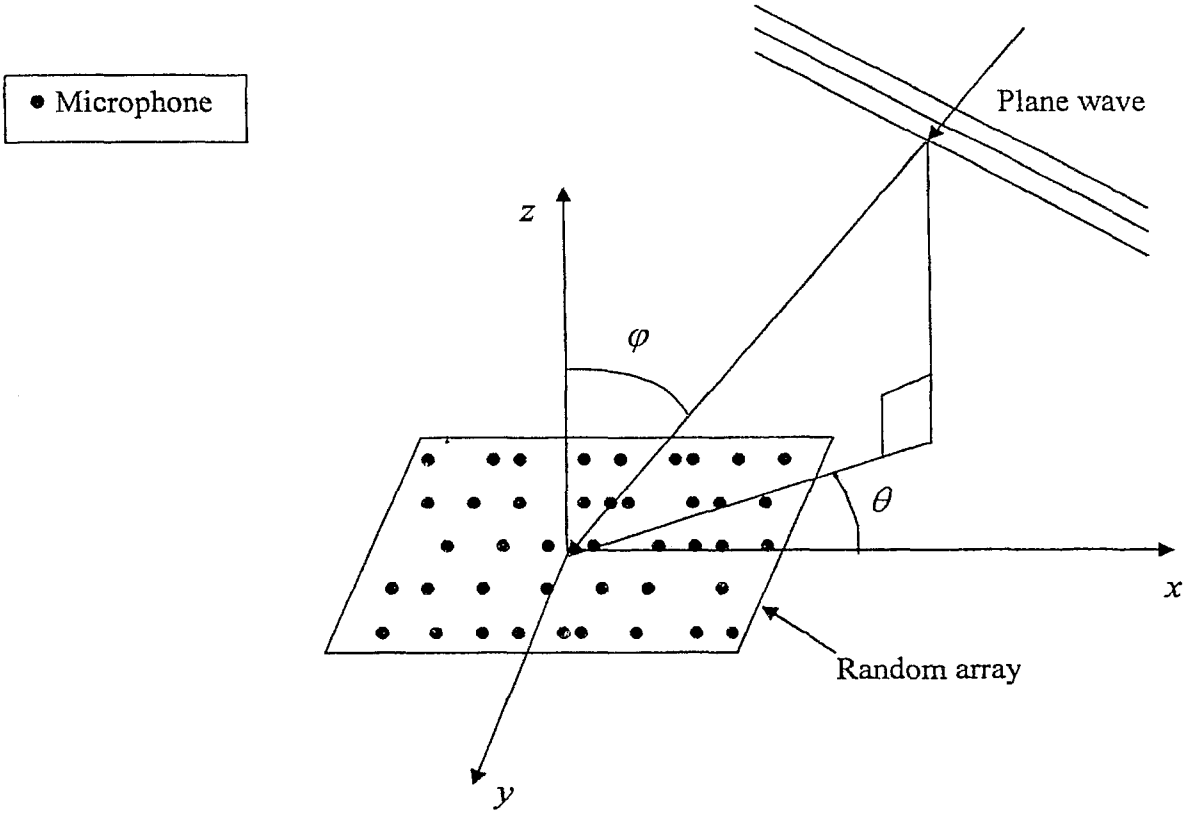

Figure 2.8: Random array with a far field source.

Chapter 3
Sensitivity analysis-simulation data

3.0 Introduction

The present chapter focuses on the sensitivity analysis of the beamforming technique using simulation data. This analysis investigates the impact of various parameters, such as, the number of microphones (N), the frequency of the signal (f), and the number of data blocks (L). Different array geometries, viz., a uniform linear array (ULA), a uniform planar array (UPA), and a spiral array, are included in the analysis.

The purposes of the beamforming technique are the localization of acoustic sources and the determination of their sound level spectra. The beamforming map, which is a plot of the array power, provides the necessary information about the source location. As mentioned in section 2.0, the primary lobe in the beamforming map is called the mainlobe and the secondary lobes are called sidelobes. It should be noted that the position of the mainlobe within the map corresponds to the source location and the height of the mainlobe corresponds to the source power. The performance of a microphone array is measured by using the following two beamforming evaluators: the array resolution and the height of the sidelobes of a beamforming map. These two evaluators are discussed below.

Array resolution

The array resolution defines the capability of an array to localize an acoustic source and is determined by the mainlobe width measured at a point which is –3 dB below the peak of the mainlobe. This width is called the beamwidth (BW), and the array resolution is defined as:

$$\text{Array resolution} = 1/\ (BW\ ) \tag{3.1}$$

Clearly, the array resolution will increase when the beamwidth becomes narrow, and the source can be pinpointed easily, as shown in Figure 3.1. In this Figure, the BW decreases from 0.21 radians to 0.021 radians for an increase of N from 10 to 80.

An optimum array design is one with as small a BW value as possible. In addition, the 'goodness' of the resolution can be expressed in terms of an error band for source localization defined as,

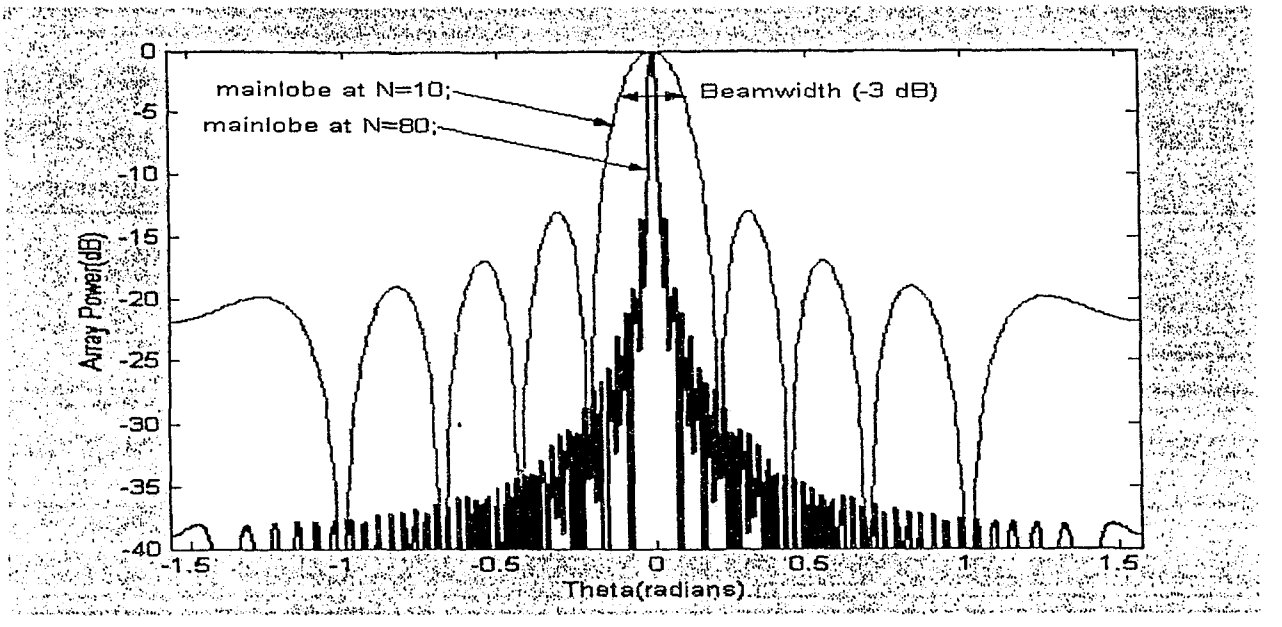

Figure 3.1: Array resolution for N=10 and N=80.

$$\text{Error band} = \pm \tfrac{1}{2} (BW) \tag{3.2}$$

Sidelobes

The sidelobes indicate the ability of an array to filter out signals propagating from directions other than the direction of the desired signal [1]. Generally, the level of the highest sidelobe is measured. The difference between the mainlobe and the highest sidelobe is called the dynamic range, as shown in Figure 2.1, and should be at least 10 dB for accurate localization. If the sidelobes are high, the acoustic source can not be localized easily. In other words, the sidelobe level should be as low as possible to improve the array's capability to localize an acoustic source.

Array resolution and sidelobes are the *central focus* for the sensitivity analysis.

3.1 Simulation details

In order to simulate the pressure signals, $y_n(t)$, $n = 1, 2, 3, \ldots, N$, received by any array of N microphones, as depicted in Figure 2.2, digital versions of the following equations, which are based on equations (1.6) and (1.11), were used:

$$y_n(t) = A \sin \omega t \tag{3.3}$$

in the case of a far-field source, and

$$y_n(r_n,t) = \left(\frac{A}{r_n}\right)\sin\left[\omega(t-\frac{r_n}{c}\right] \tag{3.4}$$

in the case of a near field source, where r_n is the distance between the acoustic source and the *nth* microphone.

The digital data collected by the microphone array were stored for post-processing, as discussed in section 2.2.3, and the MATLAB code was applied for the sensitivity analysis (see Appendix A).

3.2 Uniform Linear Array - far field beamforming

The basic microphone array geometry is a uniform linear array (ULA) (see Figure 2.3). Moreover, if the source is far from the array, then a plane wave reaches the microphone array at an angle θ. In the present case, the ULA was designed for far field simulated signals with a maximum frequency of 8000 Hz. The inter-microphone distance was, therefore, set at 2 cm to satisfy Shannon's theorem. The plane wave, $A\sin\omega t$, was generated at each microphone location, with the appropriate delay. It should be noted that each block of data contained 1024 points, i.e., M=1024, and yielded 513 (M/2+1) frequency bins. For each of these bins, the beamforming map was obtained by calculating steering vectors for various assumed source locations ranging from $-\pi/2$ radians to $\pi/2$ radians. The source signal spectrum was determined from the maximum values of the beamforming maps in the various frequency bins.

The following parameters were chosen for the analysis of ULA - far field beamforming:

- Number of microphones ($N \rightarrow 2$ to 50).
- Signal frequency ($f \rightarrow 500$ to 8000 Hz).
- Integer and non-integer number of cycles and time windows.
- Inter-microphone distance (d).
- Source position.
- Multiple frequencies.
- Number of number of data blocks (L) without noise.
- Noise with a single block of data.
- Noise with several (L) blocks of data.

3.2.1 Effect of number of microphones (N)

The number of microphones changes the aperture of an array, which is defined as $D=Nd$. As the number of microphones increases, the acoustic field fluctuations can be measured at more spatial positions and the beamforming results can be improved. To investigate this aspect, the plane wave signal was generated at a frequency of 4500 Hz, with $\theta = 0$ radians, an inter-microphone spacing of 2 cm and an integer number of cycles. The number of microphones (N) was varied from 2 to 50.

The beamforming results are presented in Figure 3.2 (a) and (b) for N=2 and N=50. Figure 3.2(a) shows the array power as a function of the DOA, and Figure 3.2 (b) shows the sound pressure level (SPL) spectrum. The beamwidth and the dynamic range were obtained from the various beamforming maps. The beamwidth, array resolution, the error band and the dynamic range are summarized in Table 3.1, and a plot of the array resolution versus number of microphones is presented in Figure 3.3.

The poor quality in source localization is evident from Figure 3.2 (a) when the array aperture is small (N=2). Moreover, the error band of ± 1.375 radians (corresponding to about ± 44 % with respect to the DOA range of π radians) is relatively large (see Table 3.1). Although the source localization capability is inadequate in this case, the frequency resolution with respect to the SPL spectrum is excellent [Figure 3.2(b)]. It should be noted that this resolution is independent of N.

As one increases the size of the aperture, i.e., the number of microphones, the results clearly show that the localization capability of the beamforming technique improves progressively and is quite satisfactory for N=50. It should be pointed out, however, that the simulation signals are generated with "optimum" values for the other relevant parameters, such as the inter-microphone spacing (d), source frequency and source position.

Figure 3.3 shows the improvement in array resolution as a function of number of microphones. It can be seen that the resolution increases linearly with N. Table 3.1 shows that the error band decreases rapidly as N increases, for this simple case (with "optimum" values for relevant parameters). It is seen that a relatively small array size, as small as 5 microphones, provides an acceptable error band of ± 0.375 radians (corresponding to about ± 12 %) for source localization and an array dynamic range of 13 dB, which remains constant for $N \geq 5$.

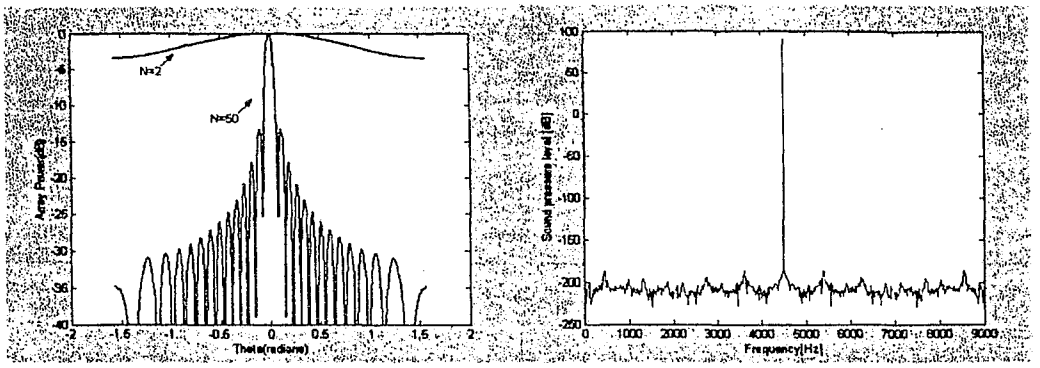

(a) (b)

Figure 3.2: Beamforming results, for N=2 & 50, f =4500 Hz; (a) Array power plot (b) SPL spectrum.

Table 3.1 Effect of number of microphones

Number of Microphones (N)	Beamwidth (radians)	Resolution (1/radians)	Error band (radians)	Dynamic range (dB)
2	2.75	0.3636	±1.375	N.A.⊕
3	1.37	0.7272	± 0.687	N.A.
5	0.75	1.333	± 0.375	13
9	0.37	2.670	± 0.187	13
17	0.208	4.800	± 0.104	13
50	0.069	14.50	± 0.034	13

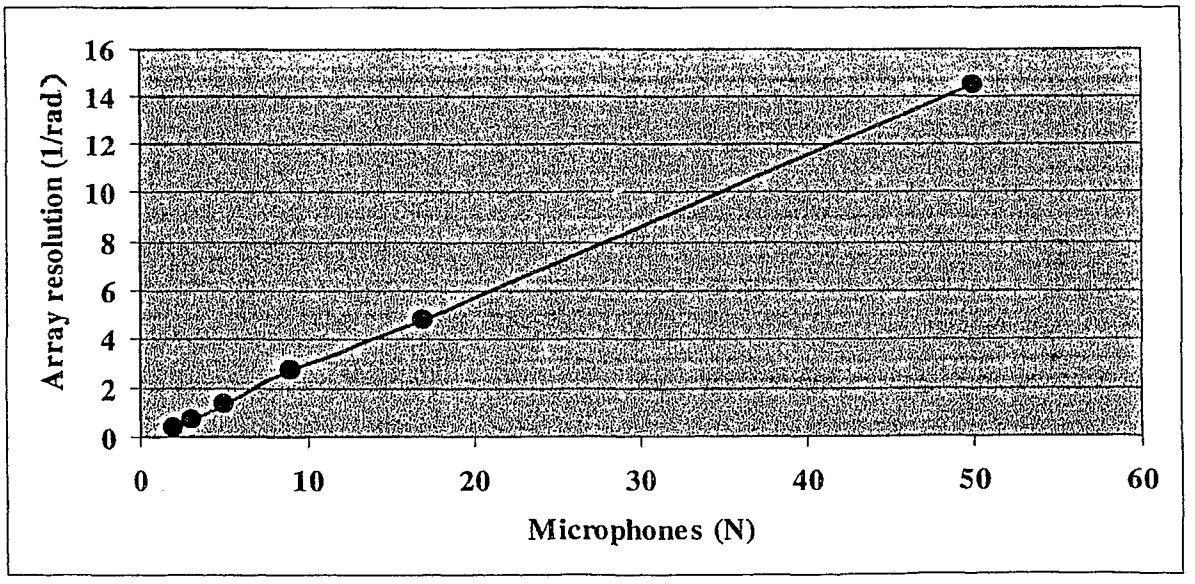

Figure 3.3: Effect of number of microphones on array resolution.

⊕ N.A. denotes not applicable.

3.2.2 Effect of source signal frequency (f)

Since it may be possible to change beamforming results by changing the source signal frequency, the plane wave signal was generated at different frequencies ranging from 500 to 8000 Hz for different array apertures (N =2 to 50) with $\theta = 0$ radians and an inter-microphone distance of 2 cm. Again, the sine wave generated at each microphone had an integer number of cycles.

The beamforming results for f=500 Hz and f=8000 Hz are depicted in Figures 3.4 and 3.5 for N=2 and N=50 respectively. Figure 3.4 (a) and 3.5 (a) show the array power for the two different frequencies. Figures 3.4 (b) and 3.5 (b) show the corresponding spectra. The beamwidth and the dynamic range were obtained from the various beamforming maps for different frequencies ranging from 500 Hz to 8000 Hz at different array apertures. The beamwidth, array resolution, the error band and the dynamic range are summarized in Table 3.2, and a plot of the array resolution versus signal frequency is presented in Figure 3.6.

When N=2 (i.e., the aperture is small), it can be seen from Figure 3.4 (a) that the array power is a straight line for f=500 Hz. The corresponding array resolution is therefore zero and the error band is infinite (Table 3.2 (a)), signifying that the beamforming method is futile under these circumstances. The array resolution increases with the increase of frequency to 8000 Hz, but the dynamic range cannot be defined, and the error band of ± 0.583 radians (± 18.5 %) is fairly large. Thus, the source localization capability of the array, although improved, is poor.

When N is increased to 50, for 500 Hz, the array power sidelobes are at -13 dB and the error band is reduced to ± 0.3213 radians (± 10 %) [Figure 3.5 (a) and Table 3.2 (d)]. This error band and hence the ability of the microphone array for source localization are acceptable. The error band changes rapidly with the increase of frequency to f=8000 Hz [Table 3.2(d)]. Specifically, the error changes from ± 10 % for 500 Hz to less than ± 1 % for 8000 Hz. With such a small error and a dynamic range of 13 dB, the acoustic source localization capability of the beamforming technique is quite satisfactory. Figure 3.6 indicates that the array resolution increases linearly with the increase of signal frequency for any array aperture.

Notice that the frequency resolution of the spectra is very good for both f=500 Hz and f=8000 Hz [Figure 3.4(b) and 3.5(b)]. This resolution is independent of frequency, as well as number of microphones (see subsection 3.2.1).

The results of this section serve to demonstrate that, at low frequencies, the source localization capability of the beamforming technique is very poor for small array apertures; however, this capability can be improved by increasing the array aperture. It is evident that the resolution of an array is a function of array aperture ($D=Nd$) and signal frequency [30]. At low frequencies, signal wavelengths are large, and to improve the array resolution large apertures are required; moreover, for a constant aperture, the array resolution increases with the increase of frequency⊕. The results also show that once the dynamic range can be defined in the beamforming maps, it is independent of frequency.

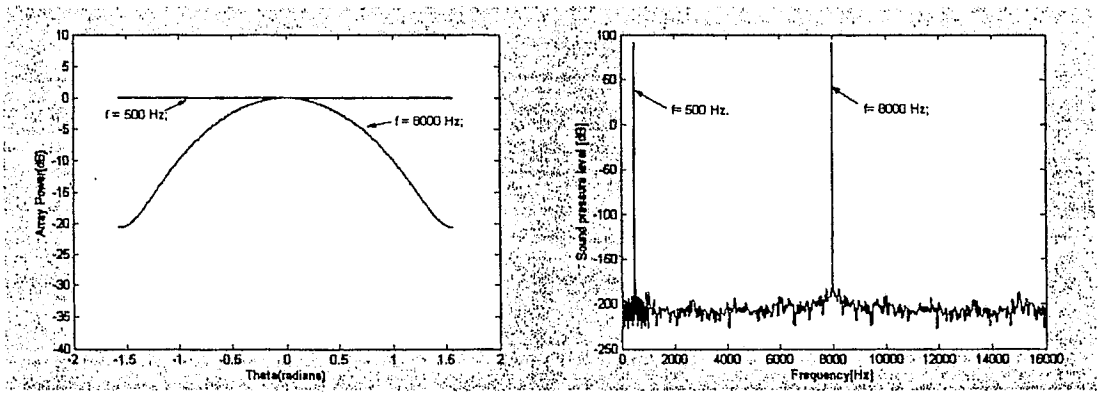

(a) (b)

Figure 3.4: Beamforming results, for N=2, f=500 Hz & 8000 Hz; (a) Array power plot (b) SPL spectrum.

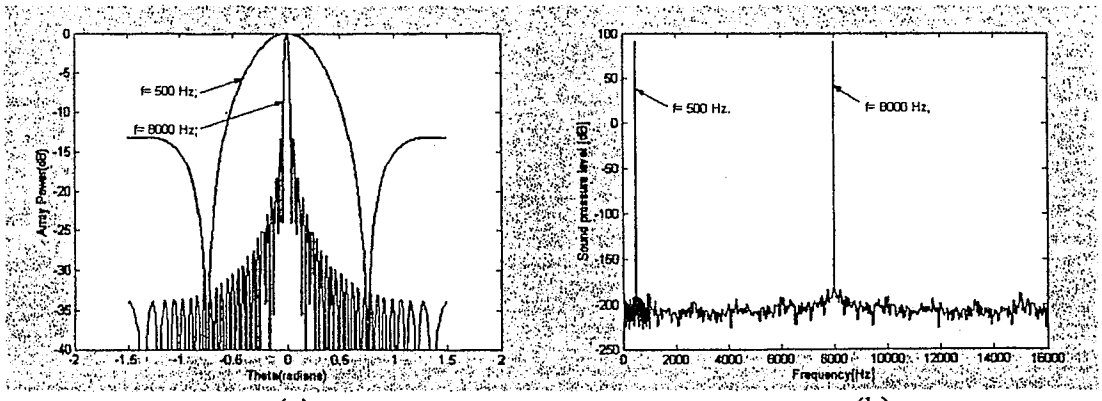

(a) (b)

Figure 3.5: Beamforming results, for N=50, f=500 Hz & 8000 Hz; (a) Array power plot (b) SPL spectrum.

⊕ These traits can be shown via the array pattern results (see Appendix B, equation B.5)

Table 3.2 Effect of source signal frequency

(a) *N*=2

Frequency (Hz)	Beamwidth (radians)	Resolution (1/radians)	Error band (radians)	Dynamic range (dB)
500	∞	0.00	∞	N.A.
3000	∞	0.00	∞	N.A.
4500	2.75	0.3636	± 1.3750	N.A.
6500	1.458	0.6857	± 0.7291	N.A
8000	1.166	0.8576	± 0.5830	N.A.

(b) *N*=5

Frequency (Hz)	Beamwidth (radians)	Resolution (1/radians)	Error band (radians)	Dynamic range (dB)
500	∞	0.00	∞	N.A.
3000	1.125.	0.888.	±0.5625	N.A.
4500	0.75	1.333	±0.3750	13
6500	0.50	2.0	±0.2500	13
8000	0.4166	2.40	±0.2083	13

(c) *N*=9

Frequency (Hz)	Beamwidth (radians)	Resolution (1/radians)	Error band (radians)	Dynamic range (dB)
500	∞	0.00	∞	N.A.
3000	0.666	1.50.	±0.3330	13
4500	0.375	2.67	±0.1875	13
6500	0.291	3.42	±0.1458	13
8000	0.25	4.0	±0.1250	13

(d) *N*=50

Frequency (Hz)	Beamwidth (radians)	Resolution (1/radians)	Error band (radians)	Dynamic range (dB)
500	0.6426	1.556	±0.3213	13
3000	0.1071	9.34	±0.0535	13
4500	0.0714	14.00	±0.0357	13
6500	0.0535	18.67	±0.0267	13
8000	0.042	23.80	±0.0210	13

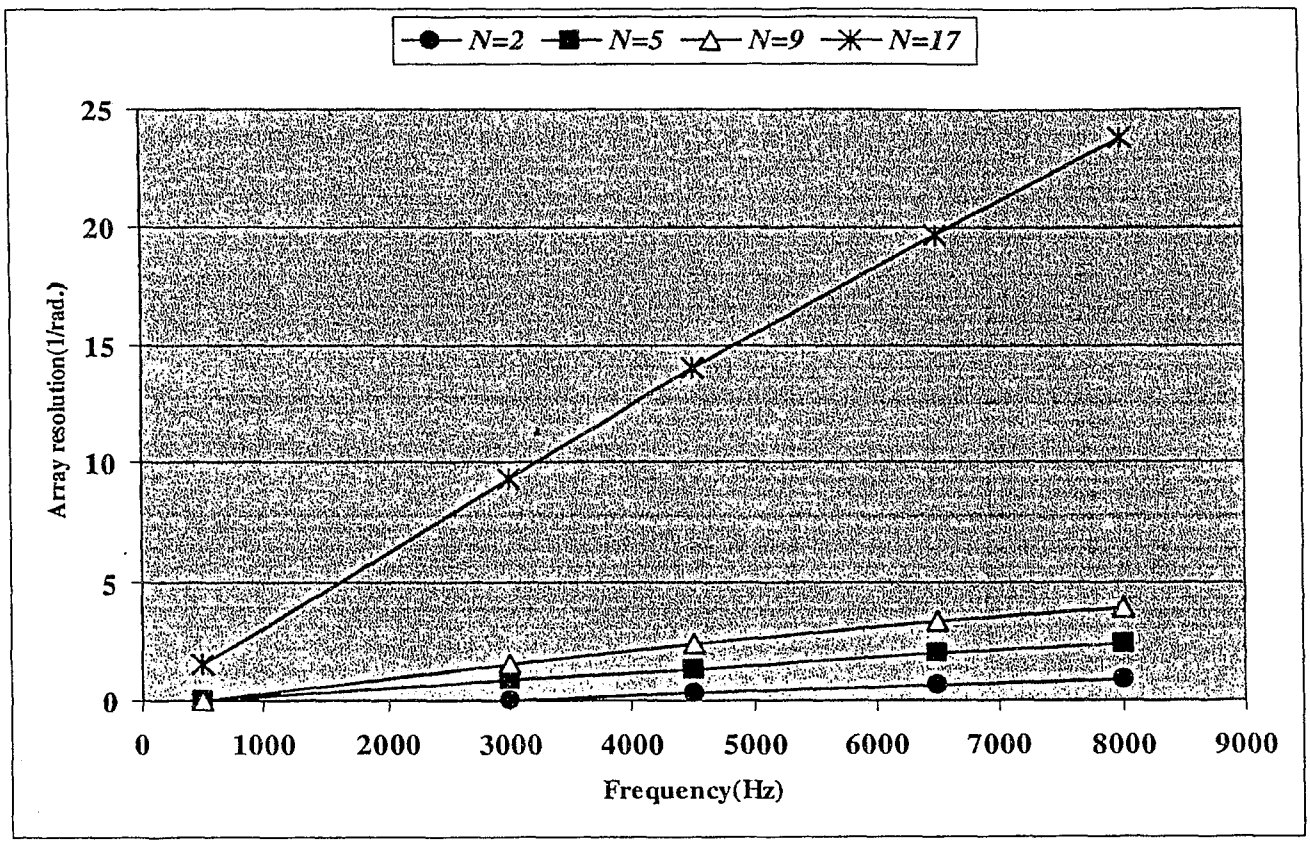

Figure 3.6: Effect of source signal frequency on array resolution.

3.2.3 Effect of integer and non-integer number of cycles with time windows

In general, measured periodic acoustic signals have non-integer numbers of cycles. The primary objective of this subsection was to examine the beamforming results when the acoustic signals have non-integer numbers of cycles. The impact of a time window, viz., the Hanning window, on the beamforming results with non-integer and integer number of cycles was also analyzed. The plane wave signal was generated at 4500 Hz, with $\theta = 0$ radians and an inter-microphone distance of 2 cm. The number of microphones was increased from 2 to 17 for the case of non-integer number of cycles with the default rectangular window.

The relevant beamforming results are presented in Figures 3.7, 3.8, 3.9 and 3.10, and Table 3.3. Figure 3.7 shows the results for a non-integer number of cycles with the rectangular window for f=4500 Hz and N=17. Figure 3.8 depicts the results for a non-integer number of cycles with the Hanning and rectangular windows, for f=4500 Hz and N=17. Figure 3.9 shows the beamforming results for an integer number of cycles with the Hanning and rectangular

windows for f=4500 Hz and N=17. The beamwidth, array resolution, the error band and the dynamic range, obtained from the various beamforming plots (N=2 to 17) for a non-integer number of cycles with the Hanning window, are summarized in Table 3.3. A plot of the array resolution versus number of microphones is presented in Figure 3.10.

When a non-integer number of cycles is used, the beamforming results indicate that the array power is distributed in various "frequency bins", as depicted in Figure 3.7 (a)-(e). But there is only one bin which "contains" the highest array power and which corresponds to the signal frequency. In this case (f=4500 Hz and N=17), it is the 348th frequency bin. Figure 3.10 depicts the array resolution calculated from the correct or dominant frequency bins for various array apertures. This figure indicates that array resolution increases linearly with the number of microphones. The resolution and error band values are exactly the same as those calculated in sub-section 3.2.1, where an integer number of cycles were used (Tables 3.3 and 3.1). However, there is energy leakage from the correct bin into adjacent bins [Figure 3.7 (a)-(e)]; consequently, the frequency resolution of the spectrum is reduced [Figure 3.7 (f)].

As shown in Figure 3.8 (a), the beamforming map is unaffected by the Hanning window, when the signal has a non-integer number of cycles. Moreover, Figure 3.8 (b) shows that the Hanning window noticeably alleviates the leakage problem associated with the spectrum, as compared to the rectangular (default) window.

When the Hanning window is applied with an integer number of cycles, the beamforming map is again unaffected, as shown in Figure 3.9(a). However, the frequency resolution of the spectrum is significantly degraded, as compared to the resolution when the rectangular window is used [Figure 3.9(b)].

From the results in this sub-section, it can be concluded that the beamforming map is independent of whether or not the signal contains an integer number of cycles, and the source can be localized from the correct or dominant frequency bin. Moreover, windows have no effect on the beamforming map. However, a window (other than the rectangular window) reduces the leakage from the spectrum when the signal has a non-integer number of cycles. Hence, in practice, a special window should always be prescribed in order to alleviate the leakage problem and to improve the resolvability of the estimated spectrum. But such a window is not required for a signal with an integer number of cycles.

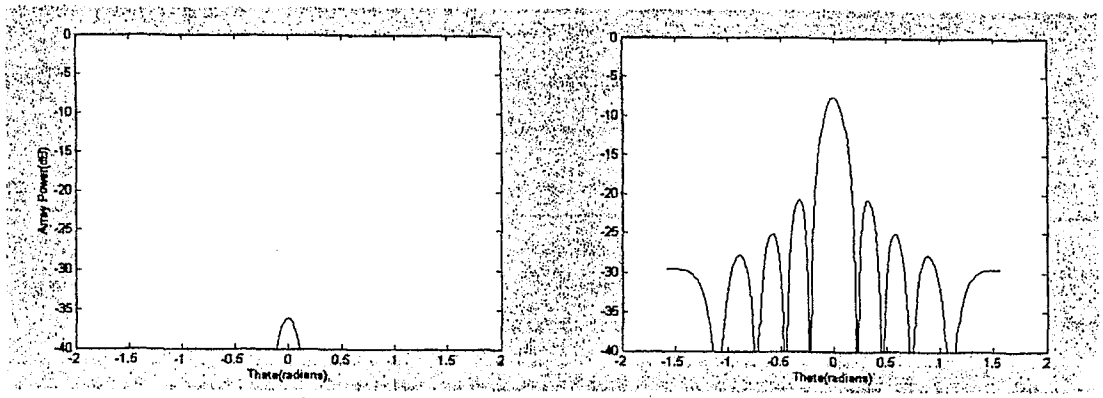

(a): 346th (b): 347th

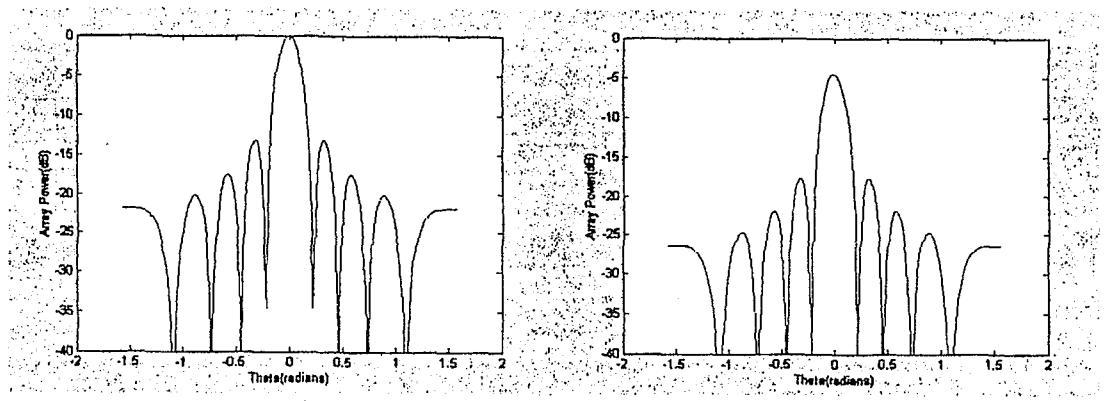

(c): 348th (d): 349th

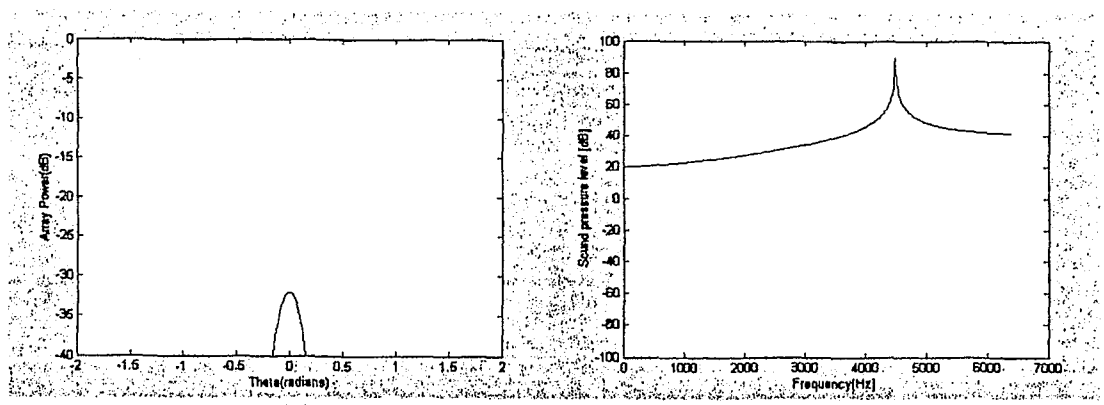

(e): 350th (f)

Figure 3.7: Beamforming results, for N=17, f= 4500 Hz, with a non-integer number of cycles and rectangular window; (a) - (e) Array power plots for 346th, 347th, 348th, 349th, 350th frequency bins (f) SPL spectrum.

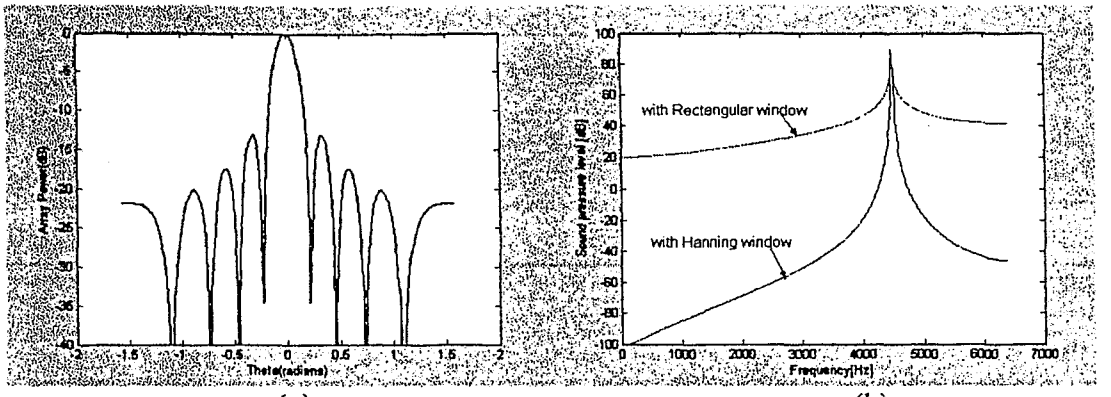

(a) (b)

Figure 3.8: Beamforming results, for N=17, f= 4500 Hz, with a non-integer number of cycles with Rectangular and Hanning windows; (a) Array power plot (b) SPL spectrum.

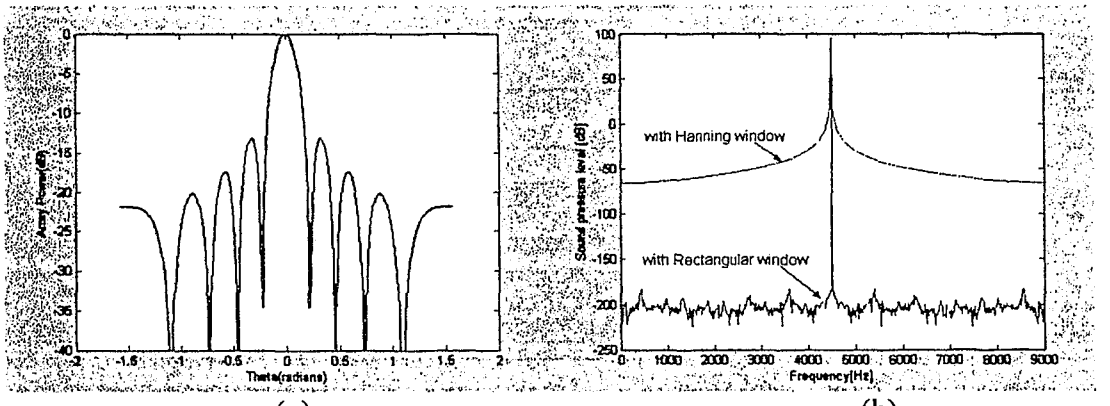

(a) (b)

Figure 3.9: Beamforming results, for N=17, f= 4500 Hz, with an integer number of cycles with Rectangular and Hanning windows; (a) Array power plot (b) SPL spectrum.

Table 3.3 Effect of non-integer number of cycles with Hanning window

Number of Microphones (N)	Beamwidth (radians)	Resolution (1/radians)	Error band (radians)	Dynamic range (dB)
2	2.750	0.363	±1.375	N.A.
3	1.375	0.727	± 0.6875	N.A.
5	0.750	1.333	± 0.375	13
9	0.375	2.670	± 0.1875	13
17	0.208	4.800	± 0.104	13

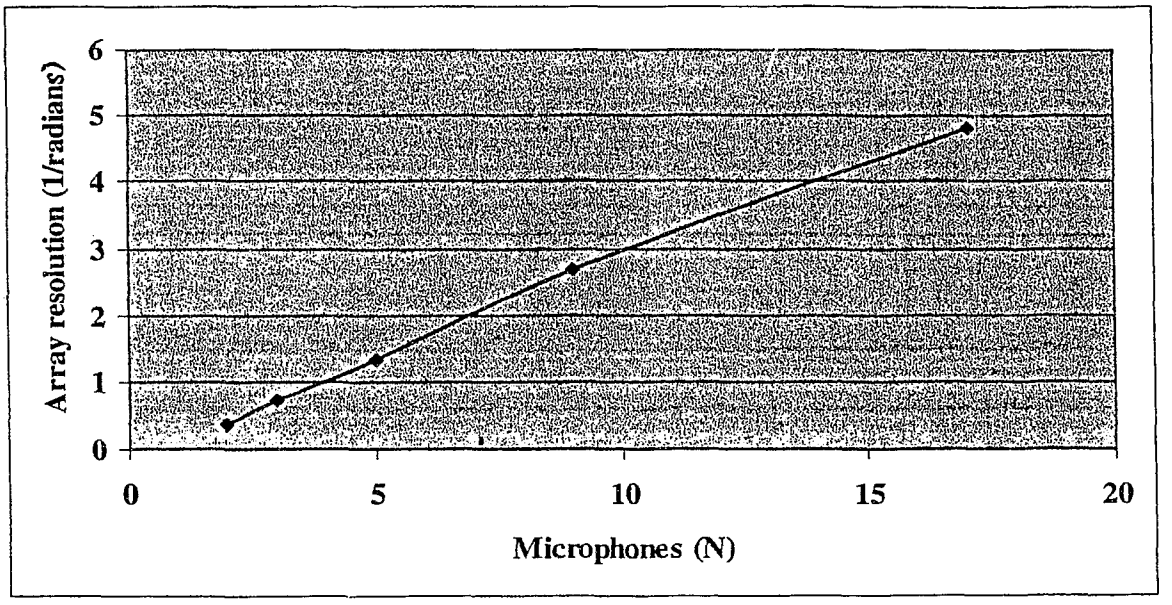

Figure 3.10: Effect of non-integer number of cycles on array resolution.

3.2.4 Effect of inter-microphone distance (d)

The distance between microphones (d) controls the spurious (grating) lobes in the beamforming map as discussed in subsection 2.2.1. With the violation of the Shannon criterion ($d > \lambda/2$), grating lobes appear in the beamforming map, as shown in Figure 2.3. The purpose of this sub-section was to explore what happens if $d > \lambda/2$, $d = \lambda/2$ and $d < \lambda/2$. The plane wave signal was generated at a frequency of 8000 Hz, with $\theta = 0$ radians, N=17 and an integer number of cycles. The inter-microphone spacing was changed from 6 cm to 1 cm. The inter-microphone spacing required to satisfy Shannon's criterion ($d^* = \lambda/2$) was 2 cm.

The beamforming results for d=3d^* (6 cm), d^* (2 cm), and $d^*/2$ (1 cm) are presented in Figures 3.11, 3.12, and 3.13 respectively. Figures 3.11(a), 3.12(a), and 3.13(a) show the array power as the function of DOA. Figures 3.11(b), 3.12(b), and 3.13(b) show the corresponding SPL spectra.

Grating lobes appear in the beamforming map when d=3d^* and their magnitude is as high as that of the mainlobe (Figure 3.11(a)). Due to these grating lobes, beamforming source localization is futile. When the distance between microphones is reduced to d=d^* (which satisfies Shannon's criterion) the grating lobes are suppressed and a beamforming map with adequate dynamic range (13 dB) results (Figure 3.12 (a)). When the distance between

microphones is further reduced to $d=d^*/2$, the mainlobe width increases (Figure 3.13 (a)), and the error band increases by 3 times, i.e., from ± 0.0357 radians for $d=d^*$ to ± 0.107 radians for $d=d^*/2$; but the dynamic range is unaffected. It should be noted that the inter-microphone distance has no effect on the sound pressure spectrum [Figures 3.11(b), 3.12(b), and 3.13 (b)].

It is clear from the above results that an acoustic source can be localized once $d \leq d^*$, i.e., when Shannon's criterion is met. Moreover, when $d < d^*$, the array resolution is degraded. Thus, it can be concluded that the maximum array resolution is obtained when $d=d^*$. (In practice, d is fixed at d^* for a specific application with a given array design.) The results also show that the inter-microphone distance has no impact on the SPL spectrum of the signal.

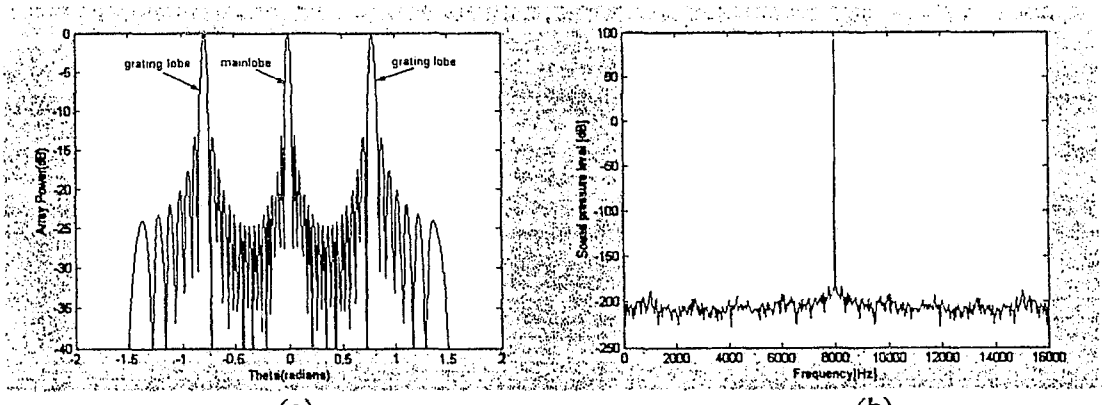

(a) (b)

Figure 3.11: Beamforming results for $d = 3d^*$; (a) Array power plot (b) SPL spectrum.

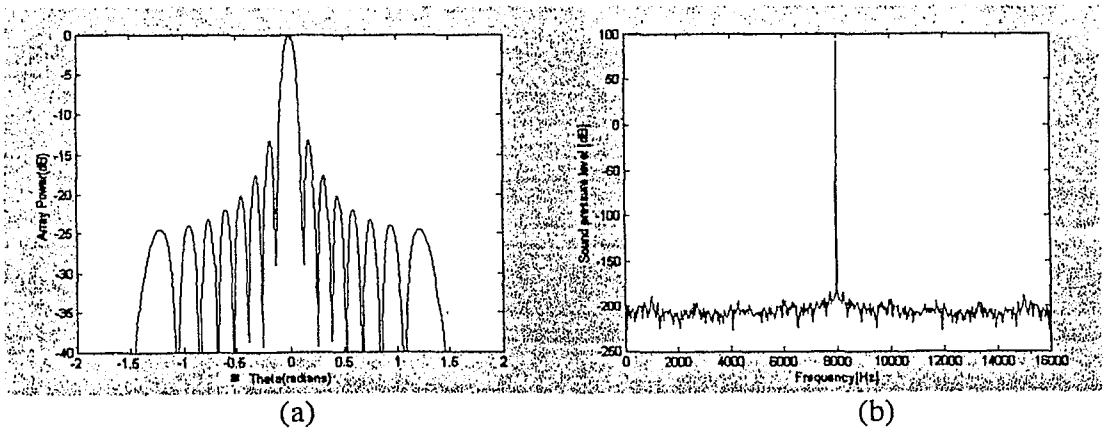

(a) (b)

Figure 3.12: Beamforming results for $d = d^*$; (a) Array power plot (b) SPL spectrum.

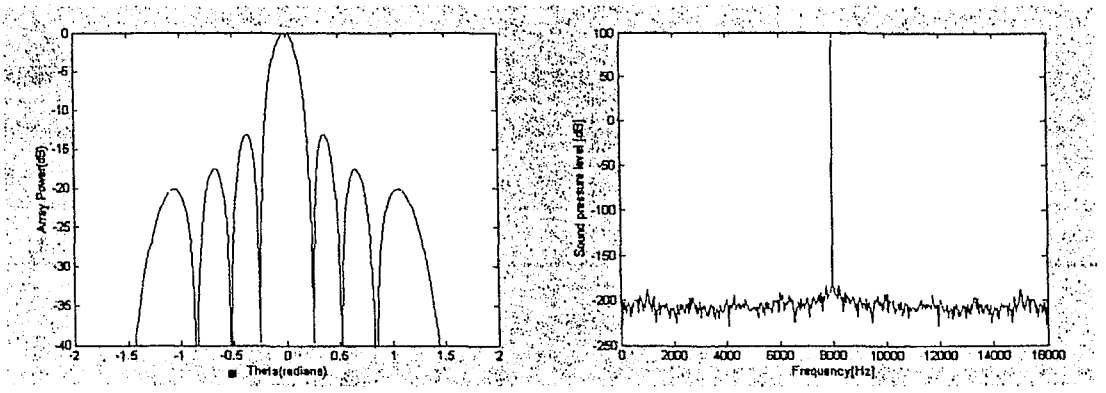

(a) (b)

Figure 3.13: Beamforming results for $d = d^*/2$; (a) Array power plot (b) SPL spectrum.

3.2.5 Effect of source position

An acoustic source can be located between – 90 degrees and + 90 degrees for the ULA far field beamforming, and the signal direction of arrival (DOA) may change the array capability. To examine this aspect, a plane wave signal was generated at 8000 Hz, with 17 microphones, an inter-microphone spacing of 2 cm and an integer number of cycles. The source was placed at different positions from -1.0 radians to 1.0 radians with respect to broadside ($\theta = 0$ radians).

The beamforming results are shown in Figure 3.14 for θ =-1.0 radians and 0 radians. Figure 3.14 (a) shows the array power for two different DOA's. Figure 3.14 (b) presents the corresponding SPL spectra. The beamwidth, the array resolution, the error band and the dynamic range, obtained from the various beamforming plots (θ = -1.0 radians to 1.0 radians) are summarized in Table 3.4. A plot of the array resolution versus DOA is presented in Figure 3.15.

When the signal impinges at $\theta = 0$ radians, the error band is ± 0.0625 radians, and the dynamic range is 13 dB [Figure 3.14 (a)]. The error band increases to ± 0.1304 radians with the change of DOA to $\theta = \pm$ 1.0 radians (Table 3.5). This error band is almost double that obtained at $\theta = 0$ radians. Also, it should be noted that the sidelobes become asymmetric with the change of direction of propagation of the signal from $\theta = 0$ radians to θ =-1.0 radians. The DOA has no impact on the SPL spectrum [Figures 3.14(b)]. Figure 3.15 shows that the array resolution is maximum for θ=0 radians and decreases non-linearly as $|\theta|$ increases.

It is evident that the array resolution depends upon the DOA of the signal, with the maximum resolution occurring when an acoustic source is at $\theta = 0$ radians (i.e., at broadside). However, the dynamic range remains unaffected by the DOA.

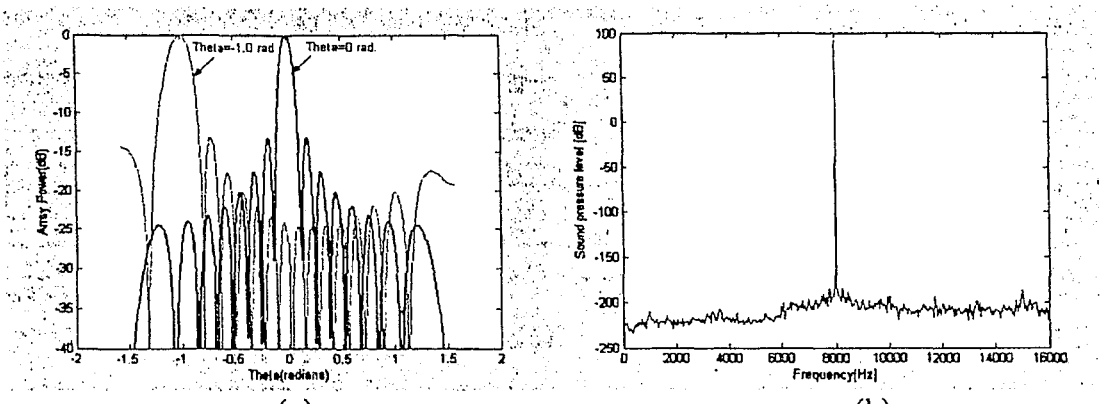

(a) (b)

Figure 3.14: Beamforming results for $\theta = -1.0$ radians, $\theta = 0$ radians; (a) Array power plot (b) SPL spectrum.

Table 3.4 Effect of source position

DOA (radians)	Beamwidth (radians)	Resolution (1/radians)	Error band (radians)	Dynamic range (dB)
-1.0	0.2608	3.834	±0.1304	13
-0.5	0.1522	6.57	±0.0760	13
0	0.125	8.00	±0.0625	13
0.5	0.1522	6.57	±0.0760	13
1.0	0.2608	3.834	±0.1304	13

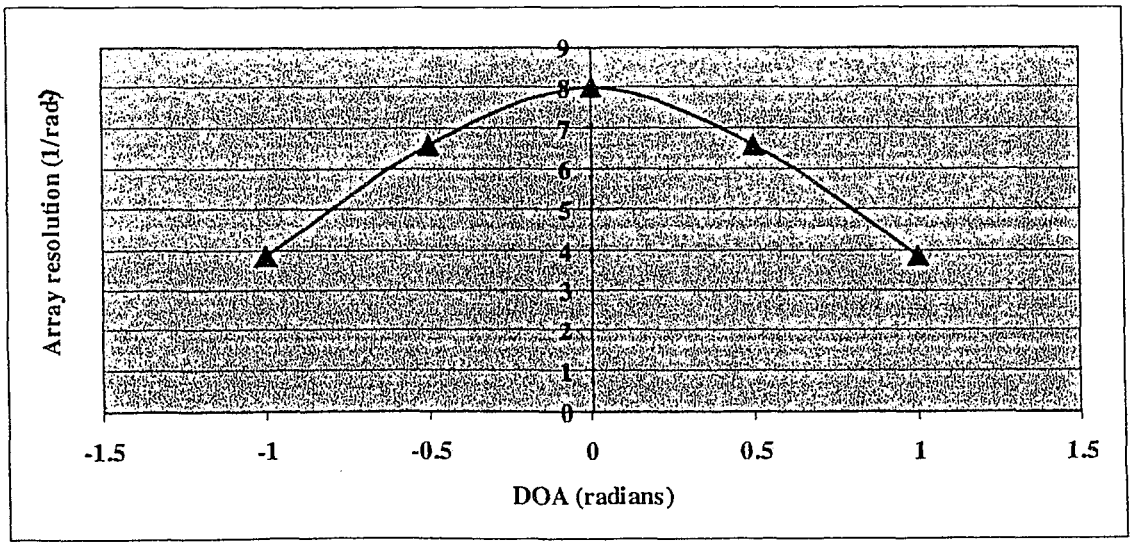

Figure 3.15: Effect of source location on array resolution.

3.2.6 Effect of multiple frequencies

Single frequency signals, which are generally similar to narrowband signals, have been discussed in the previous subsections. In practice, however, broadband signals, i.e., signals containing a large number of frequencies, are often encountered. The purpose of this subsection was to analyze a signal with multiple frequencies in order to gain some insight into the beamforming technique in the case of broadband signals. To this end, a plane wave signal containing three components at frequencies of 4500 Hz, 6500 Hz, and 8000 Hz, was generated, with θ=0 radians, an inter-microphone of 2 cm, and an integer number of cycles. The microphone array consisted of 17 microphones.

The beamforming results are presented in Figure 3.16. Figure 3.16 (a)-(c) depicts the array power in different frequency bins and Figure 3.16 (d) shows the SPL spectrum.

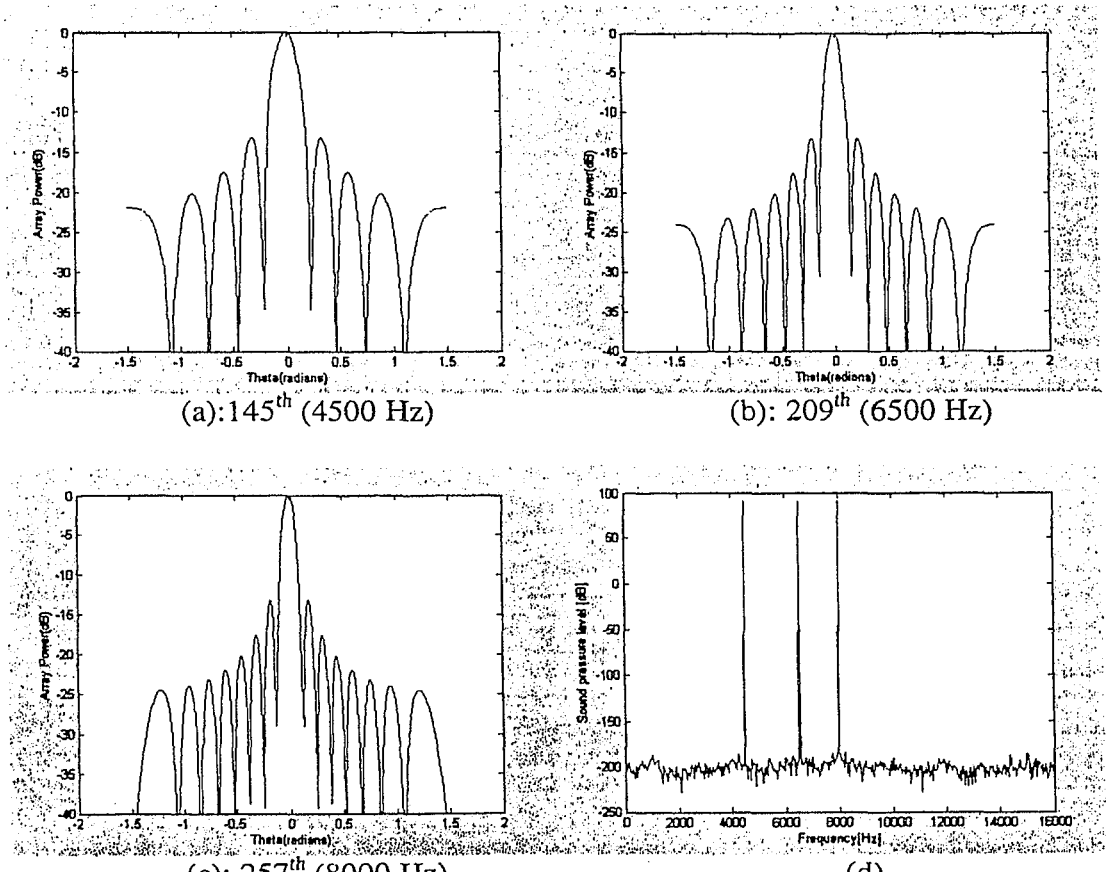

(a):145th (4500 Hz) (b): 209th (6500 Hz)

(c): 257th (8000 Hz) (d)

Figure 3.16: Beamformimg results, for N=17, multiple frequency signal;
(a)-(c) Array power plots for145th, 209th, and 257th frequency bins (d) SPL spectrum.

It can be seen that the beamforming maps corresponding to the three signal frequencies (4500 Hz, 6500 Hz and 8000 Hz) are contained in specific dominant frequency bins. Moreover, the error band pertaining to the different beamforming maps are ± 0.2083 radians for 4500 Hz, ± 0.150 radians for 6500 Hz, and ± 0.125 radians for 8000 Hz, in accordance with the fact that the error band decreases (or the array resolution increases) as frequency increases (see subsection 3.2.2). It should be noted that the array dynamic range remains constant at 13 dB for the different frequencies.

It is evident that for a signal with multiple frequencies (or a broadband signal), with the use of time windows, source localization is possible by finding the relevant dominant frequency bins. The implication of these results is that the beamforming technique is robust, i.e., it is capable of resolving the source localization problem regardless of the nature of the signal, i.e., narrowband or broadband.

3.2.7 Effect of number of data blocks without noise

The purpose of this sub-section was to examine the effect of the number of data blocks when an acoustic signal is free of extraneous noise. The plane wave signal was generated at a frequency of 8000 Hz, with $\theta = 0$ radians, an inter-microphone spacing of 2 cm and an integer number of cycles. The microphone array consisted of 17 microphones.

The beamforming results for L=1 and L=10 are presented in Figures 3.17 and 3.18 respectively. Figures 3.17(a) and 3.18(a) show the array power as a function of DOA. Figures 3.16 (b) and 3.18(b) show the corresponding SPL spectra.

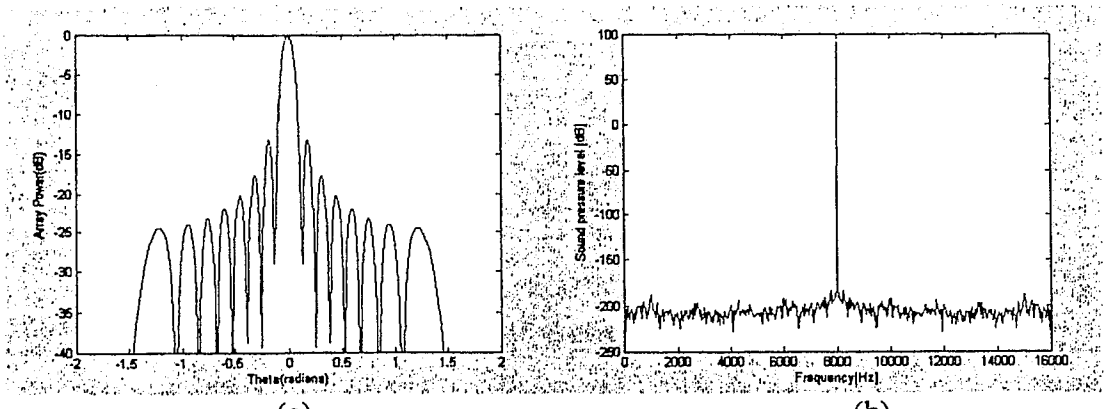

(a) (b)

Figure 3.17: Beamforming results for L=1; (a) Array power plot (b) SPL spectrum.

When a single block of data is used, the beamforming map has an error band of ± 0.0625 radians with array dynamic range of 13 dB [Figure 3.17 (a)]. When 10 blocks are used, the results remain exactly the same [Figure 3.18(a)]. The SPL spectra [Figures 3.17(b) and 3.18 (b)] are also unaffected by the number of blocks.

The above results serve to establish that block averaging is really not required when the signal contains no extraneous noise, as pointed out previously in section 2.2.

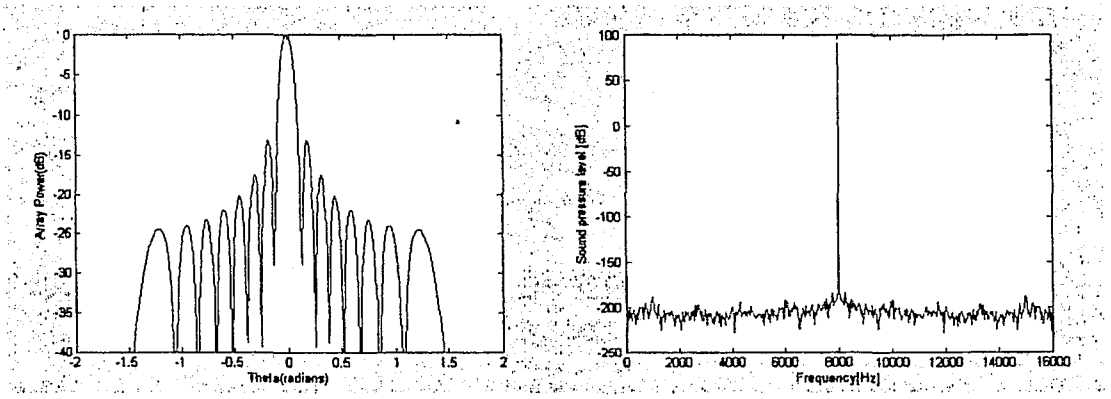

(a) (b)

Figure 3.18: Beamforming results for L=10; (a) Array power plot (b) SPL spectrum.

3.2.8 Effect of noise for a single block of data

The signals used in the previous sub-sections were noise free. But in practice, extraneous noise is often present in acoustic signals. If this noise is statistically independent with respect to the various microphones in an array, then frequency domain averaging, i.e., averaging several blocks (L) of frequency-domain data, can be used to improve the beamforming results. Moreover, the signal-to-noise ratio (SNR) of the array is significantly greater than that of a single microphone (SNR_o), as discussed in Appendix C.

The purpose of this sub-section was to investigate the effect of the noise on the beamforming results. The plane wave signal was generated at a frequency of 6500 Hz, with θ=0 radians, an inter-microphone spacing of 2 cm and an integer number of cycles. Statistically independent noise was added to each microphone signal. The amplitude of the noise was varied so that three different signal-to noise ratios (i.e., SNR_o values) were obtained, viz., 0.52, 0.0012, and 0.00030. Four different array apertures corresponding to N=10, 17, 33,

45, were used. Only a single block of noisy data containing 1024 data points (L=1, M=1024) was used for this analysis.

The beamforming results for SNR_o values of 0.52, 0.0012, and 0.0003, and for N values of 10 and 45, are presented in Figures 3.19-3.24. Each figure depicts an array power plot and the associated SPL spectrum.

For SNR_o=0.52 and N=10 [Figure 3.19(a)], the error band is ± 0.25 radians (± 8 %), and the dynamic range is 13 dB. This error band is adequate for source localization. The associated SPL spectrum [Figure 3.19 (b)] shows that the spectrum of the acoustic signal dominates that of the noise, with the difference between the two spectra being approximately 29 dB.

When SNR_o decreases from 0.52 to 0.0012, for N=10 [Figure 3.20 (a)], the sidelobe levels increase, and the dynamic range decreases to 3.6 dB. Also, the associated SPL spectrum [Figure 3.20 (b)] shows that spectrum of the signal and that of the noise are indistinguishable. Therefore, the beamforming method is of very limited use in this case.

As SNR_o decreases further to 0.0003, for N=10 [Figure 3.21(a)], the sidelobe levels increase to such a height that the dynamic range is zero and the associated SPL spectrum [Figure 3.21(b)] shows that the spectrum of the signal is buried in that of the noise. Therefore, the beamforming method is futile in this case.

For SNR_o=0.52 and N=45 [Figure 3.22 (a)], the error band is reduced from ± 0.25 radians (± 8 %) to ± 0.055 radians (± 0.18 %), and the dynamic range is 13 dB. The decrease in the error band with the increase in the number of microphones (from N=10 to 45) is consistent with the results of sub-section 3.2.1. The effect of the noise on the associated SPL spectrum [Figure 3.22(b)] is also reduced, because the array SNR increases (see Appendix C) as the number of microphones increases, and the signal spectrum dominants the noise spectrum by about 39 dB.

When SNR_o decreases from 0.52 to 0.0012, for N=45 [Figure 3.23(a)], the sidelobe levels increase and the dynamic range decreases to 7.65 dB. The associated SPL spectrum [Figure 3.23(b)] shows that the signal spectrum is distinguishable from the noise spectrum, the difference between the two spectra being about 5 dB. The beamforming method is limited in this case but it is better than in the case of SNR_o=0.0012 and N=10.

As SNR_o decreases to 0.0003, for N=45 [Figure 3.24(a)], the sidelobe levels increase further and the dynamic range decreases to 2.7 dB. The associated SPL spectrum [Figure

3.24(a)] shows that the signal spectrum is buried in the noise spectrum. Therefore, the beamforming method is futile in this case.

It can be concluded that once the signal to noise ratio (SNR_o) is greater than about 0.5 and the number of microphone is 10 or more, the beamforming method is viable *with a single block of data*, when the noise affecting the various microphones is statistically independent. If SNR_o is very much smaller than 0.5 (say, less than 0.001), then an adequate *array* signal to noise ratio (SNR) can not be achieved using a single block of data, even with a relatively large number of microphones (N=45); consequently, both source localization and signal spectrum detection are difficult. In other words, the beamforming technique becomes increasingly deficient as SNR_o decreases, when a single block of data is used. To overcome this deficiency, block averaging is used.

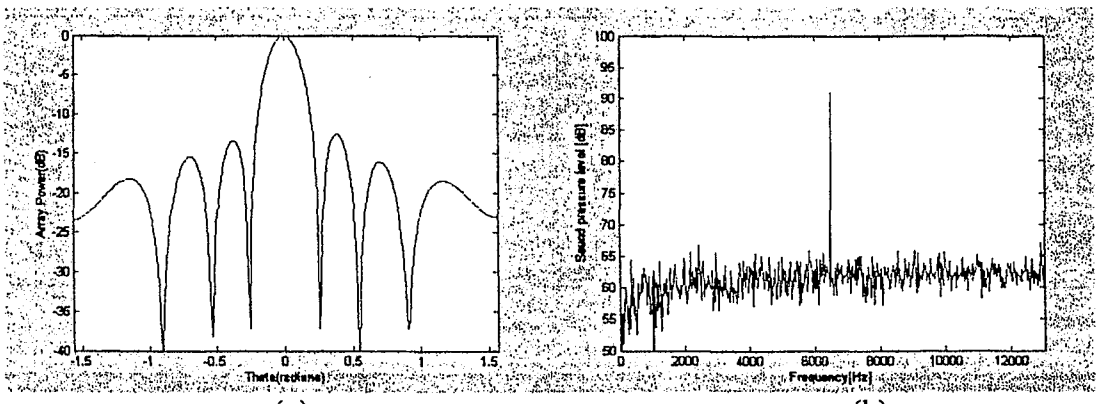

(a) (b)

Figure 3.19: Beamforming results for SNR_o=0.52, N=10; (a) Array power plot (b) SPL spectrum.

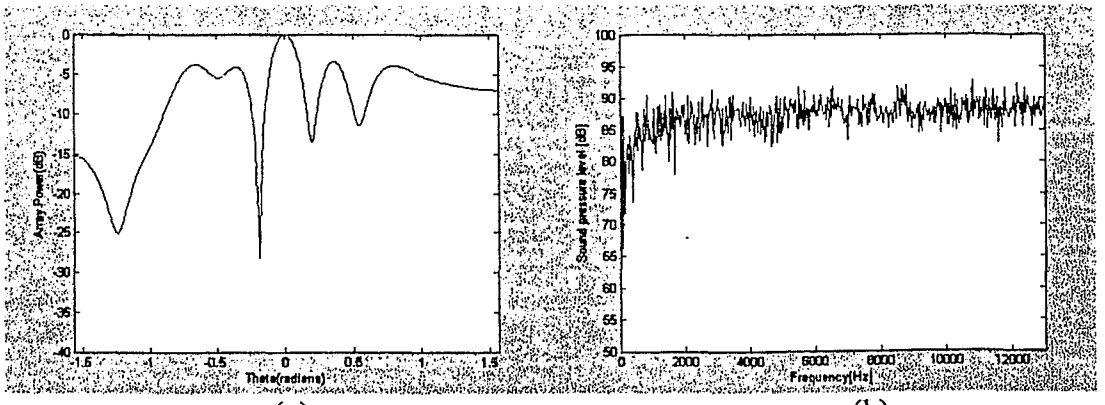

(a) (b)

Figure 3.20: Beamforming results for SNR_o=0.0012, N=10; (a) Array power plot (b) SPL spectrum.

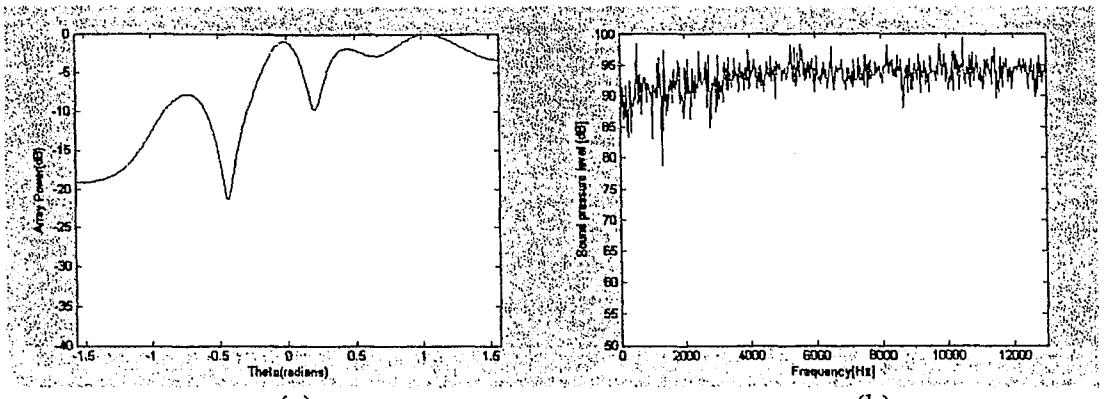

(a) (b)

Figure 3.21: Beamforming results for SNR_o=0.0003, N=10; (a) Array power plot (b) SPL spectrum.

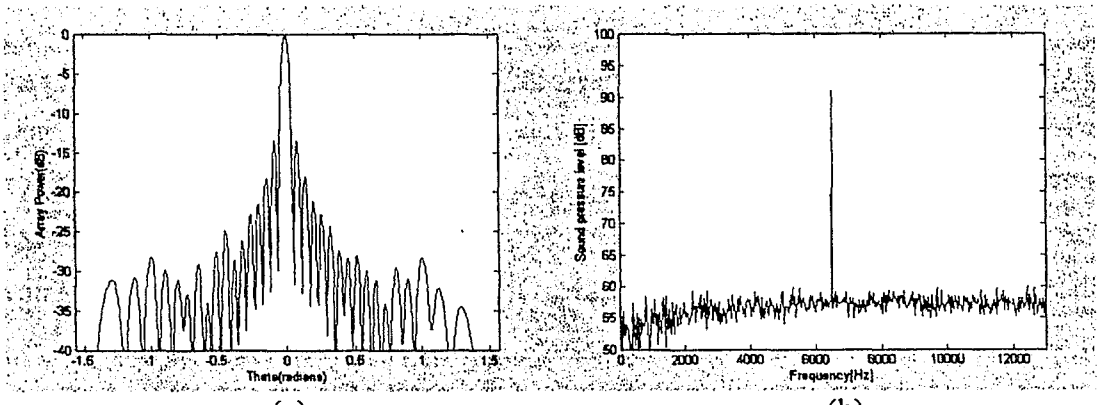

(a) (b)

Figure 3.22: Beamforming results for SNR_o=0.52, N=45; (a) Array power plot (b) SPL spectrum.

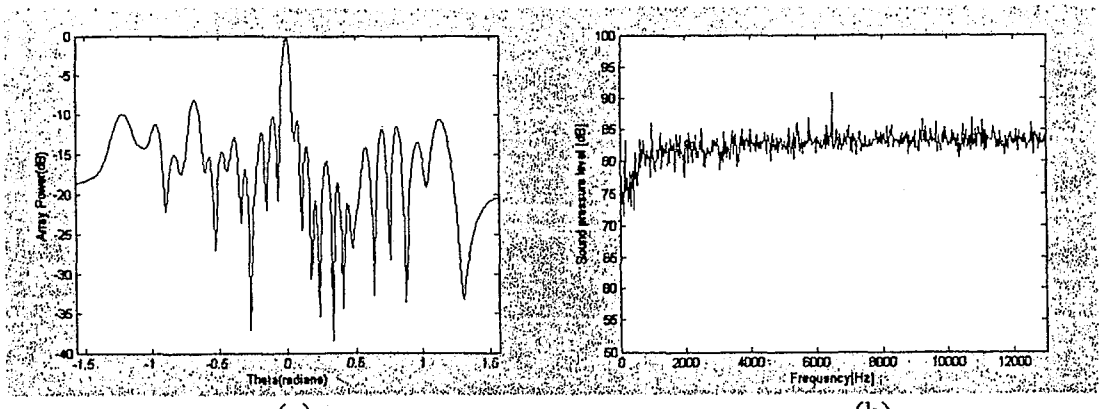

(a) (b)

Figure 3.23: Beamforming results for SNR_o=0.0012, N=45; (a) Array power plot (b) SPL spectrum.

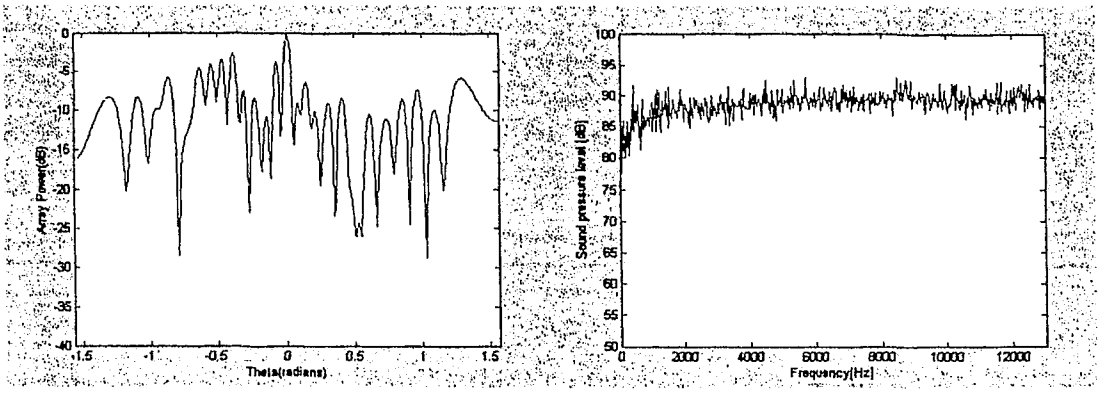

(a) (b)

Figure 3.24: Beamforming results for SNR_o=0.0003, N=45; (a) Array power plot (b) SPL spectrum.

3.2.9 Effect of noise with several blocks (L) of data

The results in the last subsection indicate that the noise dominated the source signal for SNR_o=0.0012 and 0.0003 (i.e., for relatively low SNR_o values), and both source localization and signal spectrum detection were difficult. The aim of this sub-section was to demonstrate the impact of the number of data blocks (i.e., block averaging), when *statistically independent* noise affects the microphones in an array. The data for each microphone were divided into a number of blocks (L), and the FFT was applied to each block, as discussed in 2.2.3.1. The plane wave signal was generated at a frequency of 6500 Hz, with θ=0 radians, an inter-microphone spacing of 2 cm and an integer number of cycles. Statistically independent noise was added to each microphone signal. The SNR_o values used were 0.0012 and 0.0003, and the number of microphones was varied from 10 to 45. Beamforming results were obtained for various combinations of SNR_o and N, with different numbers of data blocks, i.e., L values, being used for *each combination*. The "optimum" number of blocks of frequency-domain data to be averaged for each combination was determined on the basis of consistency of the beamforming maps obtained using different L values. As L increases, the beamforming map for any given SNR_o -N combination evolves from a relatively disorganized form [e.g., Figure 3.24 (a)] to a structured form [e.g., Figure 3.28(a)]. The value of L beyond which the map ceases to change in any significant fashion is the optimum L value.

Beamforming results based on the optimum number of blocks for different combinations of SNR_o and N are presented in Figures 3.25-3.28. Each figure depicts the "evolved" array

power and associated SPL spectrum. A plot of the optimum number of blocks versus number of microphones for different SNR_o values is presented in Figure 3.29.

Figure 3.25 depicts the beamforming results for SNR_o=0.0012 and N=10. The optimum number of blocks is 23 for source localization via the beamforming method. The beamforming map in Figure 3.25(a) for L=23 can be compared to that in Figure 3.20(a) for L=1. It can be seen that the array dynamic range increases from 3.6 dB (which is poor) to 6.3 dB, due to the increase in L from 1 to 23. With respect to the SPL spectrum, the noise effect is alleviated by about 6 dB for L=23 [Figure 3.25 (b)], as compared to 0 dB for L=1 [Figure 3.20(b)].

Figure 3.26 shows the beamforming results for SNR_o=0.0003 and N=10. The optimum number of blocks is 40 for source localization, and the array dynamic range is 3 dB. The beamforming map in Figure 3.26(a) for L=40 is seen to be organized compared to that shown in Figure 3.21(a) for L=1. Also, the SPL spectrum indicates that the noise effect is alleviated by about 3 dB for L=40 [Figure 3.26 (b)], as compared to 0 dB for L=1 [Figure 3.21(b)]. But the dynamic range of 3 dB is unacceptable.

The beamforming results for SNR_o=0.0012 and N=45 are presented in Figure 3.27. The optimum number of blocks is 10, and the array dynamic range is 10.8 dB, which is reasonable. The beamforming map in Figure 3.27(a) for L=10 is clearly much more organized than that shown in Figure 3.23(a) for L=1. With respect to the SPL spectrum, the noise effect alleviation is about 12 dB for L=10 [Figure 3.27(b)], as compared to about 6 dB for L=1 [Figure 3.23(b)].

The beamforming results for SNR_o=0.0003 and N=45 are presented in Figure 3.28. The optimum number of blocks is 15, and the array dynamic range is 7.2 dB, which is acceptable. With respect to the SPL spectrum, the noise effect alleviation is about 7 dB for L=15 [Figure 3.28(b)], as compared to about 0 dB for L=1 [Figure 3.24(b)].

A comparison of Figure 3.25 for SNR_o=0.0012 and N=10, and Figure 3.27 for SNR_o=0.0012 and N=45, indicates that for a given SNR_o value, *once the optimum L is used*, both the dynamic range and the noise effect alleviation increase as N increases; in other words, the capability of the beamforming technique improves as the array aperture increases, as expected. It should be noted, however, that for low SNR_o values (e.g., 0.0003), fairly large apertures are required to obtain reasonable results (see Figure 3.26, for N=10 and Figure 3.28, for N=45).

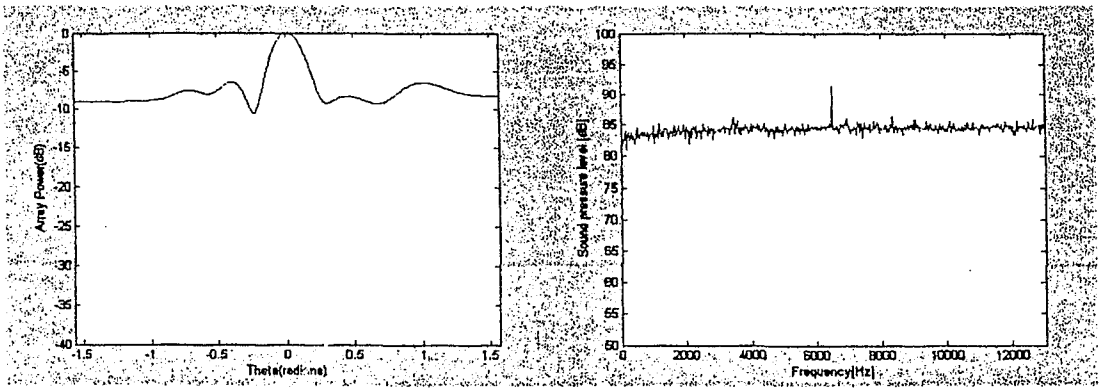

(a) (b)

Figure 3.25: Beamforming results for SNR_0=0.0012, N=10, L=23; (a) Array power plot (b) SPL spectrum.

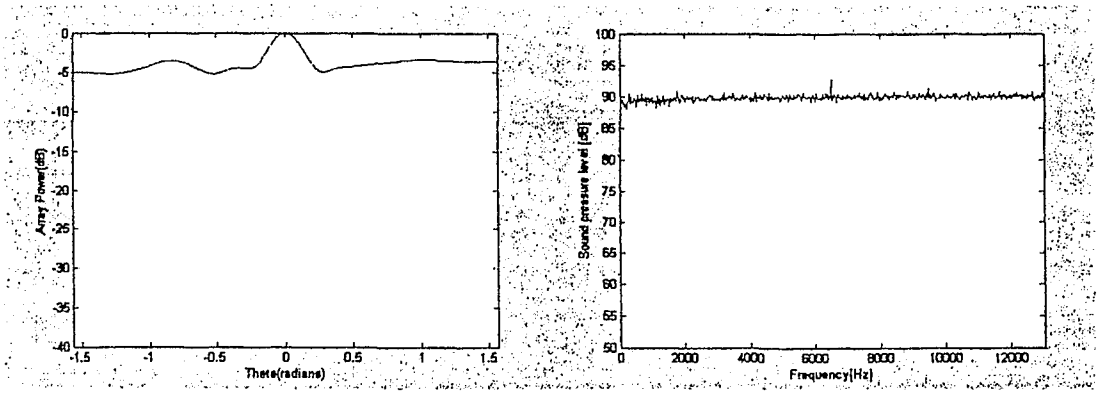

(a) (b)

Figure 3.26: Beamforming results for SNR_0=0.0003, N=10, L=4; (a) Array power plot (b) SPL spectrum.

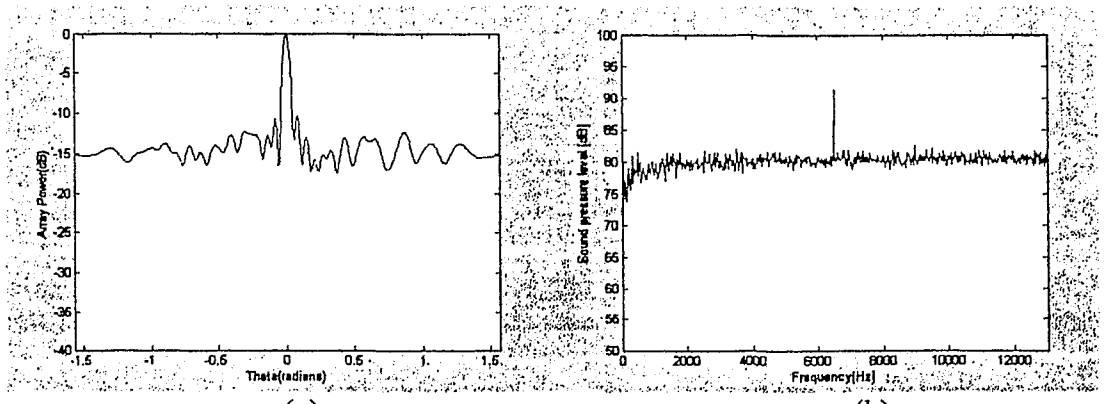

(a) (b)

Figure 3.27: Beamforming results for SNR_0=0.0012, N=45, L=10; (a) Array power plot (b) SPL spectrum.

It can be seen from Figure 3.29 that for a given SNR_o value, the optimum number of blocks decreases essentially linearly as the number of microphones (or the array aperture) increases; moreover, for a given number of microphones, the optimum number of blocks decreases as the SNR_o value increases.

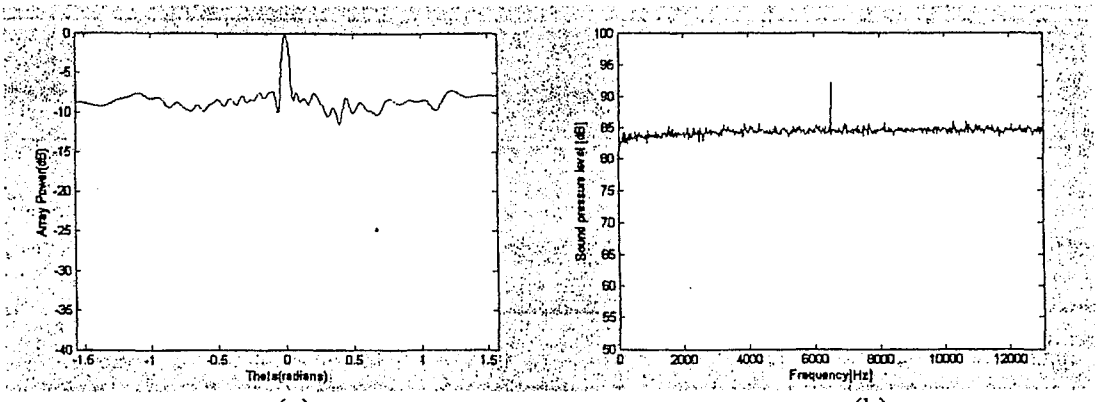

(a) (b)

Figure 3.28: Beamforming results for SNR_o=0.0003, N=45, L=15; (a) Array power plot (b) SPL spectrum.

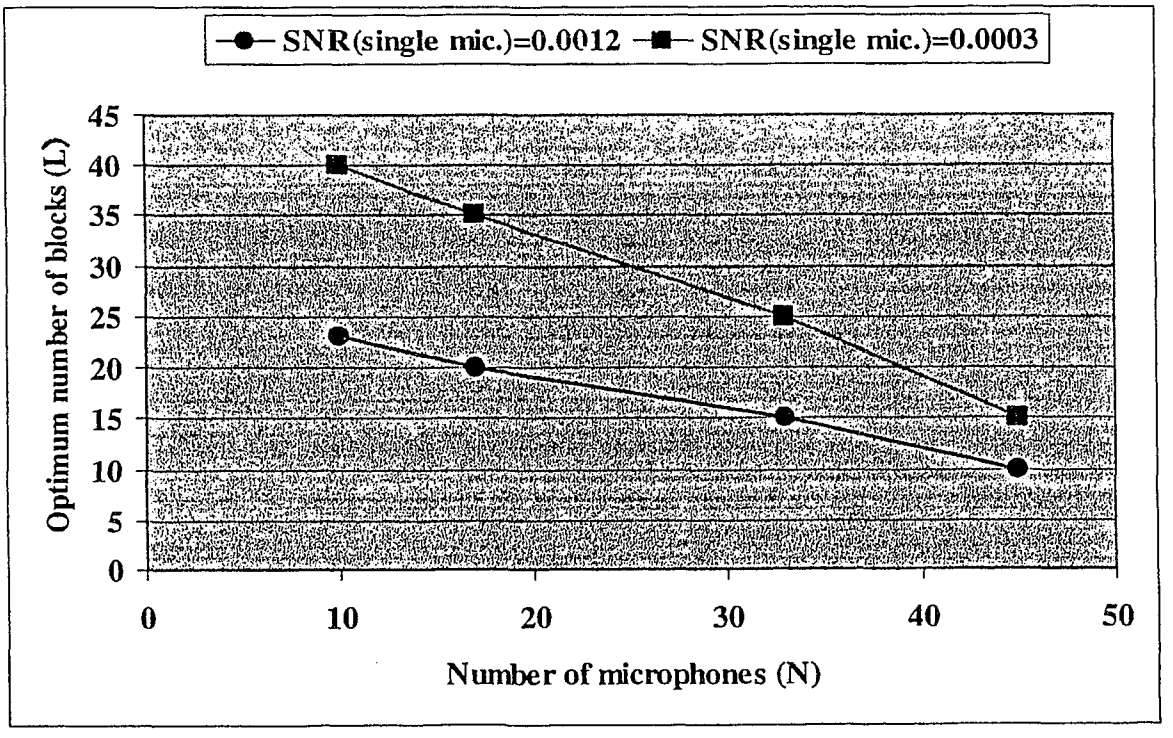

Figure 3.29: Plot between optimum numbers of blocks (L) versus number of microphones (N) for SNR_o = 0.0012 and SNR_o = 0.0003.

The results of this sub-section demonstrate that a source can be localized in a noisy environment by means of block averaging, when *statistically independent* noise affects the microphones in an array. In such an environment, the enhancement of the signal-to-noise ratio of an array over that of a single microphone is insufficient, and block averaging should be used to reduce the variability of the beamforming results.

In the above section (3.2), a detailed sensitivity analysis of a uniform linear array (ULA) with a source placed in the far field has been carried out. In the next section, the sensitivity analysis of the ULA with the source placed in the near field is presented.

3.3 Uniform Linear Array - near field beamforming

In certain aeroacoustic situations, for example, a sound source placed in the test section of a wind tunnel, a microphone array can be located near to a sound source. In such a situation, the acoustic wave front is spherical and beamforming is complicated, in comparison with a planar wave situation. As mentioned in section 1.1.2, for near field source localization, both the range and the DOA of the acoustic source need to be determined. The purpose of this section was to examine beamforming results pertaining to a ULA with a near field source. The ULA was designed for near field simulated signals with a maximum frequency of 3000 Hz. The inter-microphone spacing was therefore set at 5.7 cm to satisfy Shannon's theorem. The signals at each microphone had an integer number of cycles. Each block of data for the digital signals contained 1024 points, i.e., M=1024, and yielded 513 (M/2+1) frequency bins.

The ULA was taken along the x-axis, and a spherical wave was generated at each microphone location by means of the formula $(A/r_n)\sin[\omega(t-r_n/c)]$, as discussed in sub-section 3.1. For this arrangement, the wave front reaches the microphone array centre at an angle θ as depicted in Figure 3.30, where r is the distance between the acoustic source and the array centre.

For each frequency bin, the beamforming map was obtained by computing steering vectors for various assumed source locations in the x-y plane (e.g., -0.5 m to 0.5 m along the x-axis and 0.1 to 1.1 m along the y-axis). The sound pressure level (SPL) spectrum was obtained from the maximum values of the beamforming maps in the various frequency bins.

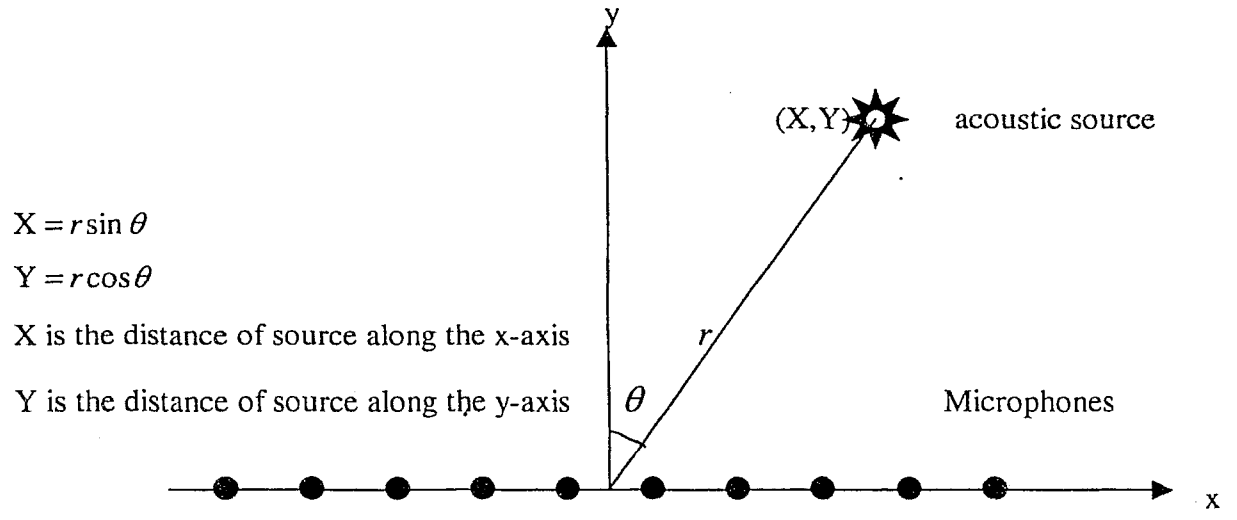

Figure 3.30: Depiction of Uniform Linear Array with a near field source.

The following parameters were chosen for the sensitivity analysis in this case.

- Number of microphones ($N \rightarrow 8$ to 48).
- Signal frequency ($f \rightarrow 500$ to 3000 Hz).
- Source position.
- Inter-microphone distance (d).

3.3.1 Effect of number of microphones (N) and source signal frequency (f)

The number of microphones and the signal frequency are the key parameters in beamforming, as shown by the ULA far field beamforming results (section 3.2). In this sub-section the effect of these parameters on ULA near field beamforming results was examined. The spherical wave was generated at different frequencies ranging from f=500 Hz to f=3000 Hz, and the number of microphones (N) was varied from 8 to 48. The acoustic source was placed at X=0 m, Y=0.5 m.

The beamforming maps (3D and 2D plots) for f=500 Hz and f=3000 Hz with N=8 are presented in Figures 3.31 and 3.32. The corresponding plots of the array power along the x and y axes are presented in Figure 3.33. The beamforming maps (3D and 2D plots) for f=500 Hz and f=3000 Hz with N=48 are presented in Figures 3.34 and 3.35. The corresponding plots of the array power along the x and y axes are presented in Figure 3.36. Figure 3.37 shows the

sound pressure level (SPL) spectra for f=500 Hz and f=3000 Hz with N=8 and N=48. The beamwidth and the dynamic range were obtained from the various beamforming maps for different frequencies from 500 Hz to 3000 Hz with different array apertures. The beamwidth, the array resolution, the error band and the dynamic range are summarized in Table 3.5. It should be noted that the array resolution is not the same along the x-axis and the y-axis, and the array power is portrayed in two different plots [e.g., see Figure 3.33 (a & b)]. It should also be noted that the ellipses in the 2D beamforming maps [see Figure 3.34 (b)] represent slices of the 3D maps taken at -3 dB below the peaks of the mainlobe. The plots of the array resolution along the x-axis and the y-axis versus frequency for various array apertures are presented in Figures 3.38 and 3.39.

With N=8, when the signal frequency is 500 Hz, the mainlobe width is large along the x-axis and infinite along the y-axis, and the dynamic range cannot be defined [Figure 3.31 and 3.33]. The associated error band is ± 0.5 m (corresponding to about ± 50 %) with respect to the x-axis and infinite with respect to the y-axis [Table 3.5 (a) & (b)]. Therefore, the source localization capability of a ULA is very poor under these circumstances. When the signal frequency increases to 3000 Hz, the mainlobe width is reduced and the dynamic range can be defined along the x-axis but not along the y-axis [Figure 3.32 and 3.33]. With respect to the x-axis, the associated error band is reduced to ± 0.058 m (corresponding to about ± 5.8 %) and the array dynamic range is 10.71 dB. But with respect to the y-axis the error band is still infinite [Table 3.5 (a) & (b)]. It can be seen from Figure 3.37 (a) that the frequency resolution of the spectra is very good for both f=500 Hz and f=3000 Hz.

With N=48, when the signal frequency is 500 Hz, the error is ± 0.128 m (corresponding to about ± 13 %), which is satisfactory, and the dynamic range is 6.65 dB with respect to the x-axis; the error band is ± 0.414 m (corresponding to about ± 42 %), which is not satisfactory, and the dynamic range cannot be defined along the y-axis [Figure 3.34 & 3.36 and Table 3.5 (g) & (h)]. When the signal frequency increases to 3000 Hz, the x-axis and y-axis error bands reduce to ± 0.021 m (± 2.1 %) and ± 0.072 m (± 7.2 %) respectively, both of which are satisfactory; also, the x-axis and y-axis dynamic ranges are 6.65 dB and 9.45 dB respectively [Figure 3.35 & 3.36 and Table 3.5 (g) & (h)]. Notice that the frequency resolution of the spectra for f=500 Hz and f=3000 Hz remains very good [Figure 3.37(a)].

It can be seen from Figures 3.38 and 3.39 that the array resolution increases (i.e., the error decreases) essentially linearly as the signal frequency increases for any array aperture (greater than some threshold value, which depends on the frequency range and the axis under consideration); also, this resolution increases progressively as the aperture increases for any given frequency. It should be noted from the results in Table 3.5 that, once sidelobes are present in the beamforming maps, the array dynamic range is independent of frequency; moreover, it decreases as the number of microphones increases. For instance, when the results for N=8, f=3000 Hz [Table 3.5 (a)] are compared to those for N=48, f=3000 Hz [Table 3.5 (g)], the dynamic range with respect to the x-axis is degraded by about 4 dB. This is entirely consistent with theoretical array pattern results (see Appendix B, Figure B.8).

The results of this sub-section serve to demonstrate that the source localization capability of the ULA with a near field source is poor for low source signal frequencies when the array aperture is small; however, this capability can be improved by increasing the aperture. When the array aperture is constant, as the signal frequency increases, the array resolution increases but the dynamic range remains the same (once sidelobes are present in the beamforming maps). When the signal frequency is constant, as the aperture increases, the array resolution increases but the dynamic range decreases. The frequency resolution of the source signal spectrum is independent of both the signal frequency and the number of microphones.

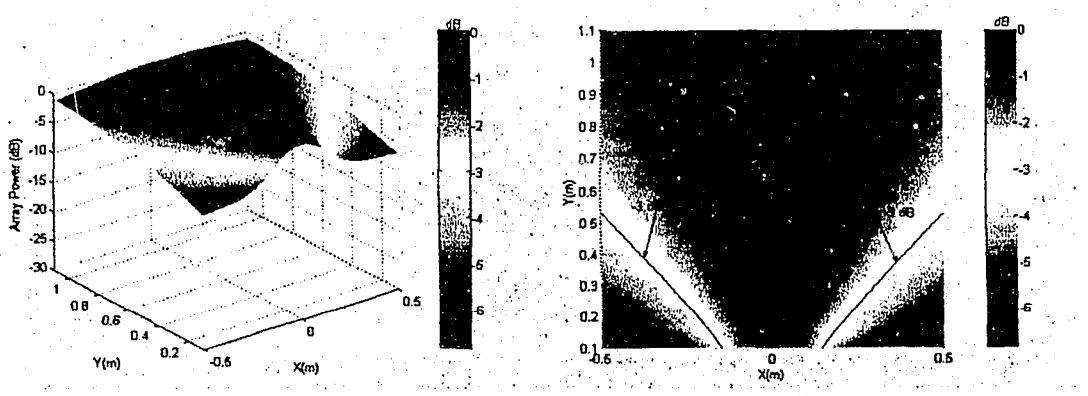

(a) (b)

Figure 3.31: Beamforming results for N=8, f= 500 Hz; (a) Beamforming map: 3D plot (b) Beamforming map: 2D plot.

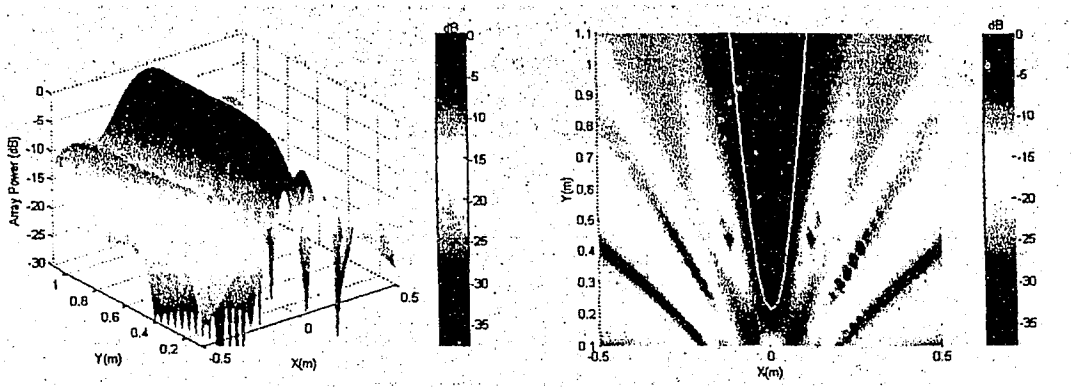

(a) (b)

Figure 3.32: Beamforming results for N=8, f= 3000 Hz; (a) Beamforming map: 3D plot (b) Beamforming map:2D plot (line at -3 dB).

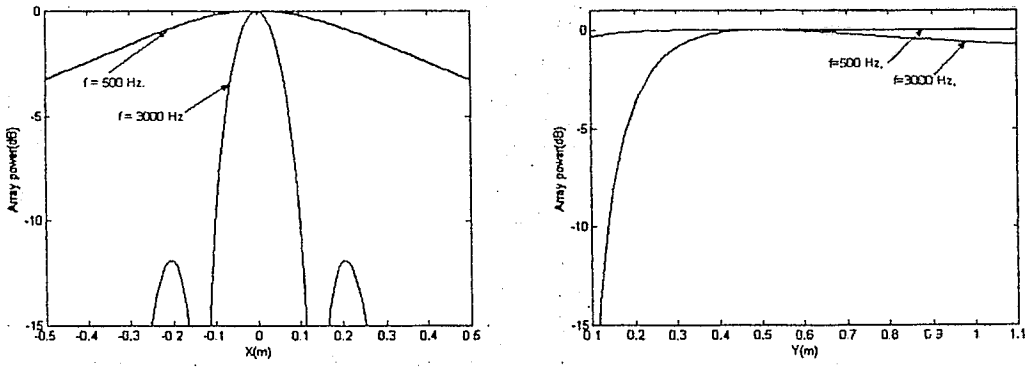

(a) (b)

Figure 3.33: Beamforming results for N=8; (a) Array power along x-axis for f =500 Hz and 3000 Hz (b) Array power along y-axis for f=500 Hz and 3000 Hz.

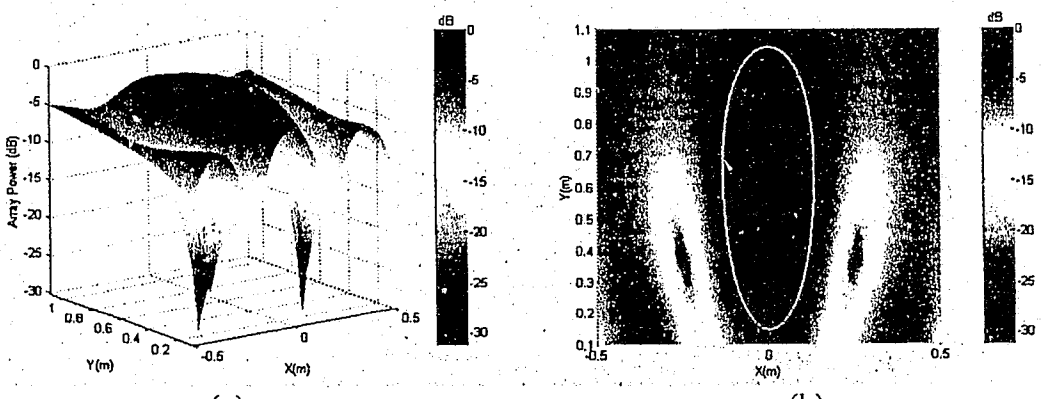

(a) (b)

Figure 3.34: Beamforming results for N=48, f= 500 Hz; (a) Beamforming map: 3D plot (b) Beamforming map: 2D plot (ellipse at -3 dB).

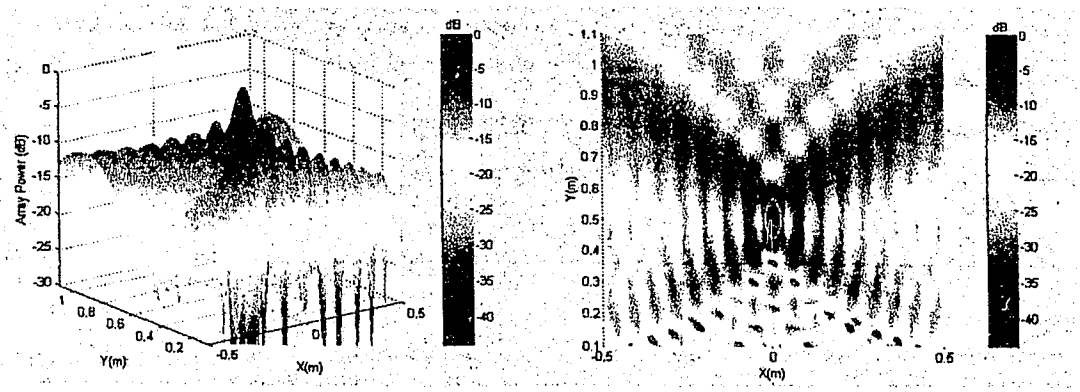

(a) (b)

Figure 3.35: Beamforming results for N=48, f= 3000 Hz; (a) Beamforming map: 3D plot (b) Beamforming map: 2D plot (ellipse at -3 dB).

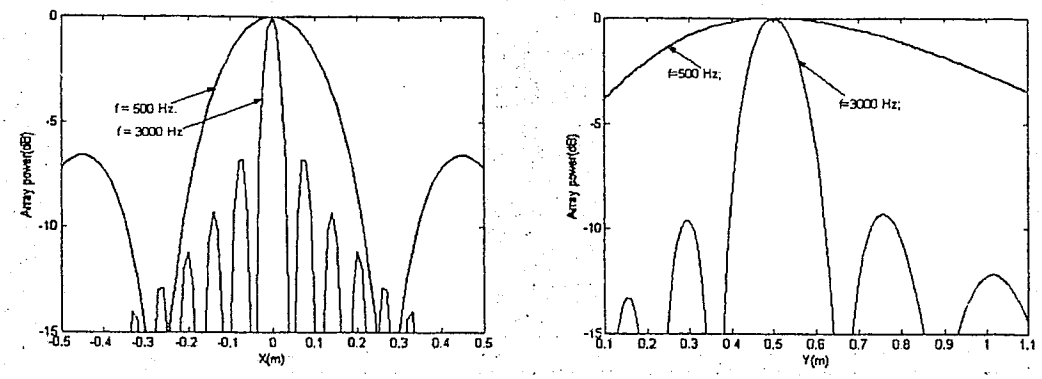

(a) (b)

Figure 3.36: Beamforming results for N=48; (a) Array power along x-axis for f =500 Hz and 3000 Hz (b) Array power along y-axis for f=500 Hz and 3000 Hz.

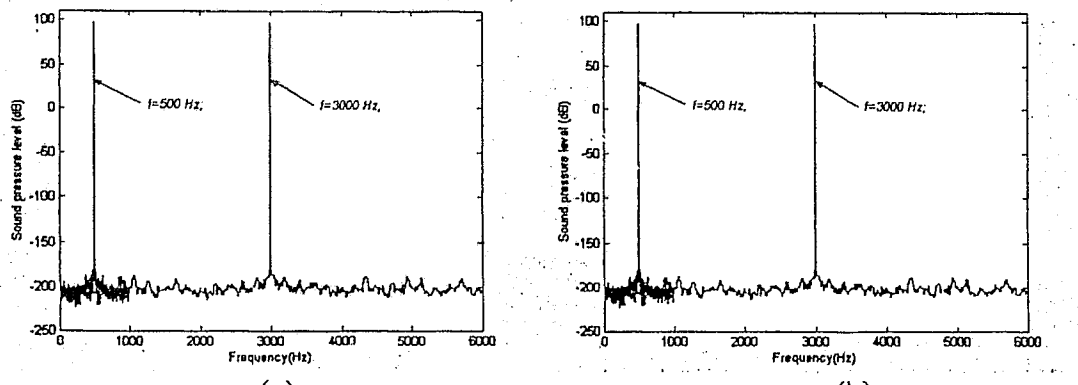

(a) (b)

Figure 3.37: (a) SPL spectrum for f= 500 Hz and 3000 Hz, with N=8, (b) SPL spectrum for f= 500 Hz and 3000 Hz, with N=48.

Table 3.5 Effect of number of microphones (N) and signal frequency (f)

(a) N=8

Array resolution, error band and the dynamic range along the x-axis

Frequency (Hz)	Beamwidth (m)	Resolution (1/m)	Error band (m.)	Dynamic range (dB)
500	1.0	1.0	± 0.50	N.A.
1000	0.4.	2.5	± 0.20	N.A.
1500	0.263	3.80	± 0.13	10.71
2000	0.20	5.00	± 0.10	10.71
2500	0.153	6.59	± 0.076	10.71
3000	0.117	8.55	: 0.058	10.71

(b) N=8

Array resolution, error band and the dynamic range along the y-axis

Frequency (Hz)	Beamwidth (m)	Resolution (1/m)	Error band (m)	Dynamic range (dB)
500	∞	0	∞	N.A.
1000	∞	0	∞	N.A.
1500	∞	0	∞	N.A.
2000	∞	0	∞	N.A.
2500	∞	0	∞	N.A.
3000	∞	0	∞	N.A.

(c) N=16

Array resolution, error band and the dynamic range along the x-axis

Frequency (Hz)	Beamwidth (m)	Resolution (1/m)	Error band (m)	Dynamic range (dB)
500	0.472	2.12.	± 0.236	N.A.
1000	0.236.	4.237	± 0.118	10.23
1500	0.144	6.94	± 0.072	10.23
2000	0.108	9.25	± 0.054	10.23
2500	0.090	11.11	± 0.045	10.23
3000	0.072	13.88	± 0.036	10.23

-Table 3.5 continued-

(d) N=16

Array resolution, error band and the dynamic range along the y-axis

Frequency (Hz)	Beamwidth (m)	Resolution (1/m)	Error band (m)	Dynamic range (dB)
500	∞	0	∞	N.A.
1000	∞	0	∞	N.A.
1500	0.846	1.1820	± 0.423	N.A.
2000	0.702	1.4245	± 0.351	N.A.
2500	0.504	1.9841	± 0.252	10.23
3000	0.414	2.4154	± 0.207	10.23

(e) N=32

Array resolution, error band and the dynamic range along the x-axis

Frequency (Hz)	Beamwidth (m)	Resolution (1/m)	Error band (m)	Dynamic range (dB)
500	0.308	3.246	± 0.154	8.0
1000	0.144	6.945	± 0.072	8.0
1500	0.099	10.10	± 0.495	8.0
2000	0.072	13.88	± 0.036	8.0
2500	0.058	17.24	± 0.290	8.0
3000	0.049	20.20	± 0.024	8.0

(f) N=32

Array resolution, error band and the dynamic range along the y-axis

Frequency (Hz)	Beamwidth (m)	Resolution (1/m)	Error band (m)	Dynamic range (dB)
500	1.1	0.909.	± 0.55	N.A.
1000	0.558	1.792	± 0.279	N.A.
1500	0.378	2.645	± 0.189	N.A.
2000	0.279	3.584	± 0.139	9.75
2500	0.216	4.629	± 0.108	9.75
3000	0.18	5.550	± 0.09	9.75

-Table 3.5 continued-

(g) N=48

Array resolution, error band and the dynamic range along the x-axis

Frequency (Hz)	Beamwidth (m)	Resolution (1/m)	Error band (m)	Dynamic range (dB)
500	0.256	3.90	± 0.128	6.65
1000	0.130	7.692	± 0.065	6.65
1500	0.085	11.76	± 0.042	6.65
2000	0.065	15.38	± 0.032	6.65
2500	0.050	20.00	± 0.025	6.65
3000	0.042	23.80	± 0.021	6.65

(h) N=48

Array resolution, error band and the dynamic range along the y-axis

Frequency (Hz)	Beamwidth (m)	Resolution (1/m)	Error band (m)	Dynamic range (dB)
500	0.828	1.21	± 0.414	N.A.
1000	0.432	2.31	± 0.216	9.45
1500	0.279	3.58	± 0.139	9.45
2000	0.216	4.68	± 0.108	9.45
2500	0.162	6.17	± 0.081	9.45
3000	0.144	6.95	± 0.072	9.45

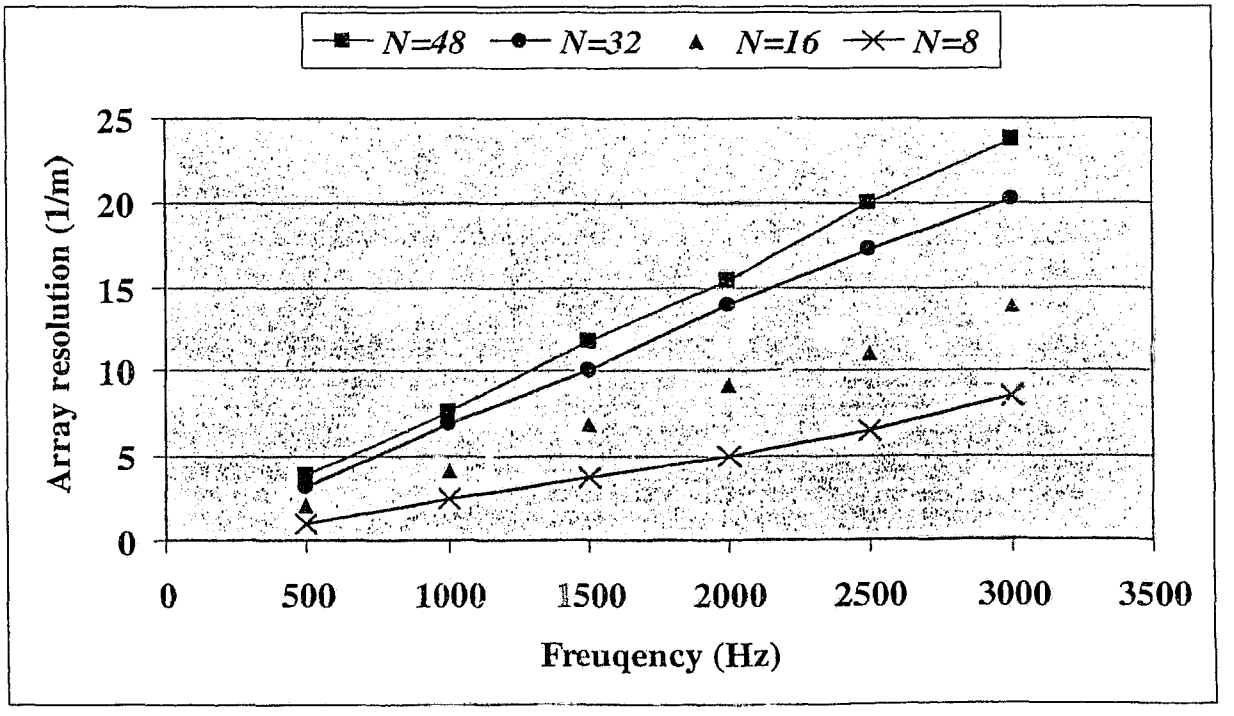

Figure 3.38: Effect of signal frequency and microphones on array resolution along x-axis.

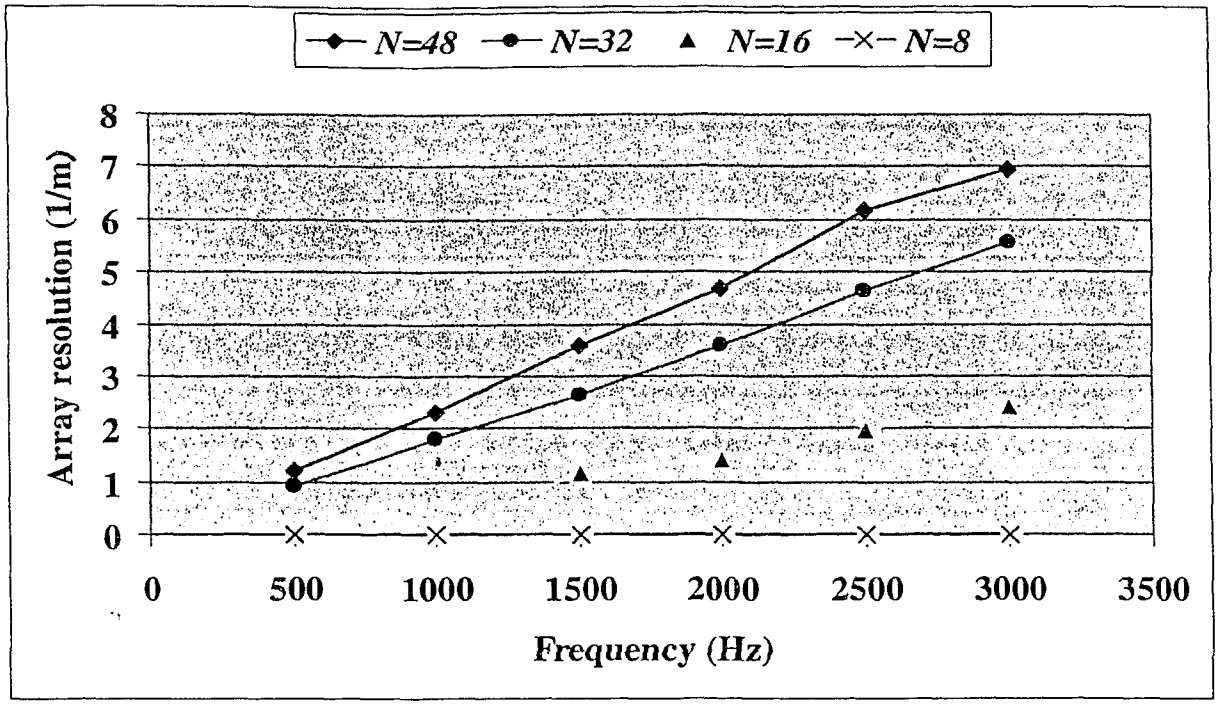

Figure 3.39: Effect of signal frequency and microphones on array resolution along y-axis.

3.3.2 Effect of source position

As mentioned before, in certain situations, aeroacoustic sources can be located near to a microphone array. These sources can be placed at various positions with respect to the array centre or the reference microphone. The source position affects the array resolution as shown in subsection 3.2.5 for a ULA with a far field source. The purpose of this sub-section was to determine the impact of the source position (in an x-y plane) on ULA near field beamforming results. Two cases were considered. For the first case, the source was placed at different positions along the x-axis varying from X= -0.4 m to X=0.4 m with the y-axis position fixed at Y= 0.5 m; the signal frequency was 2500 Hz, and 24 microphones were used. For the second case, the source was placed at different positions along the y-axis from Y=0.25 m to Y=25 m with the x-axis position fixed at X=0 m; the signal frequency was 3000 Hz, and 32 microphones were used.

Figures 3.40 and 3.41 depict the beamforming maps (2D plots) and the array power along the x-axis and the y-axis for X=-0.4 m and X=0 m with Y=0.5 m. Figures 3.42 and 3.43 depict the beamforming maps (2D plots) and the array power along the x-axis and the y-axis for Y=0.25 m and Y=1.5 m with X=0 m. Figures 3.44 and 3.45 show the beamforming maps (3D

and 2D plots) and array power plots for Y=25 m with X=0 m. The array resolution and the dynamic range were obtained from the beamforming maps and are summarized in Figures 3.46-3.49. Note that the ellipses in the beamforming maps (2D plots) represent slices of the 3D maps taken at -3 dB below the peaks of the mainlobes.

For the first case, when the source is placed at X=-0.4 m with Y=0.5 m, the error band is ± 0.0405 m (± 4 %) and the dynamic range is 5.87 dB with respect to the x-axis; also, the error band is ± 0.090 m (± 9 %) and the dynamic range is 6.65 dB with respect to the y-axis [Figure 3.40(a) and 3.41]. When the source is moved to X=0 m (so that it is perpendicular to the array centre), the x-axis error band decreases to ± 0.0315 m (± 3 %) and the dynamic range increase to 7 dB; also, the y-axis error band increases to ± 0.1351 m (± 13.5 %) and the dynamic range increases to 10.9 dB. [Figure 3.40 (b) and 3.41].

Figures 3.46 and 3.47 show the variation of the array resolution and the dynamic range when the source moves from X=-0.4 m to X=0.4 m. The dynamic ranges along the x-axis and the y-axis are maxima when the source is at X=0 m. The array resolution along the x-axis is also maximum at this position, but the array resolution along the y-axis is minimum. It should be noted that the array resolution is calculated from the array power plots (Figure 3.41), which are obtained by slicing the 3D beamforming plots along the x-axis and the y-axis. When X=-0.4 m [Figure 3.40(a)], the resolution ellipse is tilted so that the correct values of the array resolution based on the ellipse axes can not be calculated from the array power plots. This is also the case for any $X \neq 0$. In the beamforming 2D maps, the diameters of the ellipse change from 1.6 mm and 3.5 mm to 1.2 mm and 3.0 mm with the movement of the source from X=-0.4 m to 0 m [Figure 3.40 (a) & (b)]. Clearly, the correct array resolutions increase when the ellipse diameters decrease. Therefore, the array resolution is maximum when the source is at X=0 m (i.e., perpendicular to the array centre).

For the second case, when the source is placed at Y=0.25 m with X=0 m, the error band is ± 0.018 m (± 1.8 %) and the dynamic range is 3.5 dB along the x-axis; also, the error band is ± 0.036 m (± 3.6 %) and the dynamic range is 9.2 dB along the y-axis [Figures 4.42 (a) and 4.43]. When the source is moved to Y=1.5 m, x-axis error band increases to ± 0.055 m (± 5.5 %) and the x-axis dynamic range increases to 10.85 dB; also, the y-axis error band increases to

± 0.20 m (± 20 %) and the y-axis dynamic range increases to 9.4 dB [Figures 4.42 (b) and 4.43].

As the source moves from Y=0.25 m to 1.75 m, both the x-axis array resolution and the y-axis array resolution decrease non-linearly (Figure 3.48); also, the x-axis array dynamic range increases but the y-axis dynamic range remains essentially constant (Figure 3.49).

When the source is placed at X=0 m and Y=25 m, the x-axis error band is ± 0.054 m (± 5.4 %), and the mainlobe has no variation along the y-axis (Figure 3.44 and 3.45); also the x-axis dynamic range is 13 dB. It is evident from these results that near field beamforming characteristics change to far field beamforming characteristics when an acoustic source is placed sufficiently far from an array, with the mainlobe varying only along the x-axis.

The results of this sub-section serve to demonstrate the following: (i) the maximum array resolution is obtained when an acoustic source is perpendicular (i.e., broadside) to the centre of a ULA, (ii) to improve the array resolution , the source should be near to the microphone array, (iii) to improve the array dynamic range, the source should be far from the array, and (iv) a spherical wave front changes to a planar wave front when a source is sufficiently far from the array.

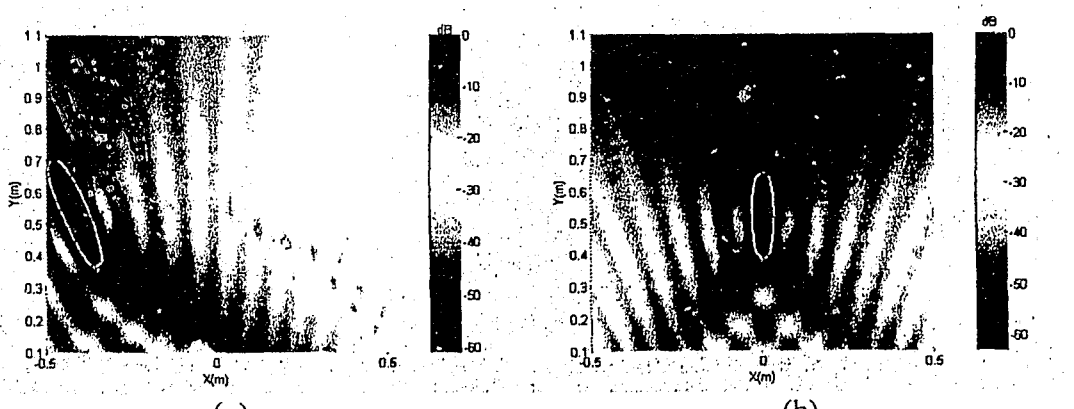

(a) (b)

Figure 3.40: Beamformimg results; (a) Beamforming map: 2D plot, for X= -0.4 m with Y=0.5 m (b) Beamforming map: 2D plot, for X=0 m with Y=0.5 m.

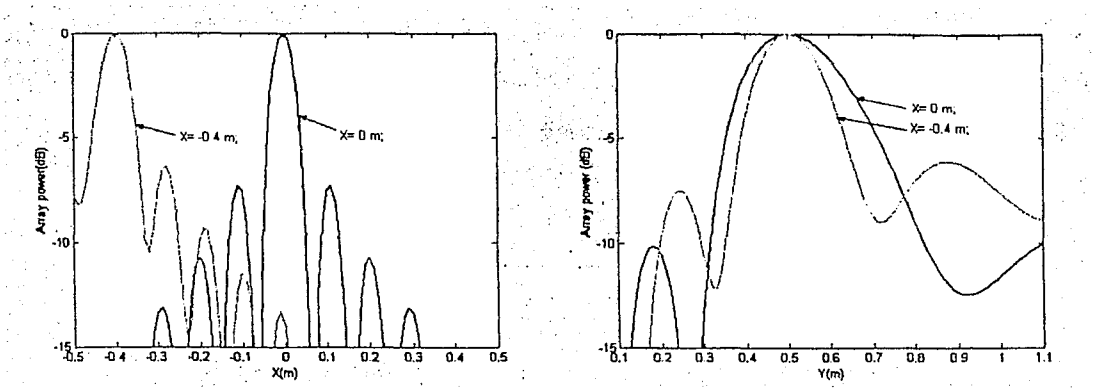

(a) (b)

Figure 3.41: Beamforming results; (a) Array power along x-axis for X=-0.4 m and X=0 m with Y=0.5 m (b) Array power along y-axis at X= -0.4 m and X=0 m with Y=0.5 m.

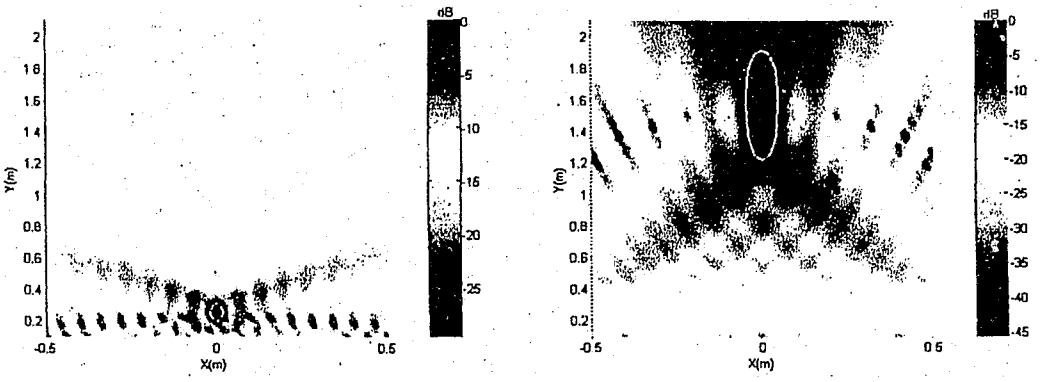

(a) (b)

Figure 3.42: Beamforming results; (a) Beamforming map: 2D plot for X=0 m with Y=0.25 m (b) Beamforming map: 2D plot for X=0 m with Y=1.5 m.

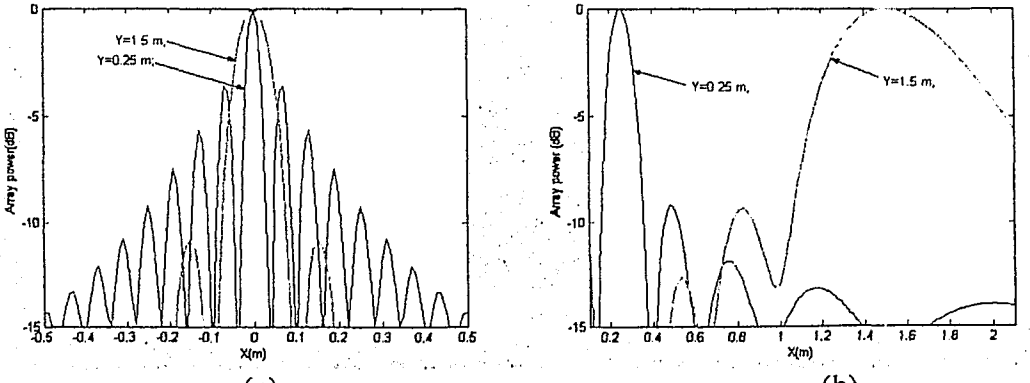

(a) (b)

Figure 3.43: Beamforming results; (a) Array power along the x-axis for Y=0.25 m, Y=1.5 m (X=0 m) (b) Array power along the y-axis for Y=0.25 m, Y=1.5 m (X=0 m).

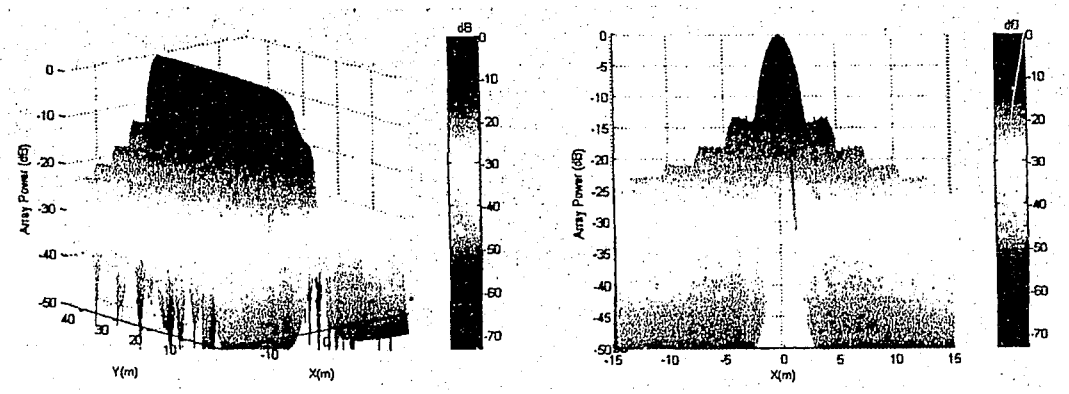

(a) (b)

Figure 3.44: Beamforming results for X=0 m and Y=25 m; (a) Beamforming map: 3D plot (b) Array power versus x-axis: 2D plot.

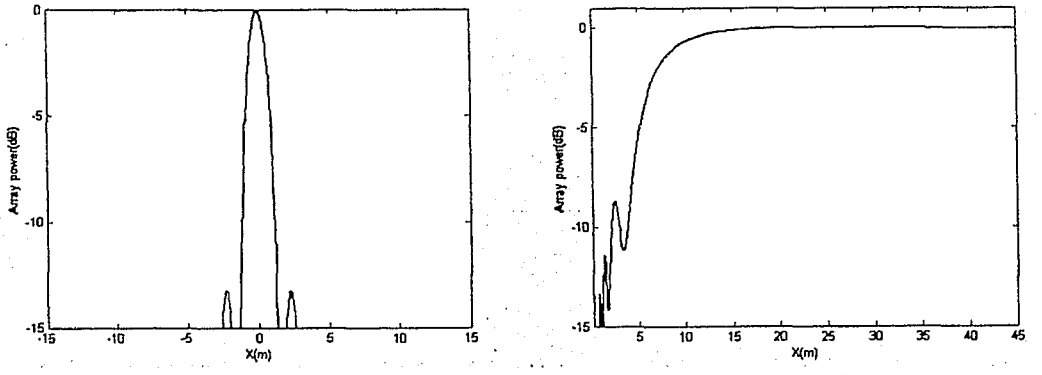

(a) (b)

Figure 3.45: Beamforming results for X=0 m and Y=25 m; Array power along the x-axis (b) Array power along the y-axis.

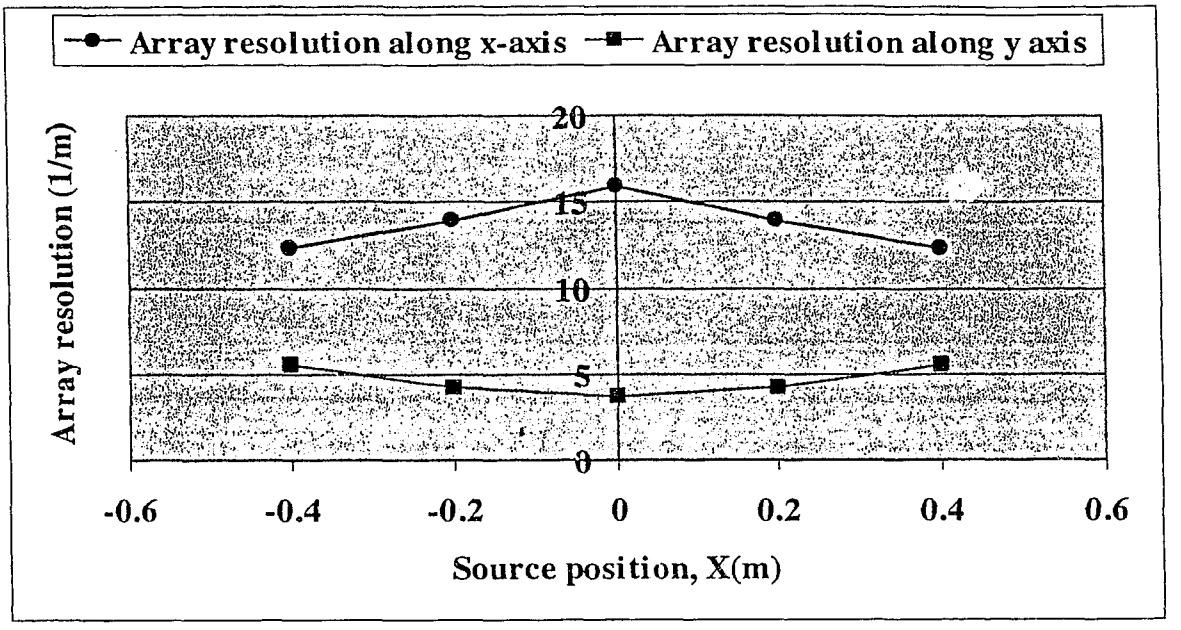

Figure 3.46: Effect of source variation on array resolution; (X=-0.4 m to X=0.4 m with Y=0.5 m).

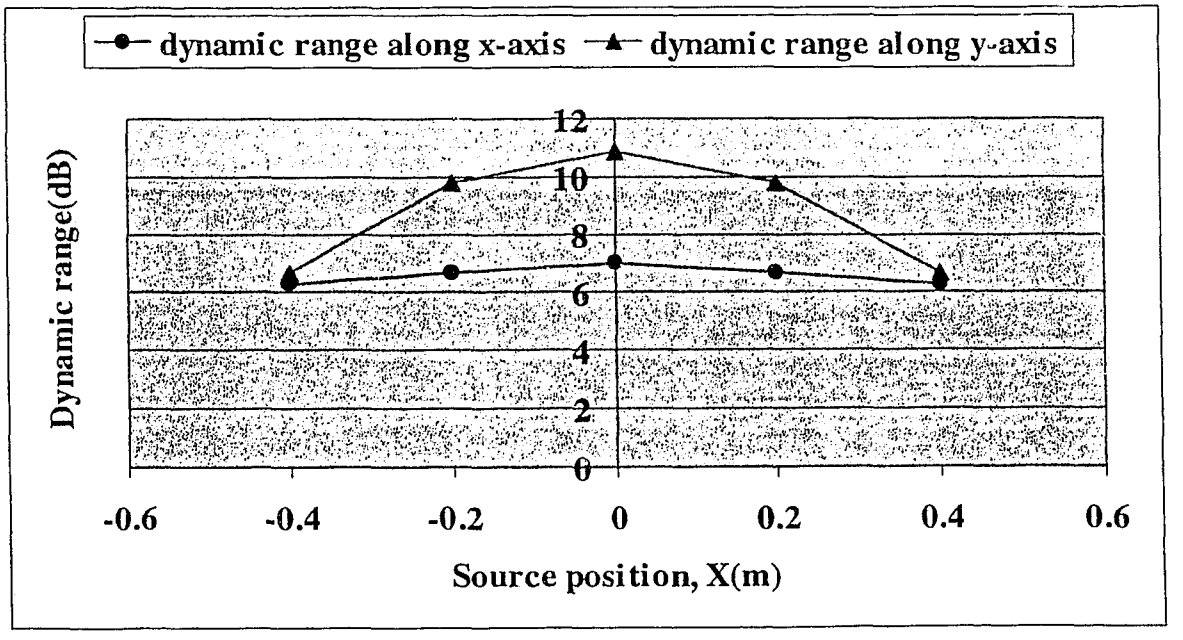

Figure 3.47: Effect of source variation on dynamic range; (X=-0.4 m to X=0.4 m with Y=0.5 m).

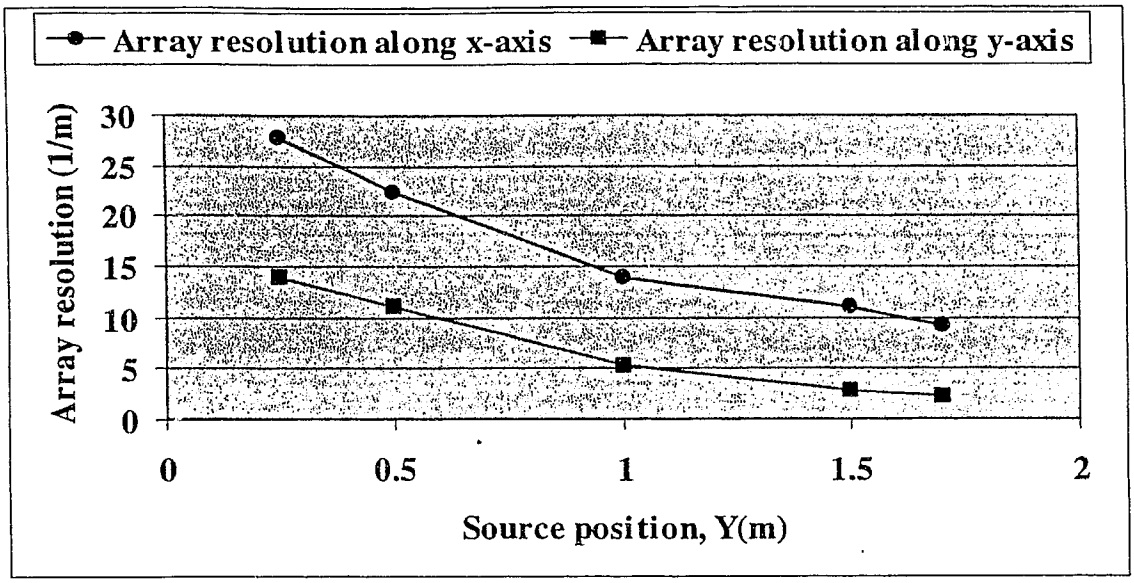

Figure 3.48: Effect of source variation on array resolution; (Y= 0.25 m to Y=1.7 m with X=0 m).

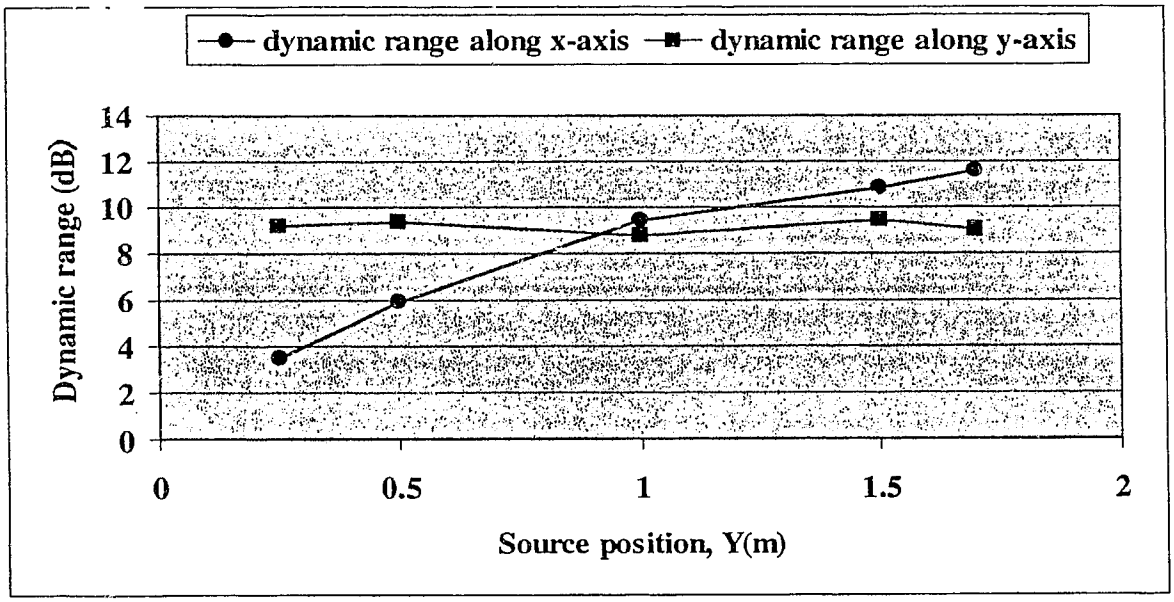

Figure 3.49: Effect of source variation on dynamic range; (Y= 0.25 m to Y=1.7 m with X=0 m).

3.3.3 Effect of inter-microphone distance (*d*)

The inter-microphone distance has an impact on beamforming, as shown in subsection 3.2.4 for the ULA with a far field source. The purpose of this sub-section was to investigate the effect of inter-microphone distance (*d*) on a ULA with a near field source. For this purpose, the

spherical wave was generated at f=3000 Hz. The number of microphones was 20, and the source was located at X=0 m and Y=0.5 m. The inter-microphone distance was changed from $8d^*$ (0.4568 m) to $d^*/2$ (0.0285 m), where d^*=0.0571 m is the distance based on Shannon's criterion, i.e., $d^*=\lambda/2$.

Figures 3.50 and 3.51 show the beamforming maps (3D and 2D plots) and the plots of the array power along the x and y axes for $d=8d^*$. Figures 3.52 and 3.53 show the beamforming maps (3D and 2D plots) and the plots of the array power along the x and y axes for $d=d^*$. Figures 3.54 and 3.55 presents the beamforming maps (3D and 2D plots) and the plots of the array power along the x and y axes for $d=d^*/2$.

Clearly, there are several dominant lobes in the beamforming maps when $d=8d^*$ (Figures 3.50 and 3.51) and this makes the beamforming method futile. When the inter-microphone distance is changed to $d=d^*$, satisfying the Shannon's criterion, there are no ambiguous lobes (Figures 3.52 and 3.53).

When the inter-microphone distance is further reduced to $d=d^*/2$, the dynamic range increases but the array resolution degrades (Figures 3.54 and 3.54). It is noted that the diameters of the resolution ellipse increases, as shown in Figures 3.52 (b) and 3.54 (b). Therefore, the overall source localization capability of the microphone array decreases.

From these results, it can be concluded that the distance between microphones should be $\leq d^*$ to avoid grating lobes; moreover, to obtain the maximum array resolution, the distance between microphones should be d^*. (In practice, d is fixed at d^* for a specific application with a given array design.)

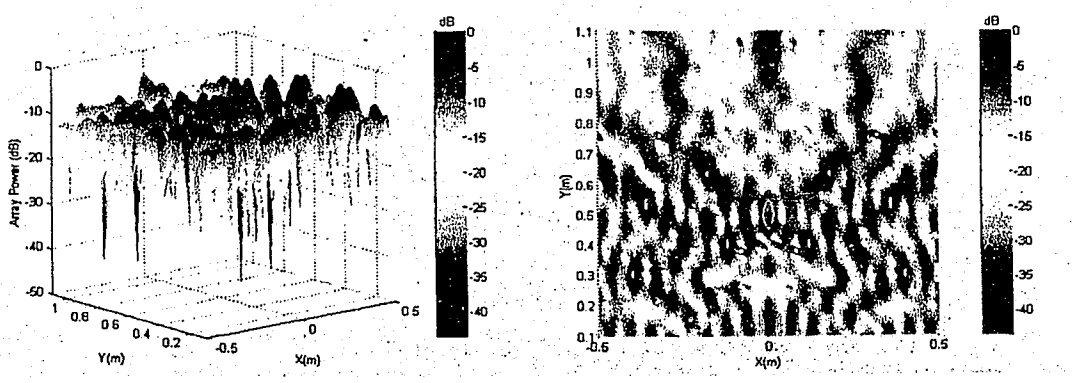

(a) (b)

Figure 3.50: Beamforming results for N=20, f=3000 Hz, $d=8d^*$;
(a) Beamforming map: 3D plot (b) Beamforming map: 2D plot.

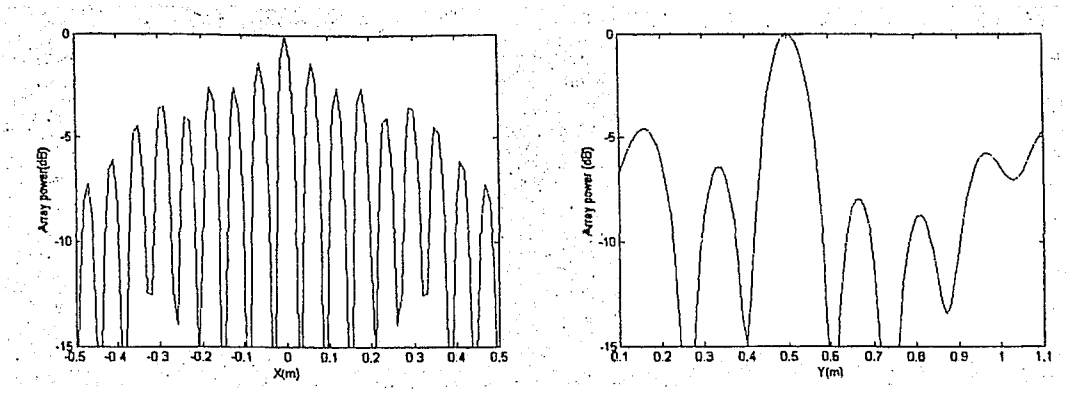

(a) (b)

Figure 3.51: Beamforming results for N=20, f=3000 Hz, d=δd*;
(a) Array power along the x-axis (b) Array power along the y-axis

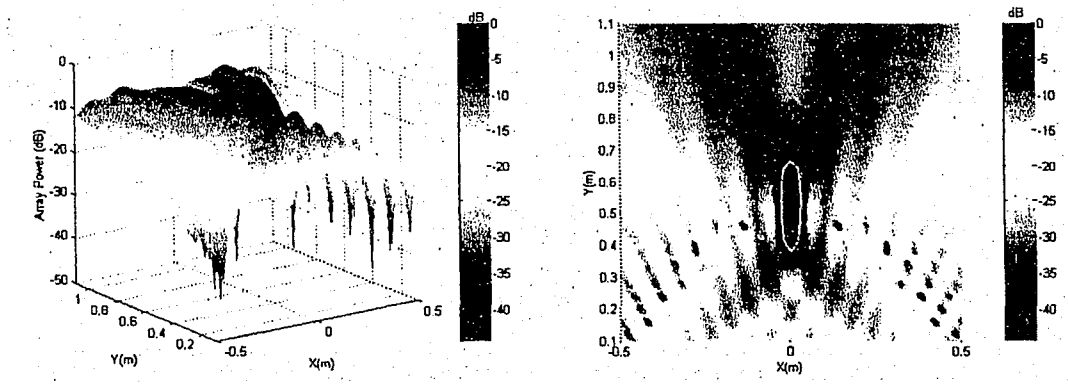

(a) (b)

Figure 3.52: Beamforming results for N=20, f=3000 Hz, d=d*;
(a) Beamforming map: 3D plot (b) Beamforming map: 2D plot.

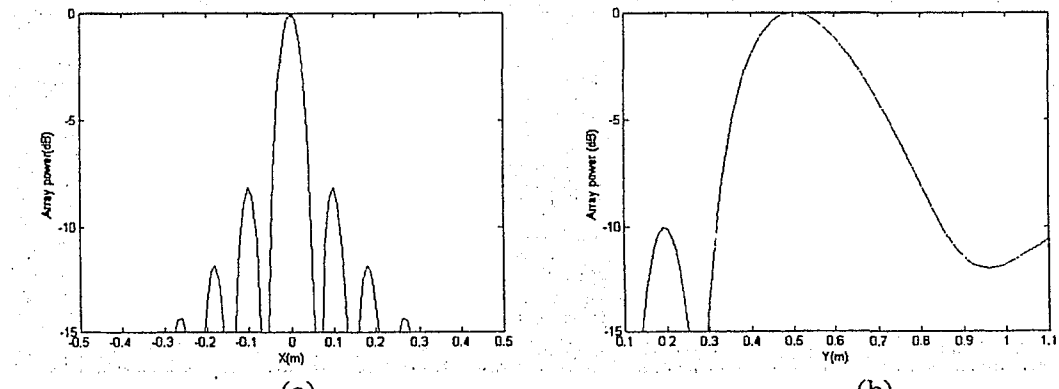

(a) (b)

Figure 3.53: Beamforming results for N=20, f=3000 Hz, d=d*;
(a) Array power along the x-axis. (b) Array power along the y-axis.

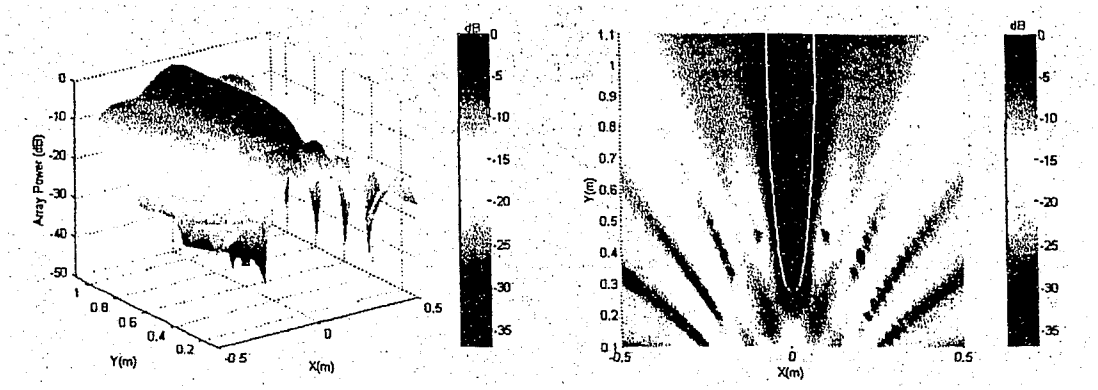

(a) (b)

Figure 3.54: Beamforming results for N=20, f=3000 Hz, d=d*/2;
(a) Beamforming map: 3D plot (b) Beamforming map: 2D plot.

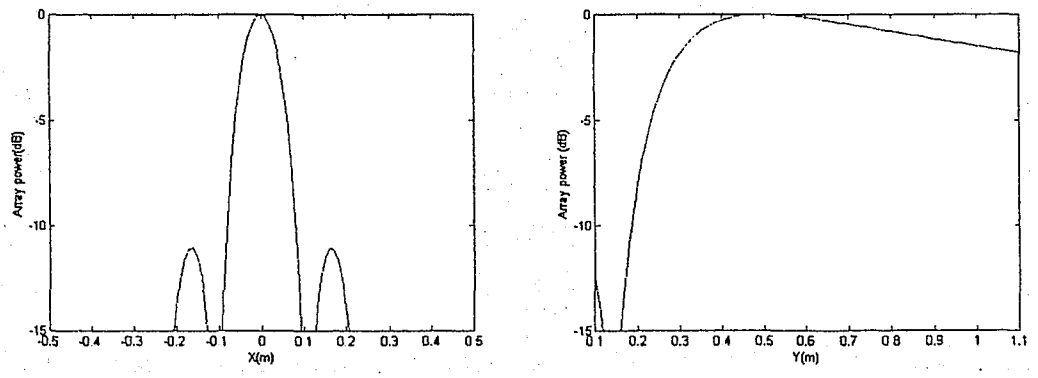

(a) (b)

Figure 3.55: Beamforming results for N=20, f=3000 Hz, d=d*/2;
(a) Array power along the x-axis (b) Array power along the y-axis.

In the above section (3.3), a sensitivity analysis of a uniform linear array (ULA) with a near field source has been carried out. In the next section, a sensitivity analysis of the uniform planar array (UPA) with a near field source is presented.

3.4 Uniform Planar Array – near field beamforming

In the case of a uniform planar array, the microphones are placed in a plane (i.e., the x-y plane), as depicted in Figure 2.6. The microphones can be arranged in any geometry, such as, a uniform square array, a uniform rectangular array, or a cross array. The purpose of this section was to examine beamforming results pertaining to a uniform planar array with a near field source. A uniform square array (USA) was chosen, with the microphones placed in a square geometry at a constant distance between each other. The USA was designed for near field

simulated signals with a maximum frequency of 8000 Hz. The inter-microphone spacing was set at 2.15 cm to satisfy Shannon's theorem. The signals at each microphone had an integer number of cycles. Each block of data for the digital signals contained 1024 points, i.e., M=1024, and yielded 513 (M/2+1) frequency bins.

The microphones were placed in x-y plane, and a spherical wave was generated at each microphone location by means of the formula $(A/r_n)\sin[\omega(t-r_n/c)]$, as discussed in section 3.1. For a uniform planar array, the source position can be defined in 3D space by an elevation angle φ, an azimuth angle θ, and a distance r between the array centre and the source. These spherical coordinates can be represented in Cartesian coordinates in terms of X, Y, and Z along the x, y, and z axes respectively. With the array lying in the x-y plane, the source can be localized by considering an x-y plane (i.e., a grid plane) at different locations along the z-axis (i.e., at different grid distances), as depicted in Figure 3.56. The grid plane contains grid points with increments along the x and y axes. The relevant beamforming maps were obtained, at different grid distances, by computing steering vectors for various assumed locations in the x-y plane. The position where the array power is maximum (i.e., where the mainlobe appears) in the grid plane corresponds to the X-Y location of the source. The position where the array power is maximum along the z-axis represents the Z location of the source.

The parameters chosen for the sensitivity analysis in this case are given below.

- Number of microphones ($N \rightarrow 16,\ 25,\ 36$).
- Signal frequency ($f \rightarrow 2000-8000$ Hz).
- Source position.
- Inter-microphone distance (d).

3.4.1 Effect of number of microphones (N) and source signal frequency (f)

In this sub-section the effect of the number of microphones and the signal frequency on a uniform square array with a near field source was examined. The spherical wave was generated at different frequencies ranging from f=2000 to f=8000 Hz. The number of microphones was varied from 16 (a square array of 4 x 4) to 36 (a square array of 6 x 6). The acoustic source was placed at X=0 m, Y=0 m and Z=0.5 m.

Figures 3.57 and 3.58 show the beamforming maps (3D and 2D plots) for f=3000 Hz and f=8000 Hz with N=16 (4 x 4). Figure 3.59 shows the corresponding array power plots. Figures 3.60 and 3.61 show the beamforming maps (3D and 2D plots) for f= 3000 Hz and f=8000 Hz with N=36 (6 x 6). Figure 3.62 shows the corresponding array power plots. The beamwidth and the dynamic range were obtained from the various beamforming maps for different frequencies ranging from 2000 Hz to 8000 Hz with different array apertures. The beamwidth, the array resolution, the error band and the dynamic range are summarized in Table 3.6. It should be noted that the array resolution (evaluated at -3 dB) is the same along the x and y axes and is plotted only along the x-axis for the beamforming analysis. It should also be noted that the rings in the 2D beamforming maps [see Figure 3.58 (b)] represent slices of the 3D maps taken at -3 dB below the peaks of the mainlobe. A plot of the array resolution versus signal frequency for different array apertures is presented in Figure 3.63.

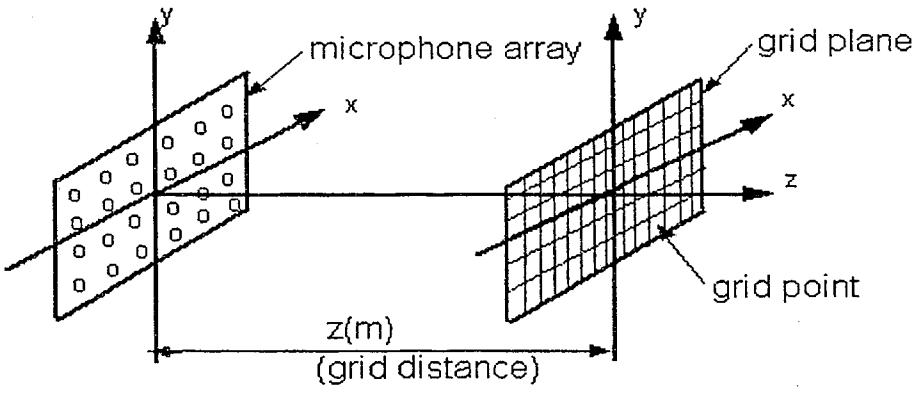

Figure 3.56: Acoustic source localization with a uniform planar array.

With N=16 (4 x 4), when the signal frequency is 3000 Hz, the error band is ± 0.37 m (corresponding to ± 18.5 %) and dynamic range cannot be defined [Figures 3.57 and 3.59 (a)]; therefore, the source localization capability of the uniform square array is poor. When the signal frequency increases to 8000 Hz, the error band is ± 0.117 m (corresponding to ± 5.8 %) and the dynamic range is 11.20 dB [Figures 3.58 and 3.59 (b)]. The values of these evaluators are quite satisfactory for source localization.

With N=36 (6 x 6), when the signal frequency is 3000 Hz, the error band is ± 0.216 m (± 10.8 %), and the dynamic range is more than 15 dB, both of which are satisfactory [Figures 3.60 and 3.62 (a)] (The sidelobes can not be seen in the array power plot because it is truncated at -15 dB). When the signal frequency increases to 8000 Hz, the error band decreases to ± 0.080 m (± 4 %), and the array dynamic range decreases to 12.43 dB, which is still satisfactory [Figures 3.61 and 3.62 (b)].

It can be seen from Figure 3.63 that the array resolution increases essentially linearly with the increase of signal frequency, for any array aperture; also, this resolution increases progressively as the aperture increases (i.e., number of microphones increases) for any given frequency. It should be noted from the results in Table 3.6 that the array dynamic range increases with the increase of number of microphones; moreover, it decreases as the signal frequency increases. For instance, when f=3000 Hz, the array power plot [Figure 3.62 (a)] has a relatively broad mainlobe and sidelobes below -15 dB. As the signal frequency increases to 8000 Hz, the mainlobe becomes sharp with sidelobes at -12.43 dB [Figure 3.62 (b)].

The results of this sub-section indicate that at low frequencies the source localization capability of the uniform square array is poor for small array apertures; however, this capability can be improved by increasing the aperture. When the signal frequency is constant, as the aperture increases, both the array resolution and the dynamic range increase. When the array aperture is constant, as the signal frequency increases, the array resolution increases but the array dynamic range decreases. However, the decrease in the dynamic range is minor, in general (e.g., for N=36 and an increase of frequency from 4000 Hz to 8000 Hz, the decrease is only 0.52 dB).

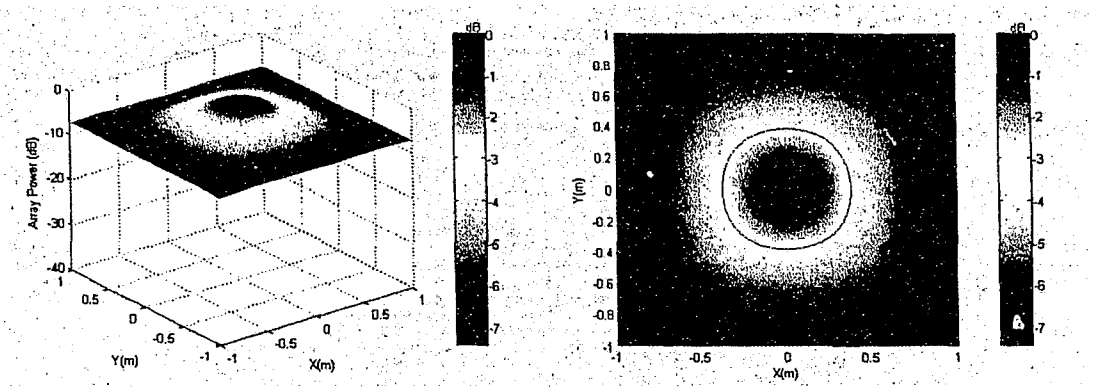

(a) (b)

Figure 3.57: Beamforming results for N=16 (a square array of 4 x 4), f = 3000 Hz; (a) Beamforming map: 3D plot (b) Beamforming map: 2D plot (ring at -3 dB).

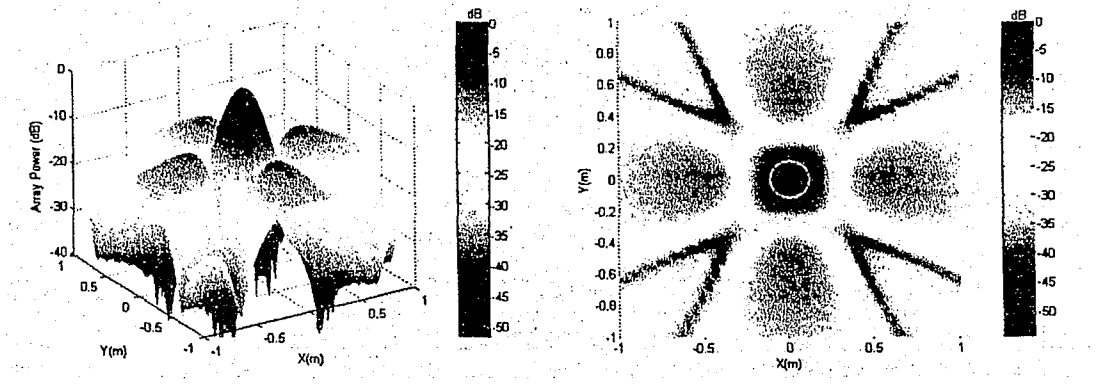

(a) (b)

Figure 3.58: Beamforming results for N=16 (a square array of 4 x 4), f = 8000 Hz; (a) Beamforming map: 3D plot (b) Beamforming map: 2D plot (ring at -3 dB).

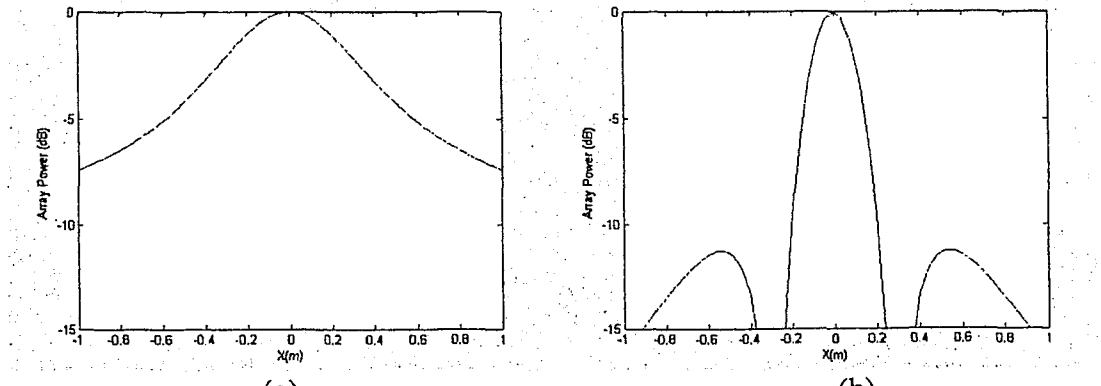

(a) (b)

Figure 3.59: Beamforming results for N=16 (a square array of 4 x 4); (a) Array power along the x-axis for f=3000 Hz (b) Array power along the x-axis for f=8000 Hz.

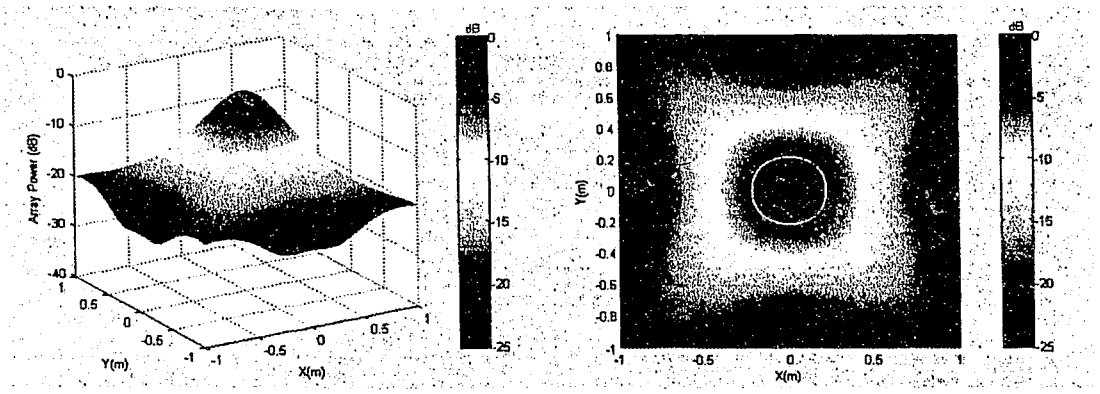

(a) (b)

Figure 3.60: Beamforming results for N=36 (a square array of 6 x 6), f = 3000 Hz; (a) Beamforming map: 3D plot (b) Beamforming map: 2D plot (ring at -3 dB).

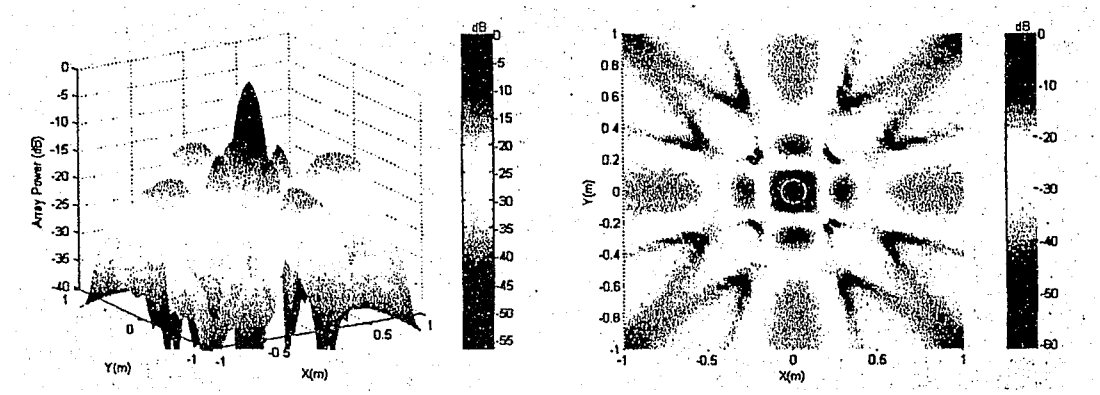

(a) (b)

Figure 3.61: Beamforming results for N=36 (a square array of 6 x 6), f = 8000 Hz; (a) Beamforming map: 3D plot (b) Beamforming map: 2D plot (ring at -3 dB).

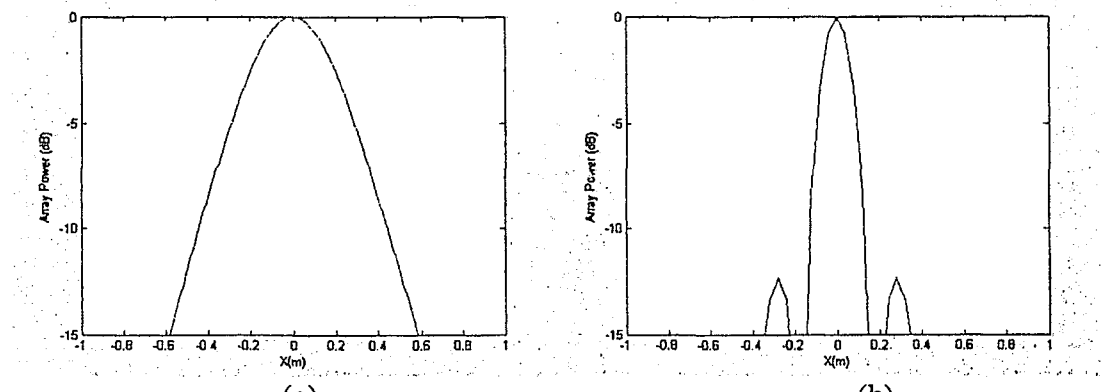

(a) (b)

Figure 3.62: Beamforming results for N=36 (square array of 6 x 6); (a) Array power along the x-axis for f=3000 Hz (b) Array power along the x-axis for f=8000 Hz.

Table 3.6 Effect of number of microphones (N) and source signal frequency (f)

(a) N=16: a square array of 4 x 4

Frequency (Hz)	Beamwidth (m)	Resolution (1/m)	Error band (m)	Dynamic range (dB)
2000	1.98	0.50	± 0.990	N.A.
3000	0.738	1.36	± 0.370	N.A
4000	0.504	1.98	± 0.252	N.A
5000	0.396	2.53	± 0.198	N.A
6000	0.324	3.09	± 0.162	11.32
7000	0.27	3.70	± 0.135	11.25
8000	0.234	4.27	± 0.117	11.20

(b) N=25: a square array of 5 x 5

Frequency (Hz)	Beamwidth (m)	Resolution (1/m)	Error band (m)	Dynamic range (dB)
2000	1.008	0.992	± 0.504	N.A.
3000	0.558	1.79	± 0.279	N.A.
4000	0.378	2.65	± 0.189	N.A.
5000	0.306	3.27	± 0.153	11.94
6000	0.252	3.96	± 0.126	11.62
7000	0.216	4.63	± 0.108	11.53
8000	0.198	5.05	± 0.099	11.40

(c) N=36: a square array of 6 x 6

Frequency (Hz)	Beamwidth (m)	Resolution (1/m)	Error band (m)	Dynamic range (dB)
2000	0.756	1.32	± 0.378	N.A.
3000	0.432	2.31	± 0.216	N.A.
4000	0.324	3.09	± 0.162	12.95
5000	0.252	3.97	± 0.126	12.70
6000	0.216	4.63	± 0.108	12.53
7000	0.18	5.55	± 0.090	12.47
8000	0.162	6.17	± 0.080	12.43

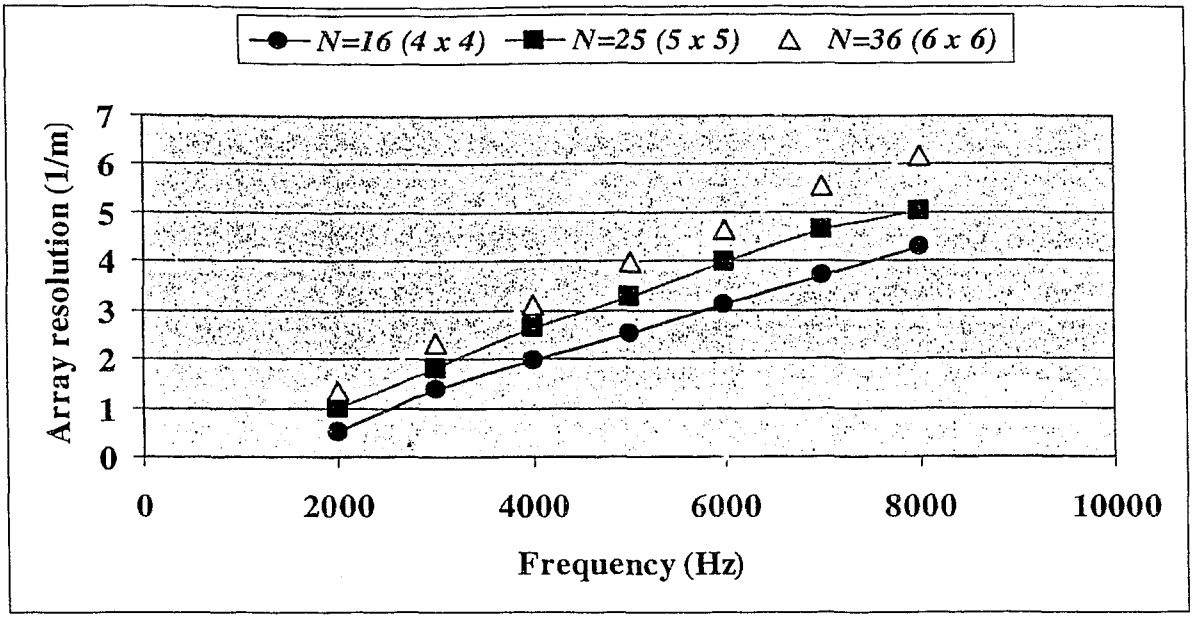

Figure 3.63: Effect of number of microphones and signal frequency on array resolution.

3.4.2 Effect of source position

The purpose of this subsection was to investigate the impact of source position on a uniform square array with a near field source. The spherical wave was generated at a frequency of 6000 Hz, and the number of microphones was 25 (a square array of 5 x 5). The source was placed at different positions along the x-axis varying from X=-0.7 m to X=0.7 m, with the y-axis and z-axis positions fixed at Y=0 m and Z=0.5 m respectively. The source was also placed at different positions along the z-axis from Z=0.25 m to Z=5 m, with the x-axis and the y-axis positions fixed at X=0 m and Y= 0 m respectively.

Figures 3.64 shows the beamforming maps (2D plots) for X=-0.7 m, X= -0.5 m, X=-0.3 m, and X=0 m with Y=0 m, Z=0.5 m. Figure 3.65 shows the array power plots for X=-0.5 m and X=0 m with Y=0 m, Z=0.5 m. Figure 3.66 shows the beamforming maps (2D plots) for Z= 0.25 m, Z=0.5 m, Z=2 m, and Z=5 m with X=0 m, Y= 0 m. Figure 3.67 shows the array power plots for Z=0.25 m and Z=2.0 m with X=0 m, Y= 0 m. The array resolution and dynamic range were obtained from the different array power plots and are summarized in Figures 3.68 - 3.71.

When the source is placed at X=-0.5 m with Y=0 m and Z=0.5 m, the error band is ± 0.31 m (corresponding to ± 8 %) and the dynamic range is 11.9 dB [Figures 3.64 (b) and 3.65 (a)]. When the source is moved to broadside, X=0 m (so that it is perpendicular to the array centre),

the error band is reduced to ± 0.063 m (corresponding to ± 1.6 %) and the dynamic range remains at 11.9 dB [Figures 3.64(d) and 3.65 (b)]. Figures 3.64 (a), (b), (c) and (d) show that as X changes from -0.7 m to 0 m, the array resolution contour changes from an ellipse to a ring.

Figures 3.68 and 3.69 show the variation of the array resolution and the dynamic range when the source moves from X=-0.7 m to X=0.7 m. It is noted that the array resolution is maximum when the source is at X=0 m, and the dynamic range remains constant.

When the source is placed at Z=0.25 m with X=0 m and Y= 0 m, the error band is ± 0.036 m (corresponding to ± 0.9 %) and the dynamic range is 11.9 dB [Figures 3.66(a) and 3.67(a)]. When the source is moved to Z=5 m, the error band increases to ± 0.62 m (corresponding to ± 16 %) and the dynamic range cannot be defined [Figures 3.66(d) and 3.67(b)]. Thus, the source localization capability of the microphone array is degraded.

As the source position along the z-axis increases, the array resolution decreases non-linearly, as shown in Figure 3.70; moreover, the array dynamic range improves in a stepwise fashion, provided that sidelobes exist, as shown in Figure 3.71.

The results of this sub-section demonstrate that the maximum array resolution is obtained when an acoustic source is perpendicular (i.e., broadside) to the centre of a uniform square array. The array source localization capability decreases as the source moves away from the array. Therefore, a model under investigation should always be placed perpendicular to the array centre. However, since the sound generated by various parts of the model would be at different angles with respect to the array centre, it would not be possible to place all the sources at the ideal position.

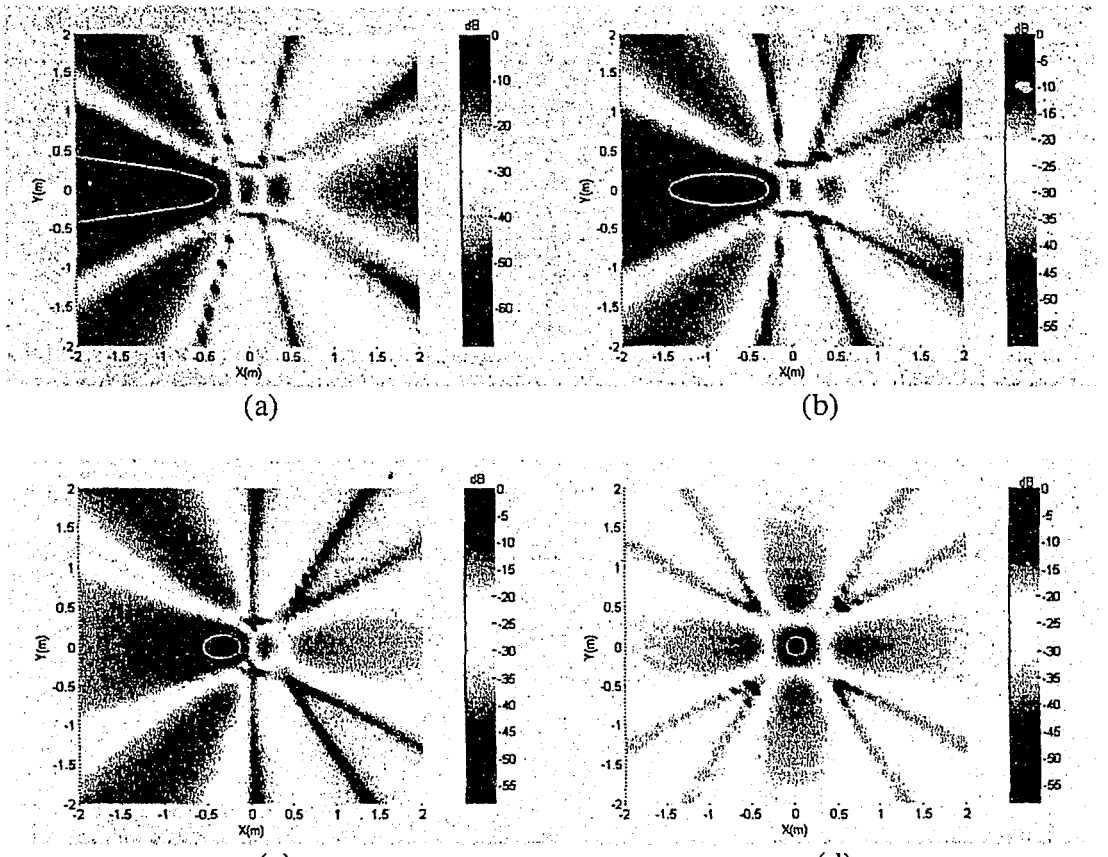

Figure 3.64: Beamforming results for N=25 (5 x 5) and f=6000 Hz; (a) Beamforming map: 2D plot for X=-0.7 m (Y=0 m, Z=0.5 m) (b) Beamforming map: 2D plot for X=-0.5 m, (Y=0 m, Z =0.5 m) (c) Beamforming map: 2D plot for X=-0.3 m (Y=0 m, Z=0.5 m) (d) Beamforming map: 2D plot for X=0 m (Y=0 m, Z=0.5 m)

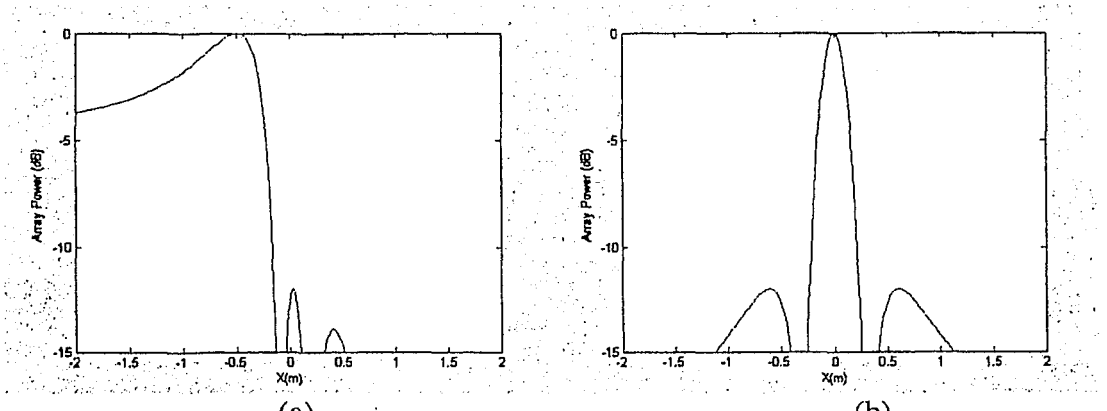

Figure 3.65: Beamforming results for N=25 (5 x 5) and f=6000 Hz; (a) Array power along the x-axis for X=-0.5 m (Y=0 m, Z=0.5 m) (b) Array power along the x-axis for X=0 m, (Y=0 m, Z=0.5 m).

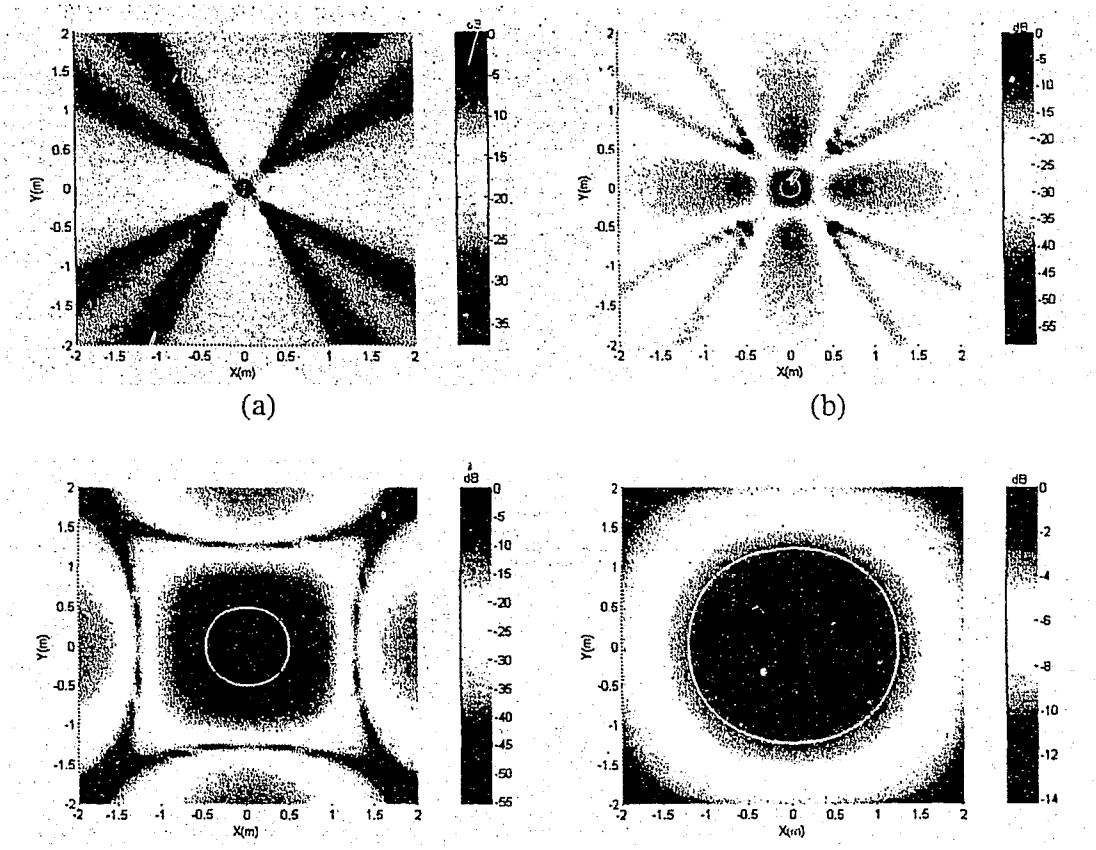

Figure 3.66: Beamforming results for N=25 (5 x 5) and f=6000 Hz; (a) Beamforming map: 2D plot for Z=0.25 m (X=0 m, Y=0 m) (b) Beamforming map: 2D plot for Z=0.5 m (X=0 m, Y=0 m) (c) Beamforming map: 2D plot for Z=2.0 m (X=0 m, Y=0 m) (d) Beamforming map, 2D plot; Z=5.0 m (X=0 m, Y=0 m).

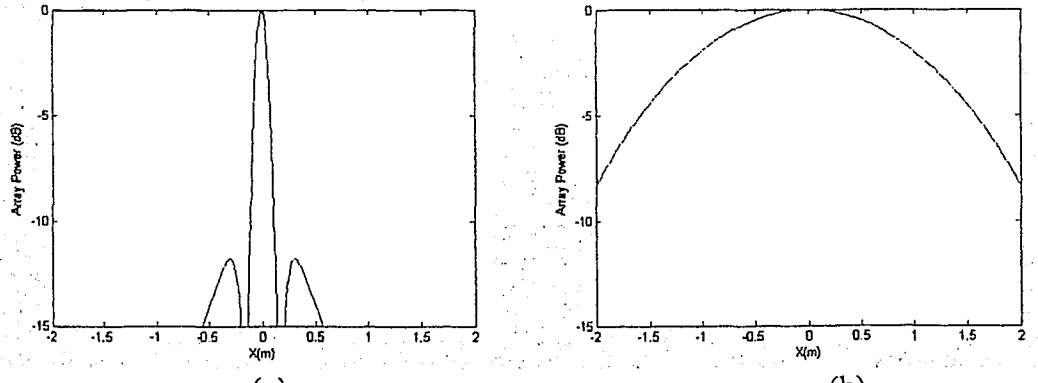

Figure 3.67: Beamforming results for N=25 (5 x 5) and f=6000 Hz;
(a) Array resolution along the x-axis for Z=0.25 m (X=0 m, Y=0 m).
(b) Array resolution along the x-axis for Z=5.0 m (X=0 m, Y=0 m).

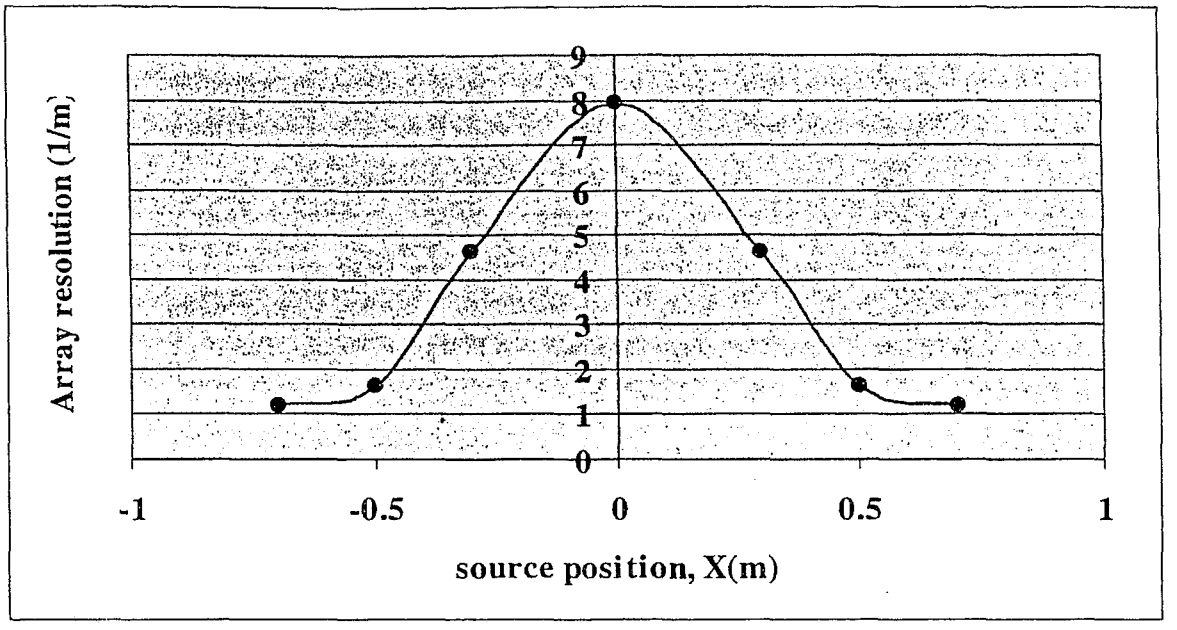

Figure 3.68: Effect of source variation on array resolution; (X=-0.7 m to X=0.7 m with Y=0 m and Z=0.5 m).

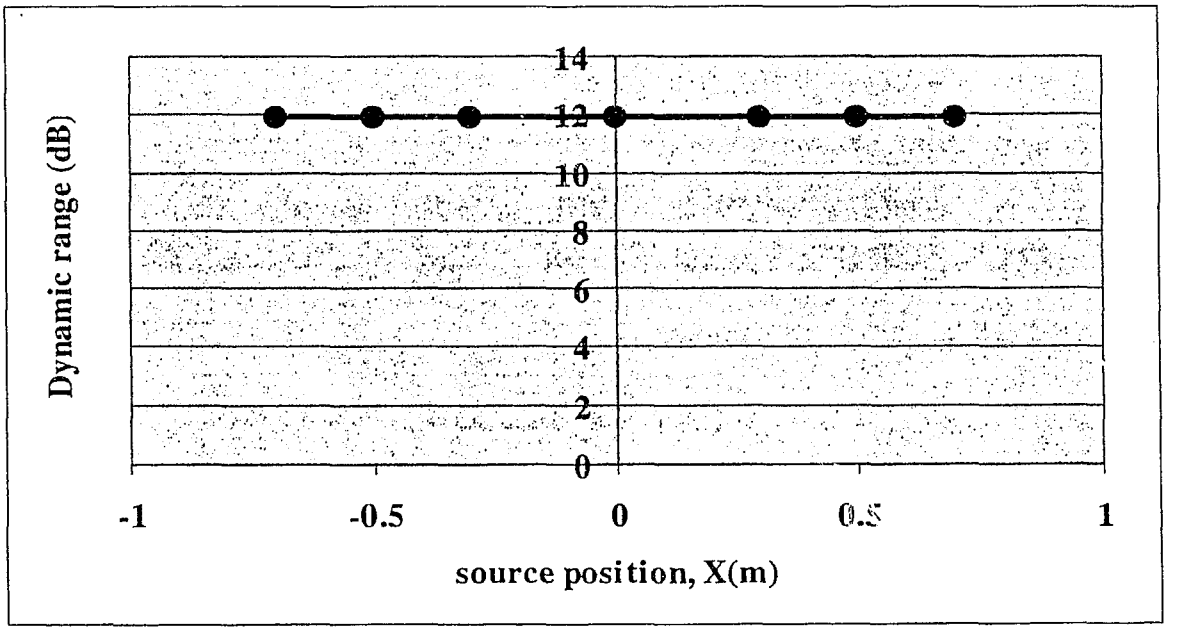

Figure 3.69: Effect of source variation on dynamic range; (X=-0.7 m to X=0.7 m with Y=0 m and Z=0.5 m).

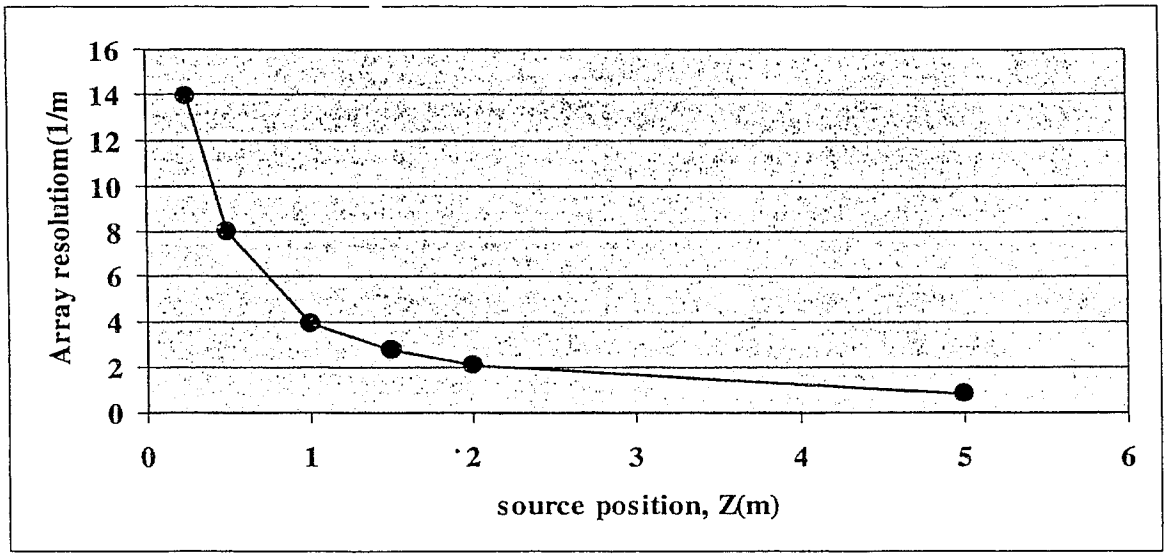

Figure 3.70: Effect of source variation on array resolution; (Z=0.25 m to Z=5 m with X=0 m and Y=0 m).

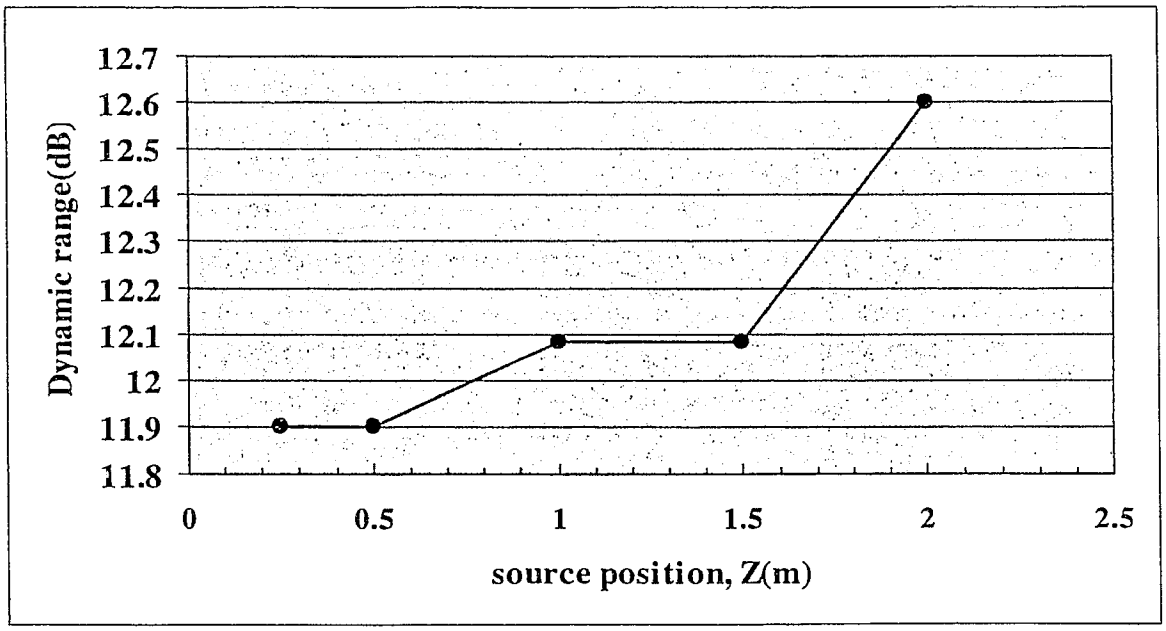

Figure 3.71: Effect of source variation on dynamic range; (Z=0.25 m to Z=5 m with X=0 m and Y=0 m).

3.4.1 Effect of inter-microphone distance (*d*)

The purpose of this sub-section was to investigate the effect of inter-microphone distance (*d*) on a uniform square array with a near field source. The spherical wave was generated at frequency of 8000 Hz, *N*=16 (4 x 4), and the source was located at X=0 m, Y=0 m and Z= 0.5

m. The inter-microphone distance along both the x-axis and the y-axis was changed from $4d^*$ (0.086m) to $d^*/2$ (0.01075 m), where d^* (0.0215 m) is the distance based on Shannon's criterion (i.e., $d^*=\lambda/2$).

The beamforming results for $d= 4d^*$, $d=d^*$ and $d=d^*/2$ are shown in Figures 3.72, 3.73 and 3.74 respectively. Each figure shows a beamforming map (3D plot) and an array power plot.

When $d=4d^*$, the mainlobe splits into a number of dominant grating lobes, and the results are ambiguous due to these lobes, as shown in Figure 3.72 (a) & (b). In contrast, there are no ambiguous (grating) lobes when Shannon's criterion is met ($d=d^*$ and $d=d^*/2$), as shown in Figures 3.73 and 3.74. But the array resolution degrades as one reduces the inter-microphone distance to $d=d^*/2$. Therefore, to avoid the grating lobes and to obtain maximum array resolution, the inter-microphone distance should be such that $d= d^*$. (In practice, d is fixed at d^* for a specific application with a given array design.)

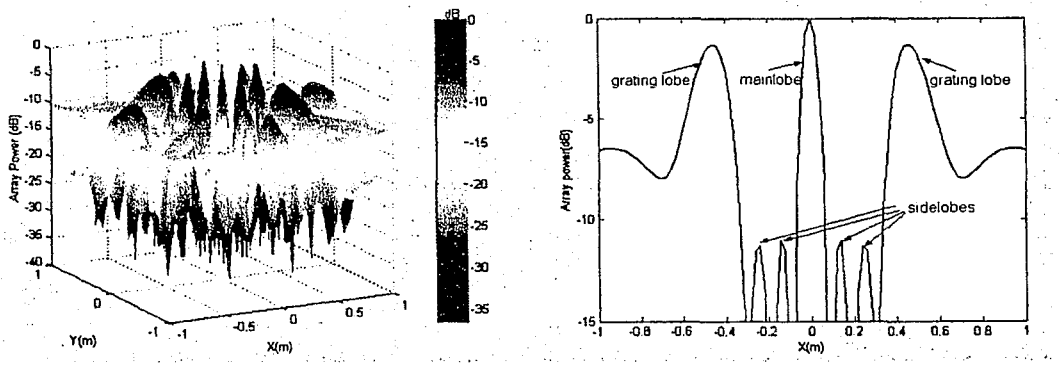

(a) (b)

Figure 3.72: Beamforming results for N=16 (a square array of 4 x 4), f = 8000 Hz, $d=4d^*$; (a) Beamforming map: 3D plot (b) Array power plot along the x-axis

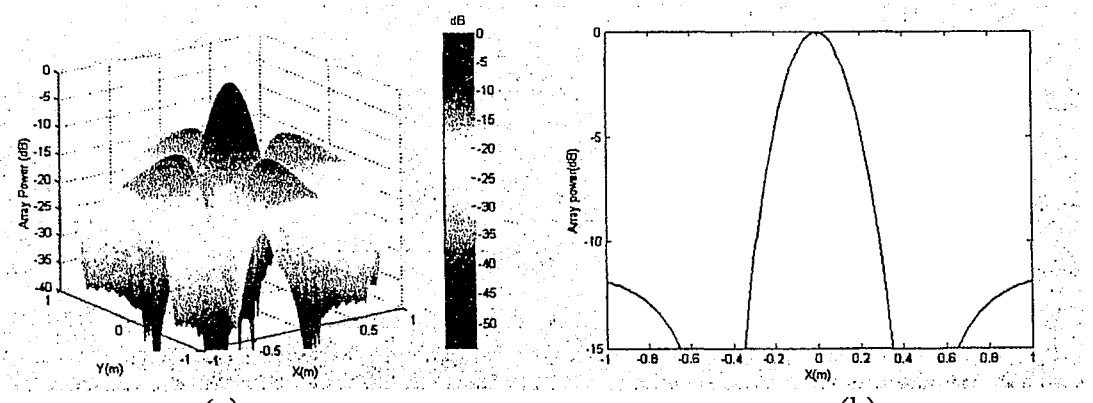

(a) (b)

Figure 3.73: Beamforming results for N=16 (a square array of 4 x 4), f = 8000 Hz, $d=d^*$; (a) Beamforming map: 3D plot (b) Array power plot along the x-axis

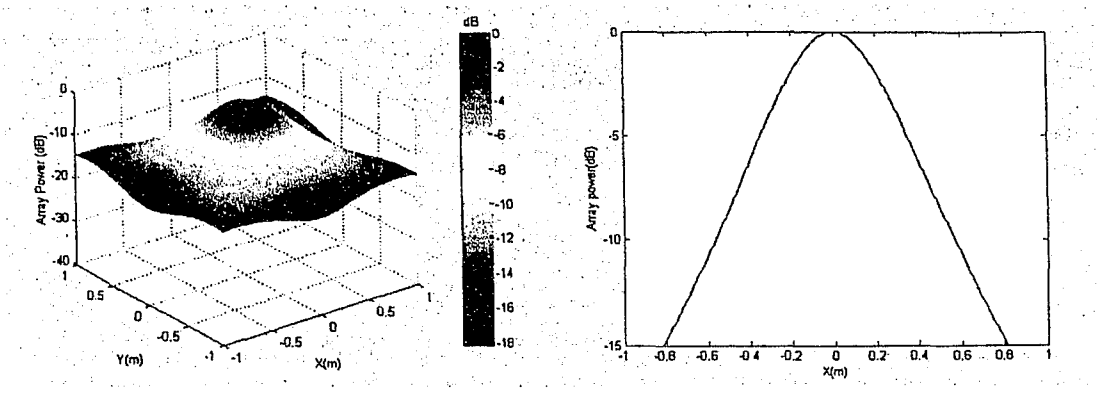

(a) (b)

Figure 3.74: Beamforming results for N=16 (a square array of 4 x 4), f = 8000 Hz, d=d*/2; (a) Beamforming map: 3D plot (b) Array power plot along the x-axis.

In this section a sensitivity analysis of a uniform planar array (specifically, a uniform square array) has been carried out with respect to the variation of the number of microphones, the signal frequency, the source position and the inter-microphone distance. In next section, a comparison between a ULA and a UPA with a near field source is discussed.

3.5 Comparison between a ULA and a UPA with a near field source

The purpose of this section is to compare the source localization capabilities of a ULA and a UPA with respect to a near field source. To this end, a spherical wave was generated at a frequency 8000 Hz with an inter-microphone spacing of 2.15 cm and an integer number of the cycles. The number of microphones was 36. Three source positions were considered, viz., X=0 m, Y=0 m, Z=0.5 m; X=0 m, Y=-0.3 m, Z=0.5 m; X=0.2 m, Y=-0.3 m and Z=0.5 m. In the case of the UPA, the 36 microphones were placed in a square (6 x 6) geometry (in the x-y plane), so that a uniform square array (USA) resulted. In the case of the ULA, the 36 microphones were placed along the x-axis and along the y-axis.

Figure 3.75 shows the beamforming results for the USA and the ULA with the microphones placed along the x-axis, with the source located at X=0 m, Y=0 m, Z=0.5 m. The corresponding array power plots are presented in Figures 3.76 and 3.77. Figure 3.78 shows the beamforming results for the ULA with the microphones placed along the x-axis and along the y-axis, with the source located at X=0 m, Y=-0.3 m, Z=0.5 m. Figure 3.79 shows the beamforming results for the USA with the source located at X=0 m, Y=-0.3 m, Z=0.5 m, and at X=0.2 m, Y=-0.3 m, Z=0.5 m.

When the source is placed at X=0 m, Y=0 m, Z=0.5 m, in the case of the USA, a mainlobe with the same resolution along the x-axis and along the y-axis is obtained, so that the resolution contour (at -3 dB) is a ring [Figures 3.75 (a) and 3.76]. This is to be expected because the same number of microphones is placed along the x-axis and the y-axis. In the case of the ULA, the mainlobe has a different resolution along the x-axis and the z-axis, so that the resolution contour is an ellipse [Figure 3.75 (b) and 3.77]. It is evident that, for the ULA, the array resolution is better along the x-axis (i.e., the axis of the array) than it is along the z-axis. It should be noted that the array resolution along the x-axis is greater for the ULA than it is for the USA, because of the larger aperture of the ULA.

When the source is placed at X=0 m, Y= -0.3 m, Z=0.5 m, and the ULA is used with the microphones placed along the x-axis, so that the localization plane is the x-z plane, the source is *incorrectly* localized at X=0 m, Y=0 m, (rather than Y=-0.3 m), Z=0.6 m (rather than Z=0.5 m) [Figure 3.78 (a)]. On the other hand, when the ULA is used with the microphones placed along the y-axis, so that the localization plane is the y-z plane, the source is *correctly* localized at X=0 m, Y=-0.3 m and Z=0.5 m [Figure 3.78 (b)]. This correct localization is a consequence of the fact that the array and the source both lie in the same plane. When the USA is used with the same source position (X=0 m, Y=-0.3 m, Z=0.5 m), the source is also *correctly* localized [Figure 3.79(a)]. Figure 3.79(b) shows the beamforming map for the USA with the source placed at a new position, viz.; X=0.2 m, Y=-0.3 m, Z=0.5 m. It can be seen that the USA again correctly localizes the source. It should be noted that for this new position, the ULA would be incapable of localizing the source correctly, regardless of whether the microphones are placed along the x-axis or along the y-axis.

The results of this section serve to demonstrate that the source localization capability of a uniform linear array (ULA) is limited to 2D situations for which the acoustic source and the ULA lie in the same plane; moreover, for a near field source, the array resolution of a ULA is better along the array axis than along the axis normal to the array axis. These results also establish that a uniform planar array (UPA), e.g., a uniform square array, is superior to a ULA (except for a situation involving a far field source lying in the same plane as the array) since, unlike a ULA, a UPA is capable of localizing a source in 3D space.

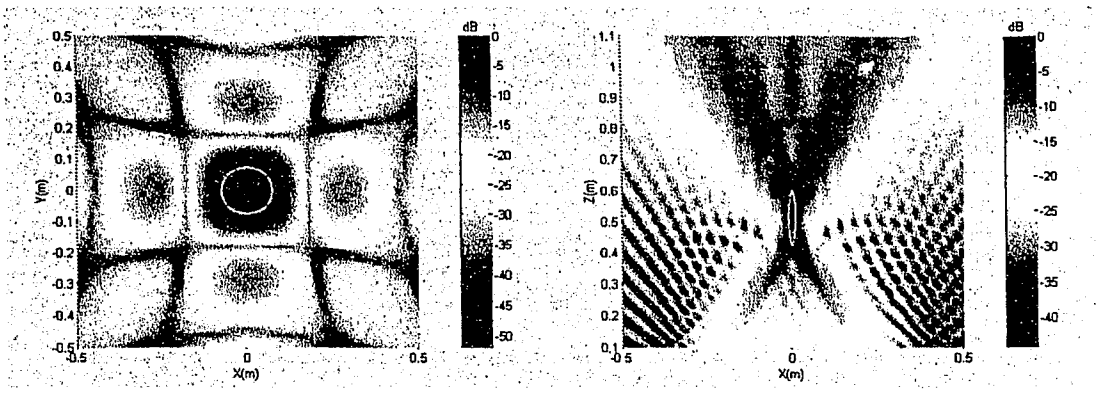

(a) (b)

Figure 3.75: Beamforming results for X=0 m, Y=0 m, Z=0.5 m; (a) Beamforming map: 2D plot for a USA with N=36 (6 x 6) (b) Beamforming map:2D plot for a ULA with 36 microphones placed along the x-axis.

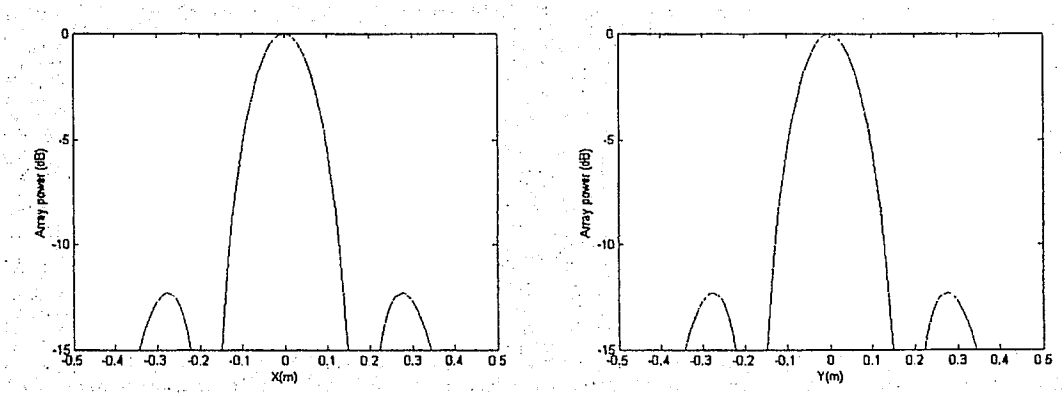

(a) (b)

Figure 3.76: Beamforming results for a USA with N=36 (6 x 6); X=0 m, Y=0 m, Z=0.5 m: (a) Array power along the x-axis (b) Array power along the y-axis.

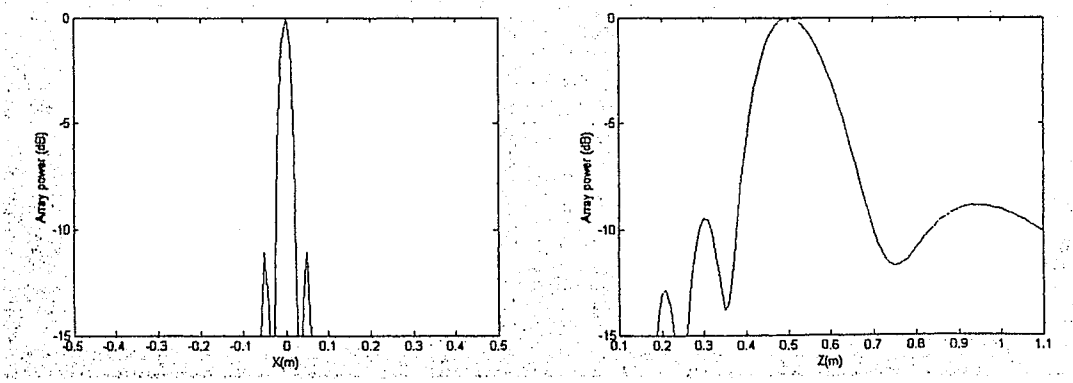

(a) (b)

Figure 3.77: Beamforming results for a ULA with 36 microphones placed along the x-axis; X=0 m, Y=0 m, Z=0.5 m: (a) Array power along the x-axis (b) Array power along the z-axis.

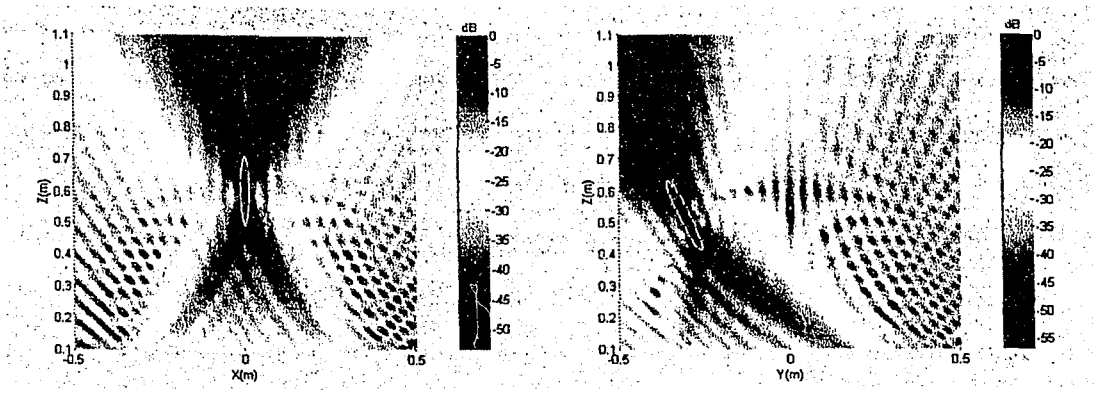

(a) (b)

Figure 3.78: Beamforming results for X=0 m, Y=-0.3 m, Z=0.5 m:
(a) Beamforming map: 2D plot for a ULA with 36 microphones placed along the x-axis
(b) Beamforming map: 2D plot for a ULA with 36 microphones placed along the y-axis.

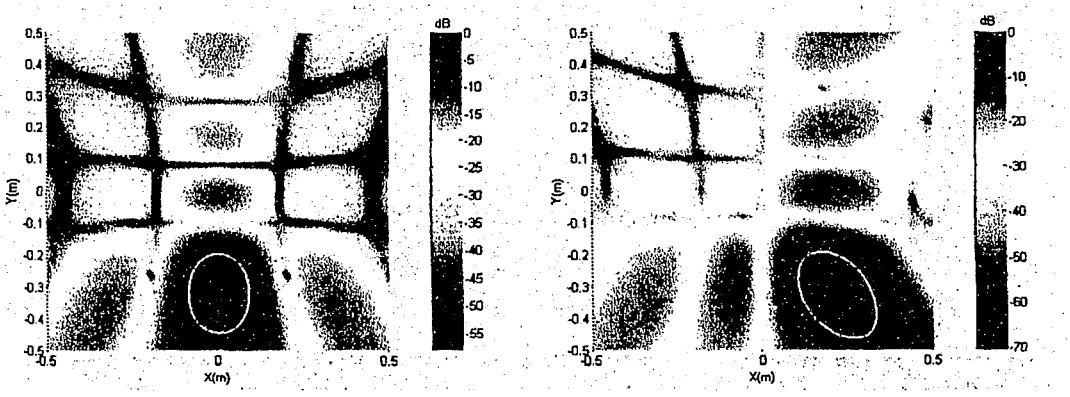

(a) (b)

Figure 3.79: Beamforming results for a USA, N=36 (6 x 6); (a) Beamforming map: 2D plot for X=0.0 m, Y=-0.3 m, Z=0.5 m (b) Beamforming map: 2D plot for X=0.2 m, Y=-0.3 m, Z=0.5 m.

In this section a comparison between a ULA and a UPA with a near field source has been carried out. In next section, the sensitivity analysis of a random array is discussed.

3.6 Random Array – near field beamforming

When microphones are placed in a random fashion (in the x-y plane) so as to break the regularities of a uniform planar array, the resulting array is called an irregular or aperiodic or random array, as depicted in Figure 2.8 (subsection 2.3.3). The purpose of this section was to examine beamforming results pertaining to a random array with a near field source. To this end, the spiral array geometry designed by NASA Langley Research Center, Hampton, VA was chosen. This array is also called a Large Aperture Directional Array (LADA)[6]. It

consists of 35 microphones placed in logarithmic spirals, and it has five spirals each having seven microphones, with the inner-most microphones lying on a 1 inch (0.0254 m) radius, and the outer-most on a 17 inch (0.4318 m) radius, as depicted in Figure 3.80. This array was designed for different frequencies ranging from 2 kHz to 30 kHz.

The microphones were placed in an x-y plane, and a spherical wave was generated at each microphone location by means of the formula $(A/r_n)\sin[\omega(t-r_n/c)]$, as discussed in section (3.1). The signals at each microphone had an integer number of cycles. Each block of data for the digital signals contained 1024 points and yielded 513 (M/2+1) frequency bins.

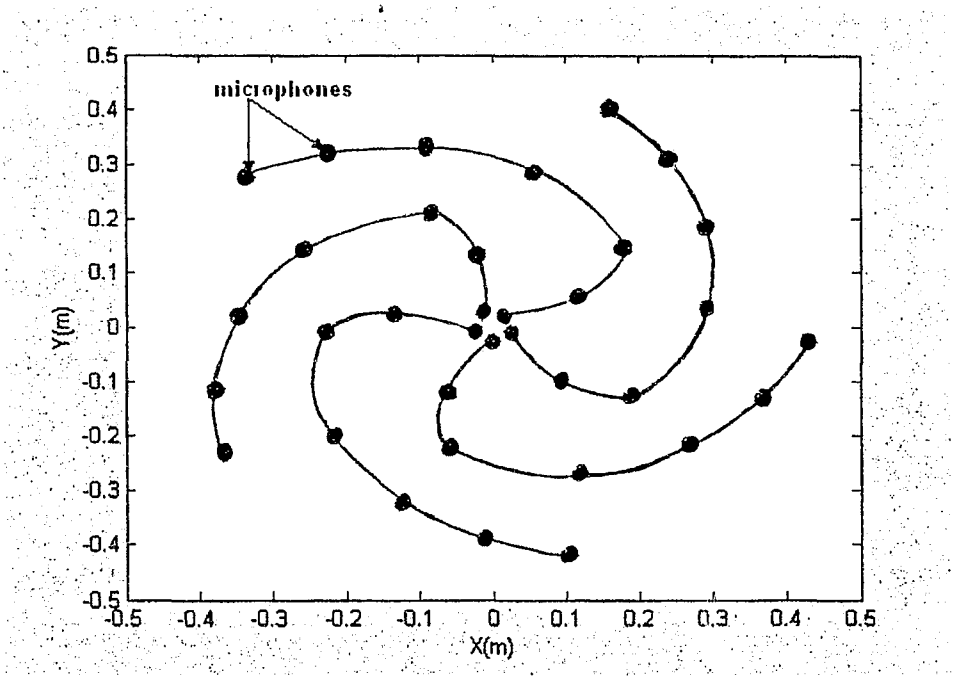

Figure 3.80: Large Aperture Directional Array (LADA)

For a spiral array, the source position can be defined in 3D space by an elevation angle φ, an azimuth angle θ, and a distance r between the array centre and the source, as in the case of a UPA (section 3.4). These spherical coordinates can be represented in Cartesian coordinates in terms of X, Y, and Z along the x, y, and z axes respectively. With the array lying in the x-y plane, the source can be localized by considering an x-y plane, (i.e., a grid plane) at different locations along the z-axis (i.e., different grid distances), as depicted in Figure 3.56. The grid plane contains grid points with increments along the x and y axes. The relevant beamforming

maps were obtained, at different grid distances, by computing steering vectors for various assumed source locations in the x-y plane. The position where the array power is maximum (i.e., where the mainlobe appears) in the grid plane corresponds to the X-Y location of the source. The position where the array power is maximum along the z-axis represents the Z location of the source.

The parameters chosen for the sensitivity analysis in this case are given below.

- Number of microphones (N).
- Signal frequency (f).
- Source position.

3.6.1 Effect of number of microphones (N)

The purpose this subsection was to examine the impact of the number of microphones on the beamforming results when a spiral array was used with a near field source. The spherical wave was generated at a frequency of 4000 Hz and the acoustic source was placed at X=0 m, Y=0 m and Z=0.5 m. The number of microphones was varied from 15 to 35.

Figures 3.81 and 3.82 show the beamforming maps (3D and 2D plots) for N=15 and N= 35. The corresponding array power plots are shown in Figure 3.83. The array resolution and the dynamic range were obtained from the various beamforming maps for different numbers of microphones ranging from 15 to 35. The plots of array resolution and array dynamic range versus number of microphones are depicted in Figures 3.84 and 3.85.

When the number of microphones is 15, the error band is ± 0.06 m (corresponding to an error of ± 5.93 %), and the array dynamic range is 8 dB [Figures 3.81 and 3.83 (a)]. When the number of microphones increases to 35, the error decreases to ± 0.032 m (corresponding to an error of ± 3.16 %) and the array dynamic range increases to 12.6 dB [Figures 3.82 and 3.83 (b)].

It can be seen from Figures 3.84 and 3.85 that both the array resolution and the array dynamic range increase progressively with the increase of number of microphones.

The results of this sub-section demonstrate that the source localization capability of a spiral array increases with the increase of number of microphones, for any given frequency.

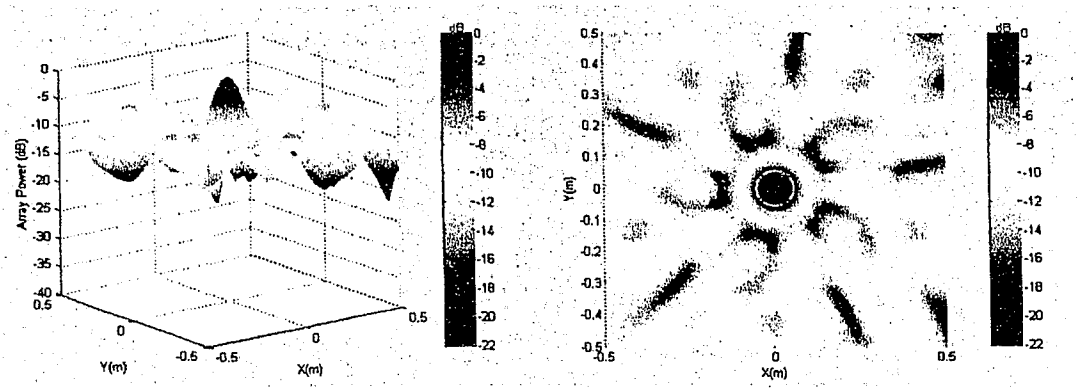

(a) (b)

Figure 3.81: Beamforming results for N=15, f=4000 Hz; (a) Beamforming map: 3D plot (b) Beamforming map: 2D plot.

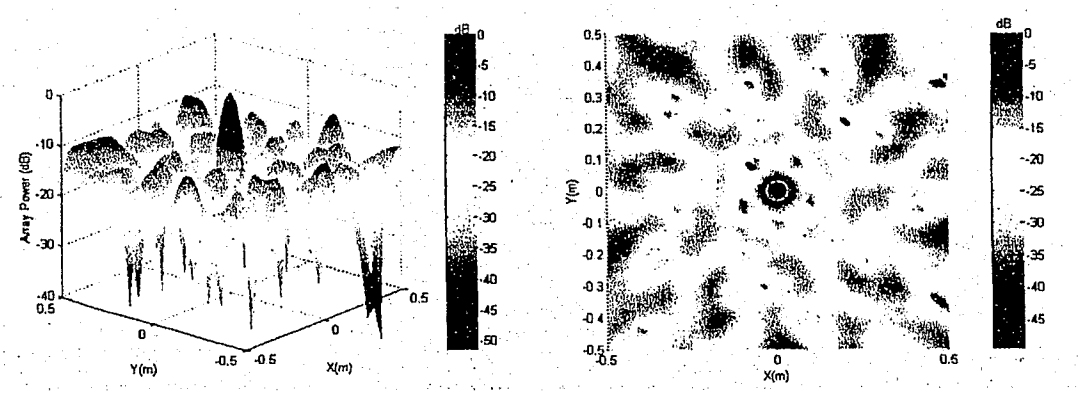

(a) (b)

Figure 3.82: Beamforming results for N=35, f=4000 Hz; (a) Beamforming map: 3D plot (b) Beamforming map: 2D plot.

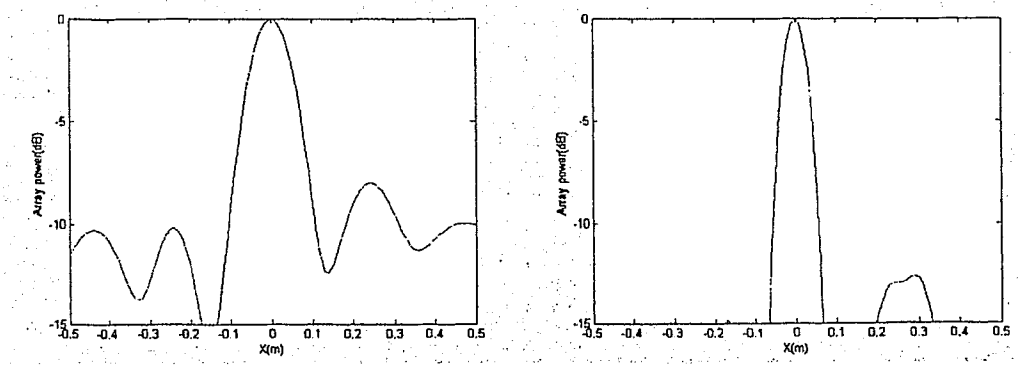

(a) (b)

Figure 3.83: Beamforming results for f=4000 Hz; (a) Array power plot for N=15 (b) Array power plot for N=35.

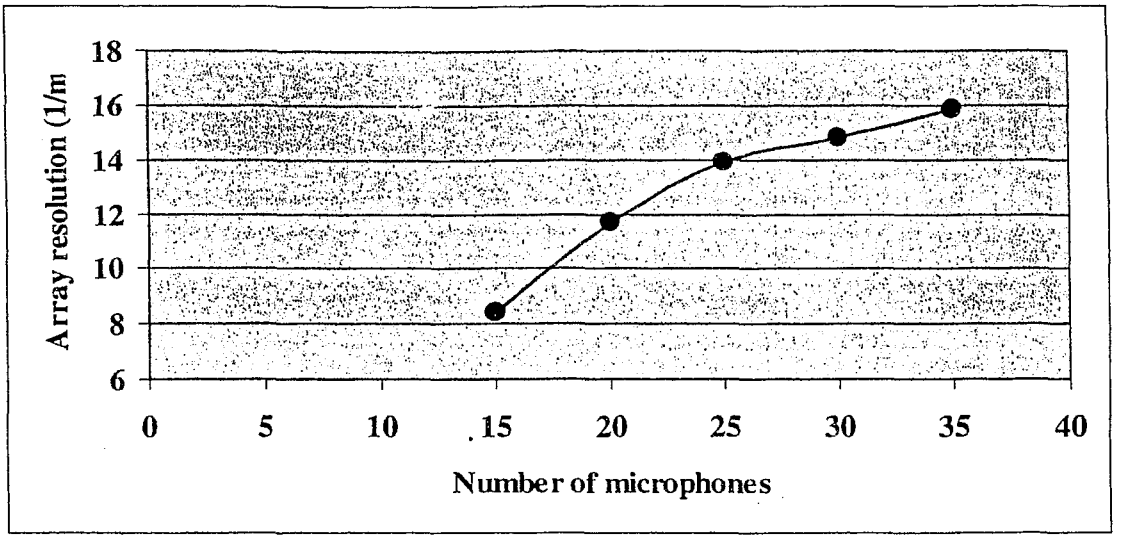

Figure 3.84: Effect of number of microphones on the array resolution.

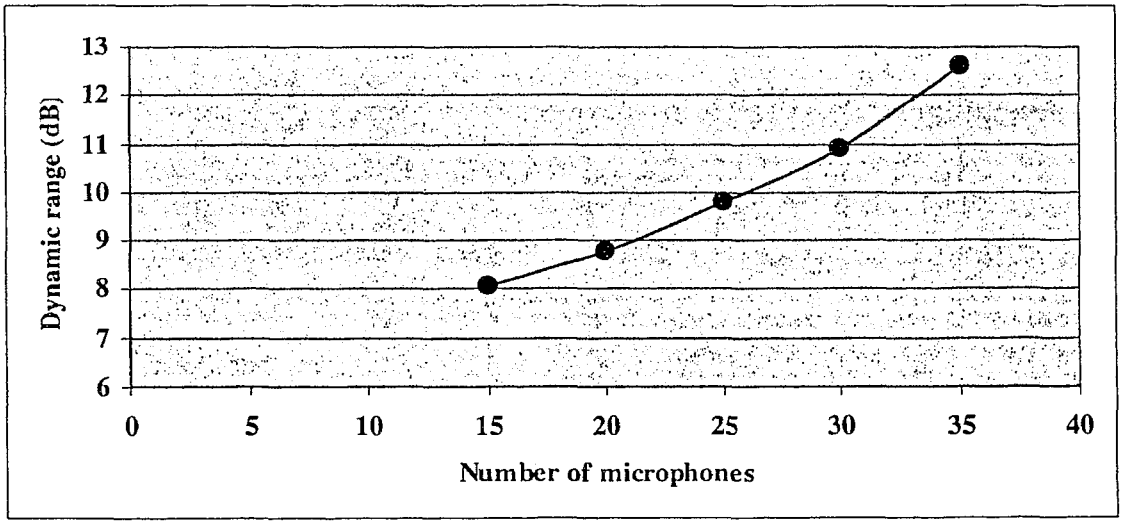

Figure 3.85: Effect of number of microphones on the dynamic range.

3.6.2 Effect of source signal frequency (*f*)

The purpose of this sub-section was to explore the effect of signal frequency on the beamforming results when a spiral array was used with a near field source. The spherical wave was generated at different frequencies ranging from f=4 kHz to f=30 kHz. Note that this frequency range is considerably larger than the frequency ranges considered for the ULA and UPA. The number of microphones was 35, and the acoustic source was placed at X=0 m, Y= 0 m and Z=0.5 m.

The beamforming results for f=4000 Hz and f=30000 Hz with N=35 are shown in Figures 3.86 and 3.87 respectively. Each figure shows a beamforming map (3D plot) and the corresponding array power plot. The array resolution and the dynamic ranges were obtained from the various beamforming maps for different frequencies ranging from 4000 Hz to 30000 Hz. The plots of the array resolution and the dynamic range versus signal frequency are presented in Figures 3.88 and 3.89 respectively.

When the signal frequency is 4000 Hz, the error band is ± 0.036 m (corresponding to error ± 3.6 %) and the array dynamic range is 12.6 dB (Figure 3.86). When the signal frequency increases to 30,000 Hz, the mainlobe becomes a spike (corresponding to 0 % error) and the array dynamic range drops to 9.45 dB, which is acceptable (Figure 3.87). Figures 3.88 and 3.89 show that, as the signal frequency increases, the array resolution increases markedly while the array dynamic range decreases only slightly.

The above results demonstrate that a spiral array provides particularly effective source localization over a broad range of frequencies, without any spatial aliasing, with a limited number of microphones.

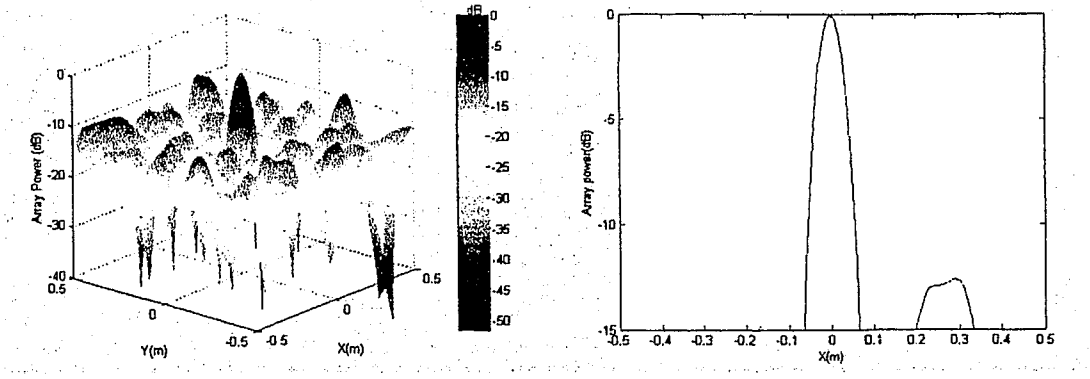

(a) (b)

Figure 3.86: Beamforming results for N=35, f=4000 Hz; (a) Beamforming map: 3D plot (b) Array power along the x-axis

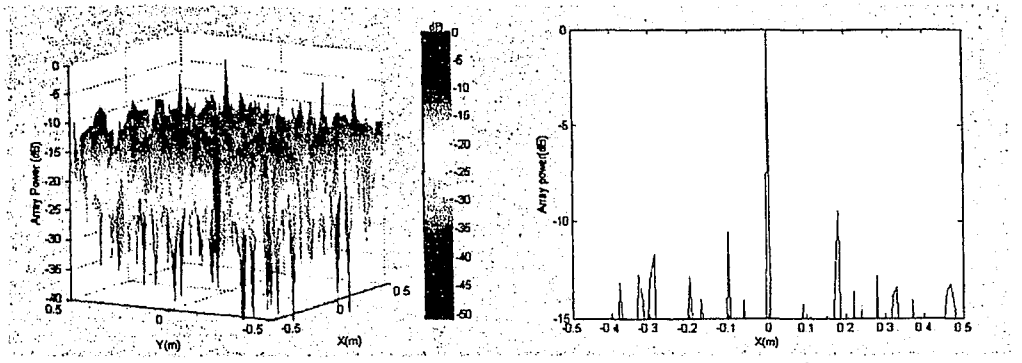

(a) (b)

Figure 3.87: Beamforming results for N=35, f=30,000 Hz; (a) Beamforming map: 3D plot (b) Array power along the x-axis.

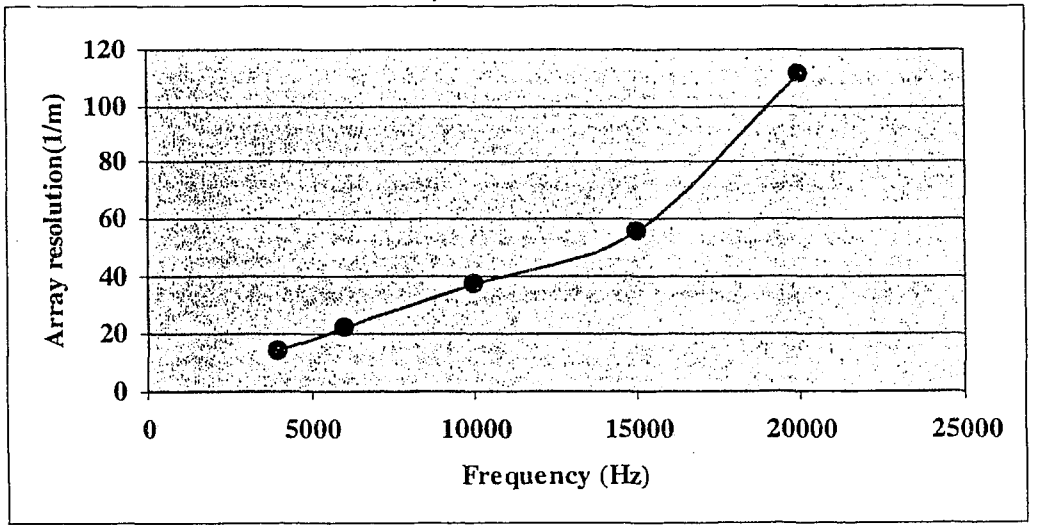

Figure 3.88: Effect of source signal frequency on the array resolution.

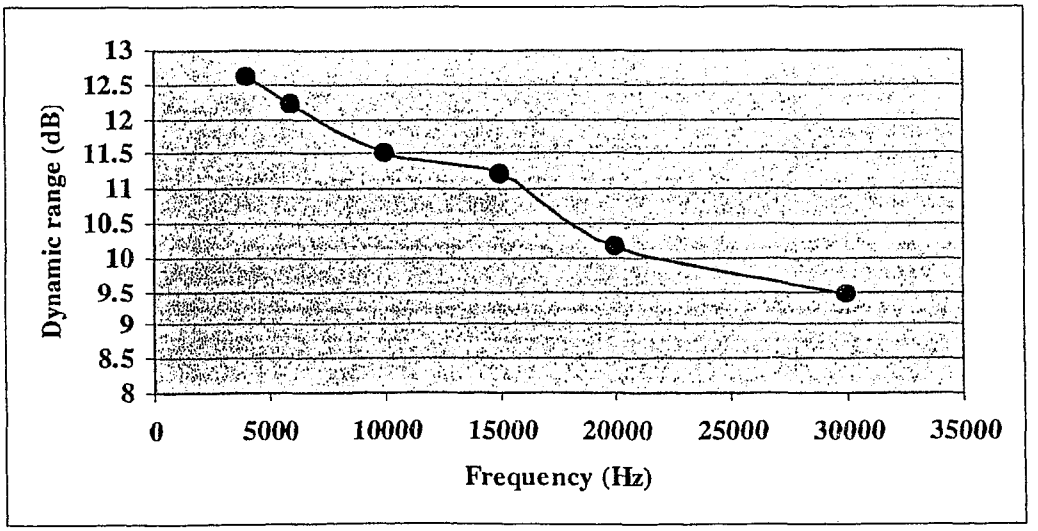

Figure 3.89: Effect of source signal frequency on the dynamic range.

3.6.3 Effect of source position

The purpose of this sub-section was to determine the impact of the source position for a spiral array with a near field source. The spherical wave was generated at a frequency of 4000 Hz, and the number of microphones was 35. The source was placed at different positions along the x-axis varying from X= -0.7 m to X=0.7 m with the y-axis and z-axis positions fixed at Y=0 m and Z=0.5 m respectively. The source was also placed at different positions along the z-axis varying from Z=0.25 m to Z=5 m with the x-axis and y-axis positions fixed at X=0 m and Y=0 m respectively.

Figures 3.90 and 3.91 show the beamforming maps (2D plots) and the array power plots for X=-0.7 m and X=0 m with Y=0 m and Z=0.5 m. Figures 3.92 and 3.93 show the beamforming maps (2D plots) and the array power plots for Z=0.25 m and Z=5 m with X=0 m and Y=0 m. Figure 3.94 shows the array power plots for Z=0.5 m and Z=1.5 m with X=0 m and Y=0 m. The array resolution and the array dynamic range were obtained from the various beamforming maps for the different source positions. The plots of array resolution and dynamic range versus the source position along the x-axis are depicted in Figures 3.95 and 3.96. Figure 3.97 presents the array resolution versus the source position along the z-axis.

When the source is placed at X=-0.7 with Y=0 m and Z=0.5 m, the error band is ± 0.108 m (corresponding to ± 5.4 %) and the dynamic range is 10.67 dB (Figure 3.90). When the source is moved to X=0 m, the error band decreases to ± 0.032 m (corresponding to ± 1.6 %) and the dynamic range increases to 12.77 dB (Figures 3.91). Figures 3.95 and 3.96 show that both the array resolution and the dynamic range increase (i.e., the source localization capability improves) when the source moves from X= ± 0.7 m to X=0 m.

When the source is placed at Z=0.25 m with X=0 m and Y=0 m, the error band is ± 0.022 m (± 2.2 %) and the dynamic range is 10.36 dB (Figure 3.92). When the source is moved to Z=5 m, the error band increases to ± 0.27 m (± 27 %) and the dynamic range cannot be defined (Figures 3.93). It can be seen from Figure 3.97 that the array resolution decreases non-linearly as the source position along the z-axis increases. But the dynamic range increases as the source moves away from the microphone array (Figure 3.94). For instance, when Z=0.5 m, the dynamic range is 12.6 dB, and when Z=1.5 m, the dynamic range is more than 15 dB.

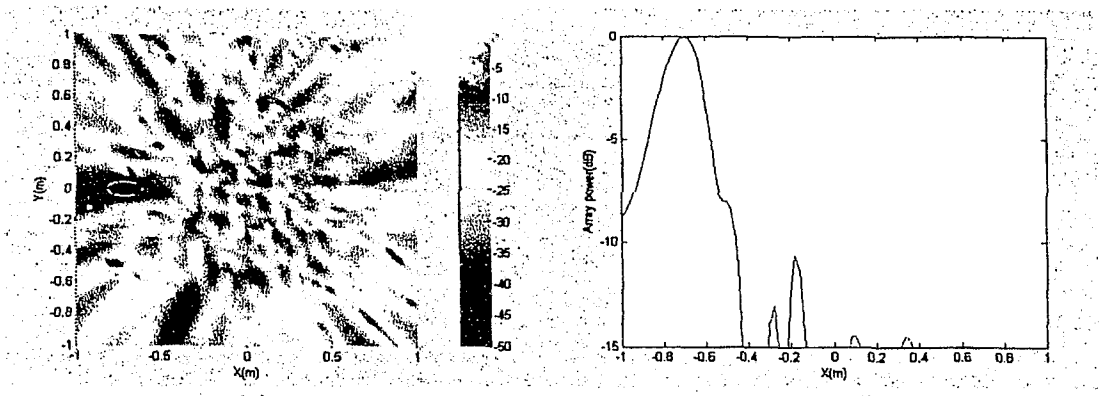

(a) (b)

Figure 3.90: Beamforming results for N=35, f=4000 Hz, X=-0.7 m (Y=0 m and Z=0.5 m): (a) Beamforming map: 2D plot (b) Array power along the x-axis.

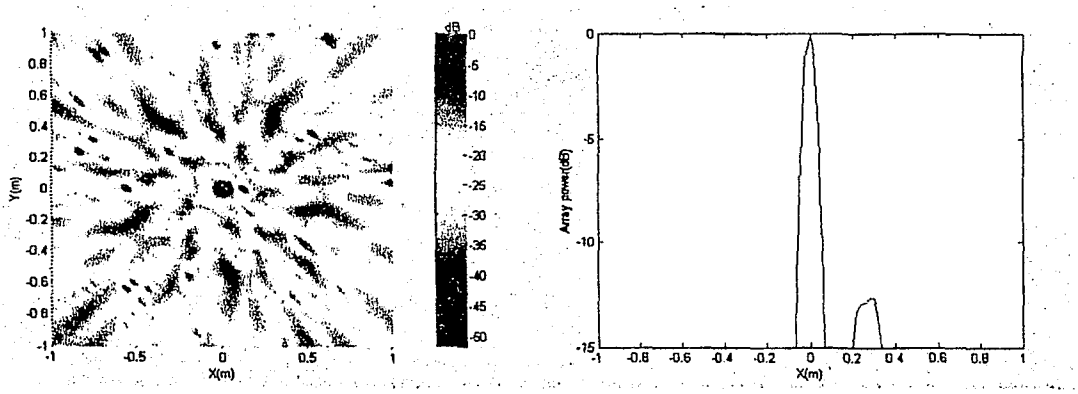

(a) (b)

Figure 3.91: Beamforming results for N=35, f=4000 Hz, X=0 m (Y=0 m and Z=0.5 m); (a) Beamforming map: 2D plot (b) Array power along the x-axis.

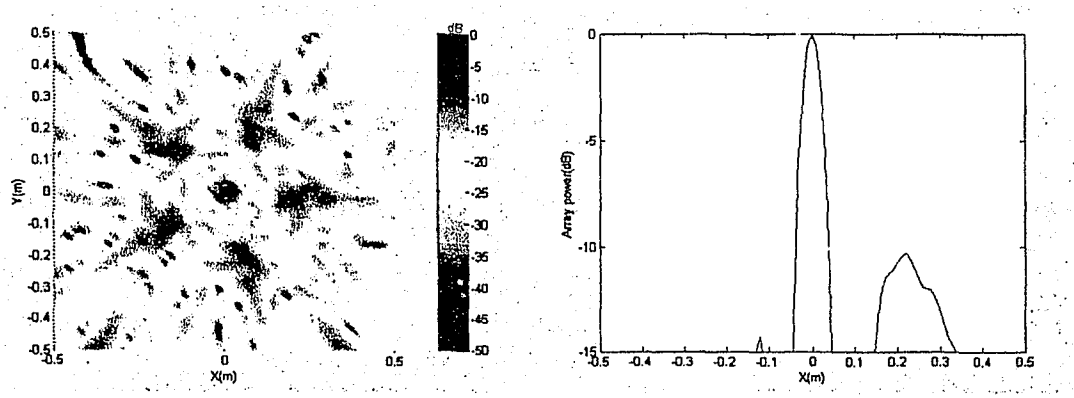

(a) (b)

Figure 3.92: Beamforming results for N=35, f=4000 Hz, Z=0.25 m (X=0 m and Y=0 m) (a) Beamforming map: 2D plot (b) Array power along the x-axis.

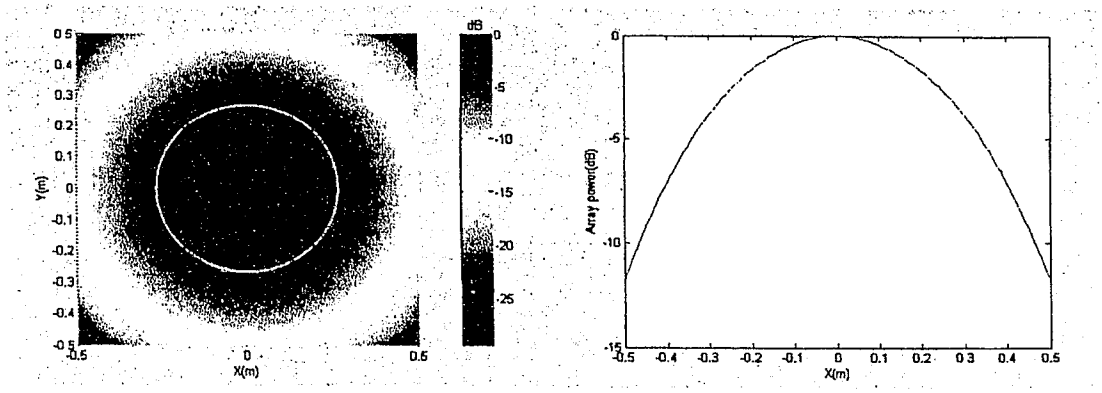

(a) (b)

Figure 3.93: Beamforming results for N=35, f=4000 Hz, Z=5 m, (X=0 m and Y=0 m) (a) Beamforming map: 2D plot (b) Array power along the x-axis.

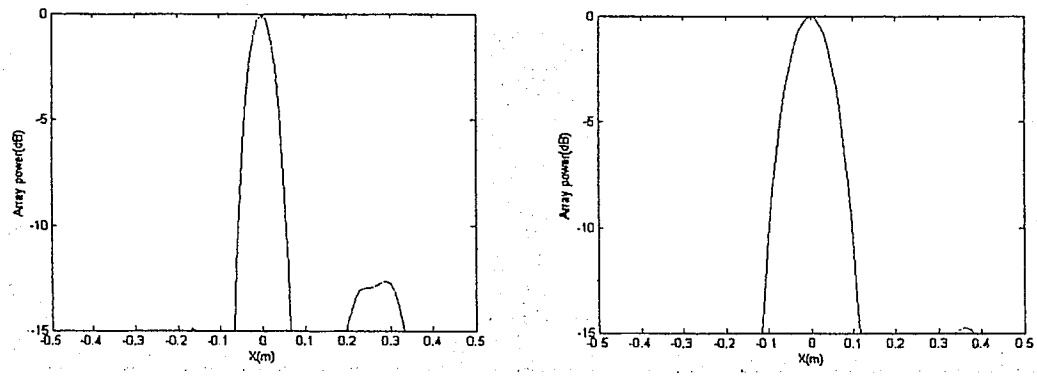

(a) (b)

Figure 3.94: Beamforming results for N=35, f=4000 Hz; (a) Array power along the x-axis for Z=0.5 m, (X=0 m and Y=0 m); (a) Array power along the x-axis for Z=1.5 m, (X=0 m and Y=0 m).

The results of this sub-section demonstrate that the maximum array resolution is obtained when an acoustic source is perpendicular (i.e., broadside) to the centre of a spiral array. The array resolution decreases as the source moves away from the array. Therefore, a model under investigation should always be placed perpendicular to the array centre. However, since the sound generated by various parts of the model would be at different angles with respect to the array centre, it would not be possible to place all the sources at the ideal position.

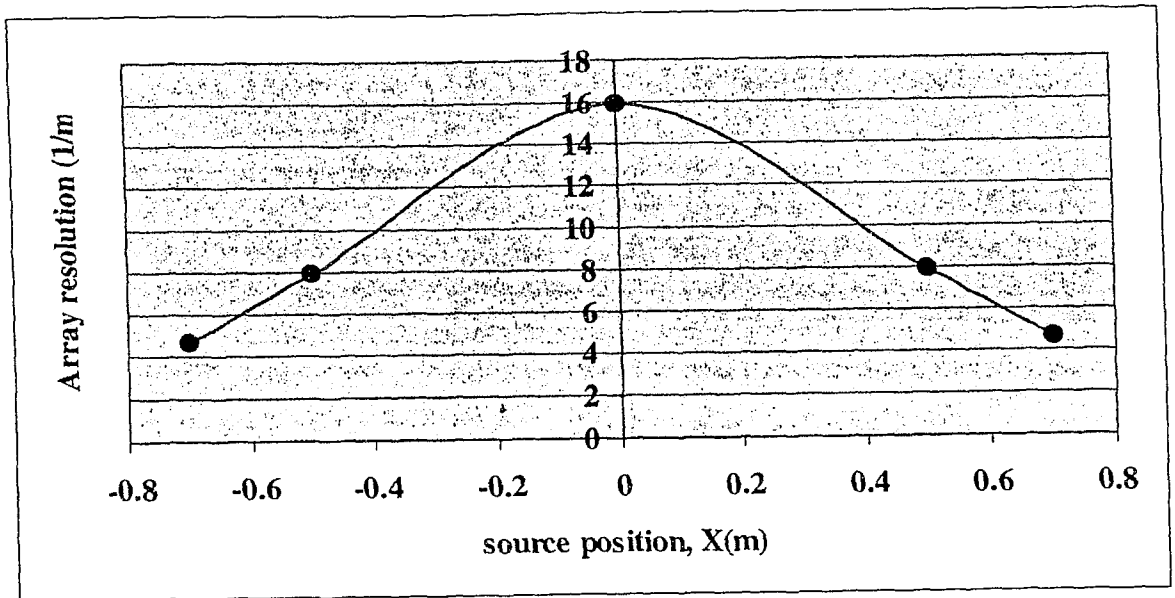

Figure 3.95: Effect of source variation along the x-axis on the array resolution; (X=-0.7 m to X=0.7 m with Y=0 m and Z=0.5 m).

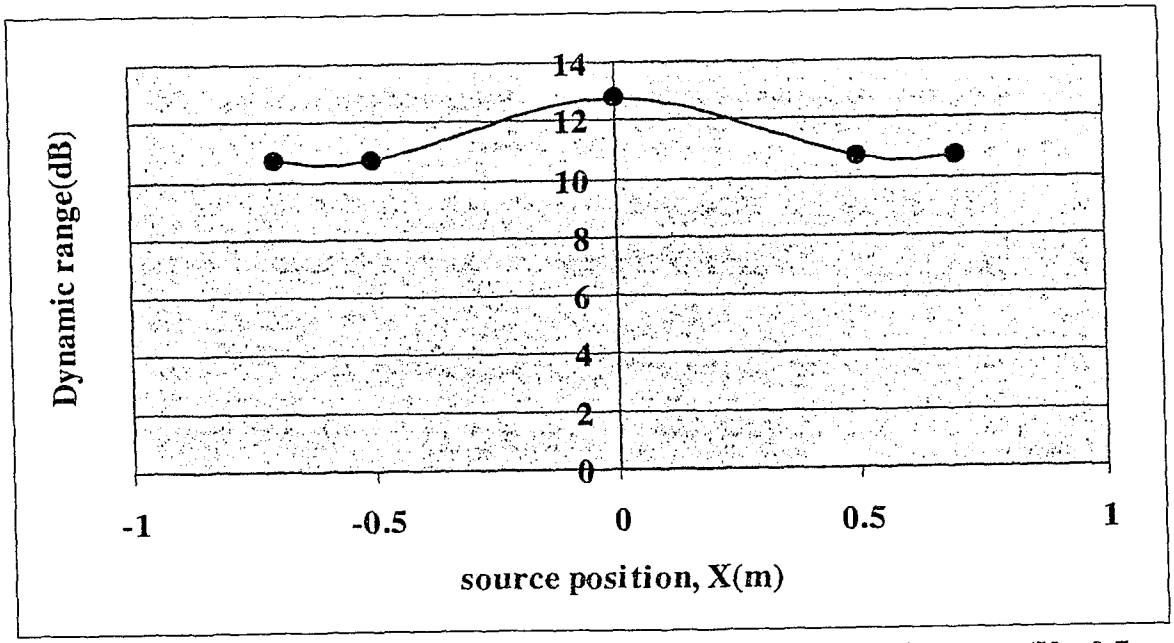

Figure 3.96: Effect of source variation along the x-axis on the dynamic range; (X=-0.7 m to X=0.7 m with Y=0 m and Z=0.5 m).

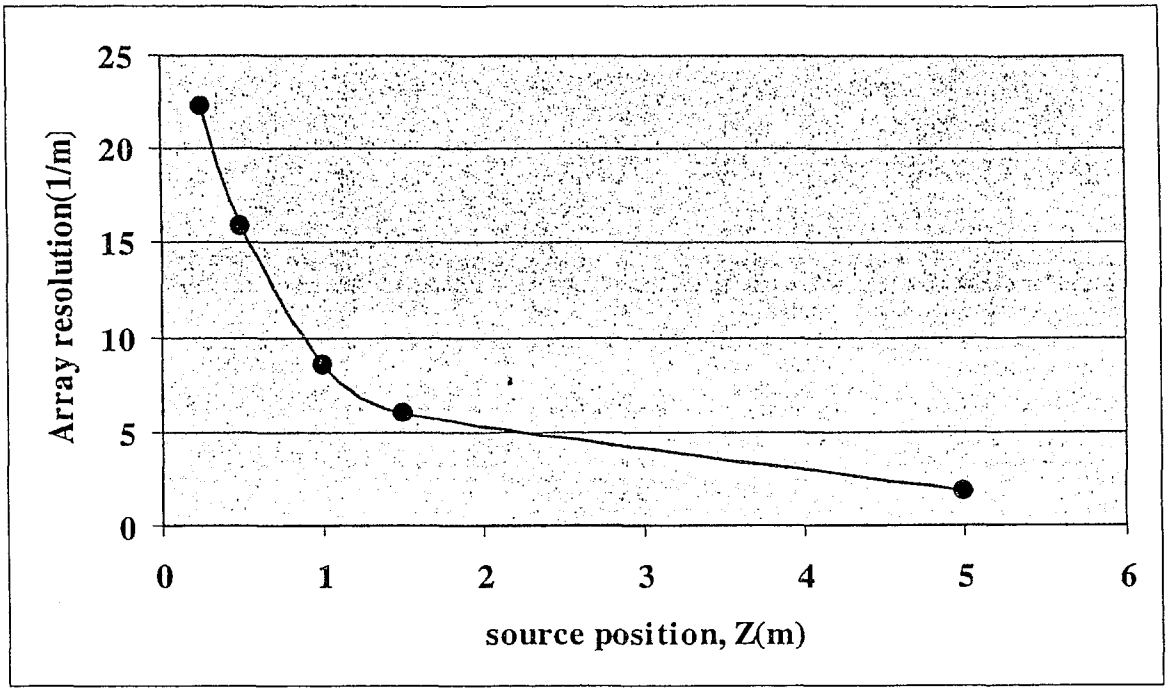

Figure 3.97: Effect of source variation along the z-axis on the array resolution; (Z=0.25 m to Z=5 m with X=0 m and Y=0 m).

Chapter 4

Sensitivity analysis-experimental data

4.0 Introduction

The present chapter focuses on the sensitivity analysis of the beamforming technique using *experimental data*. In this analysis, the impact of the number of microphones (N), the source position, and the inter-microphone distance (d) is examined. Experiments were conducted with two different array geometries, viz., a horizontal uniform linear array (HULA) and a cross array (which is analogous to a uniform planar array), at the laboratory of the Institute of Aerospace Research (IAR), National Research Council (NRC) of Canada, Ottawa.

As mentioned in section 3.0, the performance of a microphone array is measured by the beamforming evaluators, *array resolution* and *array dynamic range*. These evaluators characterize the capability of an array to localize an acoustic source. The array resolution is determined by the mainlobe width and increases as the mainlobe becomes narrower. In addition, the 'goodness' of the microphone array can be expressed in terms of an error band. The array dynamic range is determined by the highest sidelobe level.

The array resolution (or the error band) and the array dynamic range remain the central focus for this sensitivity analysis.

4.1 Experimental setup and data acquisition system

4.1.1 Experimental setup

A loudspeaker was used as an acoustic source producing a sine wave at a frequency of 2859 Hz. The different array geometries used for the experiments are shown in Figure 4.1. The horizontal uniform linear array (HULA) and the cross array consisted of, respectively, 16 and 32 Bruel & Kjaer model 4941A ¼ inch microphones, which were fixed on aluminum bars. Except for the central microphones, the inter-microphone distance (d) was 2 inches (0.0508 m) to satisfy Shannon's criterion (based on a frequency of 2859 Hz). The central microphones were separated by $2d$. The aluminum bars were attached to a tripod (see Figure 4.1). The data recorded at the different microphones were passed through preamplifiers (inside the microphones) and supplied to an A/D converter as depicted in Figure 4.1(b).

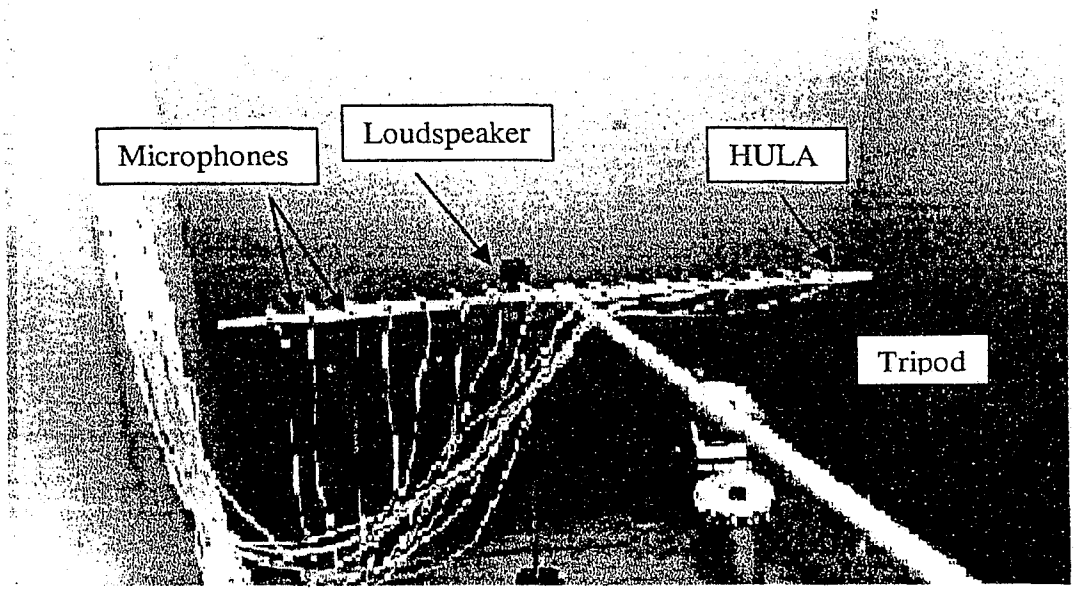

(a)

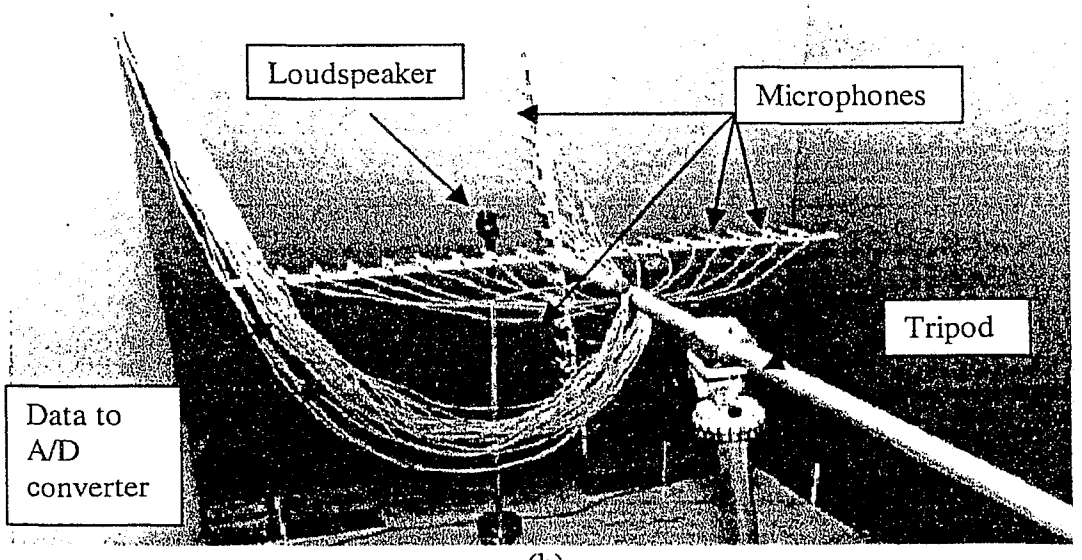

(b)

Figure 4.1: (a) Horizontal uniform linear array (HULA) (b) Cross array.

Note that the laboratory test section was not an anechoic chamber, so that the microphones were affected by reflection of the sound waves from the sidewalls, the ceiling and the floor of the test section. Non-overlapping blocks were used for the data processing. A Cartesian coordinate system was used, with the x-axis parallel to the laboratory floor and perpendicular to the side walls of the test section. In one case, the z-axis was taken perpendicular to the

laboratory floor, i.e., the vertical direction; in other cases, the y-axis was taken perpendicular to the laboratory floor.

4.1.2 Data acquisition system

The data acquisition system is shown in Figure 4.2. The internal details of this system are shown in Figure 4.3. Two Bruel & Kjaer model 2694B 16-channel signal conditioners were used to amplify the microphone signals. Each conditioner was connected to a 32-channel analog to digital (A/D) converter, model ICS-610, which was run by LabVIEW software. The data were converted with 24-bit precision at a sampling rate of 16 kHz. The digital data were sent to a StreamStor disk drive array, model 816-FX2, using a Front Panel Data Port (FPDP). The FPDP transfers 32-bit data continuously at a rate of 480 megabytes per second. The data were stored for post processing on the hard drive of a computer with 80 GB capacity.

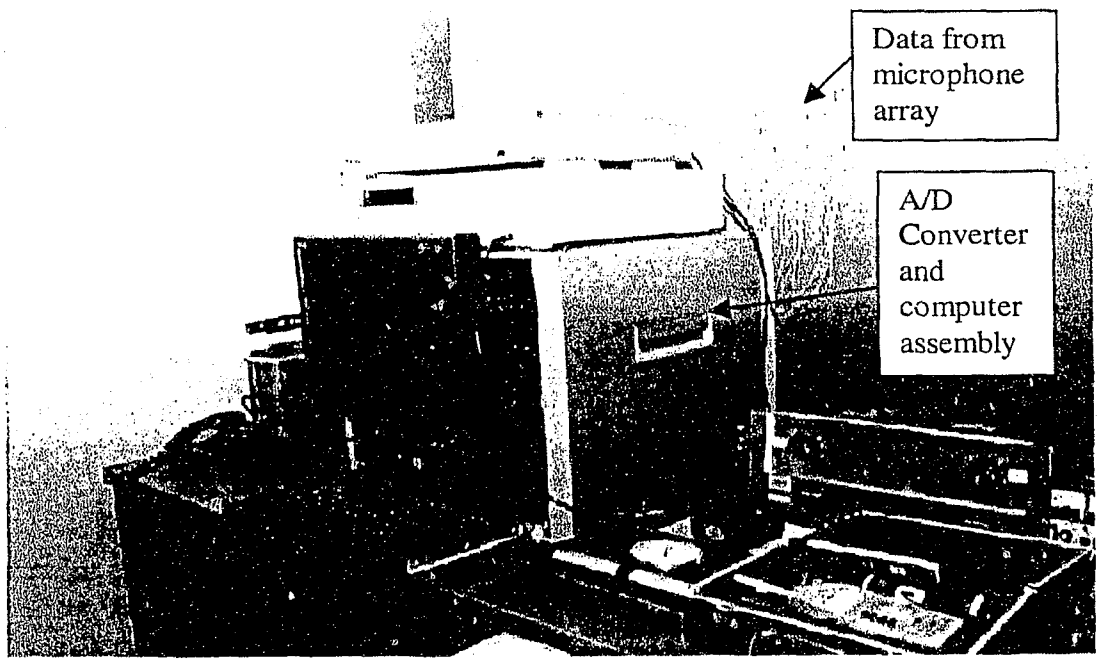

Figure 4.2: Data acquisition system.

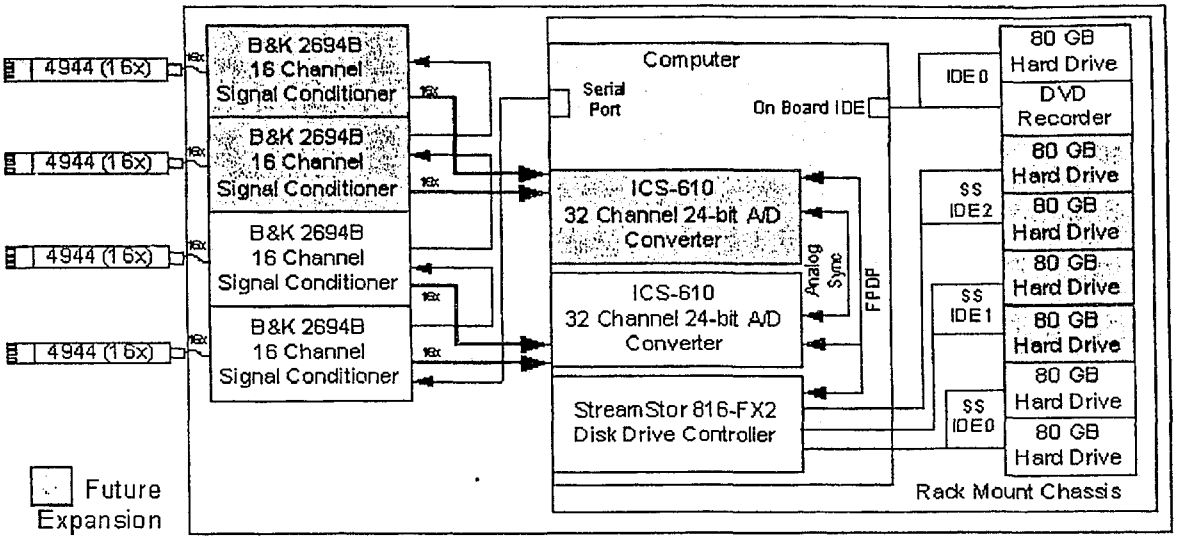

Figure 4.3: Internal details of data acquisition system (Courtesy: NRC, Ottawa).

4.2 Horizontal Uniform Linear Array (HULA)

For this horizontal uniform linear array (HULA), the microphones were placed along the x-axis (i.e., parallel to the laboratory floor) and the vertical axis was the z-axis, as shown in Figure 4.1(a). The HULA microphone coordinates are shown in Table 4.1. The acoustic source (loudspeaker) was placed in the x-y plane, within 1 m from the array, so that a spherical wave front occurred at the microphones, i.e., the loudspeaker was a near field source. The data were collected for 8 seconds at each microphone at a sampling rate of 16 KHz and were divided into non-overlapping blocks, each containing 1024 data points (i.e., M=1024). With the sampling rate being 16 KHz, the frequency resolution was 15.62 Hz.

The digital data collected by the microphone array were stored for post-processing as discussed in sub-section 4.1.2, and the MATLAB code was applied to obtain the beamforming results (see Appendix A). For each of the 513 ($M/2$ +1) frequency bins, the beamforming map was obtained by computing steering vectors for various assumed source locations in the x-y plane (e.g., -0.5 m to 0.5 m along the x-axis and 0.1 to 1.1 m along the y-axis).

The following parameters were used for the sensitivity analysis of the HULA.

- Number of microphones (N).
- Source position.
- Inter-microphone distance (d).

Table 4.1 Horizontal Uniform Linear Array Microphone Coordinates

Mic #	X location	Y location	Z location
	(m)	(m)	(m)
1	0.4064	0.00	0.00
2	0.3556	0.00	0.00
3	0.3048	0.00	0.00
4	0.2540	0.00	0.00
5	0.2032	0.00	0.00
6	0.1524	0.00	0.00
7	0.1016	0.00	0.00
8	0.0508	0.00	0.00
9	-0.0508	0.00	0.00
10	-0.1016	0.00	0.00
11	-0.1524	0.00	0.00
12	-0.2032	0.00	0.00
13	-0.2540	0.00	0.00
14	-0.3048	0.00	0.00
15	-0.3556	0.00	0.00
16	-0.4064	0.00	0.00

4.2.1 Effect of number of microphones (N)

The aim of this sub-section was to examine the effect of the number of microphones using experimental data. The number of non-overlapping blocks (L) was 120. The source was placed at X=0.02 m and Y=0.49 m, and the number of microphones (N) was varied from 4 to 16.

Figures 4.4 and 4.6 show the beamforming plots (3D and 2D plots) for N=4 and N=16 respectively. Figures 4.5 and 4.7 show the plots of array power along the x-axis and along the y-axis for N=4 and N=16 respectively. Figures 4.8 and 4.9 show the beamforming results (i.e., array power plots) using *simulation data* for different numbers of microphones, from N=4 to N=40. The array resolution and the dynamic range were obtained from the various beamforming maps. The beamwidth, the array resolution, the error band and the dynamic range are summarized in Table 4.2. It should be noted that the array resolution along the x-axis and the y-axis are not the same, and the array power is portrayed in two different plots [e.g., see Figure 4.5 (a) &(b)]. It should also be noted that the ellipses (resolution contours) in the 2D beamforming maps [see Figure 4.6 (b)] represent slices of the 3D maps taken at -3 dB below

the mainlobe peak. Plots of the dynamic range along the x-axis versus the number of microphones are presented in Figure 4.10, and plots of the array resolution along the x-axis and the y-axis versus the number of microphones are presented in Figure 4.11.

For N=4, the error band is ± 0.099 m (corresponding to ± 10 % error) along the x-axis and infinite along the y-axis (Figures 4.4 & 4.5 and Table 4.2). The dynamic range along the x-axis is 4.2 dB, while the dynamic range along the y-axis is undefined. Although, the error band along the x-axis is small, the dynamic range is not adequate. The beamforming map (2D plot) [Figure 4.4 (b)] is such that the resolution at -3 dB corresponds to two lines (rather than a closed loop). This shows that the source localization capability of the HULA is very poor under these circumstances (i.e., N=4), and beamforming is not possible.

For N=16, the error band is reduced to ± 0.039 m (corresponding to ± 3.9 % error) along the x-axis and ± 0.099 m (± 4.12 % error) along the y-axis (Figures 4.6 & 4.7 and Table 4.2). The dynamic ranges along the x-axis and the y-axis are 9.45 dB and 7.3 dB respectively (Table 4.2). These evaluators are satisfactory and the source localization capability of the microphone array is improved. Also, the array resolution contour at -3 dB [Figure 4.6(b)] is an ellipse, as compared to two lines for N=4 [Figure 4.4(b)].

For the simulation data (sub-section 3.3.1), the dynamic range decreases as the number of microphones increases. In contrast, for the experimental data, the dynamic range increases as the number of microphones increases (Table 4.2). This discrepancy is due to the fact that the separation distance between the two central microphones (the 8th and 9th microphones) was $2d$ in the case of the experimental data, whereas the separation distance was d in the case of the simulation data. Additional simulation results for N=4, 8 and 40 at a frequency of 2859 Hz are presented in Figures 4.8 and 4.9 for the separation distance between the central microphones equal to $2d$ (0.1016 m) and d (0.0508 m) respectively. Figure 4.8 (pertaining to a separation distance of $2d$) shows that the sidelobe level is high for small array apertures (i.e., N=4) and decreases initially as N increases but then increases for large N (N=40), signifying that the dynamic range increases then decreases as the number of microphone increase. Figure 4.9 (pertaining to a separation distance of d) shows *exactly* the same behavior as that shown in sub-section (3.3.1), i.e., the sidelobe level increases as the number of microphones increases, for all N, signifying that the dynamic range decreases as the number of microphones increases. The behaviour of the simulation results pertaining to the separation distance of $2d$ was not

portrayed by the experimental results because only 16 microphones were used in this HULA, as evidenced by the results presented in Figure 4.10.

Figure 4.11 indicates that the array resolution increases progressively along the x-axis and along the y-axis with the increase of number of microphones.

The results of this sub-section demonstrate that the source localization capability of HULA is poor for small array apertures, but can be improved by increasing the aperture. Overall, these experimental results are consistent with the simulation results.

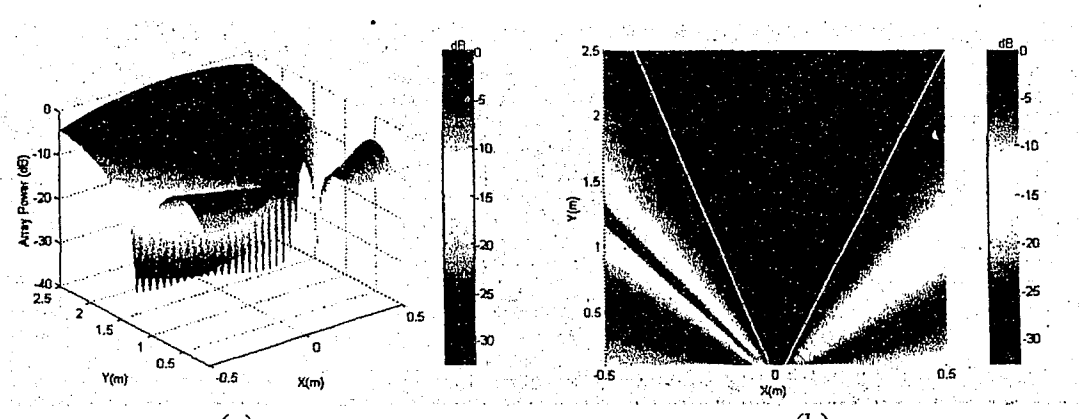

(a) (b)

Figure 4.4: Beamforming results for N=4; (a) Beamforming map: 3D plot (b) Beamforming map: 2D plot (white lines at -3 dB).

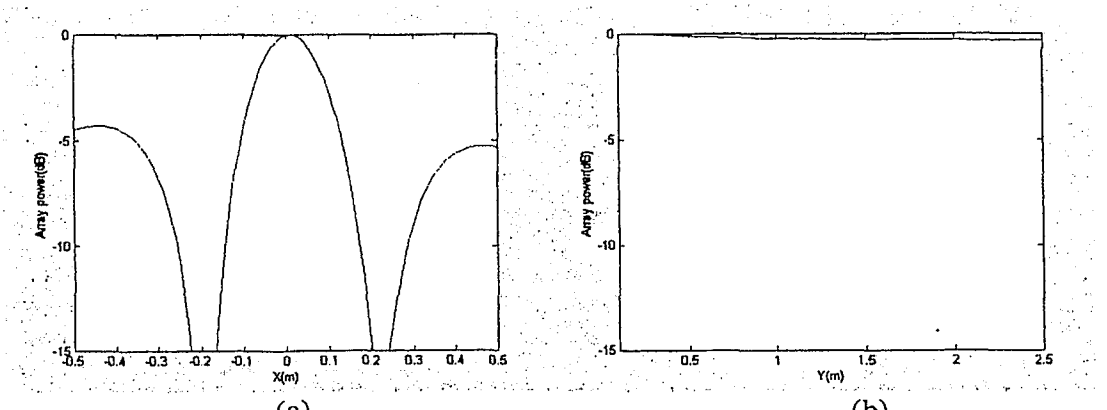

(a) (b)

Figure 4.5: Beamforming results for N=4; (a) Array power along the x-axis (b) Array power along the y-axis.

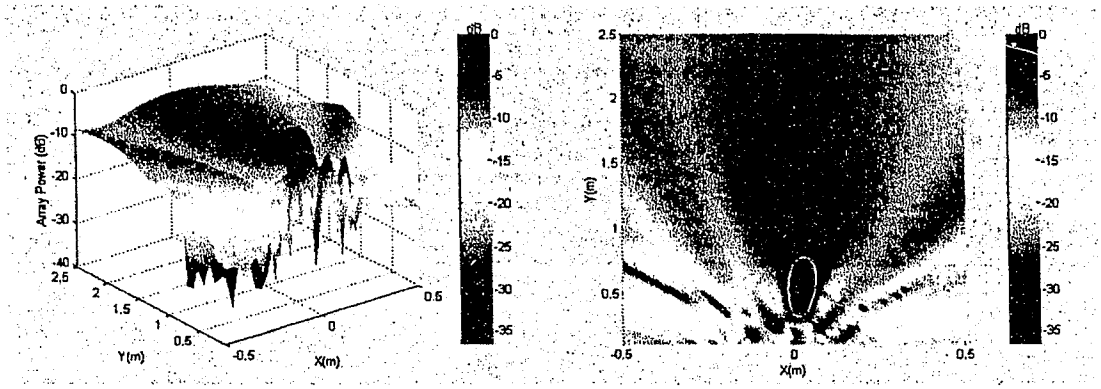

(a) (b)

Figure 4.6: Beamforming results for N=16; (a) Beamforming map: 3D plot (b) Beamforming map: 2D plot (ellipse at -3 dB).

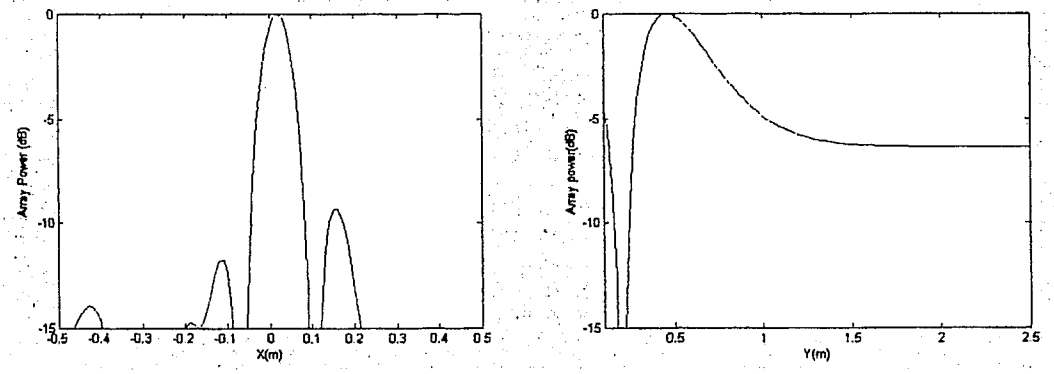

(a) (b)

Figure 4.7: Beamforming results for N=16; (a) Array power along the x-axis (b) Array power along the y-axis.

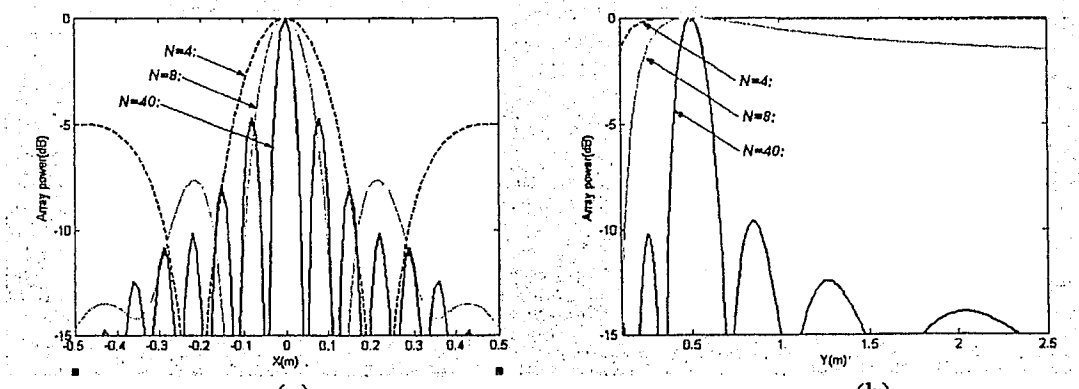

(a) (b)

Figure 4.8: ULA beamforming results *using simulation data* when the separation distance between the central centre microphones is $2d$ (0.1016 m), for N=4, N=8, N=40; (a) Array power along the x-axis (b) Array power along the y-axis.

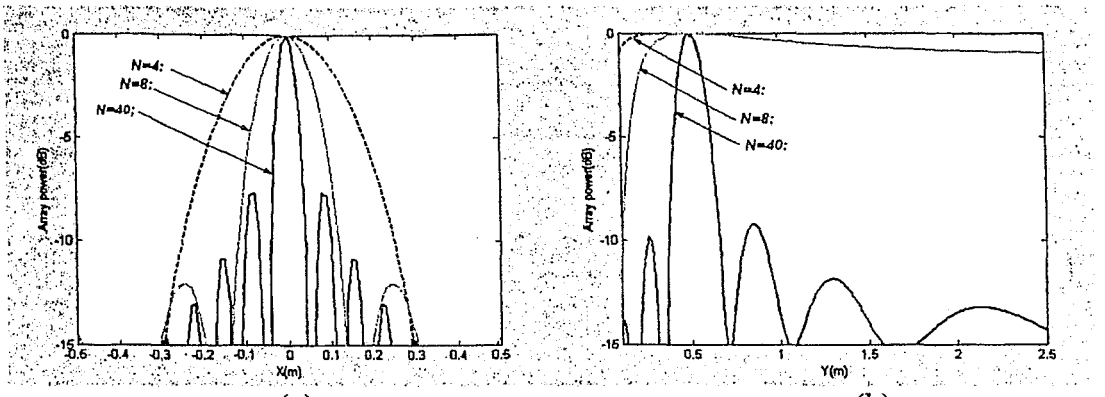

(a) (b)

Figure 4.9: ULA beamforming results *using simulation data* when the separation distance between the central microphones is d (0.0508 m), for N=4, N=8, N=40; (a) Array power along the x-axis (b) Array power along the y-axis.

Table 4.2 Effect of number of microphones

Array resolution, error band and the dynamic range along the x-axis

Number of microphones	Beamwidth (m)	Resolution (1/m)	Error band (m)	Dynamic range (dB)
4	0.198	5.02	± 0.099	4.2
8	0.117	8.54	± 0.058	6.9
12	0.090	11.11	± 0.045	8.5
16	0.079	12.62	± 0.039	9.45

Array resolution, error band and the dynamic range along the y-axis

Number of microphones	Beamwidth (m)	Resolution (1/m)	Error band (m)	Dynamic range (dB)
4	∞	0.00	∞	0
8	0.954	1.05	± 0.477	2.1
12	0.450	2.22	± 0.225	4.9
16	0.198	5.05	± 0.099	7.3

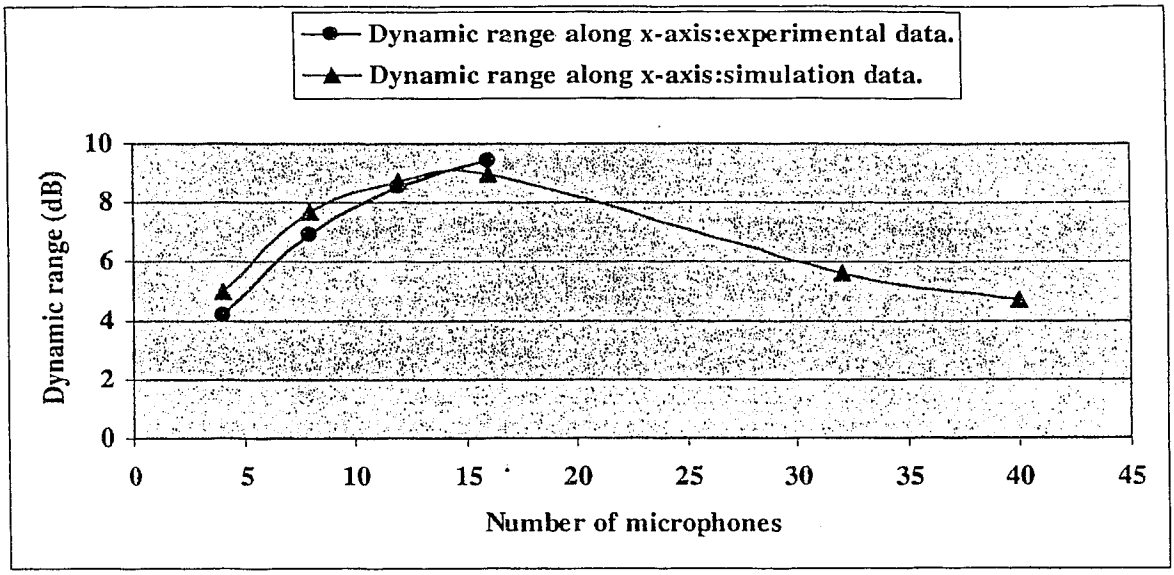

Figure 4.10: Effect of number of microphones on dynamic range along the x-axis when the separation distance between the central microphones of ULA is 2*d*: *experimental* and *simulation* data.

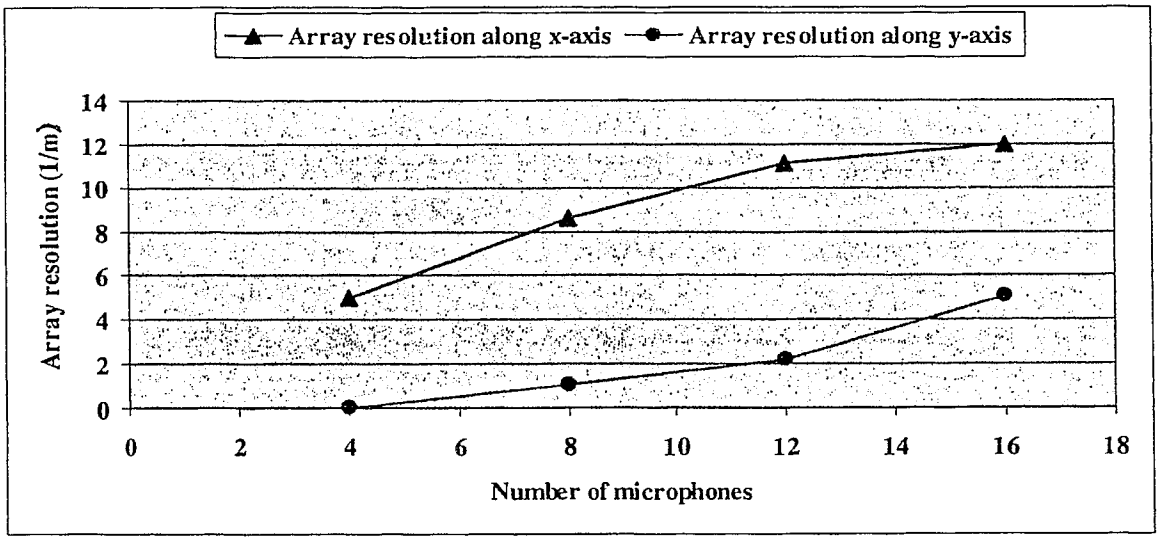

Figure 4.11: Effect of number of microphones on array resolution along the x-axis and along the y-axis when the separation distance between the central microphones of ULA is 2*d*: *experimental data.*

4.2.2 Effect of source position

The purpose of this sub-section was to determine the impact of source position using experimental data. Again, the number of non-overlapping blocks was 120. The number of microphones (N) was 16 and the acoustic source (i.e., the loudspeaker) was placed at three

positions, viz., (X=0.02, Y=0.49) m, (X=-0.18, Y=0.51) m and (X=0.01, Y=0.87) m with respect to the array centre.

Figures 4.12, 4.14 and 4.16 show the beamforming maps (3D and 2D plots) for the source at (0.02, 0.49) m, (-0.18, 0.51) m and (0.01, 0.87) m respectively. The corresponding plots of array power along the x-axis and along the y-axis are shown in Figures 4.13, 4.15 and 4.17. The array resolution and dynamic range were obtained from the various beamforming maps for different source positions. The beamwidth, the array resolution, the error band and the dynamic range are summarized in Table 4.3.

When the source is placed at (0.02, 0.49) m, the error band is ± 0.039 m (± 3.9 % error) along the x-axis and ± 0.099 m (± 4.12 % error) along the y-axis. (Figure 4.13 and Table 4.3). The dynamic ranges along the x-axis and along the y-axis are 9.45 dB and 7.3 dB respectively.

When the source is placed at (-0.18, 0.51) m, the error band is ± 0.0405 m (± 4.05 % error) along the x-axis and ± 0.069 m (± 2.9 % error) along the y-axis. (Figure 4.15 and Table 4.3). The dynamic ranges along the x-axis and along the y-axis are 7.8 dB and 4.2 dB respectively.

With the movement of the source from (0.02, 0.49) m to (-0.18, 0.51) m, the array dynamic range (along both the x-axis and the y-axis) is degraded. The x-axis error band increases and the y-axis error band decreases with this movement. It should be noted that the array resolution is calculated from the array power plots (Figures 4.13 and 4.15), which are obtained by slicing the 3D beamforming plots along the x-axis and the y-axis. When X=-0.18 m, the resolution ellipse is tilted [Figure 4.14 (b)], so that, as in the case of the simulation results (sub-section 3.3.2), the correct values of the array resolution based on the ellipse axes can not be calculated from the array power plots. In the beamforming 2D maps, the diameters of the ellipse change from 3.6 mm and 13mm to 3.5 mm and 8.5 mm with the movement of the source from X=-0.18 m to 0.02 m (~Y=0.5 m) [Figure 4.12 (b) & 4.14 (b)]. Clearly, the correct array resolution increases when the ellipse diameters decrease. Therefore, the array resolution is greater when the source is at X=0.02 m (i.e., perpendicular to the array centre) than when the source is at X=-0.18 m.

When the source is placed at (0.01, 0.87) m, the error band is ± 0.0630 m (± 6.3 % error) along the x-axis and ± 0.369 m (± 15.37 % error) along the y-axis. (Figure 4.16 & 4.17, Table 4.3). The dynamic range along the x-axis is 7.7 dB, while the dynamic range along the y-axis is undefined. Therefore, the error band along the x-axis and along the y-axis increases; also, the

dynamic range along the x-axis decreases when the source moves from (0.02, 0.49) m to (0.01, 0.87) m, i.e., the array source localization capability is degraded.

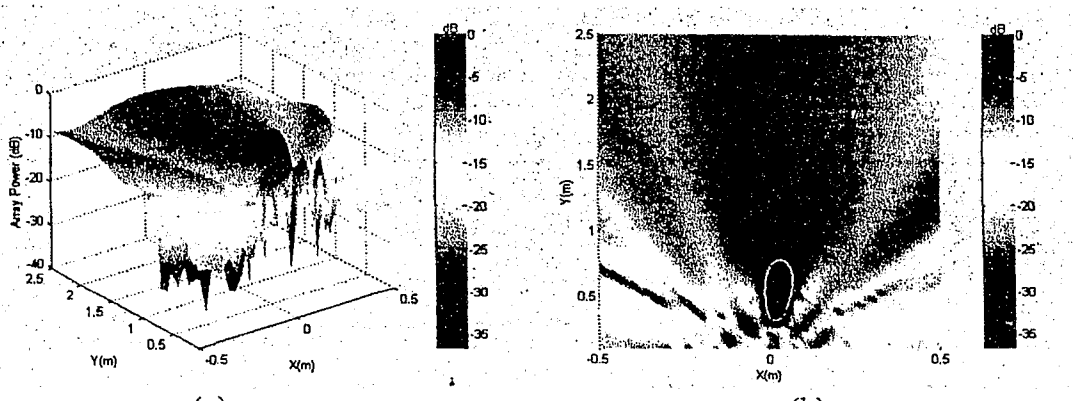

(a) (b)

Figure 4.12: Beamforming results for X=0.02 m, Y=0.49 m; (a) Beamforming map: 3D plot (b) Beamforming map: 2D plot (ellipse at -3 dB).

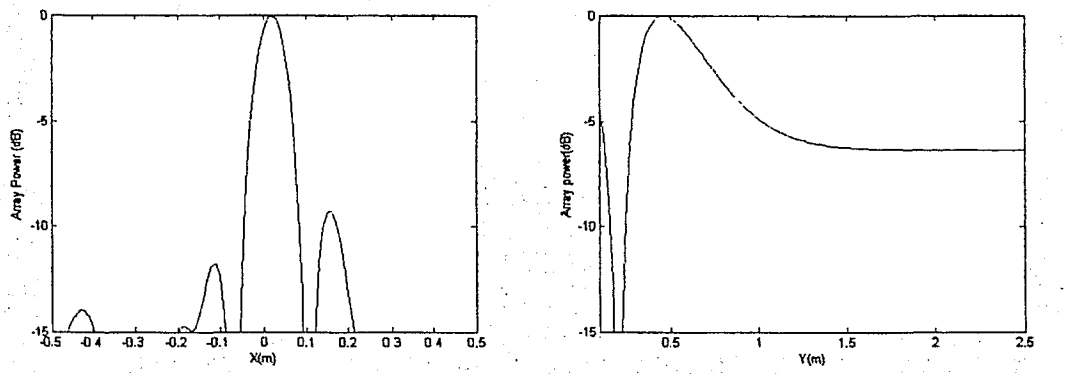

(a) (b)

Figure 4.13: Beamforming results for X=0.02 m, Y=0.49 m; (a) Array power along the x-axis (b) Array power along the y-axis.

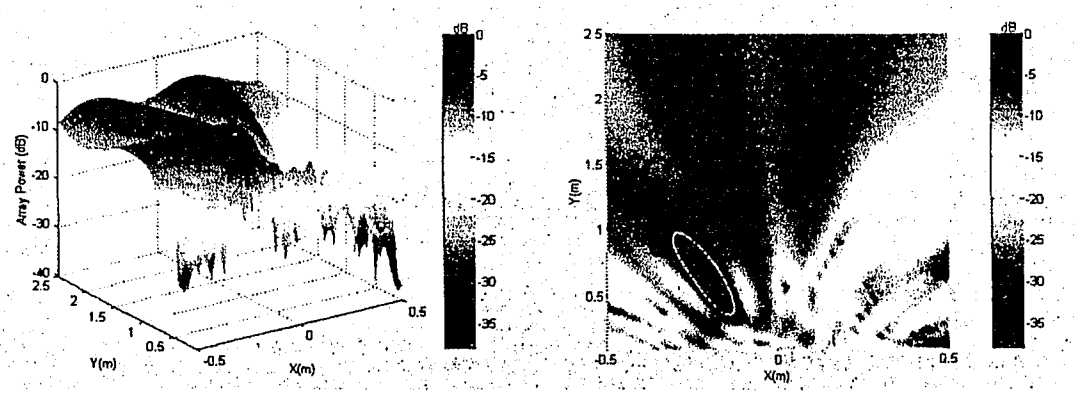

(a) (b)

Figure 4.14: Beamforming results for X=-0.18 m, Y=0.51 m; (a) Beamforming map: 3D plot (b) Beamforming map: 2D plot (ellipse at -3 dB).

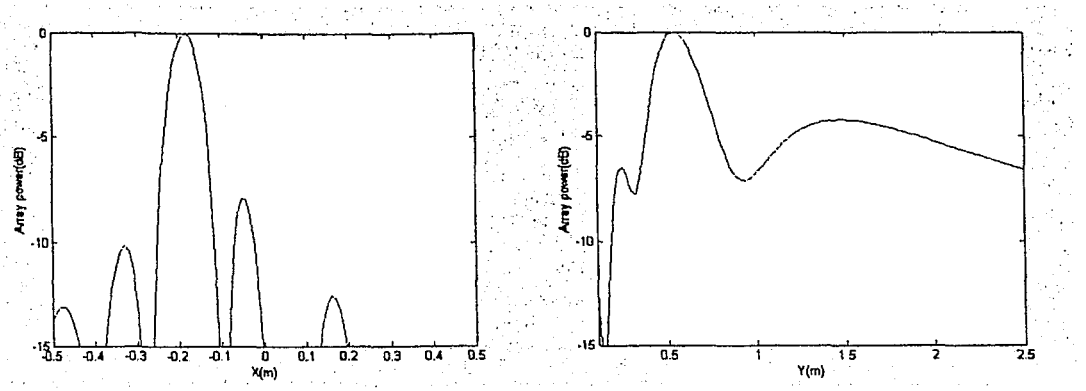

(a) (b)

Figure 4.15: Beamforming results for X=-0.18 m, Y=0.51 m; (a) Array power along the x-axis (b) Array power along the y-axis.

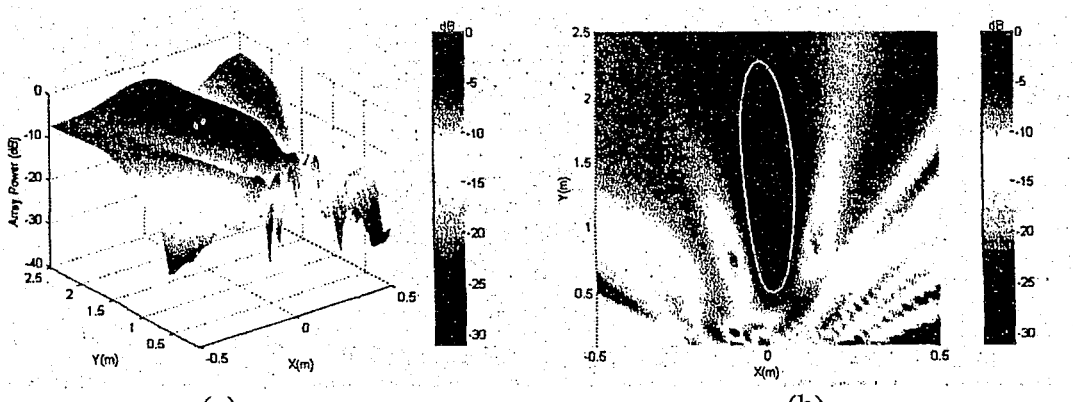

(a) (b)

Figure 4.16: Beamforming results for X=0.01 m, Y=0.87 m; (a) Beamforming map: 3D plot (b) Beamforming map: 2D plot (ellipse at -3 dB).

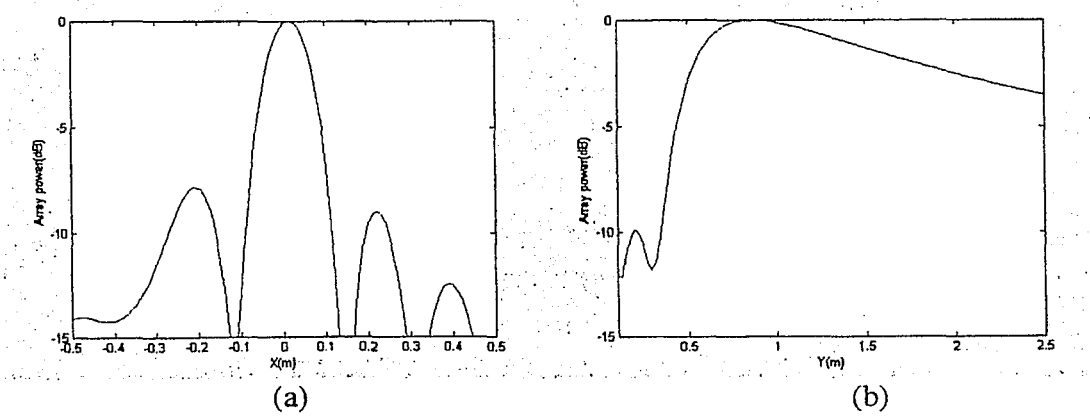

(a) (b)

Figure 4.17: Beamforming results for X=0.01 m, Y=0.87 m; (a) Array power along the x-axis (b) Array power along the y-axis.

Table 4.3 Effect of source position

Array resolution, error band and the dynamic range along the x-axis

Source Position (m)	Beamwidth (m)	Resolution (1/m)	Error band (m)	Dynamic range (dB)
X=0.02, Y=0.49	0.079	12.62	± 0.0395	9.45
X=-0.18,Y=0.51	0.081	12.34	± 0.0405	7.80
X=0.01, Y=0.87	0.126	7.95	± 0.0630	7.70

Array resolution, error band and the dynamic range along the y-axis

Source Position (m)	Beamwidth (m)	Resolution (1/m)	Error band (m)	Dynamic range (dB)
X=0.02, Y=0.49	0.198	5.05	± 0.099	7.3
X=-0.18,Y=0.51	0.138	7.21	± 0.069	4.2
X=0.01, Y=0.87	0.738	1.36	± 0.369	N.A.

The above results serve to demonstrate that the microphone array has maximum capability when the source is placed perpendicular to the array centre (i.e., broadside). This is in agreement with the simulation results. Also, the array capability degrades (i.e., array resolution and dynamic range decrease) as the source moves away from the array. But the simulation results (Figure 3.43) show that the array resolution decreases and dynamic range increases when a source moves away from the array. This difference between simulation and experimental results is due to the fact that, in the experiments, when the source moved away from the array, extraneous noise due to reflections from the floor and walls affecting the microphone array increased, causing the sidelobe level to increases; hence, the dynamic range decreased. Clearly, for source localization using a uniform linear array, the array centre should be placed as close as possible and perpendicular to the source.

4.2.3 Effect of inter-microphone distance (d)

The purpose of this sub-section was to examine the impact of inter-microphone distance using the experimental data. The source (i.e., the loudspeaker) was placed at (0.02, 0.49) m. The number of non-overlapping blocks was 120. Two cases were considered. For the first case, N=8 and d=4 inches (0.1016 m). For the second case, N=4 and d=8 inches (0.4064 m). It should be noted that the inter-microphone distance required to satisfy Shannon's criterion was d^*=2 inches (0.0508 m), for f= 2859 Hz.

Figure 4.18 shows the beamforming maps (3D and 2D plots) for N=8 and d=2d*. Figure 4.19 shows the beamforming maps (3D and 2D plots) for N=4 and d=4d*. Figure 4.20 shows the plots of array power along the x-axis and the y-axis for N=4 and d=4d*.

For N=8 and d=2d*, the beamforming map shows that the sidelobes are high and the array resolution contour at -3 dB has a distorted shape (Figure 4.18). In this case, the array source localization capability is degraded. For N=4 and d=4d*, the mainlobe splits into a number of lobes (i.e., grating lobes appear in the beamforming map) [Figure 4.19]. The magnitude of each grating lobe is same as that of the mainlobe, and this makes the beamforming method futile (Figure 4.20).

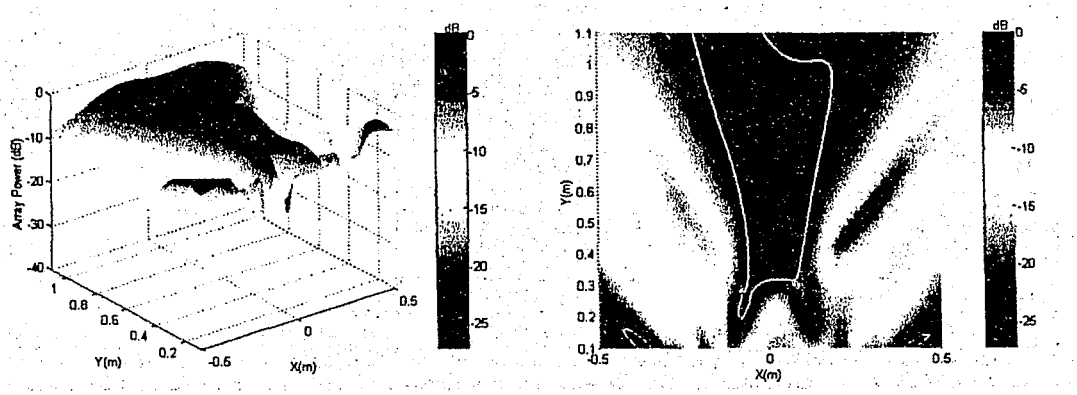

(a) (b)

Figure 4.18: Beamforming results for N=8, d= 2d*; (a) Beamforming map: 3D plot (b) Beamforming map: 2D plot (white irregular line at -3 dB).

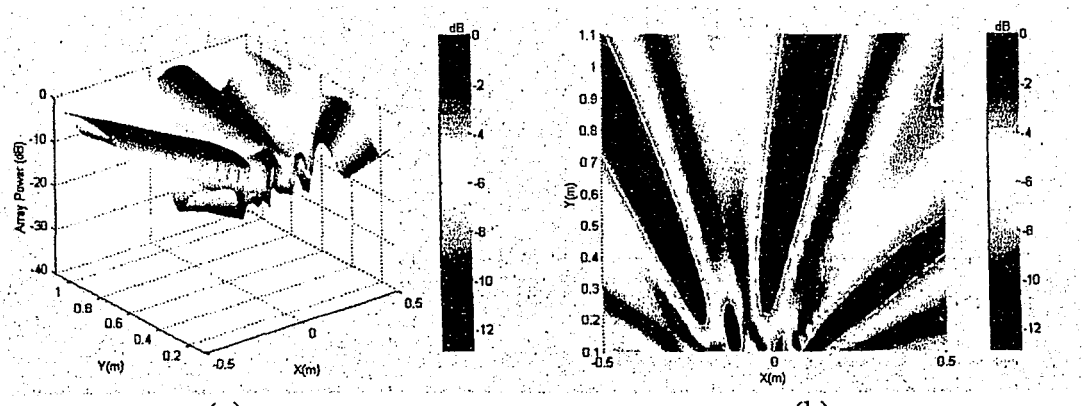

(a) (b)

Figure 4.19: Beamforming results for N=4, d=4d*; (a) Beamforming map: 3D plot (b) Beamforming map: 2D plot (white lines at -3 dB).

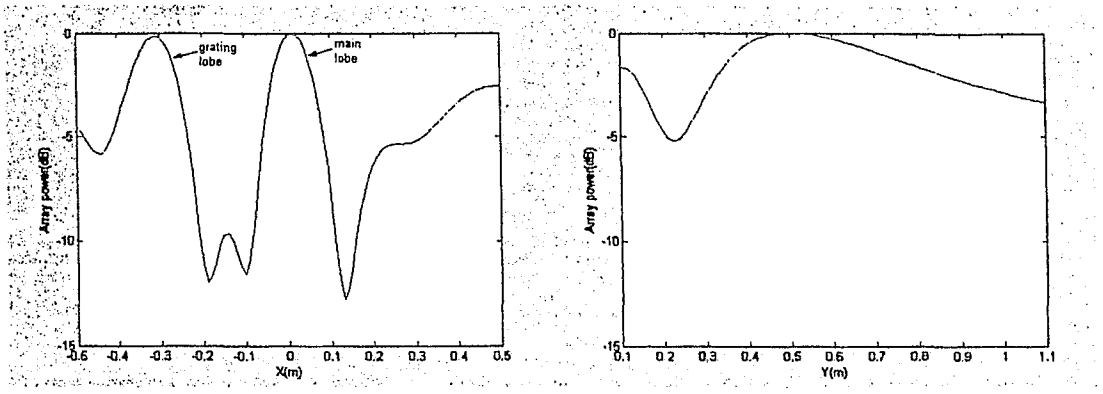

(a) (b)

Figure 4.20: Beamforming results for N=4, d=4d*; (a) Array power along the x-axis (b) Array power along the y-axis.

The above experimental results are in general agreement with the simulation results presented in sub-section 3.3.3, and it is clear from these results that an acoustic source cannot be localized when Shannon's criterion is not met.

4.3 Comparison between a Vertical Uniform Linear Array (VULA) and an HULA

The purpose of this section was to compare beamforming results obtained via a *vertical* uniform linear array (VULA) with those obtained via an HULA. The VULA consisted of the cross array microphones located along the vertical axis, perpendicular to the floor, which was taken to be the y-axis. The HULA consisted of the cross array microphones located along the axis parallel to the floor, which was taken to be the x-axis. It should be noted that in the previous case, the vertical axis was the z-axis. The source was placed along the z-axis. The beamforming maps were obtained by computing steering vectors for various assumed source locations in the x-z plane for HULA and in the y-z plane for VULA.

The source was placed at (0.01, 0.01, 0.53) m and the number of microphones was 16 for both the HULA and the VULA. The microphone coordinates of the HULA and the VULA are given in Tables 4.2 and 4.4. For the HULA, the microphones were placed 30 inches (1.52 m) above the laboratory floor, and for the VULA, the 1st microphone and 16th microphone were 46 inches (2.34 m) and 14 inches (0.7112 m) respectively above the floor.

The experimental data were collected for 8 seconds for both the HULA and the VULA at a sampling rate of 16 KHz. The data points collected at each microphone were divided into 120 non-overlapping blocks, each containing 1024 data points (i.e., M=1024).

Table 4.4 VULA Microphone Coordinates

Mic #	X location	Y location	Z location
	(m)	(m)	(m)
1	0.00	0.4064	0.00
2	0.00	0.3556	0.00
3	0.00	0.3048	0.00
4	0.00	0.2540	0.00
5	0.00	0.2032	0.00
6	0.00	0.1524	0.00
7	0.00	0.1016	0.00
8	0.00	0.0508	0.00
9	0.00	-0.0508	0.00
10	0.00	-0.1016	0.00
11	0.00	-0.1524	0.00
12	0.00	-0.2032	0.00
13	0.00	-0.2540	0.00
14	0.00	-0.3048	0.00
15	0.00	-0.3556	0.00
16	0.00	-0.4064	0.00

Figures 4.21 and 4.22 show the beamforming maps (3D and 2D plots) and plots of array power along the x and y axes for the VULA (N=16). Figures 4.23 and 4.24 show the beamforming maps (3D and 2D plots) and plots of array power along the x and y axes for the HULA (N=16). Figure 4.25 shows plots of array power along the x and y axes based on simulation data for the VULA and the HULA with N=16. The array resolution and the dynamic range were obtained from the beamforming maps. The beamwidth, the array resolution, the error band and the dynamic range are summarized in Table 4.5.

For the VULA, with N=16, the error band is ± 0.045 m and the array dynamic range is 7.7 dB along the y-axis (i.e., along the array axis) (Figure 4.21, 4.22, Table 4.5). The error band is ± 0.335 m and the array dynamic range is 5.95 dB along the z-axis. The source position is localized at (Y=0.01 m, Z=0.6 m).

For the HULA, with N=16, the error band is ± 0.041 m and the array dynamic range is 9.63 dB along x-axis (i.e., along the array axis) (Figures 4.23, 4.24 and Table 4.5). The error band is ± 0.287 m and the array dynamic range is 11.55 dB along the z-axis. The source position is localized at X=0.01 m and Z=0.53 m.

The error band decreases and the dynamic range increases as the array geometry changes from the VULA to the HULA, i.e., the array source localization capability improves. On the other hand, the beamforming results obtained by using simulation data (without extraneous noise) show that there is no impact on the beamforming results whether the HULA or the VULA is used (Figure 4.25).

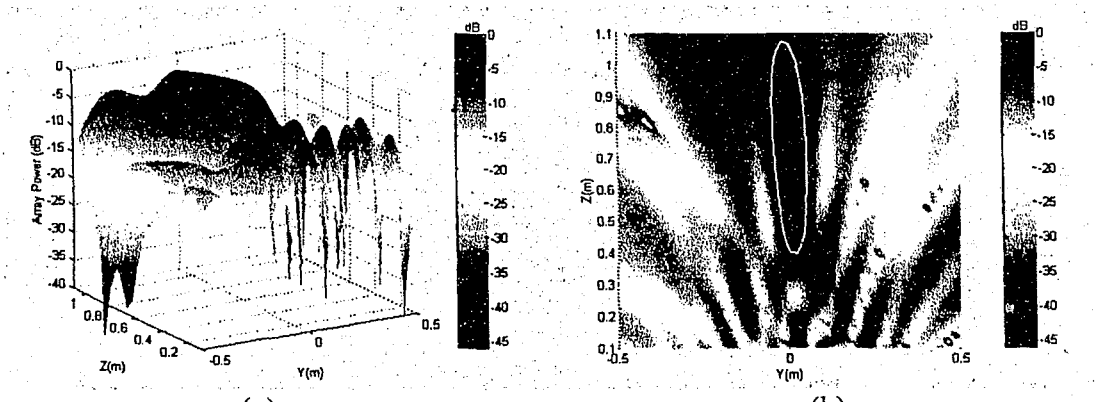

(a) (b)

Figure 4.21: Beamforming results for VULA, N=16; (a) Beamforming map: 3D plot (b) Beamforming map: 2D plot (ellipse at -3 dB).

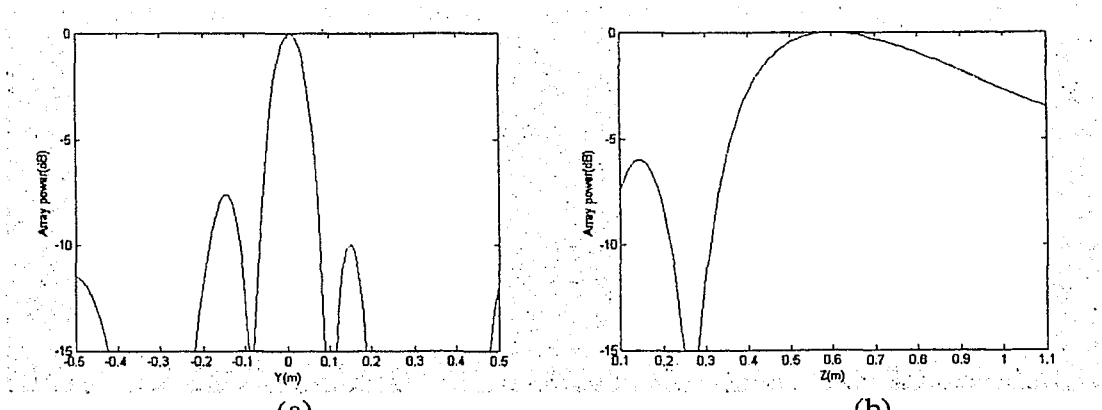

(a) (b)

Figure 4.22: Beamforming results for VULA, N=16; (a) Array power along the x-axis (b) Array power along the y-axis.

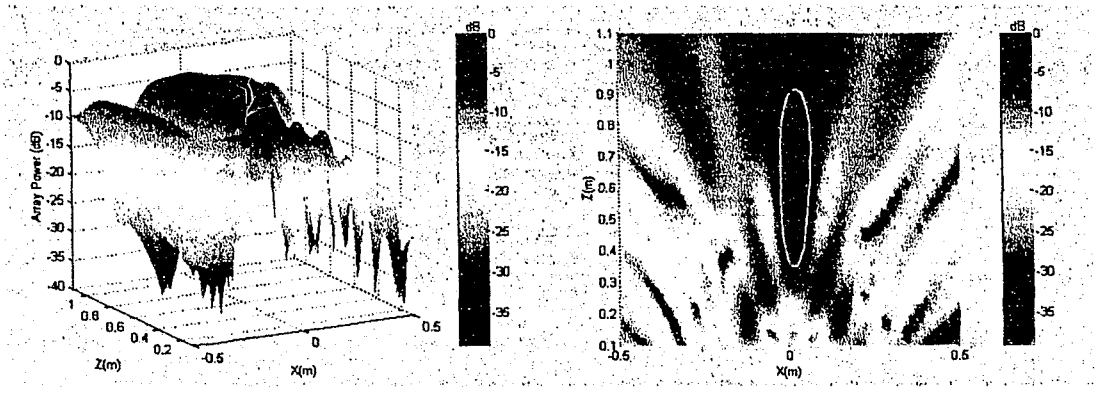

(a) (b)

Figure 4.23: Beamforming results for HULA, N=16; (a) Beamforming map: 3D plot (b) Beamforming map: 2D plot (ellipse at -3 dB).

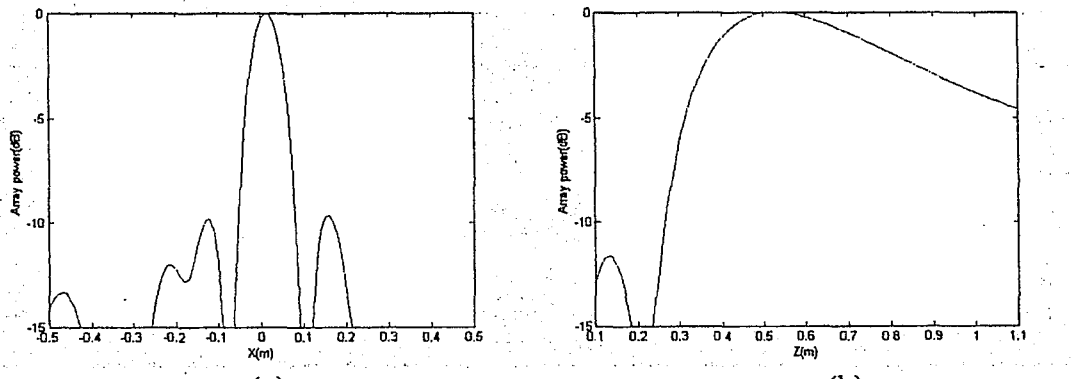

(a) (b)

Figure 4.24: Beamforming results for HULA, N=16; (a) Array power along the x-axis (b) Array power along the y-axis.

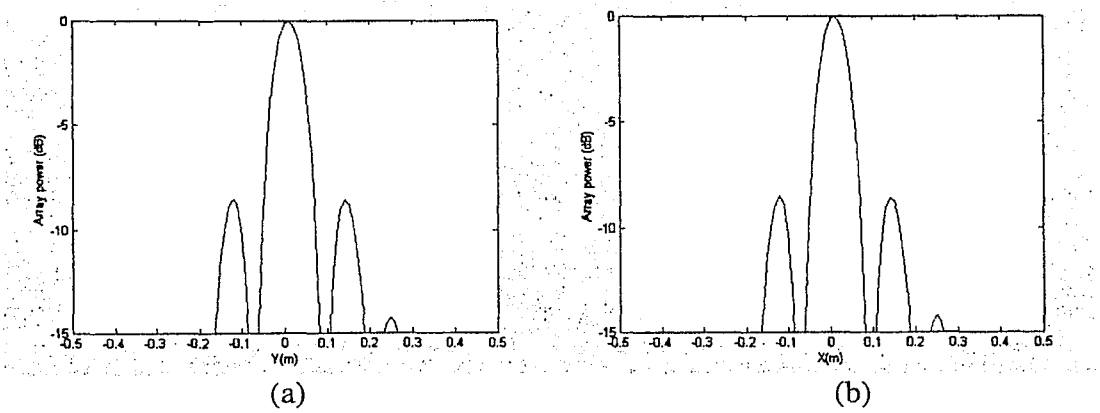

(a) (b)

Figure 4.25: Beamforming results *using simulation data* for N=16; (a) Array power along the x-axis for VULA (b) Array power along the x-axis for HULA.

Table 4.5 Effect of ULA geometry (HULA versus VULA)

Array resolution, error band and the dynamic range along the y-axis (VULA)

N (type of array)	Beamwidth (m)	Resolution (1/m)	Error band (m)	Dynamic range (dB)
16 (VULA)	0.090	11.11	± 0.045	7.7

Array resolution, error band and the dynamic range along the x-axis (HULA)

N (type of array)	Beamwidth (m)	Resolution (1/m)	Error band (m)	Dynamic range (dB)
16 (HULA)	0.081	12.35	± 0.041	9.63

Array resolution, error band and the dynamic range along the z-axis (HULA and VULA)

N (type of array)	Beamwidth (m)	Resolution (1/m)	Error band (m)	Dynamic range (dB)
16 (VULA)	0.671	1.49	± 0.335	5.95
16 (HULA)	0.575	1.74	± 0.287	11.55

The experimental results of this sub-section serve to demonstrate that a horizontal uniform linear array (HULA) is better than a vertical uniform linear array (VULA). The simulation results show that the array geometry has no effect on the beamforming results for a noise free environment (e.g., in an anechoic chamber). The change in the experimental results, with the change of the array geometry, is due to the position of the VULA microphones. Specifically, the lower VULA microphones (i.e., the 25^{th} to the 32^{nd}), which were near to the hard floor, were affected significantly by extraneous floor-reflection noise.

4.4 Cross Array

When microphones are separated by a constant distance in a plane (i.e., the x-y plane) to form a cross, the array is called a cross array as shown in Figure 4.1(b). The cross array was used for the experiments because it was relatively easy to arrange the microphones in a cross. Note that this array is a type of uniform planar array. The cross array consisted of 32 microphones, with the separation distance between the central microphones equal to $2d$ .The microphone array coordinates are given in Table 4.6. The acoustic source (i.e., the loudspeaker) was placed within 1 m from the array so that a spherical wave front occurred at

the microphones, i.e., the loudspeaker was a near field source. The data were collected for 8 seconds at each microphone with a sampling rate of 16 KHz and were divided into non-overlapping blocks, each containing 1024 data points (i.e., M=1024). With the sampling rate being 16 KHz, the frequency resolution was 15.62 Hz.

The digital data collected by the microphone array were stored for post-processing, as discussed in sub-section 4.1.2, and the MATLAB code was applied to obtain the beamforming results (see Appendix A). With the array lying in the x-y plane, the source can be localized by considering an x-y plane (i.e., a grid plane) at different locations along the z-axis (i.e., at different grid distances), as depicted in Figure 3.56. The grid plane contains grid points with increments along the x and y-axes. The relevant beamforming maps were obtained, at different grid distances, by computing steering vectors for various assumed locations in the x-y plane. The position where the array power is maximum (i.e., where the mainlobe appears) in the grid plane corresponds to the X-Y location of the source. The position where the array power is maximum along the z-axis represents the Z location of the source.

Table 4.6 Cross Array Microphone Coordinates

Mic #	X location (m)	Y location (m)	Z location (m)	Mic #	X location (m)	Y location (m)	Z location (m)
1	0.4064	0.00	0.00	17	0.00	0.4064	0.00
2	0.3556	0.00	0.00	18	0.00	0.3556	0.00
3	0.3048	0.00	0.00	19	0.00	0.3048	0.00
4	0.2540	0.00	0.00	20	0.00	0.2540	0.00
5	0.2032	0.00	0.00	21	0.00	0.2032	0.00
6	0.1524	0.00	0.00	22	0.00	0.1524	0.00
7	0.1016	0.00	0.00	23	0.00	0.1016	0.00
8	0.0508	0.00	0.00	24	0.00	0.0508	0.00
9	-0.0508	0.00	0.00	25	0.00	-0.0508	0.00
10	-0.1016	0.00	0.00	26	0.00	-0.1016	0.00
11	-0.1524	0.00	0.00	27	0.00	-0.1524	0.00
12	-0.2032	0.00	0.00	28	0.00	-0.2032	0.00
13	-0.2540	0.00	0.00	29	0.00	-0.2540	0.00
14	-0.3048	0.00	0.00	30	0.00	-0.3048	0.00
15	-0.3556	0.00	0.00	31	0.00	-0.3556	0.00
16	-0.4064	0.00	0.00	32	0.00	-0.4064	0.00

The following parameters were used for the sensitivity analysis of the cross array.

- Number of microphones (N).
- Source position.

4.4.1 Effect of number of microphones (N)

The purpose of this sub-section was to examine the impact of number of microphones on the beamforming results. The number of non-overlapping blocks was 120. The source was placed at X=0.01 m, Y=0.01 m, Z=0.53 m, and the number of microphones (N) was varied from N=8 (a cross of 4 x 4) to N=32 (a cross of 16 x 16).

Figures 4.26 and 4.27 show the beamforming maps (3D and 2D plots) and the plots of array power along the x-axis and along the y-axis for N =8 (a cross array of 4 x 4). Figures 4.28 and 4.29 show the beamforming maps (3D and 2D plots) and the array power plots along the x-axis and along the y-axis for N =32 (a cross array of 16 x 16). Figures 4.30 and 4.31 show cross array beamforming results (array power plots) using *simulation data* for N=8, 20 and 32, with the separation distance between the central microphones equal to $2d$ and d respectively. The array resolution and the dynamic range were obtained from the various beamforming maps using the experimental data. The beamwidth, the array resolution, the error band and the dynamic range pertaining to these data are summarized in Table 4.7.

For N=8, the error band is ± 0.198 m along the x-axis and ± 0.144 m along the y-axis (Figures 4.26, 4.27 and Table 4.7). The mainlobe is wide and the dynamic range cannot be defined. For this small array aperture, the source is localized at X=0.02 m, Y=0.05 m and Z=0.53 m, as opposed to X=0.01 m, Y=0.01 m and Z=0.53 m (the correct location). Thus, the source localization capability is poor for N=8.

For N=32, the error band decreases to ± 0.054 m along the x-axis and to ± 0.059 m along the y-axis (Figures 4.28, 4.29 and Table 4.7). The array dynamic range along the x-axis is 6.65 dB and along the y-axis is 3.50 dB. The array resolution increases and sidelobes appear in the beamforming results. Moreover, the source is correctly localized at (0.01, 0.01, 0.53) m. Thus, the source localization capability is improved for N=32.

The error bands and the array dynamic ranges along the x-axis and along the y-axis decrease as the number of microphones increases from N=8 to N=32 (Table 4.7). The decrease of dynamic range with the increase of microphones is unexpected based on the simulation

results for the uniform square array (sub-section 3.4.1). However, the cross array simulation results pertaining to a separation distance between the central microphones equal to $2d$, exhibit *exactly* the same behavior, i.e., the dynamic range decreases as the number of microphones increases (Figure 4.30). Therefore, the experimental results are consistent with the simulation results. It is noted that the array resolution and the sidelobe levels are the same along the x-axis and the y-axis for the simulation results. On the other hand, for the experimental results, the array resolution and the sidelobe levels are not the same along the x-axis and the y-axis. This discrepancy is due to the fact that the lower y-axis cross array microphones (i.e., the 25th to the 32nd) are near to the hard floor, and are affected significantly by extraneous floor-reflection noise.

The simulation results pertaining to a separation distance between the central microphones equal to d presented in Figure 4.31 display the same behaviour, i.e., the dynamic range decreases as the number of microphones increases. Therefore, these simulation results serve to demonstrate that the cross array is not as good as the square array, as far as dynamic range is concerned.

The results of this sub-section establish that the source localization capability of a cross array is poor for small array apertures. As the aperture increases, the array resolution increases, but the dynamic range decreases. It is evident that the cross array geometry is inferior to the square array geometry [33]. The cross array was used for these experiments because it was relatively easy to arrange the microphones in a cross.

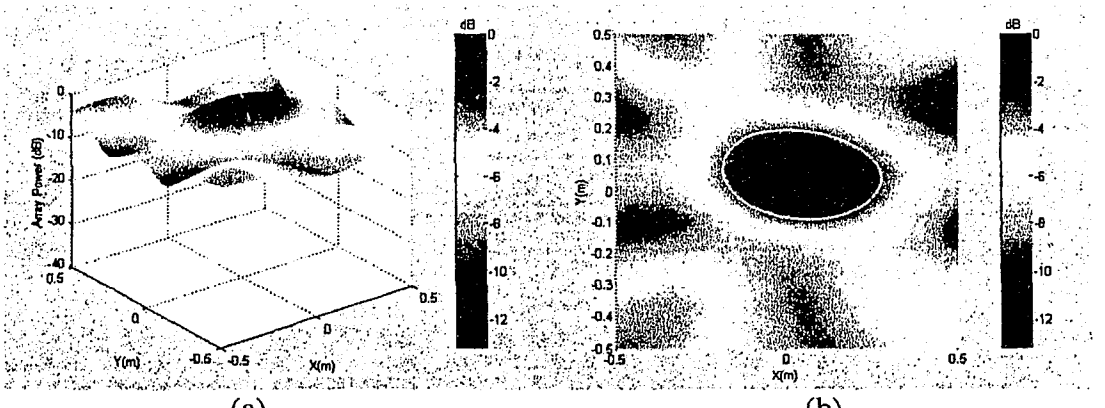

(a) (b)

Figure 4.26: Beamforming results for N=8 (a cross array of 4 x 4); (a) Beamforming map: 3D plot (b) Beamforming map: 2D plot (ring at -3 dB).

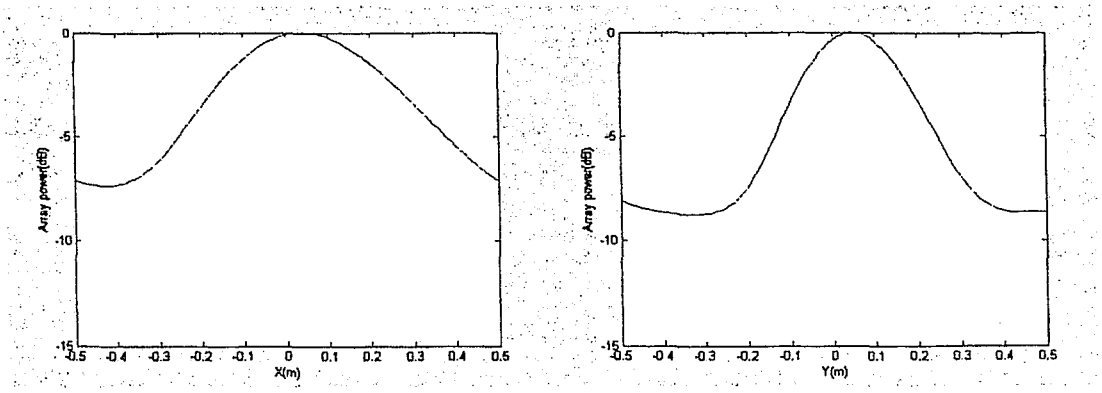

(a) (b)

Figure 4.27: Beamforming results for N=8 (a cross array of 4 x 4); (a) Array power along x-axis (b) Array power along y-axis.

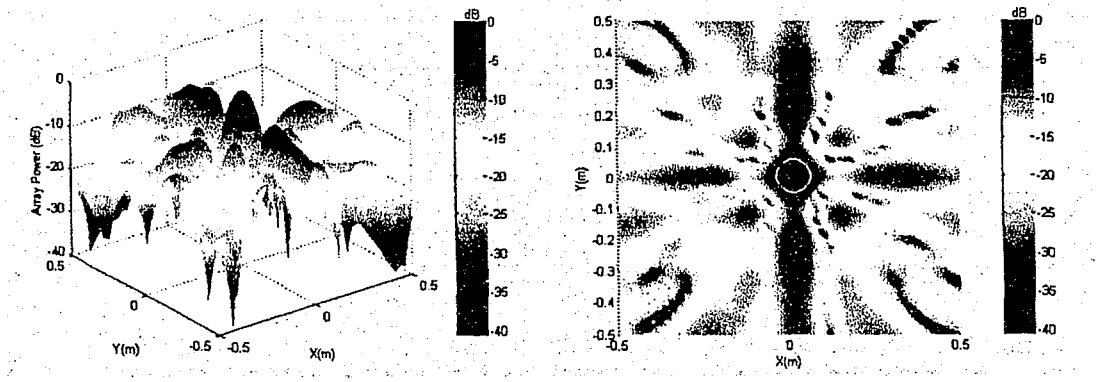

(a) (b)

Figure 4.28: Beamforming results for N=32 (a cross array of 16 x 16);
(a) Beamforming map: 3D plot (b) Beamforming map: 2D plot (ring at -3 dB).

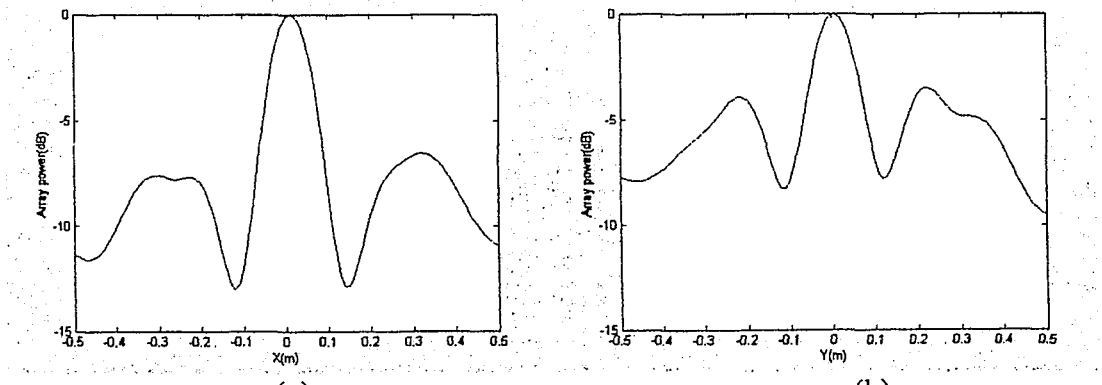

(a) (b)

Figure 4.29: Beamforming results for N=32 (a cross array of 16 x 16);
(a) Array power along x-axis (b) Array power along y-axis.

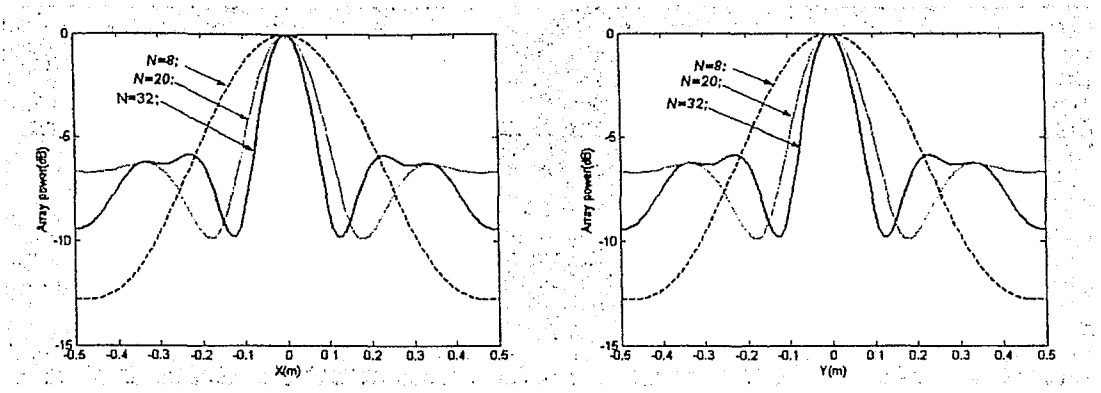

(a) (b)

Figure 4.30: Cross array beamforming results *using simulation data* when the separation distance between the central centre microphones is $2d$ (0.1016 m), for N=8, N=20, N=32; (a) Array power along the x-axis (b) Array power along the y-axis

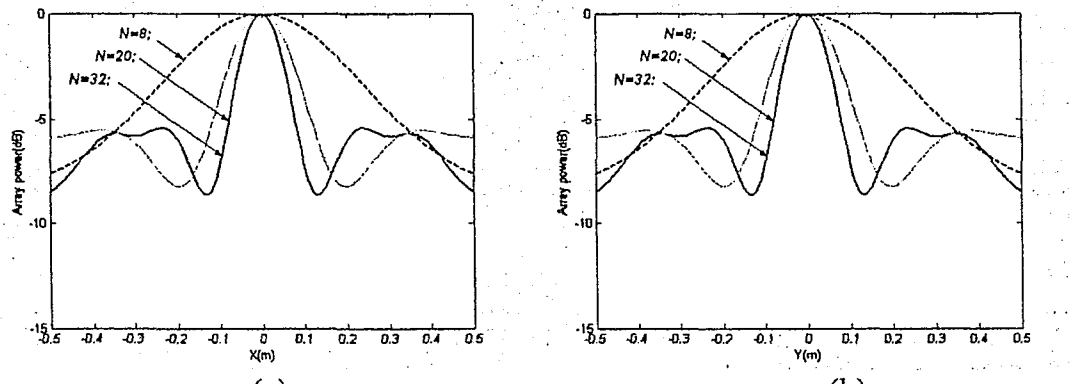

(a) (b)

Figure 4.31: Cross array beamforming results *using simulation data* when the separation distance between the central centre microphones is d (0.0508 m), for N=8, N=20, N=32; (a) Array power along the x-axis (b) Array power along the y-axis

Table 4.7 Effect of number of microphones

Array resolution, error band and the dynamic range along the x-axis

Number of microphones	Beamwidth (m)	Resolution (1/m)	Error band (m)	Dynamic range (dB)
8	0.396	2.52	± 0.198	N.A.
12	0.198	5.05	± 0.099	N.A.
20	0.126	7.94	± 0.063	8.23
28	0.117	8.55	± 0.059	7.18
32	0.108	9.26	± 0.054	6.65

-Table 4.7 continued-

Array resolution, error band and the dynamic range along the y-axis

Number of microphones	Beamwidth (m)	Resolution (1/m)	Error band (m)	Dynamic range (dB)
8	0.288	3.47	± 0.144	N.A.
12	0.250	4.00	± 0.125	N.A.
20	0.198	5.05	± 0.099	4.03
28	0.135	7.41	± 0.067	3.70
32	0.117	8.55	± 0.059	3.50

4.4.2 Effect of source position

The purpose of this sub-section was to determine the impact of source position on the cross array beamforming results obtained using experimental data. The number of non-overlapping blocks was 120. The number of microphones (N) was 32, (a cross array of 16 x 16), and the source (i.e., the loudspeaker) was placed at three different positions, viz., (0.01, 0.01, 0.53) m, (0.31, 0.02, 0.52) m, and (0.01, -0.05, 0.76) m with respect to the array centre.

Figures 4.32 and 4.33 show the beamforming maps (3D and 2D plots) and the plots of array power along the x-axis and along the y axis for the source at (0.01, 0.01, 0.53) m. Figures 4.34 and 4.35 show the beamforming maps (3D and 2D plots) and the plots of array power along the x-axis and the y-axis for the source at (0.31, 0.02, 0.52) m. Figure 4.36 shows plots of normalized array pressure versus X and Y for the source at (0.01, 0.01, 0.53) m and (0.31, 0.02, 0.52) m. Figures 4.37 and 4.38 show the beamforming maps (3D and 2D plots) and the plots of array power along the x-axis and along the y-axis for the source at (0.01, -0.05, 0.76) m. The array resolution and the dynamic range were obtained from the various beamforming maps for different source positions. The beamwidth, the array resolution, the error band and the dynamic range are summarized in Table 4.8.

When the source is placed at (0.01, 0.01, 0.53) m, the error band and the array dynamic range are ± 0.054 m and 6.65 dB respectively along the x-axis, and ± 0.059 m and 3.50 dB respectively along the y-axis (Figures 4.32, 4.33 and Table 4.8).

When the source is placed at (0.31, 0.02, 0.52) m, the error band and the array dynamic range are ± 0.063 m and 5.00 dB respectively along the x-axis, and ± 0.068 m and 5.6 dB

respectively along the y-axis (Figures 4.34 and 4.35, Table 4.8). Thus, with the movement of the source from (0.01, 0.01, 0.53) m to (0.31, 0.02, 0.52) m, the error band increases along both axes, while the dynamic range decreases along the x-axis but increases along the y-axis. It should be noted that the dynamic range is calculated from the array power plots (Figure 4.35) and these plots are obtained by slicing the 3D beamforming plot [Figure 4.34 (a)] along the x-axis and the y-axis. As can be seen in Figure 4.34 (b), the y-axis sidelobes lie outside of the slicing region. This is reason why the dynamic range increases along the y-axis. Figure 4.36 (a) & (b) show that the number of sidelobes increases and the sidelobes are more asymmetric at (0.31, 0.02, 0.52) m than at (0.01, 0.01, 0.53) m. Therefore, the array source localization capability is degraded as the source moves from (0.01, 0.01, 0.53) m to (0.31, 0.02, 0.52) m.

When the source is placed at (0.01, -0.05, 0.76) m, the error band and the array dynamic range are ± 0.081 m and 5.07 dB respectively along the x-axis, and ± 0.076 m and 4.7 dB respectively along the y-axis (Figures 4.37 and 4.38, Table 4.8). Thus, with the movement of the source from (0.01, 0.01, 0.53) m to (0.01, -0.05, 0.76) m., the error bands increase along both the x-axis and the y-axis, while the dynamic range decreases along the x-axis but increases along the y-axis.

The above results serve to establish that the cross array has maximum source localization capability when a source is placed perpendicular to the array centre. Moreover, this capability is degraded as the distance between the source and the array increases.

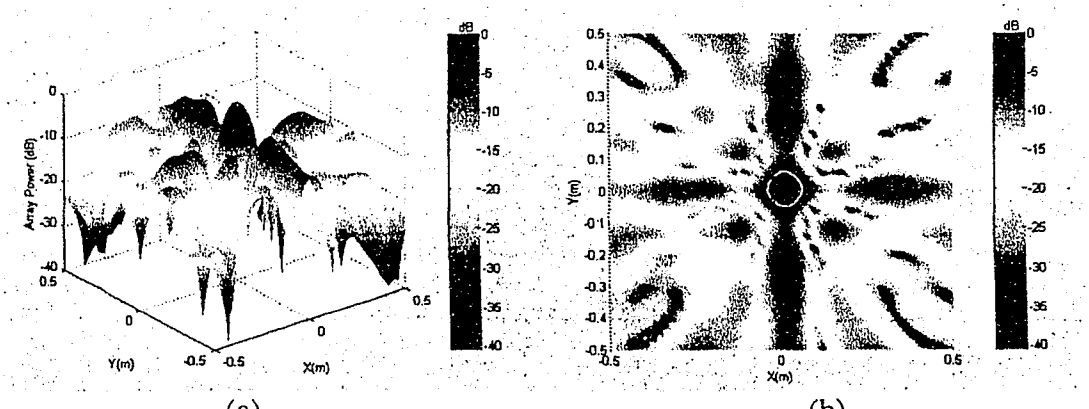

(a) (b)

Figure 4.32: Beamforming results for (0.01, 0.01, 0.53) m; (a) Beamforming map: 3D plot (b) Beamforming map: 2D plot (ring at -3 dB).

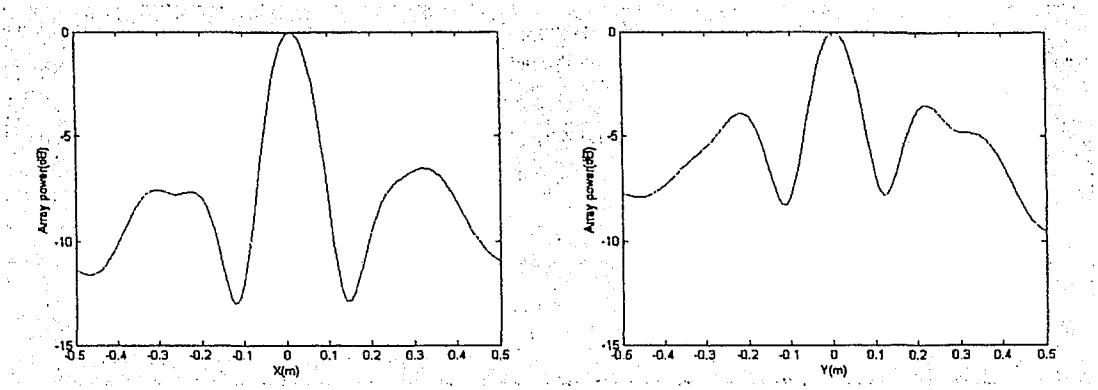

(a) (b)

Figure 4.33: Beamforming results for (0.01, 0.01, 0.53) m; (a) Array power along the x-axis (b) Array power along the y-axis.

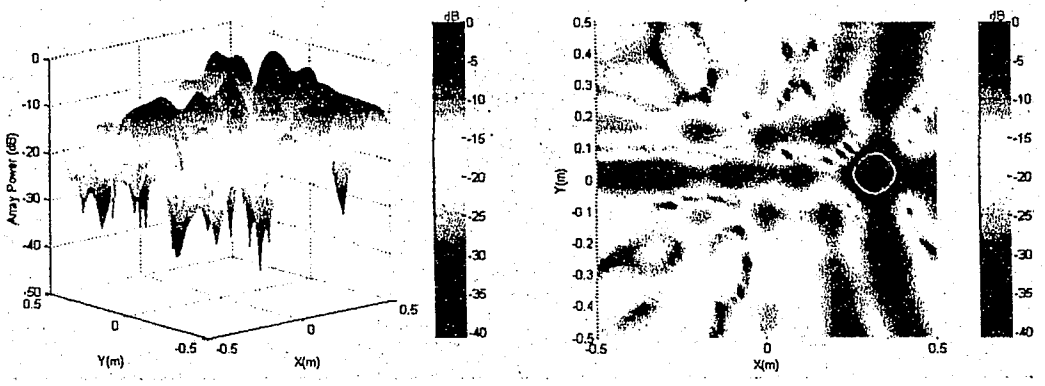

(a) (b)

Figure 4.34: Beamforming results for (0.31, 0.02, 0.52) m; (a) Beamforming map: 3D plot (b) Beamforming map: 2D plot (ring at -3 dB).

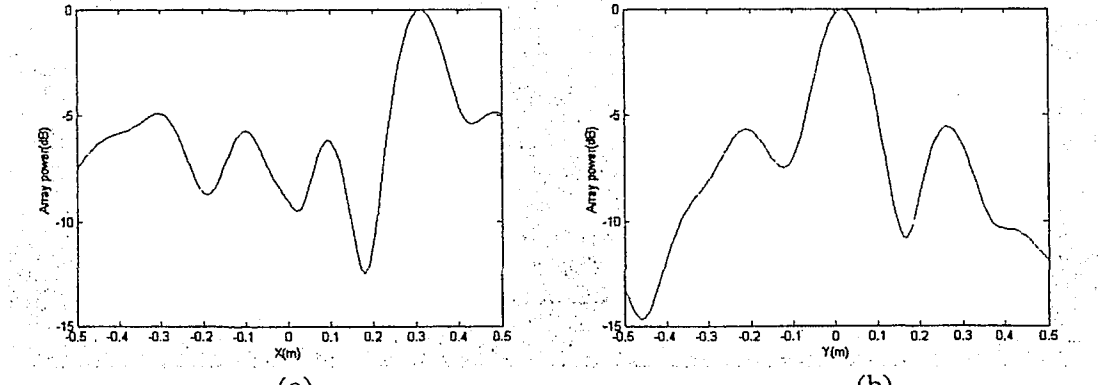

(a) (b)

Figure 4.35: Beamforming results for (0.31, 0.02, 0.52) m; (a) Array power along the x-axis (b) Array power along the y-axis.

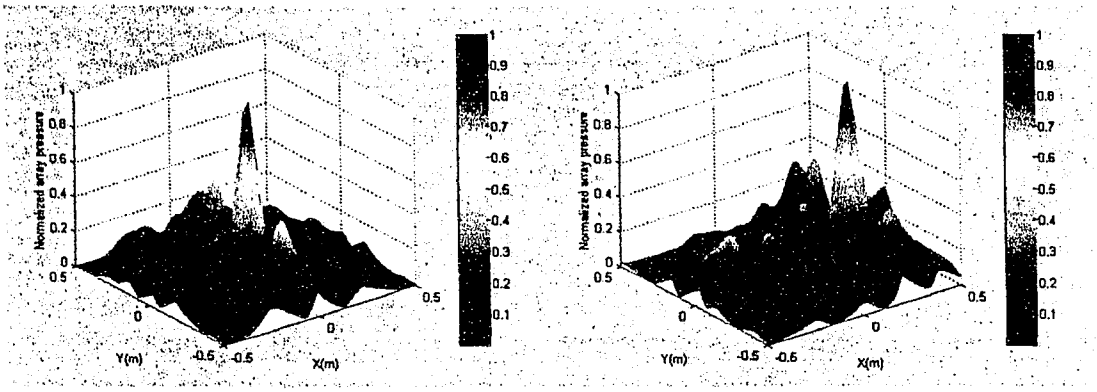

(a) (b)

Figure 4.36: Beamforming results (a) plot of normalized array pressure for (0.01, 0.01, 0.53) m (b) plot of normalized array pressure for (0.31, 0.02, 0.52) m.

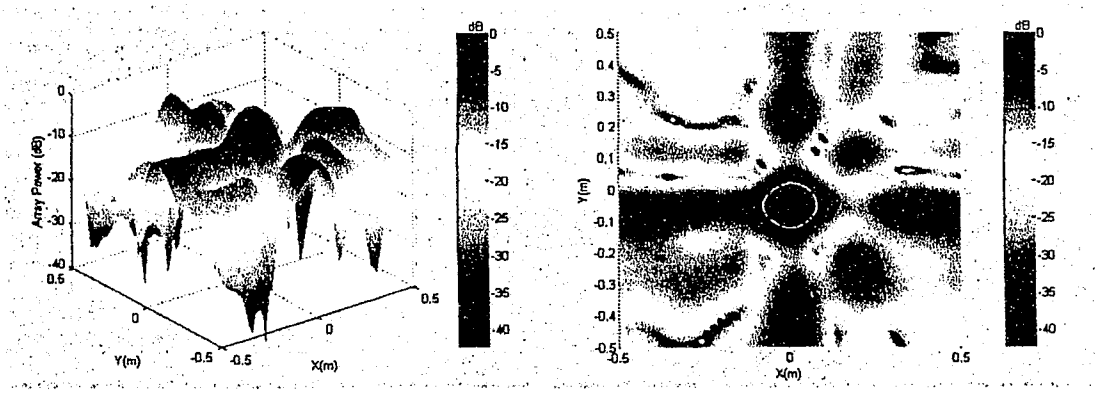

(a) (b)

Figure 4.37: Beamforming results for (0.01, -0.05, 0.76) m; (a) Beamforming map: 3D plot (b) Beamforming map: 2D plot (ring at -3 dB).

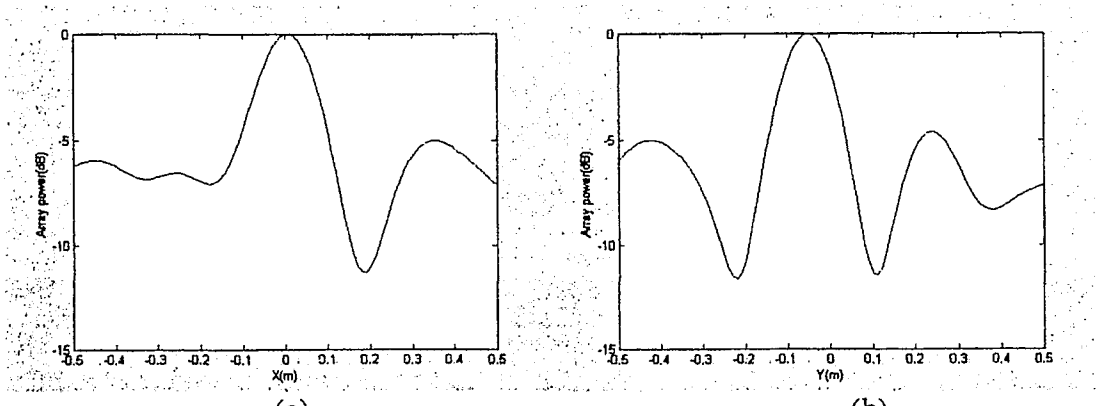

(a) (b)

Figure 4.38: Beamforming results for (0.01, -0.05, 0.76) m; (a) Array power along the x-axis (b) Array power along the y-axis.

Table 4.8 Effect of source position
Array resolution, error band and the dynamic range along the x-axis

Source Position (m)	Beamwidth (m)	Resolution (1/m)	Error band (m)	Dynamic range (dB)
(0.01, 0.01, 0.53)	0.108	9.26	± 0.054	6.65
(0.31,0.02, 0.52)	0.126	7.94	± 0.063	5.00
(0.01, -0.05, 0.76)	0.162	6.17	± 0.081	5.07

Array resolution, error band and the dynamic range along the y-axis

Source Position (m)	Beamwidth (m)	Resolution (1/m)	Error band (m)	Dynamic range (dB)
(0.01, 0.01, 0.53)	0.117	8.55	± 0.059	3.5
(0.31,0.01, 0.52)	0.135	7.41	± 0.068	5.6
(0.01, -0.05, 0.76)	0.153	6.54	± 0.076	4.7

4.5 Comparison between an HULA, a VULA, and a Cross array

In the previous sections, the sensitivity analysis of an HULA, a comparison between a VULA and an HULA, and the sensitivity analysis of a cross array have been carried out. The purpose of this section was to compare the three different microphone array geometries (i.e., an HULA, a VULA and a cross array). For this comparison, the data were collected for 8 seconds at each microphone at a sampling rate of 16 KHz and were divided into 120 non-overlapping blocks each containing 1024 data points (i.e., M=1024)). Two cases were considered. For the first case, N=8, the source was placed at X=0.01 m, Y=0.01 m, Z= 0.53 m, and an HULA, a VULA, and a cross array were used. For the second case, the source was placed at X=-0.29 m, Y=-0.01 m, Z= 0.5 m, and an HULA with N=16, a VULA with N=16, and a cross array with N=32 were used. It should be noted that, for both cases, the source localization plane was the x-z plane for the HULA and the y-z plane for the VULA.

Figure 4.39 and 4.40 show the beamforming maps (3D and 2D plots) and the plots of array power along the x-axis and the z axis for the HULA (N=8) with the source at (0.01, 0.01, 0.53) m. Figures 4.41 and 4.42 show the corresponding beamforming maps (3D and 2D plots) and the plots of array power along the y-axis and the z-axis for the VULA. Figures 4.43 and 4.44 show the corresponding beamforming maps (3D and 2D plots) and the plots of array power along the x-axis and the y-axis for the cross array. Figures 4.45(a), 4.45(b), and 4.46 show the beamforming maps (2D plots) for the HULA (N=16), the VULA (N=16) and the cross array

(N=32) with the source position at (-0.29, 0.01, 0.50) m. Figures 4.47-4.49 show the plots of array power for the corresponding array geometries with the source position at (-0.29, 0.01, 0.50) m.

When the source is placed at (0.01, 0.01, 0.53) m, for the HULA (N=8), the error band is ± 0.180 m along the x-axis and infinite along the y-axis, while the dynamic range is in excess of 15 dB along the x-axis (Figures 4.39 and 4.40). With the change of the array geometry to the VULA (N=8), the error band is ± 0.063 m along the x-axis and, again, is infinite along the y-axis, while the dynamic range is 3.5 dB along the x-axis (Figures 4.41 and 4.42). Therefore, when the VULA is used, the error band decreases, but the overall array source localization capability is degraded due to the degradation of the dynamic range. When a cross array [N=8(4 x 4)] is used, the error band is ± 0.198 m along the x-axis and ± 0.144 m along the y-axis (Figure 4.43 and 4.44). A dynamic range cannot be defined in this case. The error band along x-axis is larger for the cross array than it is for either the HULA or the VULA, but the error band along the y-axis is reduced from infinite for the HULA and VULA to ± 0.144 m for the cross array. Therefore, the source localization capability of a cross array is better as compared to a uniform linear array (horizontal or vertical).

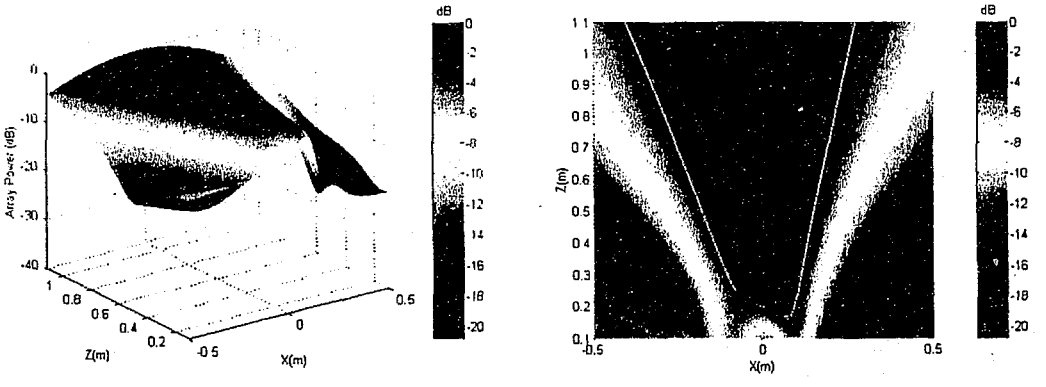

(a) (b)

Figure 4.39: Beamforming results for the HULA, N=8 at (0.01, 0.01, 0.53) m;
(a) Beamforming map: 3D plot (b) Beamforming map: 2D plot (white line at -3 dB).

When the source is placed at (-0.29, 0.01, 0.50) m, the source is localized by the HULA at X=-0.29 m and Z=0.50 m with Y=0 m [Figure 4.45(a) and 4.47] and by the VULA at Y=-0.01 m and Z=0.63 m with X=0 m [Figure 4.45(b) and 4.48]. Thus, the HULA provides the *correct* source position, whereas VULA does not. This is due to the fact that the source is placed in the

localization plane of the HULA, i.e., x-z plane, so that the HULA has the ability to localize the source. The VULA is unable to provide the correct source location because the source does not lie in its localization plane, i.e., the y-z plane. When the cross array is used, the source position is localized at X= -0.29 m Y=-0.01 m and Z=0.50 m [Figure 4.46 and 4.49]. This is the *correct* position and demonstrates that a cross array has the capability to localize an acoustic source in 3D space. It is also noted that the resolution contour for the cross array is a ring as compared to an ellipse for the uniform linear array.

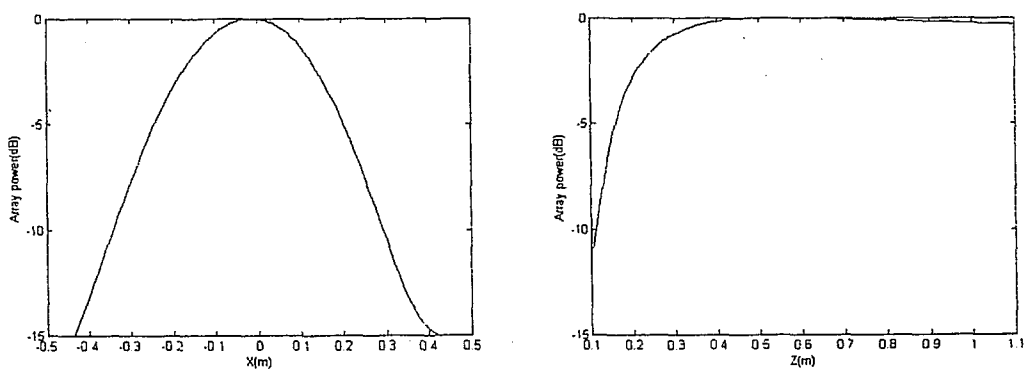

(a) (b)

Figure 4.40: Beamforming results for the HULA, N=8 at (0.01, 0.01, 0.53) m; (a) Array power along the x-axis (b) Array power along the y-axis.

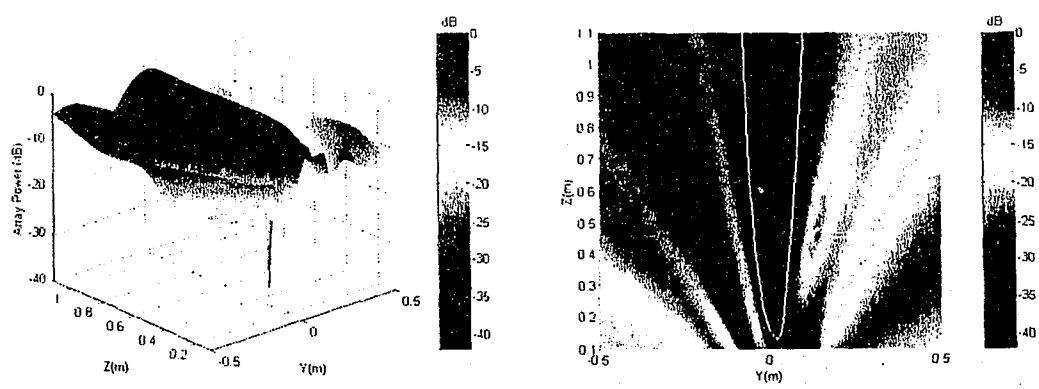

(a) (b)

Figure 4.41: Beamforming results for the VULA, N=8 at (0.01, 0.01, 0.53) m; (a) Beamforming map: 3D plot (b) Beamforming map: 2D plot (white line at -3 dB).

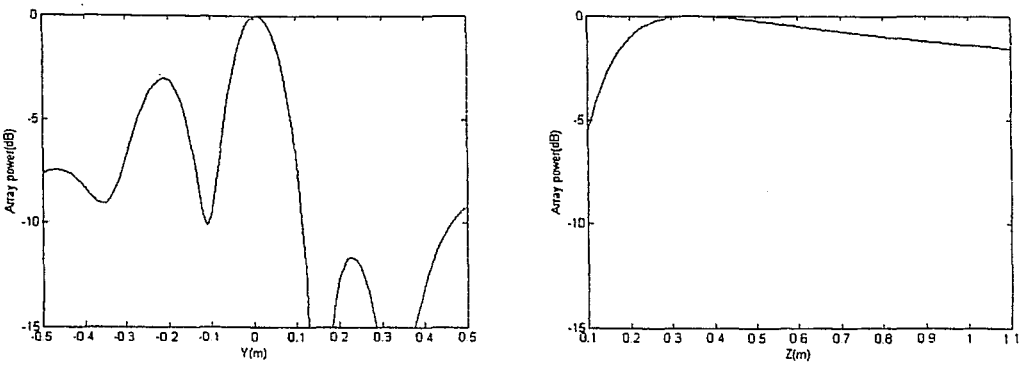

(a) (b)

Figure 4.42: Beamforming results for the VULA, N=8 at (0.01, 0.01, 0.53) m; (a) Array power along the x-axis (b) Array power along the y-axis.

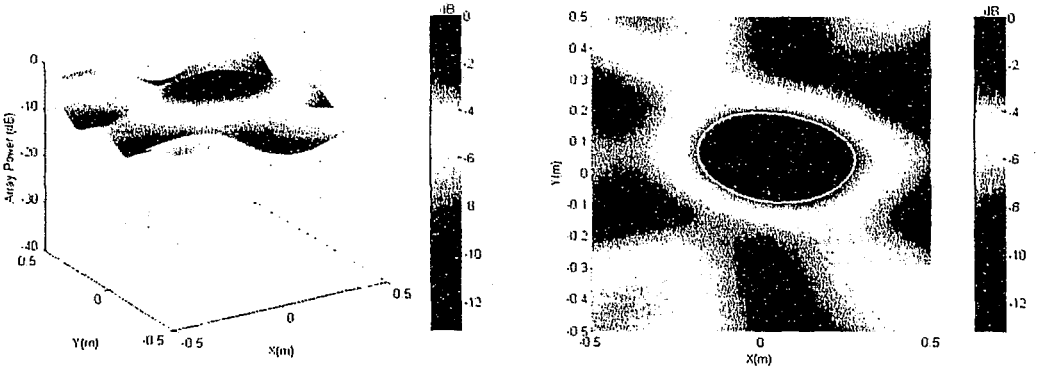

(a) (b)

Figure 4.43: Beamforming results for the cross array, N=8 at (0.01, 0.01, 0.53) m; (a) Beamforming map: 3D plot (b) Beamforming map: 2D plot (ring at -3 dB).

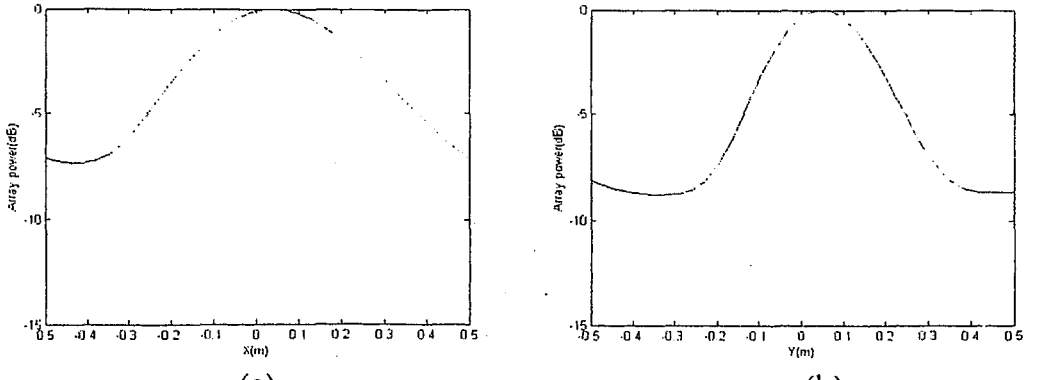

(a) (b)

Figure 4.44: Beamforming results for the cross array, N=8 at (0.01, 0.01, 0.53) m; (a) Array power along the x-axis (b) Array power along the y-axis

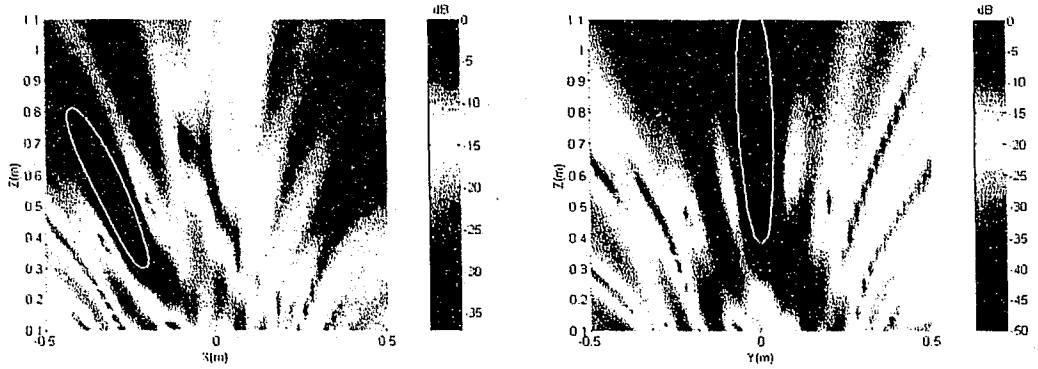

(a) (b)

Figure 4.45: Beamforming results, N=16, at (-0.29, 0.01, 0.5) m; (a) Beamforming map: 2D plot using the HULA (b) Beamforming map: 2D plot using the VULA.

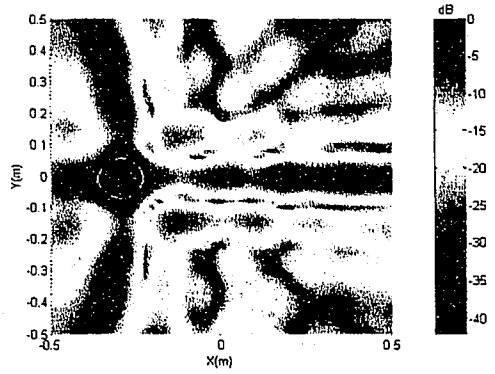

Figure 4.46: Beamforming map (2D plot), N=32 at (-0.29, 0.01, 0.5) m using the cross array.

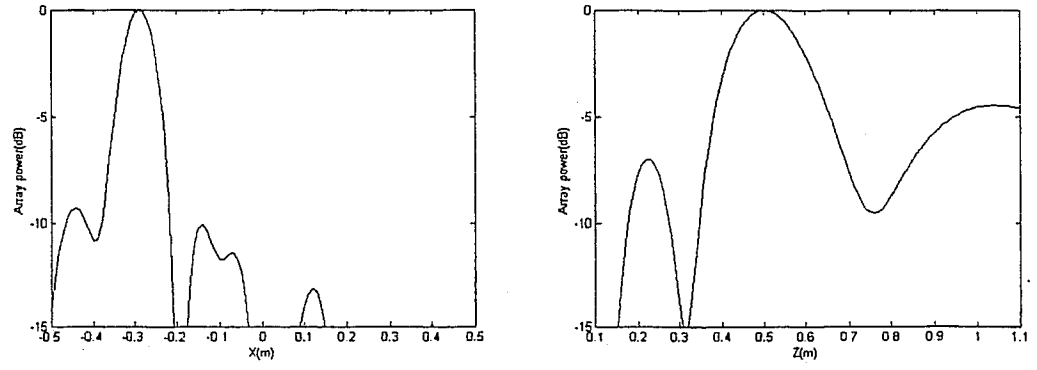

(a) (b)

Figure 4.47: Beamforming results for the HULA, N=16 at (-0.29, 0.01, 0.5) m; (a) Array power along the x-axis (b) Array power along the z-axis

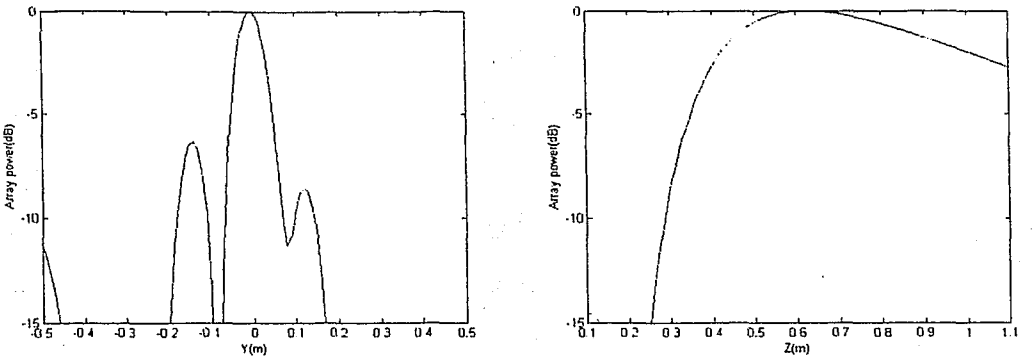

(a) (b)

Figure 4.48: Beamforming results for the VULA, N=16 at (-0.29, 0.01, 0.5) m; (a) Array power along the y-axis (b) Array power along the z-axis

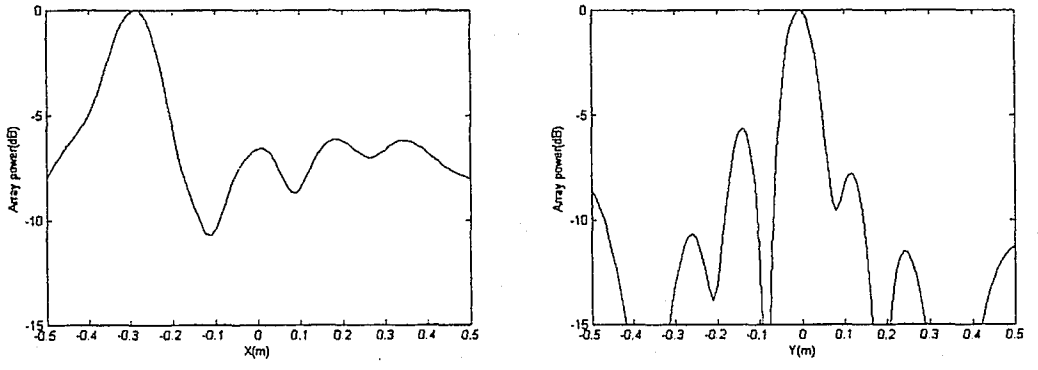

(a) (b)

Figure 4.49: Beamforming results for the cross array, N=32 at (-0.29, 0.01, 0.5) m; (a) Array power along the x-axis (b) Array power along the y-axis

The results of this section serve to demonstrate that a cross array (i.e., a uniform planar array) is better as compared to a uniform linear array (horizontal or vertical). A uniform linear array can be used only to localize a source which lies in the plane of the array (i.e., x-z plane for an HULA and y-z plane for a VULA in these experiments). In other words, when a source is located in three-dimensional (3D) space, a uniform linear array can not be used. On the other hand, a uniform planar array has the capability to localize a source in 3D space. Overall, these experimental results confirm the simulation results of section 3.5.

Chapter 5
Summary, conclusions and future work

5.0 Introduction

A sensitivity analysis of a frequency-domain beamforming technique for aeroacoustic measurements, involving an array of microphones, was performed in order to gain insight into the effects of various parameters, such as the number of microphones on the applicability and performance of the technique. Three types of arrays were considered: a uniform linear array (ULA), a uniform planar array (UPA), and a random array. Extensive simulations were carried out for each type of array; also, a selected (limited) number of experiments for the ULA and UPA were carried out for the purpose of validating the simulation results.

5.1 Summary of simulations results

5.1.1 Uniform Linear Array – far field beamforming

The sensitivity analysis of a ULA with a far field source demonstrates the working capability of the beamforming technique to localize an acoustic source placed sufficiently far from the microphone array so that plane pressure waves reach the array. The array capability improves with the increase of array aperture and the source signal frequency. The beamforming map is independent of whether or not the signal contains an integer number of cycles, and the source can be localized with a high degree of accuracy. Time windows have no impact on the beamforming map (i.e., source localization) for either an integer or a non-integer number of cycles. On the other hand, time windows must be used for a non-integer number of cycles to improve the frequency resolution of the signal spectrum. For maximum source localization capability, the inter-microphone distance should be equal to the half of the signal wavelength and the source should be at broadside (i.e., perpendicular to the reference microphone). The beamforming method has the ability to handle situations involving a signal with multiple frequencies (e.g., a broadband signal). Block averaging is really not required when a signal is free from extraneous noise. But for noisy environments, an adequate *array* signal to noise ratio (SNR) can not be achieved by using a single block of data, even with a relatively large number of microphones; consequently, both source localization and signal spectrum detection are

difficult. For such environments, block averaging must be used to reduce the variability of the beamforming results.

This analysis elucidates the source localization capability of the ULA for a far field source only. In the case of a near field source, such as an aeroacoustic source in a wind tunnel test section, for which acoustic waves are spherical, ULA far field beamforming methodology can not be used. To overcome this limitation, near field beamforming is used.

5.1.2 Uniform Linear Array – near field beamforming

The sensitivity analysis of a ULA with a near field source demonstrates the working capability of the beamforming technique to localize an acoustic source located near to the microphone array such that the pressure waves reaching the microphones are spherical. As the array aperture increases the array resolution increases but the array dynamic range decreases. As the signal frequency increases, the array resolution improves and the array dynamic range remains constant. For maximum source localization capability of the array, the source should be perpendicular to the array centre. As the source moves away from the ULA, the source localization capability decreases. When a source is placed at a sufficiently large distance from the microphone array, near field beamforming results change to far field results. To avoid grating lobes and for maximum array capability, the inter-microphone distance should be equal to the half of the signal wavelength.

For a ULA, with the microphones placed along the x-axis and the source lying in the x-y plane, the array resolution is not the same along the x-axis and the y-axis. The resolution is better along the array axis, i.e., the x-axis, as compared to the axis perpendicular to the array, i.e., the y-axis. The resolution contour at -3 dB is always an ellipse. Therefore, a source can not be pinpointed even by using large array apertures. Also, the source localization capability is limited to a two-dimensional (2D) situation in which the acoustic source lies in the plane of the array. To overcome these limitations, a uniform planar array (UPA) is used.

5.1.3 Uniform Planar Array – near field beamforming

The sensitivity analysis of a UPA (e.g., a uniform square array) with a near field source demonstrates the working capability of the beamforming technique to localize an acoustic source in a three-dimensional (3D) situation. The array resolution and the dynamic range increase with the increase of array aperture. With the increase of signal frequency, the array

resolution increases, but the array dynamic range decreases. For maximum array resolution, the source should be perpendicular to the array centre. As the source moves away from the UPA, the source localization capability decreases. To avoid grating lobes and for maximum source localization capability, the inter-microphone distance should be equal to the half of the signal wavelength.

For a square geometry, with the microphones placed in the x-y plane, the array resolution is the same along the x-axis and the y-axis, and the resolution contour at -3 dB is a ring, as compared to an ellipse for a ULA. Therefore, acoustic sources can be pinpointed when the UPA has a large aperture. Also, the UPA has the capability to localize an acoustic source in 3D space.

The main limitation of the UPA is that it does not work well when a wide range of frequencies is involved in a given aeroacoustic application. To overcome this limitation, a random array is used.

5.1.4 Random Array – near field beamforming

The sensitivity analysis of a random array (e.g., a spiral array) demonstrates the ability of the array to localize an acoustic source in 3D space over a wide frequency range (from 4 kHz to 30 KHz) without any grating lobes (i.e., spatial aliasing) and with a limited number of microphones. The array resolution and the dynamic range increase with the increase of array aperture. As the signal frequency increases, the array resolution increases, but the array dynamic range decreases. For maximum array resolution, the source should be perpendicular to the array centre. As the source moves away from the array, the source localization capability decreases.

5.2 Summary of experimental results

5.2.1 Uniform Linear Array – near field beamforming

The sensitivity analysis of a horizontal uniform linear array (HULA) shows that the array resolution increases as the number of microphones increases, as expected on the basis of the simulation results. However, in the case of the dynamic range, there is a discrepancy between the experimental results and the *original* simulation results, due to the fact that the separation distance between the two central microphones (the 8^{th} and 9^{th} microphones) was $2d$ for the experimental data, whereas the separation distance was d for the original simulation data.

Additional simulation results obtained with a separation distance of $2d$ display the same behaviour as the experimental results. The variation of the source position shows that the array has maximum array source localization capability when the source is placed perpendicular to the array centre, and the resolution degrades as the source moves away from a uniform linear array, as in the case of the simulation results. The experimental results also confirm the effect of inter-microphone distance. The comparison between the horizontal uniform linear array (HULA) and the vertical uniform linear array (VULA) indicates that the HULA is better than the VULA.

5.2.2 Cross array

When a cross array is used, the experimental results confirm the simulation results with respect to the effects of number of microphones and source position. These results also demonstrate that the array resolution increases and dynamic range decreases with the increase of the array aperture.

The comparison between three different array geometries (i.e., an HULA, a VULA and a cross array) indicates that a cross array (i.e., a type uniform planar array) is superior to a uniform linear array, in accordance with the simulation results and confirm the simulation results.

5.3 Conclusions

On the basis of the present findings, it can be concluded that a uniform planar array is superior to a uniform linear array and that a random array is the best of the three array geometries, providing particularly effective source localization over a broad range of frequencies, without any spatial aliasing and with a limited number of microphones.

5.4 Future work

Examination of the working capability of a random array using experimental data is not included in this thesis and is left for future work. Moreover, the present simulation and experimental results involved a pure tone signal. In practice, broadband signals are encountered, and acoustic measurements of interest are conducted in wind tunnels which generate significant background noise under test conditions. To remove the effect of this

background noise, and to obtain the desired results, the beamforming MATLAB code must be modified. The following procedure is recommended for handling this aspect.

STEP 1: Collect the background noise data at a specific air speed, when the source is not present in the test section.

STEP 2: Process the background noise data by the MATLAB code to determine the average CSM for the background noise, $[\hat{G}_{background}]$.

STEP 3: Place a source (or a model) in the test section and run the wind tunnel at the same speed and collect the combined background noise and source data. Process these data by the MATLAB code to determine the average combined CSM, $[\hat{G}_{combined}]$.

STEP 4: Subtract the background CSM from the combined CSM, to obtain the CSM pertaining to the source, $[\hat{G}]$, i.e.,

$$[\hat{G}] = [\hat{G}_{combined}] - [\hat{G}_{background}]$$

STEP 5: Apply the steering vector to the source CSM, $[\hat{G}]$, for each frequency bin, to obtain the beamforming maps and the SPL spectrum.

For this future work, the experimental data will be collected by means of a random array for broadband sources.

References

[1] Mueller T.J. (Editor), "*Aeroacoustic Measurements*", Springer-Verlag, Berlin, 2002.

[2] Johnson D.H. and Dudgeon D.E., "*Array Signal Processing- Concepts and Techniques*", Prentice – Hall, NJ, 1993.

[3] Sas E. (Editor), "*Advanced Techniques in Applied and Numerical Acoustics*," Katholieke Universiteit Leuven, Faculty of Engineering, Department of Mechanical Engineering, Belgium, 1996.

[4] Benesty J., "Adaptive eignvalue decomposition algorithm for passive acoustic source localization," *Journal of Acoustical Society of America*, pp. 384-391, January, 2000.

[5] Varma K., "Time–Delay estimate based direction-of-arrival estimation for speech in reverberant environments," *Masters of science (Electrical Engg.) thesis, Virginia Polytechnic Institute and state university*, 2002.

[6] Humphreys W.M., Brooks T.F., Hunter W., Meadows K.R., "Design and use of microphone directional arrays for aeroacoustic measurements," *36th Aerospace sciences Meeting &Exhibition*, January 12-15, 1998.

[7] Humphreys W.M., Brooks T.M.," Effect of directional array size on the measurement of airframe noise components," *5th AIAA/ CEAS Aeroacoustics Conference*, May 10-12, 1999.

[8] Dumbacher S.M., Brown D.L., and Bono R.W., "Overview of acoustic array techniques for noise source identification," *Inter-noise*, Christchurch, New Zealand, pp.1559-1564, November 16-18, 1998.

[9] Vaucher D., Chevret P., and Perrin F., "Use of Acoustical Holography in 3D interiors measurements," *inter-noise*, 2002.

[10] Antoine T., Cetalifaud J., and Aujard C., Metravid RDS, Lyon, France, "Meeting Noise Regulations with Near field Acoustic Holography," e-mail: thomas.antoine@metravib.fr, *Journal of Sound and vibration*, May, 2003.

[11] Krim J. and Viberg M., "Two decades of array signal processing research: The parametric approach," *IEEE Signal Processing Magazine*, pp. 67-94, July, 1996.

[12] Barry D. Van veen and Kevin M. Buckley, "Beamforming: A Versatile Approach to Spatial Filtering," *IEEE ASSP Magazine*, pp. 4-24, April, 1988.

[13] Richard J. V. (Editor), "The past, present and Future of Underwater Acoustic signal processing," *IEEE Signal processing magazine*, pp. 21-54, July, 1988.

[14] Soderman P.T. and Noble S.C, "A directional microphone array for acoustic studies of wind tunnel models," *8th AIAA Aerodynamic Testing Conference*, pp. 74-640, July 8-10, 1974.

[15] Brooks T.F., Marcolini M. A. and Pope D.S., "A directional array approach for the measurement of rotor noise source distributions with controlled spatial resolution," *Journal of Sound and Vibration*, vol.112, pp. 192-197, January, 1987.

[16] Blacodon D., Caplot M. and Elias G., "A source localization technique for helicopter rotor noise," *11th AIAA, Aeroacoustics Conference*, Oct. 19-21, 1987.

[17] Elias G., "Noise Source Localization with Focussed Antenna for Reduction purposes," Presented at the Science et Defence Conference, Transl.into english from Science et Defence (France), pp. 1-13, May 15-16, 1990.

[18] Gramann R.A. and Mocio J.W., "Aeroacoustics measurements in wind tunnels using adaptive beamforming methods," *Journal of Acoustical Society of America,* pp.3694-3701, June 1995.

[19] Brooks T.F., Marcolini M..A., Pope. D.S., "A directional array approach for the measurement of rotor noise source distribution with controlled spatial resolution," *Journal of sound and Vibrations,* vol. 112, pp.192-197, January, 1987.

[20] Underbrink R., "Practical Considerations in Focused Array Design for passive Broadband Source Mapping Applications," *Master's Thesis, The Pennsylvania State University*, May, 1995.

[21] Watts M.E., Mosher, M., and Barnes, M.J., "Microphone Array Phased Processing system (MAPPS): Phased Array System for Acoustic Measurement in a Wind Tunnel," *World Aviation Conference,* San Francisco, CA, October 19-21, 1999.

[22] Mosher, M., "Phased Array for Aeroacoustic Testing: Theoretical Development,"*2nd AIAA/CEAS Aeroacoustics Conference*, State College, PA, May 6-8, 1996.

[23] Wang. Y., Li. J., Stoica P., Sheplak M., and Nishida T., "Wideband RELAX and wideband CLEAN for aeroacoustic imaging," *Journal of Acoustical Society of America, pp.* 757-767, February, 2004.

[24] Sijtsma P. and Holthusen H., "Source localization by phased array measurements in closed wind tunnel test sections," *5th AIAA/CEAS Aeroacoustics Conference,* Greater Seattle, Washington, USA, May 10-12, 1999.

[25] Haddad K. Benoit V., "Localization of aeroacoustics sources all along a vehicle by means of the acoustical imaging system ANT64 in the semi-anechoic wind-tunnel Pininfariana," *euro-noise Naples*, 2003.

[26] Haddad K., Benoit V., "An Acoustical Imaging Processing for the Localization of Acoustic Sources inside a Vehicle: Method and test results on Road," *ACB Engineering*, France, www.acb-engineering.fr, 2003.

[27] Haddad K., Benoit V., "Capabilities of a beamforming technique for acoustic measurements inside a moving car," *The 2002 international Congress and Exposition on Noise Control Engineering Dearborn*, MI, USA, August 19-21, 2002.

[28] Haddad K., Benoit V., "Use of an acoustical imaging system for the study of the acoustic transmission of sealing system in a moving car," *ACB Engineering*, France www.acb-engineering.fr, 2002.

[29] Olson S., and Mueller T.J., "Phased Array Microphones System for Trailing Edge Noise Research," *University of Notre Dame*, Notre Dame, Indiana, June, 2003.

[30] Arnold D.P., Nishida T., Cattafesta L., Sheplak M., "MEMS- Based Acoustic Array Technology" *40th AIAA Aerospace Sciences Meeting & Exhibit*, Reno, NV, January 14-17, 2002.

[31] Kawall J.G., Lecture Notes, MIE 1805S, "Analysis of Enginering Data", Department of Mechanical and Industrial Engineering, *University of Toronto*, 2003.

[32] Van Trees H.L., "*Optimum array processing- Part IV of detection, Estimation, and Modulation Theory,*" A John Wiley & Sons, Inc., Publication 2002.

[33] Parbhakar S. Naidu, "*Sensor array signal processing*", CRC Press, 2001.

Appendix A

MATLAB code

The digital data can be generated via simulations or can be obtained via experiments. The beamforming technique utilizes a post-processing procedure, as discussed in 2.2.3. This procedure remains the same for either the simulation data or the experimental data. The MATLAB code developed at Ryerson University for post processing is given below.

A.1 ULA – far field beamforming

Variables

```
f=6500;                          % frequency of signal.
ω= 2*pi*f;                       % radian frequency of signal.
c = 344;                         % speed of sound.
d1 =d2 =d= 0.02;                 % inter-microphone distance.
N=10;                            % number of microphones.
ML=1024*1;                       % total number of data points per mic.
L=1;                             % number of non-overlapping blocks.
M=ML/L;                          % number of data points per blocks.
SR=4*f;                          % sampling rate.
S=40;                            % scaling factor to noise.
Δt=1/(SR);                       % spacing between sampling points.
t=(0:(M-1))* Δt;                 % time for M samples.
t1=(0:(M*N))* Δt;                % time for M*N samples.
noise=S.*randn (size(t1));       % noise generation.
```

Acoustic source position

```
θ=0;                             % source position.
Δ = ( ω*d*sin(θ))/(c);           % time delay per microphone.
```

Generation of simulation (digital) data⊕

```
for n = 1:N
data(n,[1:ML]) =sin( ω*t-(n-1)*Δ)+noise(:,[((n-1)*ML+1):n*ML]);
end
```

⊕ This step is omitted for the experimental data.

Cross Spectral Matrix $[\hat{G}]$

```
for n = 1:N
for e = 1:M:ML
Ye(n,[e:e+M-1]) = fft(data(n,[e:e+M-1]));          % FFT of each microphone.
end
end
M_new = M/2;
j=1;
h=1;
for n = 1:N
r = 1;
Conj_Ye = conj(Ye(n,:));
for e = 1:N
Gij(1,:) = Conj_Ye.*Ye(e,:);
total(1:M) = zeros;
for s = 1:M:ML
test=Gij(1,[s:s+ML-1]);
total = total+test;
end
G (m,[r:r+M_new-1]) = [1/(L*M*M/2)]*total(1,[1:M/2]);
r = r+M_new;
end
end
```

Steering vector and array power for each frequency bin

```
for e=1:512
ω=2*pi*(e-1)/(M*Δt);
k =e:M_new:N*M_new;
G_k = (1/(N*N))* G (:,k);                          % CSM for the kth frequency bin.
j=1;
q=1;
for θ1 ⊕=-1.5:0.01:1.5                             % possible source locations.
for x=1:N
E(x,:)=exp(i* ω *d*(x-1)*sin(θ1)/c);               % steering vector.
end
P_k =E'* G_k *E;                                   % Array power for kth frequency bin.
Q=abs( P_k );                                      % Array power in absolute value.
z(j,e)=((Q));                                      % Array power values for all bins.
j=j+1;
end
end
```

⊕ The *possible* source localization grid can be changed from a coarse to a fine grid.

Sound pressure level (SPL) spectrum

```
o=1
F(o,:)=max(z);                                  % max. value of array power/bin.
o=o+1;
fk=(0:(M/2-1))/(M*Δt);                          % frequency bins.
plot (fk,10*log10(F/(2*10^-5)^2));              % SPL (dB) versus frequency (Hz).
xlabel('Frequency[Hz]'),ylabel('Sound pressure level [dB]');
axis ([0 4*f/2 0 100])
```

Beamforming map (Array power vs. possible source locations)

```
for k=1:512
ER= max(max(z(k:k)));
z1=10*log10(z(:,[k:k])/ER);                     % array power values for kth bin.
θ1=-1.5:0.01:1.5;
plot(θ1,z1);                                    % array power plot for kth bin.
axis([-1.5 1.5 -40 0])
pause;
xlabel('Theta(radians)'),ylabel('Array Power(dB)')
end
```

Search technique

```
theta=-1.5:0.01:-0.5;
B1=max(z1([1:100],:));

theta=-0.5:0.01:0.5;
B2=max(z1([101:200],:));

theta=0.5:0.01:1.5;
B3=max(z1([201:301],:));

B1>B2
theta=-1.5:0.01:-1;
B4=max(z1([1:50],:));
display(B4);

theta=-1:0.01:-0.5;
B5=max(z1([51:100],:));
display(B5);

B2>B1
theta=-0.5:0.01:0;
B6=max(z1([101:150],:));
display(B6);

theta=0:0.01:0.5;
```

```
B7=max(z1([151:200],:));
display(B7);

B2>B3
theta=-0.5:0.01:0;
B8=max(z1([101:150],:));
display(B8);
theta=0:0.01:0.5;
B9=max(z1([151:200],:));
display(B9);

B3>B2
theta=0.5:0.01:1;
B10=max(z1([201:250],:));
display(B10);
theta=1:0.01:1.5;
B11=max(z1([251:301],:));
display(B11);

B1>B3
theta=-1.5:0.01:-1;
B12=max(z1([1:50],:));
display(B12);
theta=-1:0.01:-0.5;
B13=max(z1([51:100],:));
display(B13);

B3>B1
theta=0.5:0.01:1;
B14=max(z1([201:250],:));
display(B14);
theta=1:0.01:1.5;
B15=max(z1([251:301],:));
display(B15);
```

The maximum value out of B4, B5... B15 will determine the location of the acoustic source. Suppose B4 is the maximum, then display B4= (z1([1:50],:)) and theta=-1.5:0.01:-1. To determine the source location match the maximum value of B4 (array power) with corresponding theta (DOA). This search technique will calculate the source position with an accuracy of 0.01radians.

A.2 ULA, UPA and Random array - near-field beamforming

Variables

```
f=6500;                          % frequency of signal.
ω= 2*pi*f;                       % radian frequency of signal.
c = 344;                         % speed of sound.
d_1 =d_2 =d= 0.02;               % inter-microphone distance.
N=10;                            % number of microphones.
ML=1024*1;                       % total number of data points per mic.
L=1;                             % number of non-overlapping blocks.
M=ML/L;                          % number of data points per blocks.
SR=4*f;                          % sampling rate.
S=40;                            % scaling factor to noise.
Δt=1/(SR);                       % spacing between sampling points.
t=(0:(M-1))* Δt;                 % time for M samples.
t1=(0:(M*N))* Δt;                % time for M*N samples.
noise=S.*randn (size(t1));       % noise generation.
```

Acoustic source position

```
X=0;
Y=0;
Z=5;
```

Microphone positions for a uniform planar array (UPA)⊕

```
t = 1;
xVal = (4-1)/2*d:-d:-(4-1)/2*d;
yVal = (4-1)/2*d:-d:-(4-1)/2*d;
for index = 1:4
for index2 = 1:4
micLoc(t,1) = xVal(1,index);
micLoc(t,2) = yVal(1,index2);
t=t+1;
end
end
micLoc(:,3)=0;
```

Microphone positions for a uniform linear array (ULA)

```
micLoc = [-d*(N-1)/2:d:d*(N-1)/2]';
micLoc([1:N],2) = 0;
micLoc([1:N],3) = 0;
```

⊕ This denotes the microphone positions for a uniform square array of 4 x 4 and will change with array geometry, e.g., uniform rectangular array, cross array or random array.

Distance between various microphones and acoustic source ($R_1, R_2, \ldots R_N$)

```
for index = 1:N
R1(1,index) = sqrt((micLoc(index,1)-X)^2+(micLoc(index,2)-Y)^2+ (micLoc(index,3)-Z)^2);
end
```

Simulation data generation for a ULA and a UPA ⊕

```
t=(0:(M-1))*Δt ;
newInd=1;
for index = 1:N
data(index,:) = (1/R1(1,index))*sin( ω*(t-R1(1,index)/c))+noise(1,[newInd:index*ML]);
newInd = index*ML+1;
end
```

Cross Spectral Matrix $[\hat{G}]$

```
for n = 1:N
for e = 1:M:ML
Ye(n,[e:e+M-1]) = fft(data(n,[e:e+M-1]));          % FFT of each microphone.
end
end
M_new = M/2;
j=1;
h=1;
for n = 1:N
r = 1;
Conj_Ye = conj(Ye(n,:));
for e = 1:N
Gij(1,:) = Conj_Ye.*Ye(e,:);
total(1:M) = zeros;
for s = 1:M:ML
test=Gij(1,[s:s+ML-1]);
total = total+test;
end
G (m,[r:r+M_new-1]) = [1/(L*M*M/2)]*total(1,[1:M/2]);
r = r+M_new;
end
end
end
```

⊕ This step is omitted for the experimental data.

Steering vector and array power for each frequency bin (UPA and Random array)[⊕]

```
ω=2*pi*(e-1)/(M*Δt);                          % grid distance along the z-axis.
k =e:M_new:N*M_new;
G_k = (1/(N*N))* G (:,k);
w;
j=1;
G_k = (1/(N*N))* G (:,k);                     % CSM for the kth frequency bin.
j=1;
for X1= -1.0:0.1:1.0[⊗]                       % source localization along the x-axis.
for  Y1=-1.0:0.1:1.0[⊗]                       % source localization along the y-axis.
h=1;
Rs = sqrt(X1^2+Y1^2+Z1^2);
for index = 1:N
R11(1,index) = sqrt((micLoc(index,1)-X1)^2+(micLoc(index,2)-Y1)^2+(micLoc(index,3)-Z1)^2);
T11(1,index)=(Rs-R11(1,index))/c;
End
E(h,:)=(R11/Rs).*exp(i*ω*(T11));              % steering vector.
h=h+1;
P_k =E'* G_k *E;                              % array power for kth bin.
Q=abs( P_k );                                 % array power in absolute value.
z(j,e)=((Q));                                 % Array power values for all bins.
j=j+1;
end
end
```

Sound pressure level (SPL) spectrum

```
o=1;
F(o,:)=max(p);                                % max. value of array power/bin.
o=o+1;
fk=(0:(M/2-1))/(M*Δt)                         % frequency bins.
plot(fk,10*log10((F)/(2*10^-5)^2));           % SPL (dB) versus frequency (Hz).
axis([0 6000 0 100])
xlabel('Frequency[Hz]'),  ylabel('Sound pressure level[dB]')
```

Beamforming map (Array power vs. possible source locations)

```
X1=[-0.5:0.02:0.5];Y1=[-0.5:0.02:0.5];
R= zeros(length(Y1), length(X1));
```

⊕ For ULA, the possible source locations can be changed to z = 0, x = -1.0:0.02:1.0, y = 0.01:0.02:1.1, if the x-y plane is the localization plane; also, the area of localization can be changed, e.g., -0.5 to 0.5 along the x-axis and 0.01 to 2.1 along the y-axis.

⊗ These denotes the *possible* locations of the source in the grid plane and can be varied in selected increments, e.g., 0.1, for a coarse grid, 0.01 for a fine grid.

Beamforming map (Array power vs. possible source locations)

```
X1=[-0.5:0.02:0.5];Y1=[-0.5:0.02:0.5];
R= zeros(length(Y1), length(X1));
XX=repmat(X,[length(Y1) 1]);  YY=repmat(Y',[1 length(X1)]);
k=1;
for k=1:512
R=reshape(10*log10(p(:,[k:k])/ER),51,51);          % array power for kth frequency bin.
surf(XX,YY,R)                                      % array power versus DOA for kth bin.
axis([-1 1 -1 1  -40 0])
shading interp
xlabel('X(m)'), ylabel('Y(m)'), zlabel('Array Power (dB)')
pause
end
```

Search technique

The search technique can be applied to the beamforming maps (plots of the array power along the x-axis and array power along the y-axis) in a similar fashion to that discussed in the last section (A.1), and the acoustic source location can be determined with an accuracy of 0.01m.

Appendix B

Validation of MATLAB code

B.1 Background details

The response of the delay and sum beamformer to a monochromatic wave is often called the array pattern [2]. It is also referred to as the *theoretical response.* The array pattern, which corresponds to the wavenumber-frequency response of a spatio-temporal filter, determines the array directivity characteristics [2]. It may be used in practice for evaluating array designs for far field and near field beamforming applications [1]. The array pattern varies according to the source location (near field or far field) and according to the array geometry. The different array patterns for different array geometries and source locations (far field and near field) are discussed below.

B.1.1 Array pattern for ULA - far field beamforming

Consider a ULA containing N microphones and an acoustic (point) source located in the far field, as shown in the Figure B.1. The acoustic signal travels at the speed of sound, c, and the microphone spacing is d. The direction perpendicular to the array is called broadside. The direction of arrival (DOA) is measured with respect to broadside. Let θ be the DOA of the source. The first microphone is the reference microphone and the time delay is zero for this microphone. The time delay at the 2nd microphone is $\Delta_2 = d\sin\theta/c$, and the delays at the other microphones are multiples of Δ_2, for example, the delays at the 3rd and 4th microphone are $2\Delta_2$ and $3\Delta_2$, respectively.

If $s(t)$ is the acoustic signal emanating from the source, the output of the first microphone is $y_1(t) = s(t)$, the output of the second microphone is $y_2(t) = s(t-\Delta_2)$, and so on. The output of the nth microphone is given as:

$$y_n(t) = s(t-\Delta_n) \tag{B.1}$$

The Fourier Transform (FT) of the output of the nth microphone is given as:

$$Y_n(\omega) = \int_{-\infty}^{\infty} y_n(t)\exp(-i2\pi ft)dt$$

$$= \int_{-\infty}^{\infty} s(t-\Delta_n)\exp.(-i2\pi ft)dt$$

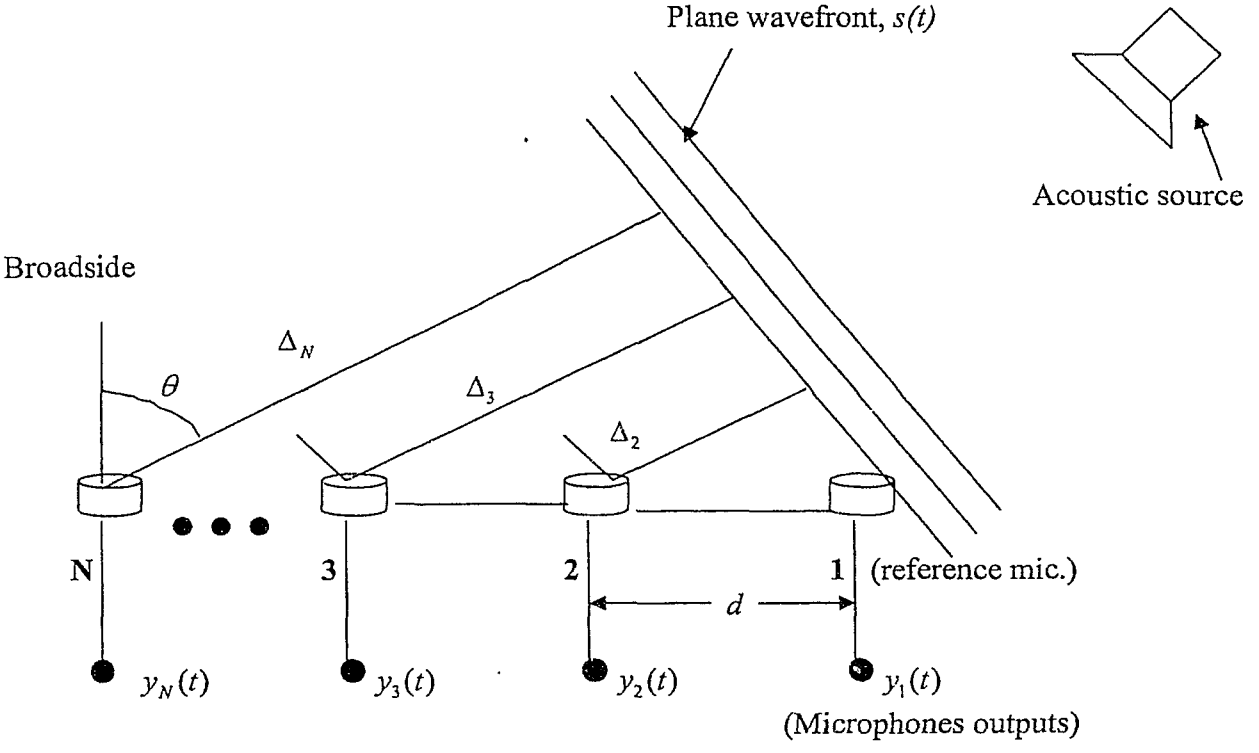

Figure B.1: Uniform Linear Array with a far field source.

With $t^* = t - \Delta_n$, so that $dt = dt^*$,

$$Y_n(\omega) = \int_{-\infty}^{+\infty} s(t^*)\exp(-i2\pi f(t^* + \Delta_n)dt^*$$

$$= \exp.(-i2\pi f\Delta_n)\int_{-\infty}^{\infty} s(t^*)\exp(-i2\pi ft^*)dt^*$$

$$= \exp(-i2\pi f\Delta_n)S(\omega) \qquad \text{(B.2)}$$

Since $W_n = 1$ for a far-field source, the output signal of the microphone array, *z(t)*, is given as:

$$z(t) = \sum_{n=1}^{N} y_n(t)$$

The FT of the output of the microphone array, $z(t)$, is given as:

$$Z(\omega) = \int_{-\infty}^{\infty} \left[\sum_{n=1}^{N} y_n(t) \right] \exp(-2\pi f t) dt$$

$$= \sum_{n=1}^{N} \left[\int_{-\infty}^{+\infty} y_n(t) \exp(-2\pi f t) dt \right]$$

$$= \sum_{n=1}^{N} Y_n(\omega)$$

$$= \left[\sum_{n=1}^{N} \exp(-i 2\pi f \Delta_n) \right] S(\omega)$$

The array pattern (function) is defined as:

$$H(\omega) = \frac{Z(\omega)}{S(\omega)} = \sum \exp(-2\pi f \Delta_n). \tag{B.3}$$

It can be shown that equation (B.3) reduces to:

$$H(\omega) = \frac{\sin(N * k_1 * d/2)}{N * \sin(k_1 * d/2)} \tag{B.4}$$

where

N = number of microphones
d = distance between microphones
$k_1 = 2\pi f \sin\theta / c = k \sin\theta$

Equation (B.4) shows that the response is maximum (1.0) only for broadside (θ =0), so that $k_1 = 0$. However, when a time delay is added to the microphone output before summation (array steering), the array can be steered in any direction [32]. Therefore, the array pattern can be modified to the steered array pattern as given below:

$$H(\omega) = \frac{\sin(N k_{11} d/2)}{N \sin(k_{11} d/2)} \tag{B.5}$$

where,

$k_{11} = 2\pi f (\sin\theta - \sin\theta_1)/c$;
θ_1 = the steered DOA, radians

The array can be steered towards θ_1, and the array response is maximum when $\theta = \theta_1$. This is illustrated by the following two examples, based on equation (B.5).

(i) ULA with N=20; d= 2 cm; an acoustic source with f = 8000 Hz, located at θ= 0 radians.

(ii) ULA with N=20; d= 2 cm; an acoustic source with f = 8000 Hz, located at θ= 0.5 radians.

The results are shown in Figures B.2.

The results of a ULA with a far field source for N=10 and N=50 are shown in Figure B.3. These results establish that the array dynamic range remains constant at 13 dB when the array aperture exceeds a certain value.

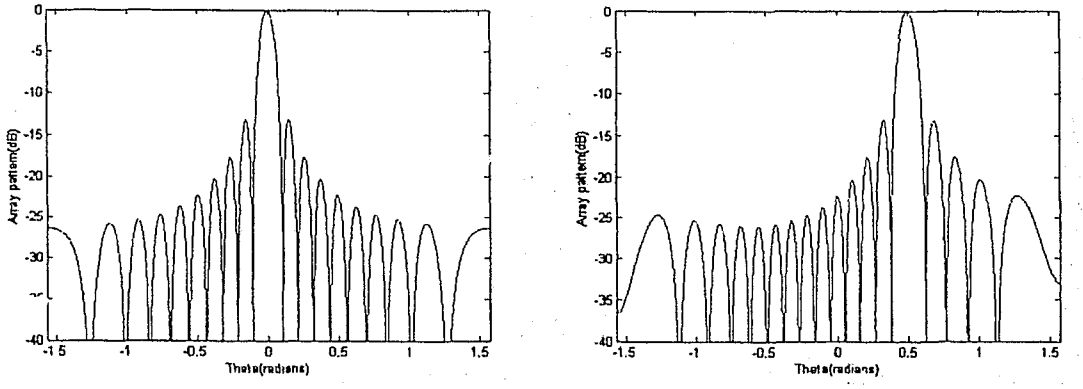

(i) (ii)

Figure B.2: Theoretical beamforming results for a ULA, far field beamforming, N=20;
(i) Array pattern (dB) vs. DOA for θ= 0 radians.
(ii) Array pattern (dB) vs. DOA for θ= 0.5 radians.

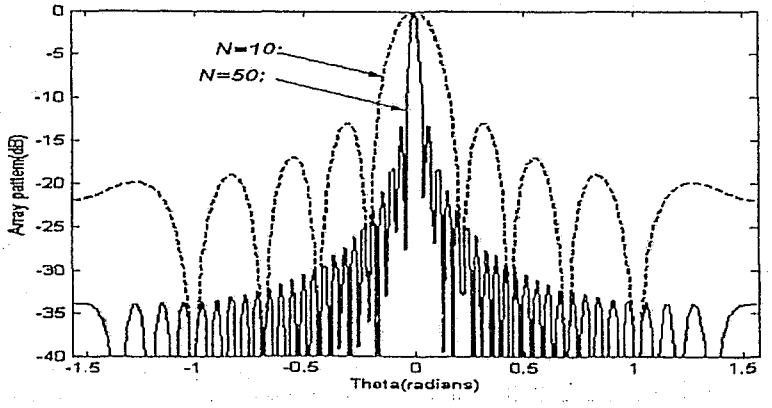

Figure B.3: Theoretical beamforming results for a ULA, far field beamforming, for θ= 0 radians, N=10 and N=50.

B.1.2 Array pattern for UPA- far field beamforming

Consider a uniform rectangular array having N_1 microphones along the x-axis and N_2 along the y-axis, as shown in Figure B.3.The inter-microphone distances between microphones along the x-axis and the y-axis are d_1 and d_2, respectively. An acoustic source is placed in the far field and the plane wave reaches the microphone array at an azimuth angle θ and at an elevation angle φ, as shown in Figure B.4.

The array pattern for the uniform planar array is a simple extension of the array pattern of a ULA. So the array pattern for the UPA can be calculated as the product of the array patterns of two ULA's along the x-axis and the y-axis. The UPA can be steered in both the azimuth direction and the elevation direction by compensating for the appropriate delay pertaining to each microphone.

The time delay for the (n_1, n_2) microphone is given below [32]:

$$\Delta_{n1n2} = n_1 d_1 \sin\varphi\cos\theta / c + n_2 d_2 \sin\varphi\sin\theta / c$$

The array pattern for a UPA (rectangular geometry) is given as:

$$H(\theta \quad) = \left[\frac{\sin(N_1(u)d_1/2)}{N_1\sin(ud_1/2)}\right]\left[\frac{\sin(N_2(v)d_2/2)}{N_2\sin(vd_2/2)}\right]$$

where,

$u = \omega\sin\varphi\cos\theta/c$; and $v = \omega\sin\varphi\sin\theta/c$; $\omega = 2\pi f$;

N_1 =Number of microphones along the x-axis.

N_2 =Number of microphones along the y-axis.

When the microphone array is steered along θ_1 and φ_1, the steered array pattern is:

$$H(\theta,\varphi) = \left[\frac{\sin(N_1(u-u_1)d_1/2}{N_1\sin(u-u_1)d_1/2}\right]\left[\frac{\sin(N_2(v-v_1)d_1/2)}{N_2\sin(v-v_1)d_1/2}\right] \tag{B.6}$$

In this expression,

$$u_1 = \omega\sin\varphi_1\cos\theta_1/c;$$

and $\quad v_1 = \omega\sin\varphi_1\sin\theta_1/c;$

where, φ_1 and θ_1 are the azimuth and the elevation angles for the steered DOA of the signal respectively.

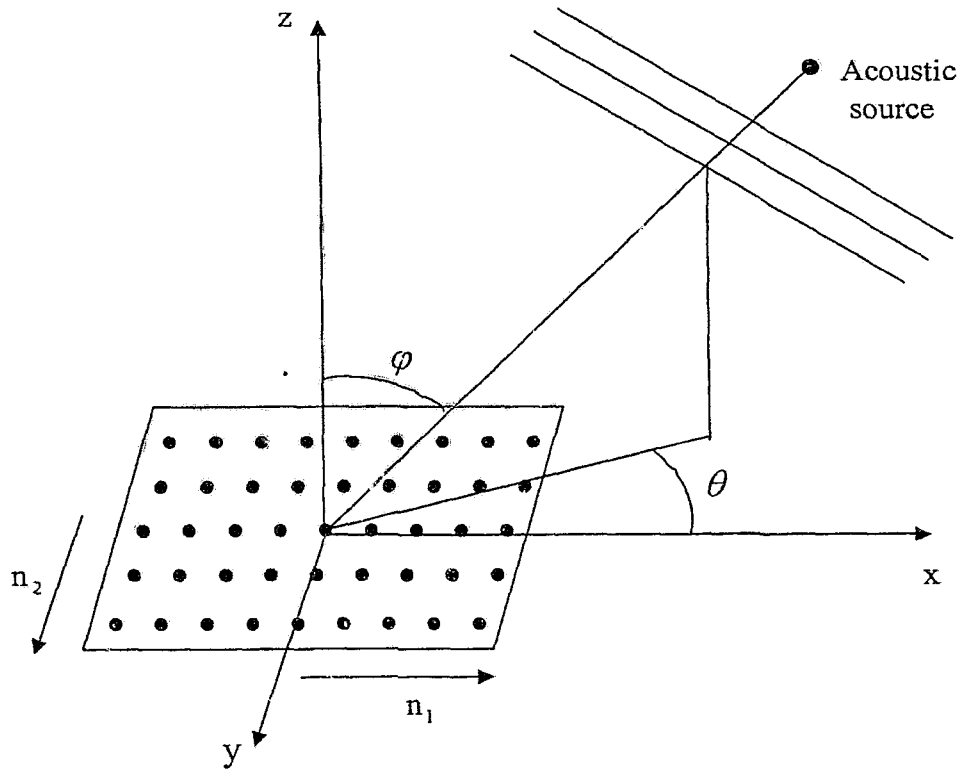

Figure B.4: Uniform rectangular array with a far field source.

The performance of the array pattern for the UPA can be illustrated by the following examples based on equation (B.6).

(i) UPA with $N_1 = N_2 = 7$ (i.e., a square grid of 7 x 7=49); $d_1 = d_2 = 0.02$ m; and an acoustic source with f=8000 Hz, located at $\varphi = 0.5$ radians and $\theta = 0.5$ radians.

(ii) UPA with $N_1 = N_2 = 7$ (i.e., a square grid of 7 x 7=49); $d_1 = d_2 = 0.02$ m; and an acoustic source with f=8000 Hz, located at $\varphi = 0.75$ radians and $\theta = 1$ radians.

The results are shown in Figure B.5.

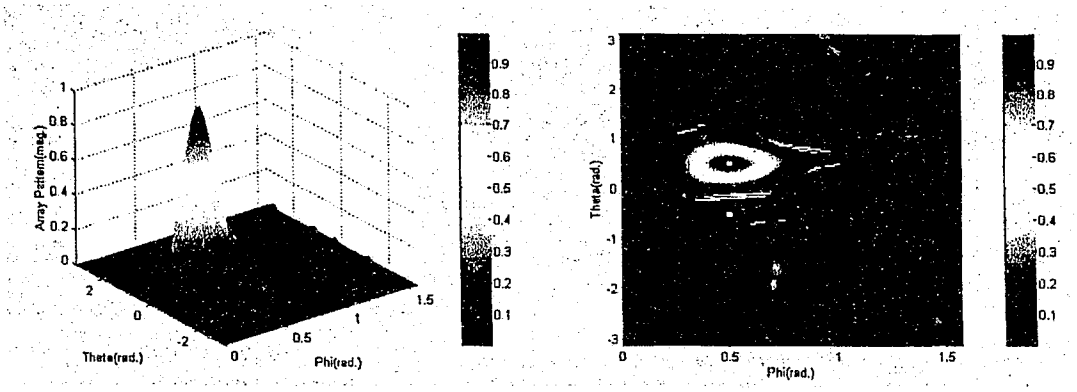

(i)(a) (i)(b)

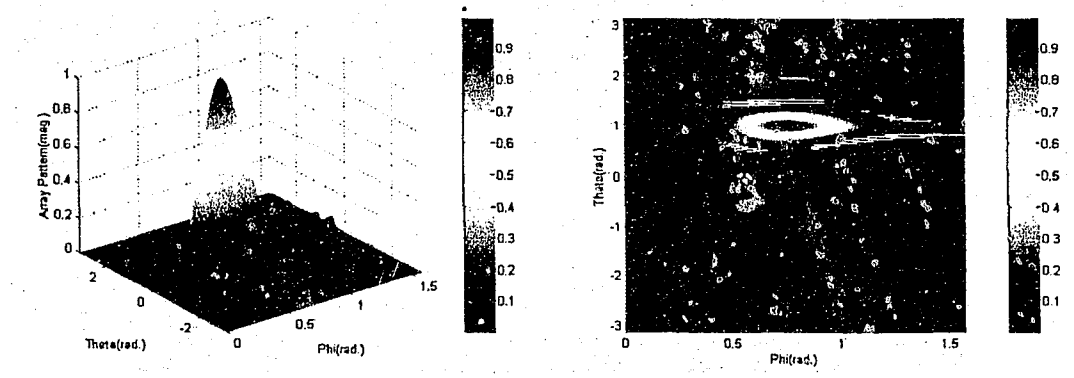

(ii)(a) (ii)(b)

Figure B.5: Theoretical beamforming results for UPA, far field beamforming: $N_1 = N_2 = 7$;
(i)(a) Array pattern (magnitude) vs. DOA for φ=0.5 radians and θ=0.5 radians, 3D plot.
(i)(b) Array pattern (magnitude) vs. DOA for φ=0.5 radians and θ=0.5 radians, 2D plot.
(ii)(a) Array pattern (magnitude) vs. DOA for φ=0.75 radians and θ=1.0 radians, 3D plot.
(ii)(b) Array pattern (magnitude) vs. DOA for φ=0.75 radians and θ=1.0 radians, 2D plot.

B.1.3 Array pattern for ULA and UPA – near field beamforming

The array pattern for a near field situation is common to both the ULA and the UPA. The relevant equation is given below [2]:

$$W(k, x', x) = \sum_{n=1}^{N} W_n \left(\frac{r}{r_n}\right) \exp\left(ik\left[(r - r_n) - (r' - r'_n)\right]\right) \tag{B.7}$$

where x' and x denote the assumed and actual locations of the point source, $r'(r)$ is the distance from the array center to the assumed (actual) source location, and $r'_n(r_n)$ is the distance from the nth microphone to the assumed (actual) source location. The array pattern based on (B.7) for the ULA and the UPA are illustrated by the following two examples.

(i) ULA with N=24; d=0.057 m; an acoustic source with f =3000 Hz, located at X = 0 m; Y = 0.5 m and at X = 0.3 m,Y= 0.7 n.

(ii) UPA with $N_1 = N_2$ =5; (square array of 5 x 5); $d_1 = d_2 = d$ =0.02 m; an acoustic source with f =8000Hz, located at X = 0 m; Y = 0m; Z = 0.5 m; and at X = 0 m, Y = 0 m, Z = 0.75 m; The results are shown in Figures B.6 and B.7.

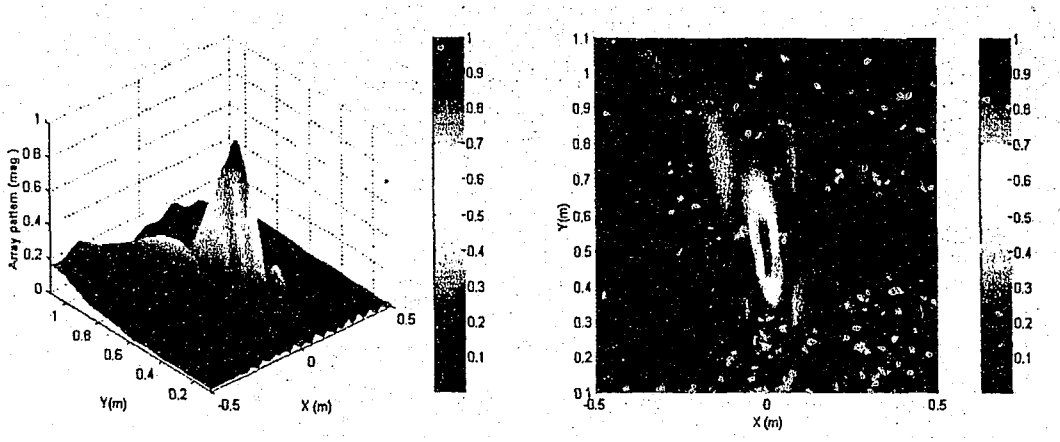

(i)(a) (i)(b)

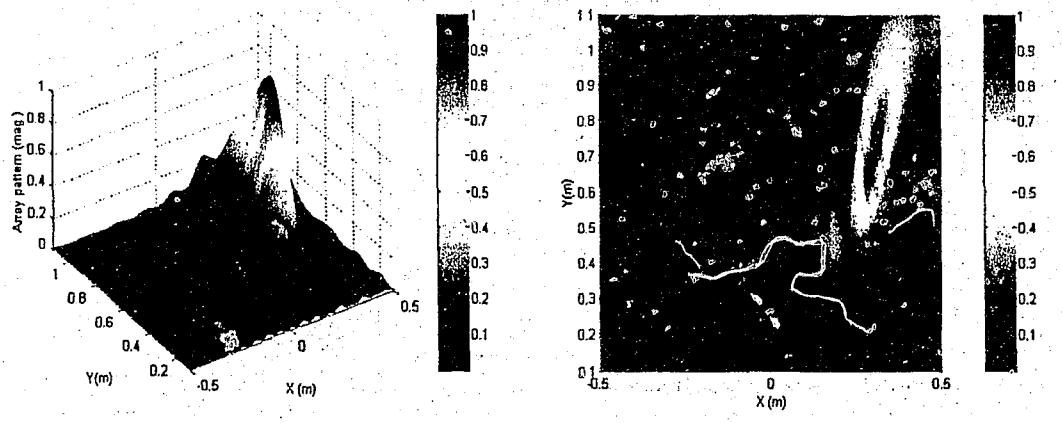

(i)(c) (i)(d)

Figure B.6: Theoretical beamforming results for a ULA, near field beamforming: N=24;
(i)(a) Array Pattern (mag.) vs X (m) & Y (m) at X=0 m; Y=0.5 m, 3D plot.
(i)(b) Array Pattern (mag.) vs X (m) & Y (m) at X=0 m; Y=0.5 m, 2D plot.
(i)(c) Array Pattern (mag.) vs X (m) & Y (m) at X=0.3 m; Y=0.7 m, 3D plot.
(i)(d) Array Pattern (mag.) vs X (m) & Y (m) at X=0.3 m; Y=0.7 m, 2D plot.

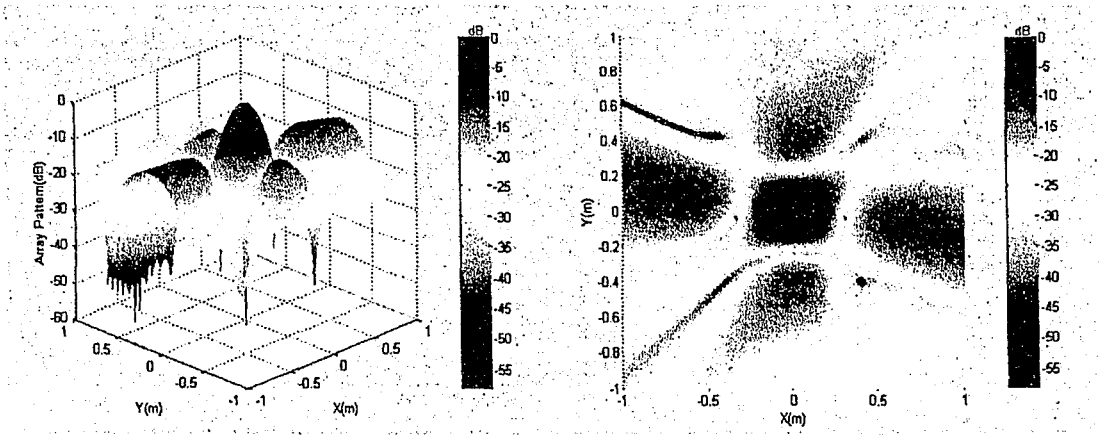

(ii)(a) (ii)(b)

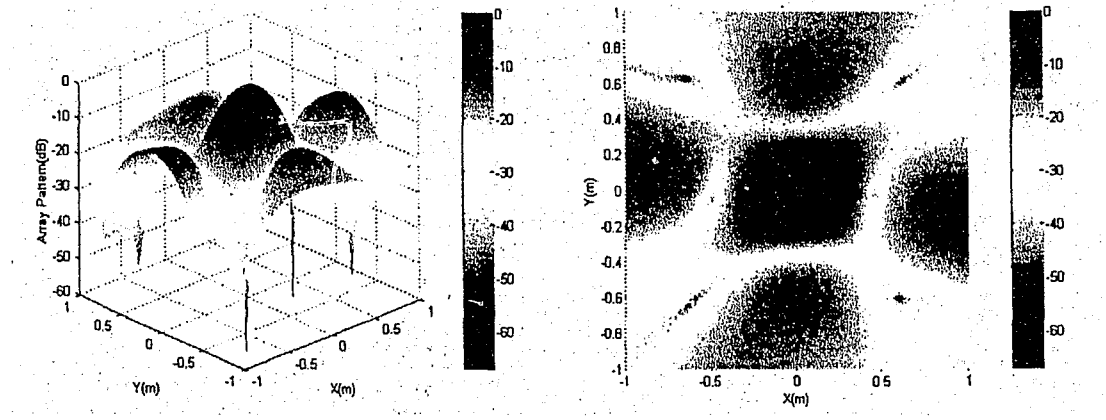

(ii)(c) (ii)(d)

Figure B.7: Theoretical beamforming results for a UPA, near field beamforming: N=25;
(ii)(a) Array Pattern (mag.) vs X (m) & Y (m) at X=0 m; Y=0.0 m, Z=0.5 m, 3D plot.
(ii)(b) Array Pattern (mag.) vs X (m) & Y (m) at X=0 m; Y=0.0 m, Z=0.5 m, 2D plot.
(ii)(c) Array Pattern (mag.) vs X (m) & Y (m) at X=0 m; Y=0.0 m, Z=0.75 m, 3D plot.
(ii)(d) Array Pattern (mag.) vs X (m) & Y (m) at X=0 m; Y=0.0 m, Z=0.75 m, 2D plot.

These examples indicate that the array pattern can be used to determine optimum array designs for beamforming applications [1].

Plots of array power for a ULA with a near field source at (0.0, 0.5) m for N=8 and N=24 are shown in Figure B.8. These results show that the dynamic range along the x-axis decreases as the number of microphones increases.

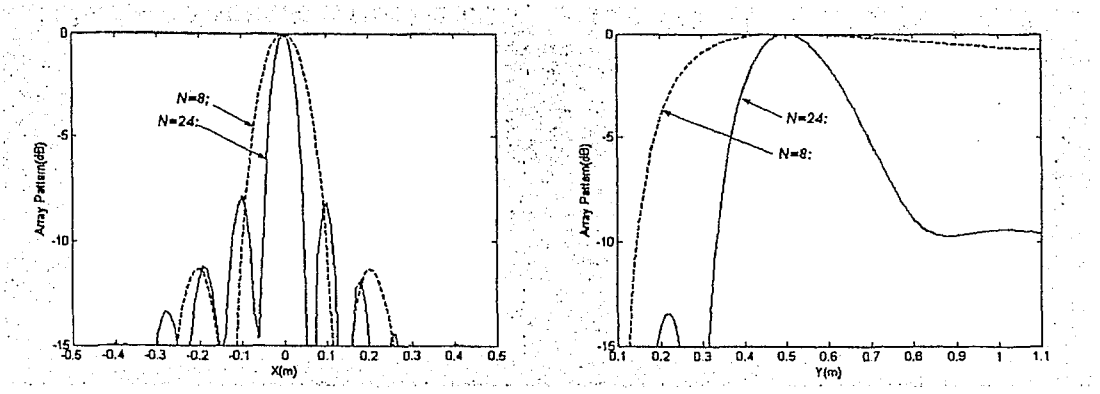

(a) (b)

Figure B.8: Theoretical beamforming results for a ULA, near field beamforming with source at (0.0, 0.5) m and N=8 & N=24; (a) array power along the x-axis (b) array power along the y-axis.

B.2 Validation of beamforming MATLAB code

Validation of the MATLAB code for the beamforming technique developed at Ryerson University (given in Appendix A) is essential before using it for the simulation and experimental data. The validation involves the following:

(i) Comparison between the theoretical array pattern for a far field ULA and the corresponding (numerical) simulation beamforming maps.

(ii) Determination of the spectrum of a far field source signal.

B.2.1 Comparison between theoretical and simulation results

The following two 2 situations were examined with simulation data and the MATLAB code. Note that the source and microphone parameters are the same as those used for the theoretical array pattern (subsection B.1.1).

(i) ULA with N=20; d=2 cm; L=1; M=1024; SR=4f; and an acoustic source with f=8000 Hz, located at θ= 0 radians.

(ii) ULA with N=20; d=2 cm; L=1; M=1024; SR=4f; and an acoustic source with f=8000 Hz, located at θ= 0.5 radians.

The results are shown in Figures B.9.

It is evident that Figures B.9 (i) and B.9 (ii) are identical to Figures B.2 (i) and B.2 (ii) respectively. This verifies that the MATLAB code is correct with respect to determination of the source location.

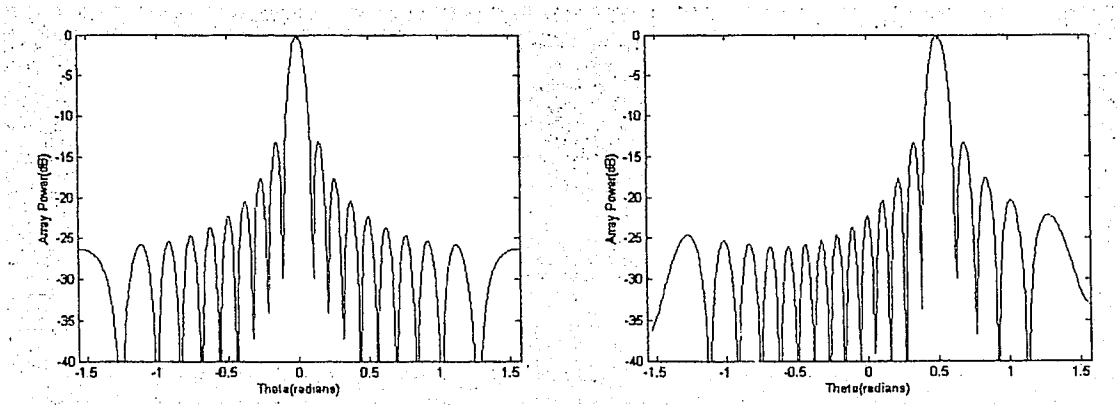

(i) (ii)

Figure B.9: Simulation beamforming simulation results for a ULA, far field beamforming, N=20; (i) Array power (dB) vs. DOA for θ= 0 radians (ii) Array power (dB) vs. DOA for θ= 0.5 radians.

B.2.2 Determination of the spectrum of the source signal

The spectrum of a source signal in the form of a sine wave with an integer number of cycles is determined first by means of a single microphone and then by means of a microphone array.

B.2.2.1 Spectrum via one microphone

Consider an acoustic source radiating a sine wave signal, $s(t)$, with an amplitude A=1, i.e.,

$$s(t) = \sin(2\pi ft).$$

The mean square value of this signal is given by.

$$\overline{s^2} = A^2/2 = 0.5,$$

or in decibels,

$$\overline{s^2}(dB) = 10\log_{10}\overline{s^2} = -3\,dB.$$

In the case of a sine wave of duration T containing an integer number of cycles, the period of the sine wave is related to T as follows:

$$T = I\,T_p,$$

where

T= signal duration, s

$T_p = 1/f$ = period of sine wave, s

and I is an integer, i.e.,

I= 1, 2, 3 ...

The digital version of $s(t)$ is generated as follows.

$$\begin{aligned} s[m] &= s(m\Delta t) \\ &= \sin(2\pi f m\Delta t) \\ &= \sin(2\pi m\Delta t / T_p) \\ &= \sin(2\pi m\Delta t I / T), \qquad m = 1, 2, 3....M \end{aligned}$$

With M being the total number of digital signal values,

$$M = T / \Delta t.$$

Hence,

$$\begin{aligned} s[m] &= \sin(2\pi m\Delta t I / M\Delta t) \\ &= \sin(2\pi m I / M), \end{aligned}$$

where $I = T / T_p = M\Delta t f = Mf / SR,$

since $SR = 1/\Delta t.$

This relationship is illustrated below.

For f=500 Hz, M= 16, and SR= 2000 Hz, it follows that

$$I = 500*16/2000 = 4$$

i.e., the generated sine wave has (exactly) 4 cycles.

A single microphone detecting $s(t)=\sin(2\pi ft)$ will yield a spectrum consisting of a single spike located at f, with a height of 0.5, representing $\overline{s^2}$, providing that T, the duration of $s(t)$, contains an integer number of cycles.

The simulation was carried out using the following parameters: f=50 Hz; M=64; SR=200 Hz. The plots of the s(t) and its spectrum are presented in the Figure B.10. It can be seen that the spectrum does in fact consists of a single spike with a height of 0.5, as required.

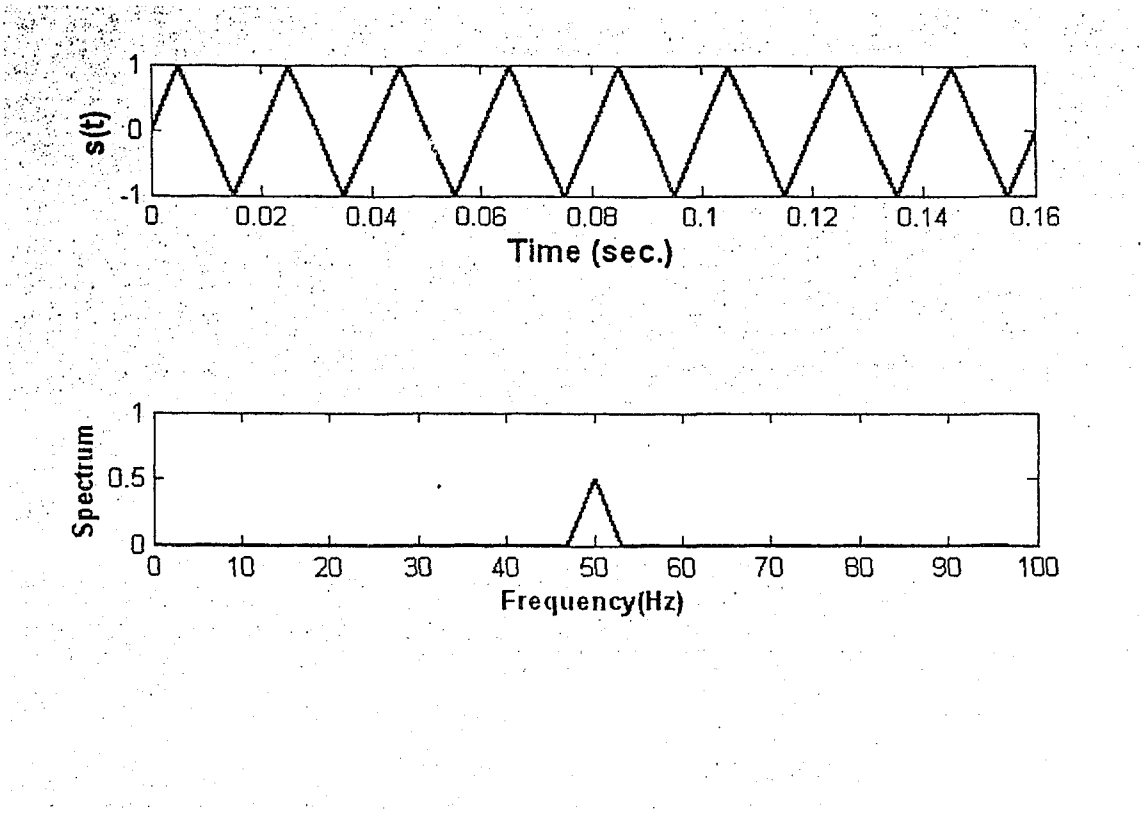

Figure B.10: Plots of $s(t)$, and the spectrum of $s(t)$.

B.2.2.2 Spectrum via microphone array

With respect to an array of N microphones, the sine wave (with an integer number of cycles) will be detected by all N microphones. Therefore, the simulation beamforming array power results should display a mainlobe centered at the location of the acoustic source, *with a height of -3 dB*. Also, the corresponding spectrum should be a spike centered at f *with a height of 0.5*.

To verify this point, two simulations were run with the following parameters:

(i) $s(t)= \sin(2\pi ft)$; N=20; f=8000 Hz; d=2 cm; M= 1024; L=1; SR= 4f; $\theta = 0$ rad.

(ii) $s(t)= \sin(2\pi ft)$; N=20; f=8000 Hz; d=2 cm; M= 1024; L=1; SR= 4f; $\theta = 0.5$ rad.

The simulation results are illustrated in Figures B.11 and B.12.These results show that the mean square value of the sine wave is in fact 0.5, establishing that the MATLAB code gives the correct spectrum of an acoustic source. Note that the MATLAB code can be validated in a similar way for other array geometries (e.g., the UPA) with both far-field and near-field source locations.

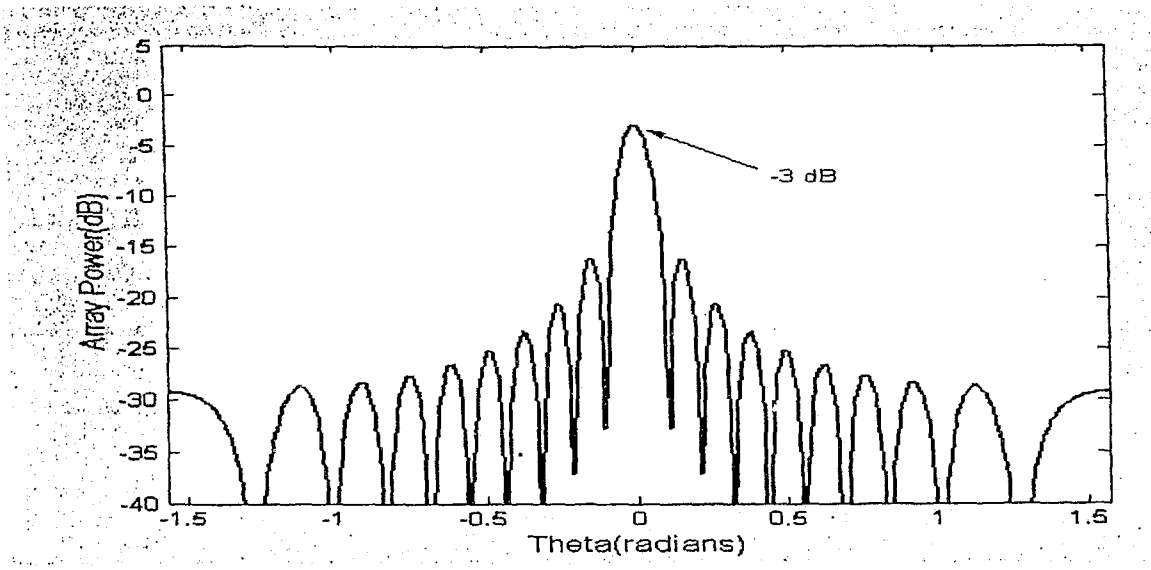

(i)

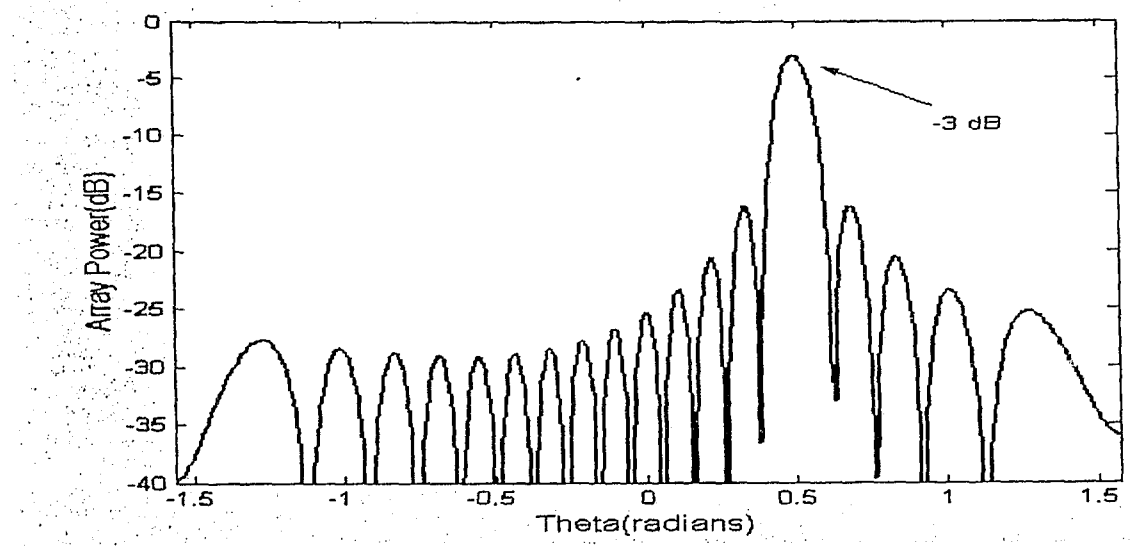

(ii)

Figure B.11: Simulation array power results obtained using MATLAB code;
(i) $\theta = 0$ radians (ii) $\theta = 0.5$ radians.

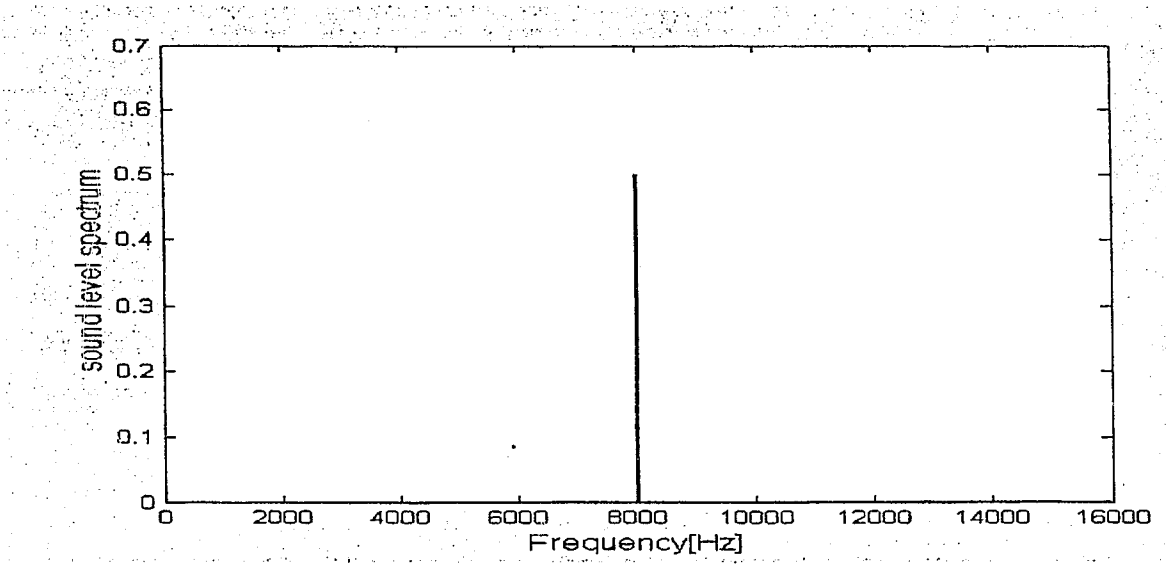

(i)

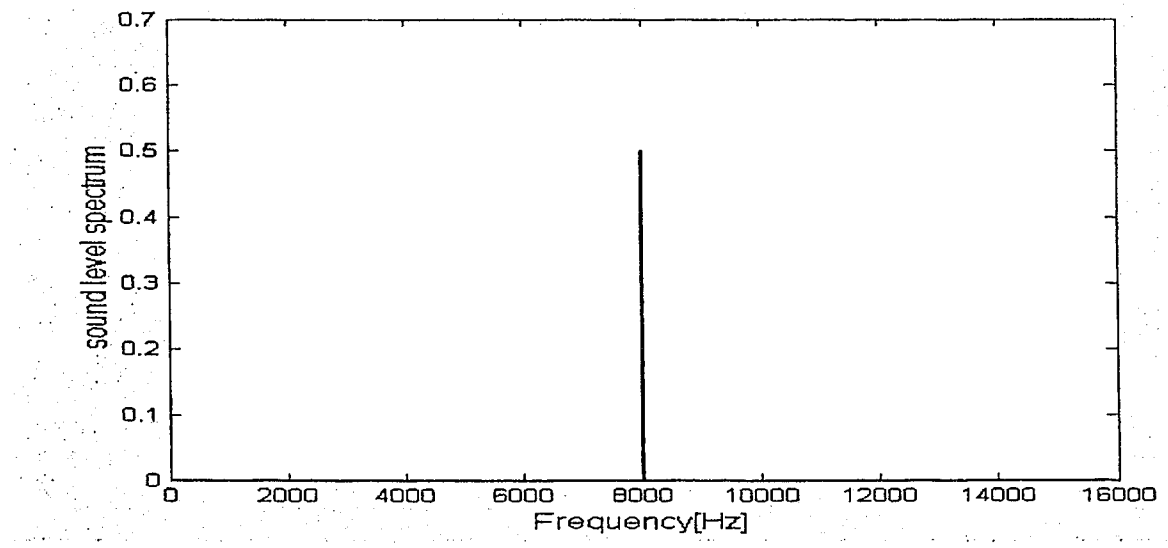

(ii)

Figure B.12: Simulation spectrum results obtained using MATLAB code;
(i) $\theta = 0$ radians and (ii) $\theta = 0.5$ radians.

Appendix C

Signal-to-noise ratio (SNR) of a microphone array

When an array of microphones is affected by noise that is statistically independent among the various microphones, the SNR of the array exceeds that of a single microphone by a factor equal to the number of microphones. This can be shown as follows. Consider an array of N microphones. The output signal of the nth microphone is given by:

$$y_n(t) = s(t) + n_n(t) \qquad n = 1, 2, 3 \ldots N,$$

where $s(t)$ is the source signal and $n_n(t)$ is the statistically independent noise signal affecting the nth microphone. Hence, the cross correlation between $s(t)$ and $n_n(t)$ is zero, i.e.,

$$R_{sn_n}(\tau) = 0,$$

where τ is the time delay between the source signal $s(t)$ and the noise signal $n_n(t)$ at the nth microphone.

It can be assumed that the noise signals have the same auto-spectrum and auto-correlation functions, i.e.,

$$G_{n_1}(f) = G_{n_2}(f) = \ldots = G_n(f)$$

and,

$$R_{n_1}(\tau) = R_{n_2}(\tau) = \ldots = R_n(\tau)$$

Also, the noise signals are uncorrelated, i.e.,

$$R_{n_i n_j}(\tau) = 0, \quad for\ i \neq j$$

Hence, the energy or mean square value of $y_n(t)$ is given by:

$$\sigma_{y_n}{}^2 = \sigma_s{}^2 + \sigma_{n_n}{}^2$$

The signal-to-noise ratio of a single microphone is given by:

$$SNR_o = \text{mean square value of signal/ mean square value of noise}$$

$$= \frac{\sigma_s{}^2}{\sigma_{n_n}{}^2}$$

The array signal is given by:

$$z(t) = \sum_{n=1}^{N} y_n(t)$$

This has the following mean square value

$$\sigma_{z(t)}^{\ 2} = N^2 \sigma_s^{\ 2} + N \sigma_{n_n}^{\ 2}$$

Thus, the signal-to-noise ratio for the array is given by:

$$\text{SNR} = \frac{N^2 \sigma_s^{\ 2}}{N \sigma_{n_n}^{\ 2}}$$

$$= N\left(\frac{\sigma_s^{\ 2}}{\sigma_{n_n}^{\ 2}}\right)$$

i.e.,

$$\text{SNR} = N\,(\text{SNR}_o)$$